# Polimery w Medycynie

## Polymers in Medicine

BIANNUAL ISSN: 0370-0747 e-ISSN: 2451-2699 polimery.umw.edu.pl

2026, Vol. 56, No. 1 (January–June)

Ministry of Science and Higher Education – 70 pts.
Index Copernicus (ICV) – 125.42 pts.

Wroclaw Medical University

Polimery w Medycynie

Polymers in Medicine

# Polimery w Medycynie
## Polymers in Medicine

ISSN 0370-0747 (PRINT) ISSN 2451-2699 (ONLINE) polimery.umw.edu.pl

**BIANNUAL**
**2026, Vol. 56, No. 1**
**(January–June)**

"Polymers in Medicine" is an independent, multidisciplinary forum to exchange scientific and clinical information, which publishes original papers (technical, analytical, experimental, clinical), preliminary reports and reviews regarding the use of polymers (natural and synthetic) and biomaterials in different specialties of medicine (biochemistry, clinical medicine, pharmacology, dentistry, implantology), biotechnology and veterinary science.

**Address of Editorial Office**
Marcinkowskiego 2–6
50-368 Wrocław, Poland
Tel.: +48 71 784 11 33
E-mail: redakcja@umw.edu.pl

**Publisher**
Wroclaw Medical University
Wybrzeże L. Pasteura 1
50-367 Wrocław, Poland

Online edition is the original version of the journal

## Editorial Policy

During the review process, the Editorial Board conforms to the "Uniform Requirements for Manuscripts Submitted to Biomedical Journals: Writing and Editing for Biomedical Publication" approved by the International Committee of Medical Journal Editors (http://www.icmje.org/). Experimental studies must include a statement that the experimental protocol and informed consent procedure were in compliance with the Declaration of Helsinki and were approved by the ethics committee.

For more information visit the following page: https://polimery.umw.edu.pl

Indexed in: Scopus, OCLC, WorldCat, PBL, EBSCO, MEDLINE, Index Copernicus

Typographic design: Monika Kolęda, Piotr Gil
Cover: Monika Kolęda
DTP: Wroclaw Medical University Press

Circulation: 11 copies

# Polimery w Medycynie
## Polymers in Medicine

BIANNUAL 2026, Vol. 56, No. 1 (January–June)

ISSN 0370-0747 (PRINT)
ISSN 2451-2699 (ONLINE)
polimery.umw.edu.pl


## Contents

# PREFACE

**Dear Readers,**

At a time when medical, pharmaceutical and environmental sciences are facing increasingly complex challenges, we are pleased to present the latest issue of *Polimery w Medycynie – Polymers in Medicine*. The articles included in this issue show how broad and dynamic contemporary polymer-related research has become, extending from wound healing and drug delivery systems to antimicrobial strategies, ophthalmic formulations, biofilm control, biomedical plasma applications, and sustainable polymer chemistry.

A significant part of this issue is devoted to alginate-based materials, which remain among the most interesting natural polymers used in medicine and pharmacy. The review article on sodium alginate in wound dressing systems presents the current state of knowledge on this biopolymer and its importance in the hemostatic, inflammatory and proliferative stages of wound healing. The bibliometric analysis included in this work confirms the increasing scientific interest in sodium alginate, which is undoubtedly related to its biocompatibility, non-toxicity and practical potential in modern wound care.

The issue also contains an original study concerning sodium alginate beads as polymeric carriers for active pharmaceutical ingredients. In this work, particular attention was paid to the influence of the drug incorporation strategy on morphology, loading efficiency and release behavior. The authors compared encapsulation during gelation with post-synthesis impregnation and demonstrated that encapsulation leads to higher drug loading, and more controlled, sustained release.

Another important pharmaceutical topic addressed in this issue is the compatibility between innovative ophthalmic preparations and polymer packaging. The study on self-emulsifying oil formulations containing suspended drug particles evaluates their interaction with commercial low-density polyethylene containers. Using modern analytical techniques such as FTIR, NIR, DSC and XRD, as well as mechanical strength testing, the authors investigated possible changes in the morphology, structure, thermal properties and mechanical performance of the packaging material. The results underline the need for careful compatibility studies between ophthalmic formulations and polymeric packaging systems, to maintain product stability and patient safety.

The present issue also reflects the growing importance of antimicrobial research in the context of global antibiotic resistance. A review article discusses selected biotechnological strategies that may support future treatment of resistant infections, including phage therapy, CRISPR-Cas9 systems, antimicrobial peptides, nanotechnology-based approaches and the therapeutic potential of the microbiome. Although further clinical studies and regulatory frameworks are still needed, the article clearly shows that biotechnology may become an important element of future antimicrobial therapy.

This subject is further developed in an original study on zinc oxide nanoparticles and their synergistic activity with imipenem against imipenem-resistant *Klebsiella pneumoniae*. The authors prepared ZnO nanoparticles using *Thymus vulgaris* leaf extract and demonstrated their ability to reduce the minimum inhibitory concentration of imipenem and decrease biofilm extracellular polymeric matrix formation. The study indicates that properly designed nanoparticles may serve as useful adjuvant agents in combating resistant and biofilm-forming pathogens.

Another original article focuses on *Pseudomonas aeruginosa* and the influence of sub-inhibitory concentrations of ceftriaxone on biofilm polymer matrix formation, bacterial adhesion and quorum-sensing regulation. The authors show that ceftriaxone, even below its inhibitory concentration, may modulate biofilm formation,

reduce adhesion to epithelial cells and downregulate genes involved in quorum sensing. Molecular docking analysis additionally suggests interactions between ceftriaxone and key regulatory proteins, including LasR and RhlR, as well as AlgD, an enzyme associated with alginate polymer biosynthesis. This study provides an interesting molecular perspective on the anti-biofilm activity of antibiotics at sub-inhibitory concentrations.

The biomedical scope of the issue is broadened by a study investigating the influence of microwave plasma on lymphocytes. The authors report that short exposure may stimulate normal lymphocyte activity and proliferation, while longer exposure may suppress abnormal cell proliferation.

Finally, this issue includes a conference report from the Tübingen Symposium on Sustainable Polymers. The report presents recent directions in polymer research, including green chemistry strategies, synthesis and degradation pathways, environmentally benign catalysts, biodegradable and biocompatible materials, as well as polymer systems for therapeutic drug delivery. This contribution reminds that the future of polymer science must be considered not only from the medical and pharmaceutical perspective, but also in relation to sustainability, resource conservation and environmental protection.

On behalf of the Editorial Team, I would like to thank all authors, reviewers and editors for their valuable contribution to the preparation of this issue of *Polimery w Medycynie – Polymers in Medicine*. I hope that the articles presented here will be of interest to our Readers and will inspire further scientific discussion, interdisciplinary cooperation and new research in the field of polymers applied in medicine, pharmacy and biotechnology.

I wish you pleasant and fruitful reading.

**Prof. Witold Musiał**
**Editor-in-Chief**
*Polimery w Medycynie – Polymers in Medicine*

# Sodium alginate for wound healing applications: A review

Muhammad Tahir[1,A–D], Simone Pettineo[2,A,B], Silvia Vicini[2,A,E,F], Maila Castellano[2,E,F], Marina Alloisio[2,E,F], Ketul Popat[3,E,F], Harishkumar Madhyastha[4,E,F], Kaoru Ohe[5,E,F], Kentaro Sakai[6,E,F], Alina Sionkowska[1,A,E,F]

[1] Laboratory for Biomaterials and Cosmetics, Faculty of Chemistry, Nicolaus Copernicus University in Torun, Poland
[2] Department of Chemistry and Industrial Chemistry, University of Genova, Italy
[3] Department of Bioengineering, George Mason University, Fairfax, USA
[4] Department of Cardiovascular Physiology, Faculty of Medicine, University of Miyazaki, Japan
[5] Center for Science and Engineering Education, Faculty of Engineering, University of Miyazaki, Japan
[6] Division for Research Facility Support Organization for Promotion of Research and Industry – Academic Regional Collaboration, University of Miyazaki, Japan

A – research concept and design; B – collection and/or assembly of data; C – data analysis and interpretation;
D – writing the article; E – critical revision of the article; F – final approval of the article

Polymers in Medicine, ISSN 0370-0747, eISSN 2451-2699 *Polim Med*. 2026;56(1):7–17

**Address for correspondence**
Muhammad Tahir
E-mail: 503438@o365.doktorant.umk.pl

**Funding sources**
None declared

**Conflict of interest**
None declared

**Acknowledgements**
None declared

Received on August 1, 2025
Reviewed on September 27, 2025
Accepted on February 26, 2026

Published online on July 30, 2026

## Abstract

Sodium alginate (SA) is a polysaccharide biopolymer widely used in wound healing applications due to its beneficial role in the hemostatic, inflammatory, and proliferative phases of tissue repair. Its hydrophilic nature supports the wound healing process by enabling efficient absorption of wound exudate and maintaining a moist microenvironment conducive to tissue regeneration. Moreover, SA can form highly porous structures that promote oxygen diffusion and provide a suitable scaffold for neovascularization and new tissue formation. This review summarizes recent advances in the application of SA in wound dressings. A bibliometric analysis of Scopus data using the keywords "sodium alginate" AND "wound healing" reveals a growing number of publications in recent years, highlighting the increasing scientific interest in this field. The expanding utilization of SA in wound healing may be attributed to its favorable properties, including biocompatibility, biodegradability, and low toxicity.

**Key words:** wound healing, sodium alginate, biopolymer, alginic acid, porous materials

**Cite as**
Tahir M, Pettineo S, Vicini S, et al. Sodium alginate for wound healing applications: A review. *Polim Med*. 2026;56(1):7–17. doi:10.17219/pim/218616

**DOI**
10.17219/pim/218616

## Introduction

Biopolymers can be extracted from bio-based materials using various techniques. They can also be produced biotechnologically or synthesized directly from building blocks derived from living organisms. Thus, in general, nature is the primary source of biopolymers.[1] Jabeen and Atif defined biopolymers as macromolecules that are primarily composed of monomeric units of natural origin.[2] Biopolymers are advantageous due to their environmentally friendly nature.[3] Nitta and Numata discussed the classification of biopolymers, which are mainly divided into 3 types: polysaccharides, nucleic acids, and proteins.[4] In the huge family of polysaccharides, one can find starch, cellulose, chitin, chitosan, and many more, for example, alginate.[5]

The primary sources of alginate reported are brown seaweed and marine algae.[6,7] Alginate has a unique non-toxic nature and biocompatibility, which make this biopolymer attractive for biomedical and cosmetic applications.[8,9] It exhibits bioadhesivity, which is the primary reason for its widespread use in pharmaceutical applications.[10] It may form sponge-like structures that are capable of absorbing water.[11] Alginate-based hydrogels are formed through ionic crosslinking.[12] Salarvand et al. reported the presence of hydroxyl and carboxyl groups in alginate, which gives the possibility of hydrogen bond formation.[13] Moreover, alginate contains negative ions capable of further interactions.[14] Wang et al. reported that sodium alginate (SA) and its oxidized derivatives show good cytocompatibility.[15] Alginate-based nanofibers are widely utilized in biomedical applications, especially in tissue engineering and wound healing.[16,17] It has recently been observed that SA applications in various areas are growing, particularly in wound healing.

## Sodium alginate

The properties of SA are widely studied. Phùng et al. mentioned the water solubility of SA,[18] whereas Yan et al. reported that SA is insoluble in ethanol.[19] Sodium alginate is highly preferred in several applications due to its outstanding ability to form films.[20,21] Yan et al. described SA as a low-cost polymer presenting high potential.[19] The presence of functional groups, such as hydroxyl and carboxyl groups, makes it easy to modify.[22] Belalia and Djelali reported the rheological behavior of SA. In their research, it was concluded that it presents shear-thinning non-Newtonian flow behavior in its aqueous form.[23] Viscosity was reduced with an increase in shear rate; this behavior has been reported as shear-thinning behavior in the literature.[24]

In the structural formula of SA, the main constituents are α-L-guluronic acid and β-D-mannuronic acid.[25,26] ChemDraw 25.0.2 software (Revvity Signals Software) was used to draw the structural formulas of SA and its constituents, which are presented in Fig. 1. The "Structure" tab of the ChemDraw software was selected, and in this tab, "Convert Name to Structure" was chosen to draw the structural formulas of SA and its constituents. The names used are also presented in the figure alongside their corresponding structural formulas. Therefore, in short, SA is a combination of 2 uronic acids. Sodium alginate sourced from algae contains a significant portion of other cations: Ca (calcium), Mg (magnesium), and Sr (strontium), which are treated with hydrochloric acid (HCl) to obtain alginic acid through a liquid wash mechanism.[27]

The addition of sodium carbonate ($Na_2CO_3$) leads to a pH range of 9–10. $Na_2CO_3$ can also be replaced with alternatives such as sodium hydroxide (NaOH), sodium bicarbonate ($NaHCO_3$), or sodium chloride (NaCl). This leads to the conversion of alginic acid (which is water-insoluble) to SA (a water-soluble form).[28] It can be followed by either the Ca-alginate or the alginic acid route. The route considering alginic acid involves the treatment of SA with HCl. The 2nd route is the Ca-alginate route, which involves the addition of calcium chloride to SA to form Ca-alginate.[29] Ca-alginate is further treated with HCl to obtain alginic acid. The alginic acid obtained from these 2 routes is further treated with $Na_2CO_3$ to produce SA in its pure form.[30]

## Porosity of sodium alginate materials

Sodium alginate materials can be fabricated into gels. Abka-Khajouei et al. reported that alginate gels presented pores, with the pore size specified in their research ranging

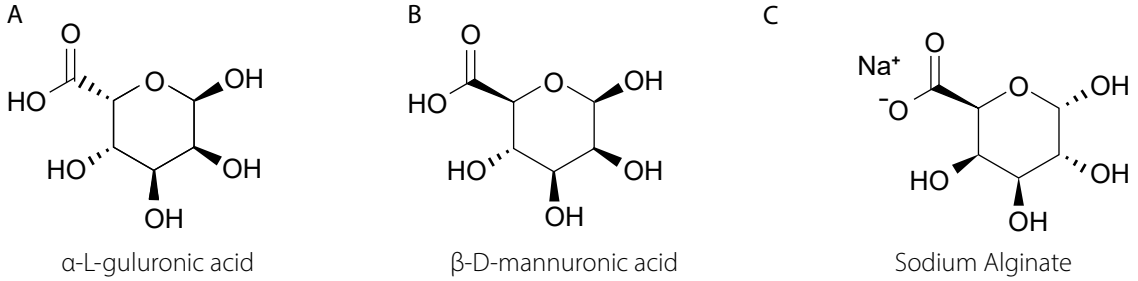


Fig. 1. Structural formulas of (A) α-L-guluronic acid, (B) β-D-mannuronic acid, and (C) sodium alginate

from 5 nm to 200 nm. They mentioned electron microscopy for pore size demonstration.[31] Da Silva et al. reported that as the SA concentration increases, it causes a decrease in the material's porosity. Therefore, an inverse relationship between SA concentration and material porosity was presented. Porosity in wound dressings is preferred because it facilitates the process of oxygenation.[32] Sinha et al. reported that wound dressings with the highest porosity had the greatest tendency to absorb wound exudate.[33] Liu et al.[34] also demonstrated that SA gel presented pores. They conducted field emission electron microscopy (FE-SEM) on SA gels with the addition of calcium ions ($Ca^{2+}$) to demonstrate the pores.

MATLAB and Python are referred to as programming languages.[35,36] They are effectively utilized for the visualization and demonstration of pores. Jenkins et al. were the developers of PoreScript (a MATLAB algorithm), and PoreScript was used to determine pore size from scanning electron microscopy (SEM) images.[37] Polez et al. utilized SEM images to determine porosity using PoreSpy,[38] a Python package that characterizes porous materials from 3D images.[39] Negut and Bita reported the use of a convolutional neural network (CNN) to identify pore size distribution in hydrogels.[40] Zhang et al. reported CNN as a deep learning model.[41] El Naqa and Murphy described deep learning as a sub-classification of machine learning, and stated that deep learning has the capacity to be trained from raw data.[42] Machine learning has been referred to as a field within artificial intelligence.[43] Three types of machine learning are reported in the literature: supervised learning, unsupervised learning, and reinforcement learning.[44,45]

Supervised machine learning utilizes labeled data.[46] Unsupervised learning is based on unlabeled data.[47] Reinforcement learning allows an agent to take actions.[48] Correct actions in reinforcement learning lead to earning rewards, whereas wrong decisions result in failure.[49] Saberian et al. utilized ImageJ software (National Institutes of Health (NIH), Bethesda, USA) to measure pores based on SEM images. The hydrogel utilized in their research was based on alginate/chitosan and also included honey and aloe vera. The prepared hydrogel was intended for use as a wound dressing.[50] Olevsky et al. developed PoreVision using a Python script. PoreVision utilizes Python libraries, primarily OpenCV, NumPy, and Pandas. It was used to measure pore size from SEM images and can be utilized for gels and porous materials, as indicated in their research.[51] Shkarin et al. developed quanfima, a Python-supported package that can be used to analyze the morphology of biomaterials, including porosity.[52] MICPY has been highlighted for pore analysis and has been reported as a Python-supported package. It can analyze SEM images.[53,54] Nair et al. utilized CTAnalyzer software for pore size determination, which was made possible by using a 3D object analyzer within the software.[55] Karaca and Aldemir Dikici utilized a deep learning model, which they named Pore $D^2$. In their study, YOLOv5 was used for object detection, and SEM images were utilized as the input. EasyOCR has been used to extract text from images, and it is a Python library that employs a deep learning approach. The output layer provided accurate information on pore size.[56]

## Wettability of sodium alginate materials

The hydrophilicity of the material's surface may be a reason for better cell adhesion. Yuan and Lee presented the relationship between the water contact angle and wettability in the context of liquid–solid interaction. According to their research, contact angles below 90° exhibited the highest wettability. A contact angle greater than 90° was a clear indication of low wettability.[57] Kumar and Prabhu described reactive and non-reactive wetting. A reaction occurring between the spreading liquid and the substrate material impacts the mechanism of wetting, which is reported as reactive wetting. If no reaction occurs between the spreading liquid and the substrate material, it is reported as inert or non-reactive wetting.[58] Xie et al. conducted contact angle analysis for membranes made of SA, and SA 100 and SA 200 were named for the lower amounts of guluronic acid. Manugel DMB was named for a higher amount of guluronic acid. A Milli-Q water drop was utilized to obtain contact angle measurements, and the analysis was conducted on alginate–chitosan–alginate (ACA) membranes. The water contact angle for SA 100, as reported in their study, was 65.9 ±1.0°. SA 200 presented a water contact angle of 68.5 ±2.4°. The water contact angle of Manugel DMB recorded in their research was 77.7 ±3.3°. These values are reported as mean ± standard error (SE). The number of analyses specified in their study was 3. In short, their results showed that an increase in guluronic acid content led to a reduction in hydrophilicity.[59] Karmakar et al. analyzed the contact angle of a hydrogel composed of SA and carboxymethyl cellulose in a 1:1 ratio, reporting a contact angle value of 48.32 ±1.5°. Contact angle measurements were recorded using distilled water, and 3 measurements were taken to obtain the mean value.[60] Mujawar et al. conducted contact angle measurements on 3D-printed samples, including those made from SA–gelatin and SA–gelatin–*Aloe barbadensis* extract. Six contact angle measurements were taken using water as the probe liquid. The recorded water contact angle for 3D-printed SA–gelatin was 42.31 ±3.23°. The water contact angle reported for SA–gelatin–*Aloe barbadensis* extract was about 53.2 ±4.7°.[61] Sisakht et al. prepared a hydrogel with a 50:50 weight ratio of SA and poly(acrylic acid). They utilized both SA and poly(acrylic acid) at a concentration of 2% wt/vol. They also analyzed the contact angle in combination with fibroblast growth factor (FGF1). Deionized water was used as the probe liquid for the contact angle analysis. Three measurements were recorded for the samples. The contact

angle reported for SA was 57.87°. In the case of the SA–poly(acrylic acid) hydrogel, the reported contact angle was 18.52°. The SA–poly(acrylic acid) hydrogel in combination with FGF1 exhibited a water contact angle of approx. 62.56°.[62] Hosseini et al. prepared a hydrogel composed of carboxymethyl cellulose and SA. Subsequently, they combined it with simvastatin, resulting in a final form known as the carboxymethyl cellulose/SA–simvastatin hydrogel. The recorded water contact angles for carboxymethyl cellulose–SA and carboxymethyl cellulose/SA–simvastatin were 43.3 ±2° and 59.1 ±4°, respectively. They utilized water as the probe liquid, and 3 measurements were recorded for each sample.[63] Table 1 presents a summary of the contact angle measurements for SA-based materials. Isa Rahim et al. specified that contact angles lower than 90° were indicative of hydrophilicity, and contact angles between 90° and 150° were indicative of hydrophobicity.[64] Chen et al. specified that a surface with a contact angle higher than 150° can be reported as superhydrophobic.[65] Choi et al. reported the use of SA for wound dressings, and the reason given in their study was its hydrophilicity.[66] Jin et al. examined the impact of hydrophilic polymers on swelling, and their study concluded that SA presented the maximum swelling among the analyzed hydrophilic polymers.[67] Feng and Wang highlighted the use of hydrogels with maximum swelling capacity for wound healing due to their ability to absorb wound exudates.[68] Singh and Pramanik reported better cell adhesion for polymeric films composed of SA and chitosan than for alginate itself, and it was also mentioned in their study that the contact angle was lower than 90°.[69]

## Sodium alginate wound healing

Zahid et al. indicated that the use of SA for wound healing applications is promising due to its liquid absorption.[70] The stages of wound healing have been demonstrated in various studies and include hemostasis, inflammation, proliferation, and remodeling phases.[71–73] Hemostasis is the first stage of wound healing, and in this phase, blood clot formation takes place.[74] Periayah et al. explained the blood coagulation mechanism in significant detail. Their study indicated the key role of platelets in thrombus formation.[75] Zhang et al. demonstrated that platelets play a vital role in vascular repair.[76] Huang et al. reported that SA can enhance platelet concentration.[77] Zhang et al. recommended SA for blood coagulation applications.[78] Chen et al. reported in their study the preparation of a hemostatic powder, which involves the presence of SA, $CaCl_2$, graphene oxide, and cerium nitrate. The concluding remarks in their study indicated that the hemostatic powder presented the ability to absorb water, resulting in a shorter hemostatic time. The hemostatic powder effectively decreased blood loss and enhanced the wound healing mechanism due to the presence of $Ce^{3+}$ (which acts as a free radical scavenger).[79] Zhou et al. analyzed the blood coagulation of a gelatin sponge individually and in combination with SA, and their study summarized that blood coagulation was enhanced due to the presence of SA.[80] Wang et al. prepared a powdered composite that included SA and poly(γ-glutamic acid) (PGA). The prepared powdered composite was found to arrest or block bleeding.[81] Li et al. presented a material composed of SA, silk fibroin, and thrombin. It was mentioned that the prepared material could promote hemostasis.[82] Xie et al. prepared a hydrogel containing SA, chitosan, and oxidized dextran. Their study results showed that the prepared hydrogel reduced blood loss, which significantly supports the basis for improved hemostasis.[83] Khattak et al. mentioned that persistent inflammation was a significant reason for the slowing down or delay of the wound healing mechanism.[84] Zhang et al. reported that inflammation was a notable challenge in wound healing.[85] Liu et al. highlighted that the anti-inflammatory effect was essential for wound healing.[86] Summa et al. prepared a wound dressing material composed of SA and povidone–iodine.

**Table 1.** Contact angle measurements for sodium alginate (SA)-based materials

| | | | | |
|---|---|---|---|---|
| SA 200 | 3 | Milli-Q water | 68.5 ±2.4° | 59 |
| SA–carboxymethyl cellulose (1:1 ratio) | 3 | distilled water | 48.32 ±1.5° | 60 |
| SA–gelatin–*Aloe barbadensis* extract | 6 | water | 53.2 ±4.7° | 61 |
| SA–poly(acrylic acid) (50:50) | 3 | deionized water | 18.52° | 62 |
| Carboxymethyl cellulose–SA | 3 | water | 43.3 ±2° | 63 |

The results of their study indicated that the prepared material exhibited an anti-inflammatory effect.[87] Zhao et al. formulated a composite that included low-viscosity SA combined with titanium dioxide and temozolomide nanoparticles. Their study reported the anti--inflammatory effect of the designed composite. Their research summarized that the anti-inflammatory effect was enhanced due to the prominent presence of SA.[88] Karmakar et al. initially prepared a SA and carboxymethyl cellulose composite, which was then crosslinked to a decellularized extracellular matrix. The crosslinker used in their study was calcium chloride, resulting in a final hydrogel composed of SA, carboxymethyl cellulose, and decellularized extracellular matrix. According to their research, the prepared hydrogel exhibited anti-inflammatory properties.[60] Zhang et al. prepared a blend of SA and carboxymethyl chitosan, which was then loaded with curcumin. $Sr^{2+}$ was used for the crosslinking of the polymers. The prepared hydrogel exhibited anti-inflammatory activity, leading to an enhanced wound healing mechanism.[89] Raguvaran et al. prepared hydrogels composed of SA and gum acacia, which were incorporated with zinc oxide nanoparticles. Their research concluded that polymers in combination with zinc oxide nanoparticles tend to boost the proliferation of fibroblasts.[90] Song et al. demonstrated that fibroblast proliferation is essential to promote the wound healing mechanism.[91] Harper et al. presented fibroblast migration as a component of the proliferative phase of wound healing.[92] Kibungu et al. reported that fibroblast cells assist in the production of collagen.[93] AlShaali et al. also described that granulation tissue starts to form during the proliferation stage.[94] Zhu et al. utilized a hydrogel based on SA, which was incorporated with *Capparis spinosa* L., and the incorporated hydrogel exhibited biocompatibility. It also boosted cell proliferation.[95] Zhou et al. reported that enhanced cell proliferation encouraged wound healing.[96] Ma et al. synthesized a nanocomposite based on SA, polyvinyl alcohol, and graphene oxide. Their research summarized that nanocomposites may result in enhanced cell proliferation.[97] Dodero et al. prepared electrospun membranes of SA, which were crosslinked with divalent cations such as $Ca^{2+}$, $Sr^{2+}$, and $Ba^{2+}$. In the final step, they prepared electrospun mats of SA loaded with zinc oxide nanoparticles, which were crosslinked with $Sr^{2+}$ ions due to excellent cell adhesion. The electrospun mat prepared in their research was recommended for wound healing applications.[98] Ding et al. utilized electrostatic spinning to synthesize a membrane based on SA and polyvinyl alcohol. Shikonin was incorporated into the electrospun membrane. It was found that the shikonin-loaded membrane boosted vascular endothelial growth factor A (VEGF-A) in the proliferative stage of wound healing.[99] Liu et al. reported shikonin as a naphthoquinone pigment useful in the preparation of shikonin-based nanomedicine.[100] Guo et al. highlighted *Lithospermum erythrorhizon* as the source of extraction for shikonin.[101] Lin et al. referred to *Lithospermum erythrorhizon* as a Chinese medicinal herb.[102] Tian et al. reported the antimicrobial and anti-inflammatory properties of shikonin in their research.[103] Guo et al. mentioned the antioxidant and antithrombotic properties of shikonin.[101] Ye et al. reported the anti-tumor effect of shikonin.[104] Several studies reported shikonin as an ideal option for the treatment of diabetic wounds.[105–107] Eming et al. described VEGF-A in relation to angiogenesis in wound healing.[108] DiPietro presented that angiogenesis results from hypoxia.[109] In the case of injury, hypoxia is primarily responsible for the recruitment of hypoxia-inducible factors such as HIF-1. It supports the mechanism of angiogenesis during wound healing.[110] Dawood et al. highlighted angiogenesis as a key feature linked to the proliferative phase of wound healing.[111] Bahadoran et al. referred to the proliferative phase by another name, the growth phase of wound healing.[112] Çerçi et al. utilized amoxicillin in combination with SA and polyvinyl alcohol. Polyvinyl alcohol was employed at a concentration of 12% wt/vol. Sodium alginate was utilized at a concentration of 1% wt/vol. The ratio selected for polyvinyl alcohol and SA was 2:1 (vol/vol) for the electrospinning solution, and 6.4 mg of amoxicillin trihydrate was added to the electrospinning solution. The electrospun nanofibrous mats were prepared by electrospinning. According to their research conclusions, the amoxicillin-loaded electrospun nanofibrous mat exhibited antibacterial properties. Based on their in vitro studies, the prepared nanofibrous mat loaded with amoxicillin was recommended for wound dressing applications.[113] Kaur et al. reported amoxicillin as an antibiotic belonging to the penicillin class.[114] Ayavoo et al. reported that the remodeling phase of wound healing was responsible for the conversion or transformation of fibroblasts into myofibroblasts.[115] The remodeling phase of wound healing tends to remodel collagen III to collagen I.[116] Yang et al. recommended a scaffold composed of SA, silk fibroin, and hyaluronic acid for extracellular matrix remodeling.[117]

## Bibliometric analysis

The bibliometric analysis was conducted using the R software v. 4.5.1 (R Foundation for Statistical Computing, Vienna, Austria) and VOSviewer (https://www.vosviewer.com/). Initially, the "bibliometrix" package was installed, followed by loading the library (bibliometrix). The biblioshiny() function was used to open the web-based interface for bibliometrix. Bibliometrix and biblioshiny were developed by Aria and Cuccurullo.[118] The data were obtained from Scopus, and the document search was conducted using the terms "Sodium Alginate" AND "Wound Healing", with the search restricted to "Article title, Abstract, Keywords" from 2010 to 2025 (access date: 27 June 2025). A total of 944 documents were generated from the search

for "Sodium Alginate" AND "Wound Healing". The annual scientific production data from Scopus for the specified search are presented in Fig. 2. The analyzed data show that the number of articles from 2018 to 2024 increased continuously, indicating the growing prominence of the presented research in recent years. The most relevant sources are depicted in Fig. 3. It represents the *International Journal of Biological Macromolecules*, the leading journal presenting pertinent articles, with 159 publications. The 2nd most relevant source was *Carbohydrate Polymers*, with 37 articles. The 3rd most relevant source was *ACS Applied Materials and Interfaces*, with 24 articles reported. The most globally cited papers were analyzed using Scopus data, and the results are presented in Fig. 4, which shows the papers with the most significant global citation impact. The impact of local citations was also investigated, and the highest number of locally cited documents was 32, as depicted in Fig. 5. Van Eck and Waltman developed VOSviewer for bibliometric mapping.[119] The Scopus data file was imported into VOSviewer, which helped identify relevant keywords through co-occurrence analysis. The co-occurrence analysis is presented in Fig. 6.

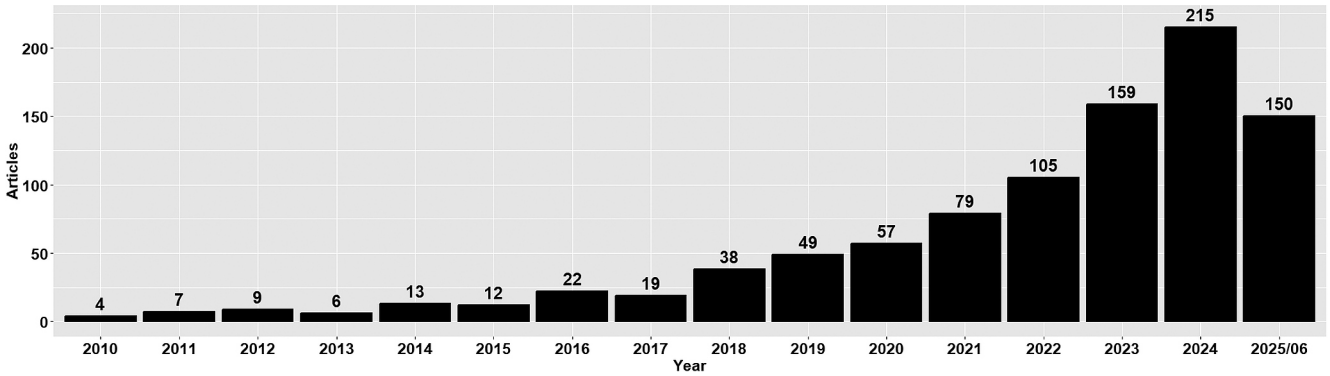


Fig. 2. Annual scientific production ("Sodium Alginate" AND "Wound Healing" search within Scopus; access date: June 27, 2025)

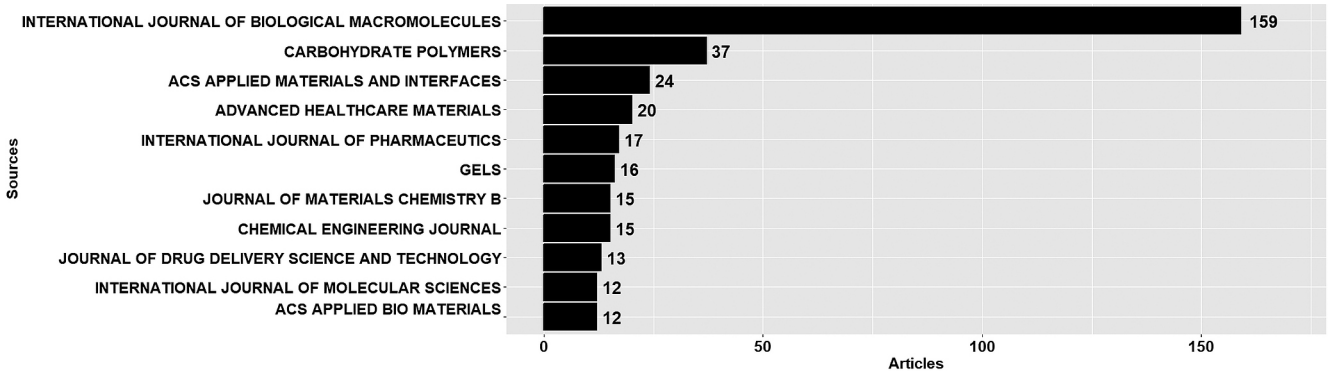


Fig. 3. Most relevant sources with the number of articles ("Sodium Alginate" AND "Wound Healing" search within Scopus; access date: June 27, 2025)

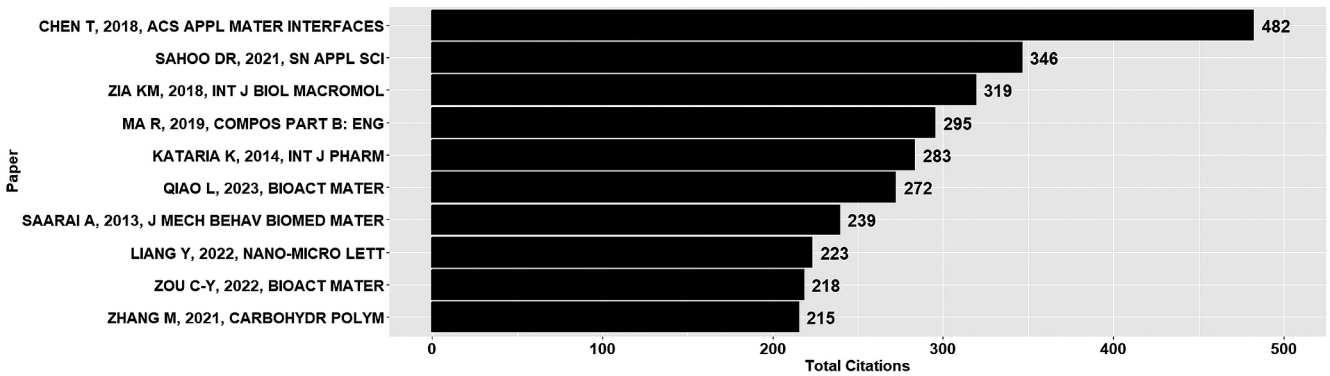


Fig. 4. Most globally cited papers ("Sodium Alginate" AND "Wound Healing" search within Scopus; access date: June 27, 2025)

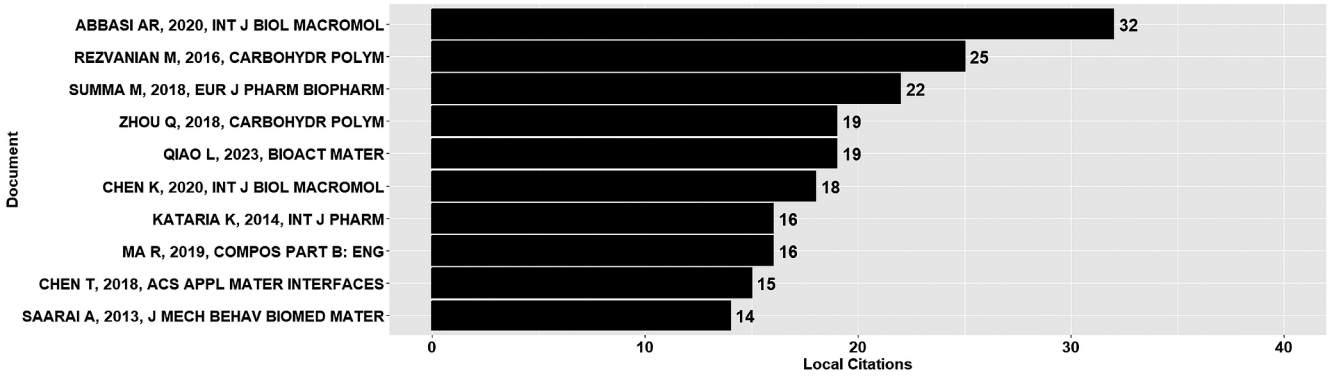


Fig. 5. Most locally cited documents ("Sodium Alginate" AND "Wound Healing" search within Scopus; access date: June 27, 2025)

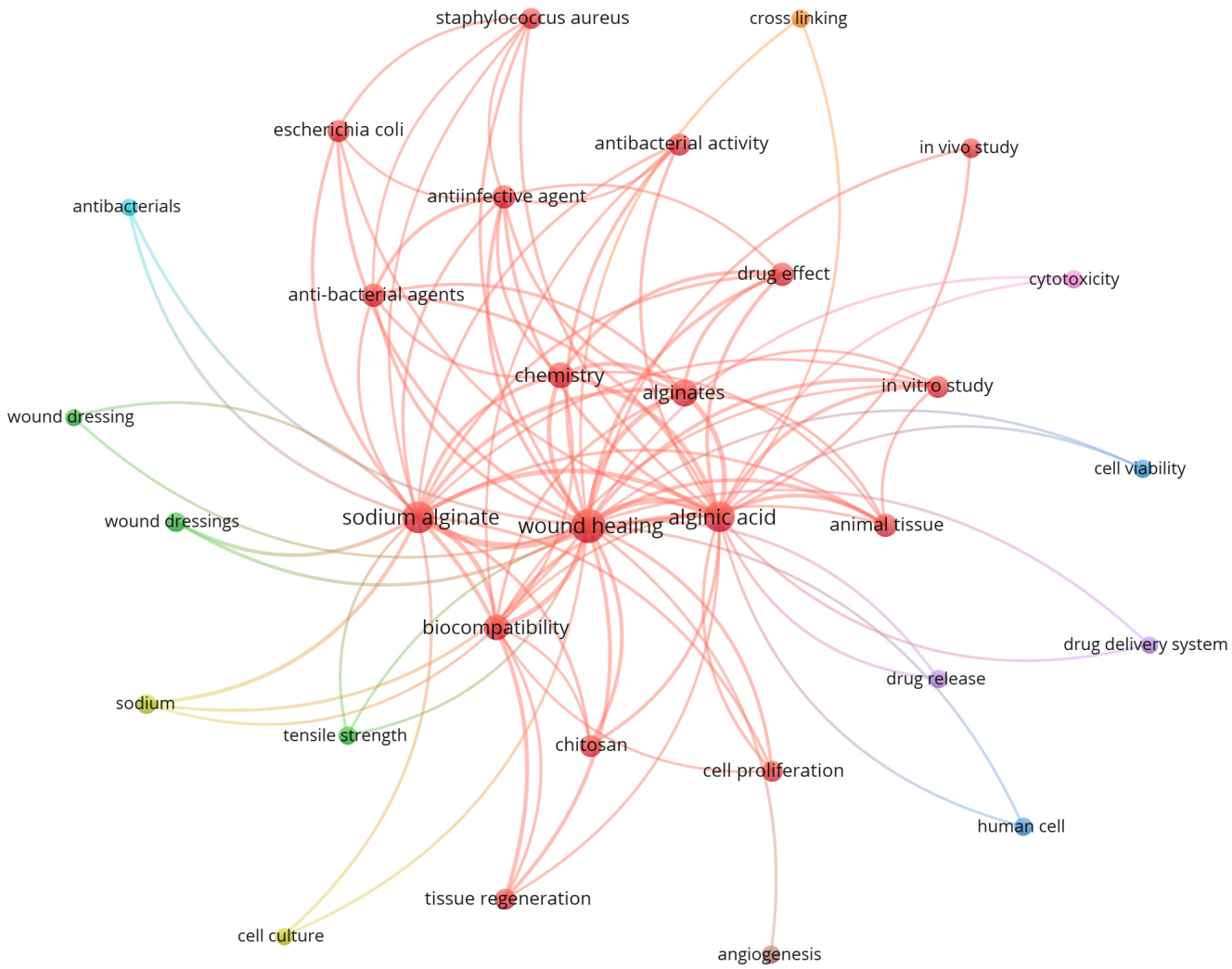


Fig. 6. Co-occurrence of keywords ("Sodium Alginate" AND "Wound Healing" search within Scopus; access date: June 27, 2025)

## Conclusions and future outlook

Several factors must be considered in the wound healing mechanism, including the hydrophilicity, porosity, and biocompatibility of wound dressing materials. Sodium alginate is primarily used in hemostatic powders for blood coagulation, as blood coagulation is the initial phase of wound healing. Wound healing is often delayed due to prolonged inflammation. Sodium alginate exhibits significant anti-inflammatory properties, facilitating early wound healing. The proliferation phase of wound healing is the combined result of angiogenesis, fibroblast

migration, and collagen deposition. Sodium alginate can effectively promote the proliferative phase of wound healing by contributing to tissue granulation. Sodium alginate scaffolds also promote extracellular matrix remodeling. Machine learning is widely used to explore porous material structures. In the future, there is a need to develop an application programming interface (API) to facilitate data communication, particularly an API for the porosity of SA-based materials. Bibliometric analysis also revealed that open-access journals are focusing on promoting research related to SA wound healing applications. Although many papers regarding the application of SA have been published so far, it can be expected that more research articles on this material will be published in the future, as many research groups worldwide are working on alginate and its combinations with other macromolecules.

## ORCID iDs

Muhammad Tahir 0000-0001-8436-1126
Simone Pettineo 0000-0002-5812-5565
Silvia Vicini 0000-0001-9369-1522
Maila Castellano 0000-0002-0930-7522
Marina Alloisio 0000-0002-6155-2912
Ketul Popat 0000-0002-2417-7789
Harishkumar Madhyastha 0000-0002-7143-4821
Kaoru Ohe 0009-0005-6343-568X
Kentaro Sakai 0000-0002-5811-8795
Alina Sionkowska 0000-0002-1551-2725

## References

1. Raina N, Rani R, Pahwa R, Gupta M. Biopolymers and treatment strategies for wound healing: An insight view. *Int J Polym Mater Polym Biomater.* 2022;71(5):359–375. doi:10.1080/00914037.2020.1838518
2. Jabeen N, Atif M. Polysaccharides based biopolymers for biomedical applications: A review. *Polym Adv Techs.* 2024;35(1):e6203. doi:10.1002/pat.6203
3. Thakur VK, Thakur MK, eds. *Functional Biopolymers.* Cham, Switzerland: Springer International Publishing; 2018. doi:10.1007/978-3-319-66417-0
4. Nitta S, Numata K. Biopolymer-based nanoparticles for drug/gene delivery and tissue engineering. *Int J Mol Sci.* 2013;14(1):1629–1654. doi:10.3390/ijms14011629
5. Ahmed HB, Mikhail MM, El-Shahat M, Emam HE. Clustering of carbon quantum dots from polysaccharides (cellulose, alginate, chitosan) versus heterocyclic compounds: Synthesis, characterization and medical applications. *Carbohydr Polym Technol Appl.* 2025;9:100738. doi:10.1016/j.carpta.2025.100738
6. Shi C, Xu R, Hu W, et al. Fabrication of alginate dialdehyde-gelatin crosslinked hydrogels incorporated with cinnamaldehyde nanoparticles for meat preservation. *Int J Biol Macromol.* 2025;298:140063. doi:10.1016/j.ijbiomac.2025.140063
7. Kulkarni VS, Butte KD, Rathod SS. Natural polymers–a comprehensive review. *Int J Res Pharm Biomed Sci.* 2012;3(4):1597-1613. Available from: https://www.researchgate.net/profile/Vishakha-gajrekulkarni/publication/236217541_Natural_Polymers-_A_comprehensive_Review/links/595b4913a6fdcc36b4daa3f7/Natural-Polymers-A-comprehensive-Review.pdf
8. Al-Roujayee AS, Hilaj E, Deepak A, et al. Alginate-based systems: Advancements in drug delivery and wound healing. *Int J Polym Mater Polym Biomater.* 2025;74(9):846–874. doi:10.1080/00914037.2024.2375343
9. Lee KY, Mooney DJ. Alginate: Properties and biomedical applications. *Prog Polym Sci.* 2012;37(1):106–126. doi:10.1016/j.progpolymsci.2011.06.003
10. Abourehab MAS, Rajendran RR, Singh A, et al. Alginate as a promising biopolymer in drug delivery and wound healing: A review of the state-of-the-art. *Int J Mol Sci.* 2022;23(16):9035. doi:10.3390/ijms23169035
11. Saberian M, Safari Roudsari R, Haghshenas N, Rousta A, Alizadeh S. How the combination of alginate and chitosan can fabricate a hydrogel with favorable properties for wound healing. *Heliyon.* 2024;10(11):e32040. doi:10.1016/j.heliyon.2024.e32040
12. Liang X, Huang C, Liu H, et al. Natural hydrogel dressings in wound care: Design, advances, and perspectives. *Chin Chem Lett.* 2024;35(10):109442. doi:10.1016/j.cclet.2023.109442
13. Salarvand S, Jalali SAH, Mahboobi Soofiani N, Allafchian A. Amine modified sodium alginate: Synthesis, characterization and in vivo evaluation in rainbow trout (*Oncorhynchus mykiss*). *Carbohydr Polym Technol Appl.* 2025;9:100699. doi:10.1016/j.carpta.2025.100699
14. Yu P, Zhong W. Hemostatic materials in wound care. *Burns Trauma.* 2021;9:tkab019. doi:10.1093/burnst/tkab019
15. Wang W, Liu M, Shafiq M, et al. Synthesis of oxidized sodium alginate and its electrospun bio-hybrids with zinc oxide nanoparticles to promote wound healing. *Int J Biol Macromol.* 2023;232:123480. doi:10.1016/j.ijbiomac.2023.123480
16. Dodero A, Alberti S, Gaggero G, et al. An up-to-date review on alginate nanoparticles and nanofibers for biomedical and pharmaceutical applications. *Adv Mater Interfaces.* 2021;8(22):2100809. doi:10.1002/admi.202100809
17. Dodero A, Alloisio M, Castellano M, Vicini S. Multilayer alginate-polycaprolactone electrospun membranes as skin wound patches with drug delivery abilities. *ACS Appl Mater Interfaces.* 2020;12(28):31162–31171. doi:10.1021/acsami.0c07352
18. Phùng TTT, Đinh HN, Ureña M, et al. Sodium alginate as a promising encapsulating material for extremely-oxygen sensitive probiotics. *Food Hydrocoll.* 2025;160:110857. doi:10.1016/j.foodhyd.2024.110857
19. Yan P, Lan W, Xie J. Modification on sodium alginate for food preservation: A review. *Trends Food Sci Technol.* 2024;143:104217. doi:10.1016/j.tifs.2023.104217
20. Astaneh ME, Hashemzadeh A, Fereydouni N. Recent advances in sodium alginate-based dressings for targeted drug delivery in the context of diabetic wound healing. *J Mater Chem B.* 2024;12(40):10163–10197. doi:10.1039/D4TB01049C
21. Luan Q, Wang Y, Chen Y, Chen H. Review on improvement of physicochemical properties of sodium alginate-based edible films. *J Food Sci.* 2025;90(2):e70016. doi:10.1111/1750-3841.70016
22. Yang JS, Xie YJ, He W. Research progress on chemical modification of alginate: A review. *Carbohydr Polym.* 2011;84(1):33–39. doi:10.1016/j.carbpol.2010.11.048
23. Belalia F, Djelali NE. Rheological properties of sodium alginate solutions. *Rev Roum Chim.* 2014;59(2):135-145. Accessed July 3, 2026. https://revroum.lew.ro/wp-content/uploads/2014/2/Art%2008.pdf
24. Karvinen J, Kellomäki M. Design aspects and characterization of hydrogel-based bioinks for extrusion-based bioprinting. *Bioprinting.* 2023;32:e00274. doi:10.1016/j.bprint.2023.e00274
25. Badawi NM, Batoo KM, Subramaniam R, et al. Highly conductive and reusable cellulose hydrogels for supercapacitor applications. *Micromachines.* 2023;14(7):1461. doi:10.3390/mi14071461
26. Pongjanyakul T. Alginate–magnesium aluminum silicate films: Importance of alginate block structures. *Int J Pharm.* 2009;365(1–2):100–108. doi:10.1016/j.ijpharm.2008.08.025
27. Pathak TS, Kim JS, Lee SJ, Baek DJ, Paeng KJ. Preparation of alginic acid and metal alginate from algae and their comparative study. *J Polym Environ.* 2008;16(3):198–204. doi:10.1007/s10924-008-0097-4
28. Bojorges H, López-Rubio A, Martínez-Abad A, Fabra MJ. Overview of alginate extraction processes: Impact on alginate molecular structure and techno-functional properties. *Trends Food Sci Technol.* 2023;140:104142. doi:10.1016/j.tifs.2023.104142
29. Saji S, Hebden A, Goswami P, Du C. A brief review on the development of alginate extraction process and its sustainability. *Sustainability.* 2022;14(9):5181. doi:10.3390/su14095181
30. Pawar SN, Edgar KJ. Alginate derivatization: A review of chemistry, properties and applications. *Biomaterials.* 2012;33(11):3279–3305. doi:10.1016/j.biomaterials.2012.01.007
31. Abka-khajouei R, Tounsi L, Shahabi N, Patel AK, Abdelkafi S, Michaud P. Structures, properties and applications of alginates. *Mar Drugs.* 2022;20(6):364. doi:10.3390/md20060364
32. Da Silva CM, Reis RL, Correlo VM, Jahno VD. The efficient role of sodium alginate-based biodegradable dressings for skin wound healing application: A systematic review. *J Biomater Sci Polym Ed.* 2024;35(3):397–414. doi:10.1080/09205063.2023.2289247
33. Sinha A, Georgoulas A, Crua C, et al. Exploring exudate absorp-

tion via sessile droplet dynamics in porous wound dressings. *Exp Therm Fluid Sci*. 2025;163:111408. doi:10.1016/j.expthermflusci.2025.111408
34. Liu S, Li H, Tang B, Bi S, Li L. Scaling law and microstructure of alginate hydrogel. *Carbohydr Polym*. 2016;135:101–109. doi:10.1016/j.carbpol.2015.08.086
35. Androniceanu M. Efficiency and prediction in human resource management using Python modules. *Theor Empir Res Urban Manag*. 2025;20(1):88-103. Available from: https://um.ase.ro/v20i1/5.pdf
36. Reis E, Gralha C, Monteiro MP. Surveying communities of users of MATLAB and clone languages. *J Comp Lang*. 2022;73:101170. doi:10.1016/j.cola.2022.101170
37. Jenkins D, Salhadar K, Ashby G, et al. PoreScript: Semi-automated pore size algorithm for scaffold characterization. *Bioact Mater*. 2022;13:1–8. doi:10.1016/j.bioactmat.2021.11.006
38. Polez RT, Ajiboye MA, Österberg M, Horn MM. Chitosan hydrogels enriched with bioactive phloroglucinol for controlled drug diffusion and potential wound healing. *Int J Biol Macromol*. 2024;265:130808. doi:10.1016/j.ijbiomac.2024.130808
39. Gostick J, Khan Z, Tranter T, et al. PoreSpy: A Python toolkit for quantitative analysis of porous media images. *J Open Source Soft*. 2019;4(37):1296. doi:10.21105/joss.01296
40. Negut I, Bita B. Exploring the potential of artificial intelligence for hydrogel development: A short review. *Gels*. 2023;9(11):845. doi:10.3390/gels9110845
41. Zhang Q, Yang LT, Chen Z, Li P. A survey on deep learning for big data. *Information Fusion*. 2018;42:146–157. doi:10.1016/j.inffus.2017.10.006
42. El Naqa I, Murphy MJ. What are machine and deep learning? In: El Naqa I, Murphy MJ, eds. *Machine and Deep Learning in Oncology, Medical Physics and Radiology*. Cham, Switzerland: Springer International Publishing; 2022:3–15. doi:10.1007/978-3-030-83047-2_1
43. Zhang B, Shi H, Wang H. Machine learning and AI in cancer prognosis, prediction, and treatment selection: A critical approach. *J Multidiscip Healthc*. 2023;16:1779–1791. doi:10.2147/JMDH.S410301
44. Chen Y, You W, Ou L, Tang H. A review of machine learning techniques for urban resilience research: The application and progress of different machine learning techniques in assessing and enhancing urban resilience. *Syst Soft Comput*. 2025;7:200269. doi:10.1016/j.sasc.2025.200269
45. Martínez Torres J, Iglesias Comesaña C, García-Nieto PJ. Review: Machine learning techniques applied to cybersecurity. *Int J Mach Learn Cyber*. 2019;10(10):2823–2836. doi:10.1007/s13042-018-00906-1
46. Rashidi HH, Tran NK, Betts EV, Howell LP, Green R. Artificial intelligence and machine learning in pathology: The present landscape of supervised methods. *Acad Pathol*. 2019;6:2374289519873088. doi:10.1177/2374289519873088
47. Dike HU, Zhou Y, Deveerasetty KK, Wu Q. Unsupervised learning based on artificial neural network: A review. In: *2018 IEEE International Conference on Cyborg and Bionic Systems (CBS)*. Shenzhen, China: IEEE; 2018:322–327. doi:10.1109/CBS.2018.8612259
48. Nayeri ZM, Ghafarian T, Javadi B. Application placement in Fog computing with AI approach: Taxonomy and a state of the art survey. *J Netw Comp Appl*. 2021;185:103078. doi:10.1016/j.jnca.2021.103078
49. Vaish R, Dwivedi UD, Tewari S, Tripathi SM. Machine learning applications in power system fault diagnosis: Research advancements and perspectives. *Eng Appl Artif Intelligence*. 2021;106:104504. doi:10.1016/j.engappai.2021.104504
50. Saberian M, Seyedjafari E, Zargar SJ, Mahdavi FS, Sanaei-rad P. Fabrication and characterization of honey and aloe vera for wound dressing applications. *J Appl Polym Sci*. 2021;138(47):51398. doi:10.1002/app.51398
51. Olevsky LM, Jacques MG, Hixon KR. PoreVision: A program for enhancing efficiency and accuracy in SEM pore analyses of gels and other porous materials. *Gels*. 2025;11(2):132. doi:10.3390/gels11020132
52. Shkarin R, Shkarin A, Shkarina S, et al. Quanfima: An open source Python package for automated fiber analysis of biomaterials. *PLoS One*. 2019;14(4):e0215137. doi:10.1371/journal.pone.0215137
53. Rouhollahi A, Ilegbusi O, Foroosh H. Segmentation and pore structure estimation in SEM images of tissue engineering scaffolds using genetic algorithm. *Ann Biomed Eng*. 2021;49(3):1033–1045. doi:10.1007/s10439-020-02638-2
54. Rouhollahi A. Integration of computational fluid dynamics and machine learning for modeling scaffold pore structure for tissue engineering [dissertation]. Orlando, FL: University of Central Florida; 2019. Accessed July 3, 2026. https://stars.library.ucf.edu/etd/6880
55. Nair M, Shepherd JH, Best SM, Cameron RE. MicroCT analysis of connectivity in porous structures: Optimizing data acquisition and analytical methods in the context of tissue engineering. *J R Soc Interface*. 2020;17(165):20190833. doi:10.1098/rsif.2019.0833
56. Karaca I, Aldemir Dikici B. Quantitative evaluation of the pore and window sizes of tissue engineering scaffolds on scanning electron microscope images using deep learning. *ACS Omega*. 2024;9(23):24695–24706. doi:10.1021/acsomega.4c01234
57. Yuan Y, Lee TR. Contact angle and wetting properties. In: Bracco G, Holst B, eds. *Surface Science Techniques*. Vol. 51. Springer Series in Surface Sciences. Berlin–Heidelberg, Germany: Springer Berlin Heidelberg; 2013:3–34. doi:10.1007/978-3-642-34243-1_1
58. Kumar G, Prabhu KN. Review of non-reactive and reactive wetting of liquids on surfaces. *Adv Colloid Interface Sci*. 2007;133(2):61–89. doi:10.1016/j.cis.2007.04.009
59. Xie H, Li X, Lv G, et al. Effect of surface wettability and charge on protein adsorption onto implantable alginate-chitosan-alginate microcapsule surfaces. *J Biomed Mater Res*. 2010;92A(4):1357–1365. doi:10.1002/jbm.a.32437
60. Karmakar R, Dixit M, Eswar K, et al. Enhanced wound healing properties by sodium alginate-carboxymethyl cellulose hydrogel enriched with decellularized amniotic membrane. *Eur J Pharm Biopharm*. 2025;207:114621. doi:10.1016/j.ejpb.2024.114621
61. Mujawar SS, Arbade GK, Bisht N, et al. 3D printed *Aloe barbadensis* loaded alginate-gelatin hydrogel for wound healing and scar reduction: In vitro and in vivo study. *Int J Biol Macromol*. 2025;296:139745. doi:10.1016/j.ijbiomac.2025.139745
62. Sisakht MM, Gholizadeh F, Shahravi Z, Doust-Vaghe YK, Nilforoushzadeh MA, Amirkhani MA. Sodium alginate/poly(acrylic acid) hydrogel composite, potential carrier for fibroblast growth factor 1 (FGF1) delivery. *Chem Biodivers*. 2025;22(2):e202401738. doi:10.1002/cbdv.202401738
63. Hosseini SMR, Heydari P, Namnabat M, et al. Carboxymethyl cellulose/sodium alginate hydrogel with anti-inflammatory capabilities for accelerated wound healing: In vitro and in vivo study. *Eur J Pharmacol*. 2024;976:176671. doi:10.1016/j.ejphar.2024.176671
64. Isa Rahim M, Aqida SN, Salwani MS, Ahmad Syarizan S. Enhancing surface hydrophobicity of AISI 304 stainless steel via laser texturing. *J Phys Conf Ser*. 2025;2933(1):012006. doi:10.1088/1742-6596/2933/1/012006
65. Chen S, Li S, Ye Z, et al. Superhydrophobic and superhydrophilic polyurethane sponge for wound healing. *Chem Eng J*. 2022;446:136985. doi:10.1016/j.cej.2022.136985
66. Choi YK, Din FU, Kim DW, et al. Amniotic membrane extract-loaded double-layered wound dressing: Evaluation of gel properties and wound healing. *Drug Dev Ind Pharm*. 2014;40(7):852–859. doi:10.3109/03639045.2013.788015
67. Jin SG, Yousaf AM, Kim KS, et al. Influence of hydrophilic polymers on functional properties and wound healing efficacy of hydrocolloid based wound dressings. *Int J Pharm*. 2016;501(1–2):160–166. doi:10.1016/j.ijpharm.2016.01.044
68. Feng W, Wang Z. Tailoring the swelling-shrinkable behavior of hydrogels for biomedical applications. *Adv Sci*. 2023;10(28):2303326. doi:10.1002/advs.202303326
69. Singh AK, Pramanik K. Fabrication and investigation of physicochemical and biological properties of 3D printed sodium alginate-chitosan blend polyelectrolyte complex scaffold for bone tissue engineering application. *J Appl Polym Sci*. 2023;140(12):e53642. doi:10.1002/app.53642
70. Zahid M, Lodhi M, Afzal A, et al. Development of hydrogels with the incorporation of *Raphanus sativus* L. seed extract in sodium alginate for wound-healing application. *Gels*. 2021;7(3):107. doi:10.3390/gels7030107
71. Almadani YH, Vorstenbosch J, Davison PG, Murphy AM. Wound healing: A comprehensive review. *Semin Plast Surg*. 2021;35(3):141–144. doi:10.1055/s-0041-1731791
72. Fahimirad S, Fattahi F, Hatami M, Shabani S, Ghorbanpour M. Nanotechnology-based biotherapeutics for physiological wound healing phases. *Ind Crops Products*. 2025;226:120608. doi:10.1016/j.indcrop.2025.120608
73. Sadeghi M, Moghaddam A, Amiri AM, et al. Improving the wound healing process: Pivotal role of mesenchymal stromal/stem cells and immune cells. *Stem Cell Rev Rep*. 2025;21(3):680–697. doi:10.1007/s12015-025-10849-0

74. Ukaegbu K, Allen E, Svoboda KKH. Reactive oxygen species and antioxidants in wound healing: Mechanisms and therapeutic potential. *Int Wound J*. 2025;22(5):e70330. doi:10.1111/iwj.70330
75. Periayah MH, Halim AS, Mat Saad AZ. Mechanism action of platelets and crucial blood coagulation pathways in hemostasis. *Int J Hematol Oncol Stem Cell Res*. 2017;11(4):319–327. PMID:29340130. PMCID:PMC5767294.
76. Zhang P, Zu R, Zhang X, et al. Unveiling the "Dark Matter" of platelet involvement in tumor microenvironment. *J Pharm Anal*. 2025;15(9):101218. doi:10.1016/j.jpha.2025.101218
77. Huang H, Chen H, Wang X, et al. Degradable and bioadhesive alginate-based composites: An effective hemostatic agent. *ACS Biomater Sci Eng*. 2019;5(10):5498–5505. doi:10.1021/acsbiomaterials.9b01120
78. Zhang J, Zhang S, Liu C, et al. Photopolymerized multifunctional sodium alginate-based hydrogel for antibacterial and coagulation dressings. *Int J Biol Macromol*. 2024;260:129428. doi:10.1016/j.ijbiomac.2024.129428
79. Chen A, Wu L, Wang K, et al. Facile synthesis of rapid hemostatic powder based on sodium alginate for promoting hemostasis and wound healing. *Int J Biol Macromol*. 2025;308:142728. doi:10.1016/j.ijbiomac.2025.142728
80. Zhou J, Li M, Hui Y, et al. Hemostatic sponge based on easily prepared crosslinked gelatin and sodium alginate for wound healing. *J Mater Sci*. 2024;59(19):8408–8426. doi:10.1007/s10853-024-09539-y
81. Wang Y, Wang P, Ji H, Ji G, Wang M, Wang X. Analysis of safety and effectiveness of sodium alginate/poly(γ-glutamic acid) microspheres for rapid hemostasis. *ACS Appl Biomater*. 2021;4(8):6539–6548. doi:10.1021/acsabm.1c00671
82. Li Y, Li M, Li C, et al. A sodium alginate – silk fibroin biosponge loaded with thrombin: Effective hemostasis and wound healing. *Heliyon*. 2024;10(6):e28047. doi:10.1016/j.heliyon.2024.e28047
83. Xie M, Zeng Y, Wu H, Wang S, Zhao J. Multifunctional carboxymethyl chitosan/oxidized dextran/sodium alginate hydrogels as dressing for hemostasis and closure of infected wounds. *Int J Biol Macromol*. 2022;219:1337–1350. doi:10.1016/j.ijbiomac.2022.08.166
84. Khattak S, Ullah I, Sohail M, et al. Endogenous/exogenous stimuli-responsive smart hydrogels for diabetic wound healing. *Aggregate*. 2025;6(2):e688. doi:10.1002/agt2.688
85. Zhang X, Li R, Li S, et al. Tri-network PVA/chitosan/gelatin hydrogel modified by tannic acid with self-healing, adhesive and anti-inflammatory properties to accelerate wound healing. *Int J Biol Macromol*. 2025;308:142280. doi:10.1016/j.ijbiomac.2025.142280
86. Liu H, Qin S, Zhang H, et al. Silk sericin-based ROS-responsive oxygen generating microneedle platform promotes angiogenesis and decreases inflammation for scarless diabetic wound healing. *Adv Funct Mater*. 2025;35(7):2404461. doi:10.1002/adfm.202404461
87. Summa M, Russo D, Penna I, et al. A biocompatible sodium alginate/povidone iodine film enhances wound healing. *Eur J Pharm Biopharm*. 2018;122:17–24. doi:10.1016/j.ejpb.2017.10.004
88. Zhao J, Yao L, Nie S, Xu Y. Low-viscosity sodium alginate combined with TiO2 nanoparticles for improving neuroblastoma treatment. *Int J Biol Macromol*. 2021;167:921–933. doi:10.1016/j.ijbiomac.2020.11.048
89. Zhang X, Liu Y, Wang Z, et al. pH-responsive and self-adaptive injectable sodium alginate/carboxymethyl chitosan hydrogel accelerates infected wound healing by bacteriostasis and immunomodulation. *Carbohydr Polym*. 2025;354:123322. doi:10.1016/j.carbpol.2025.123322
90. Raguvaran R, Manuja BK, Chopra M, et al. Sodium alginate and gum acacia hydrogels of ZnO nanoparticles show wound healing effect on fibroblast cells. *Int J Biol Macromol*. 2017;96:185–191. doi:10.1016/j.ijbiomac.2016.12.009
91. Song J, Zeng L, Ye Z, et al. The promoting effect of *Balanus albicostatus* cement protein 19k (Balcp19k) on wound healing by regulating fibroblast migration and relieving early-stage inflammation responses. *Int J Biol Macromol*. 2025;289:138781. doi:10.1016/j.ijbiomac.2024.138781
92. Harper D, Young A, McNaught CE. The physiology of wound healing. *Surgery (Oxford)*. 2014;32(9):445–450. doi:10.1016/j.mpsur.2014.06.010
93. Kibungu C, Kondiah PPD, Kumar P, Choonara YE. Recent advances in chitosan and alginate-based hydrogels for wound healing application. *Front Mater*. 2021;8:681960. doi:10.3389/fmats.2021.681960
94. AlShaali S, Atieh M, Hakam A, Alsabeeha N, Shah M. Effects of hyaluronic acid gel on initial wound healing following tooth extraction and crown lengthening procedures: A retrospective analysis. *Clin Cosmet Investig Dent*. 2025;17:225–236. doi:10.2147/CCIDE.S513987
95. Zhu P, Wu J, Chang Z, et al. Sodium alginate hydrogel loaded with *Capparis spinosa* L. extract for antimicrobial and antioxidant wound dressing applications. *Int J Biol Macromol*. 2025;289:138883. doi:10.1016/j.ijbiomac.2024.138883
96. Zhou C, Jiang T, Liu S, et al. AgNPs loaded adenine-modified chitosan composite POSS-PEG hybrid hydrogel with enhanced antibacterial and cell proliferation properties for promotion of infected wound healing. *Int J Biol Macromol*. 2024;267:131575. doi:10.1016/j.ijbiomac.2024.131575
97. Ma R, Wang Y, Qi H, et al. Nanocomposite sponges of sodium alginate/graphene oxide/polyvinyl alcohol as potential wound dressing: In vitro and in vivo evaluation. *Composites Part B Engineering*. 2019;167:396–405. doi:10.1016/j.compositesb.2019.03.006
98. Dodero A, Scarfi S, Pozzolini M, Vicini S, Alloisio M, Castellano M. Alginate-based electrospun membranes containing ZnO nanoparticles as potential wound healing patches: Biological, mechanical, and physicochemical characterization. *ACS Appl Mater Interfaces*. 2020;12(3):3371–3381. doi:10.1021/acsami.9b17597
99. Ding C, Yang J, Wang N, et al. Sodium alginate/polyvinyl alcohol nanofibers loaded with shikonin for diabetic wound healing: In vivo and in vitro evaluation. *Int J Biol Macromol*. 2024;262:129937. doi:10.1016/j.ijbiomac.2024.129937
100. Liu Z, Sun R, Huang Y, et al. The preparation of shikonin-based nanomedicine with robust GSH-responsiveness. *Coll Surf A Physicochem Eng Aspects*. 2025;705:135557. doi:10.1016/j.colsurfa.2024.135557
101. Guo C, He J, Song X, et al. Pharmacological properties and derivatives of shikonin: A review in recent years. *Pharmacol Res*. 2019;149:104463. doi:10.1016/j.phrs.2019.104463
102. Lin W, Wang X, Zhuang T, et al. Lithospermum erythrorhizon polysaccharide alleviates obesity via gut microbiota-mediated reprogramming of bile acid and short-chain fatty acid metabolism. *Int J Biol Macromol*. 2025;323:147082. doi:10.1016/j.ijbiomac.2025.147082
103. Tian M, Wu J, Du Q, et al. Revealing the mechanisms of shikonin against diabetic wounds: A combined network pharmacology and in vitro investigation. *J Diabetes Res*. 2025;2025(1):4656485. doi:10.1155/jdr/4656485
104. Ye X, Wu X, Lian S, et al. Recent advances of shikonin in the molecular mechanisms of anticancer, anti-inflammation and immunoregulation. *Am J Chin Med*. 2025;53(4):1093–1118. doi:10.1142/S0192415X25500417
105. Monga A, Kaur K, Gasso S, et al. Fabrication of starch nanofibrous scaffolds co-loaded with shikonin microsponges for accelerated diabetic wound healing: Deciphering in vitro insights and in vivo realities. *BioNanoScience*. 2025;15(3):319. doi:10.1007/s12668-025-01926-2
106. Luo B, Ding X, Hu Y, et al. Shikonin hastens diabetic wound healing by inhibiting M1 macrophage polarisation through the MAPK signaling pathway. *Mol Immunol*. 2025;177:73–84. doi:10.1016/j.molimm.2024.12.002
107. Cen LS, Cao Y, Zhou YM, Guo J, Xue JW. Shikonin protects mitochondria through the NFAT5/AMPK pathway for the treatment of diabetic wounds. *World J Diabetes*. 2024;15(12):2338–2352. doi:10.4239/wjd.v15.i12.2338
108. Eming S, Brachvogel B, Odorisio T, Koch M. Regulation of angiogenesis: Wound healing as a model. *Prog Histochem Cytochem*. 2007;42(3):115–170. doi:10.1016/j.proghi.2007.06.001
109. DiPietro LA. Angiogenesis and wound repair: When enough is enough. *J Leukoc Biol*. 2016;100(5):979–984. doi:10.1189/jlb.4MR0316-102R
110. Okonkwo U, DiPietro L. Diabetes and wound angiogenesis. *Int J Mol Sci*. 2017;18(7):1419. doi:10.3390/ijms18071419
111. Dawood HZ, Ara C, Asmatullah, Jabeen S, Islam A, Ghauri ZH. Chitosan/fibroin biopolymer-based hydrogels for potential angiogenesis in developing chicks and accelerated wound healing in mice. *Biopolymers*. 2025;116(1):e23633. doi:10.1002/bip.23633
112. Bahadoran Z, Mirmiran P, Hosseinpanah F, Kashfi K, Ghasemi A. Nitric oxide-based treatments improve wound healing associated with diabetes mellitus. *Med Gas Res*. 2025;15(1):23–35. doi:10.4103/mgr.MEDGASRES-D-24-00020
113. Çerçi A, Demir ES, Karaca E, Güzel ÇB, Osman B. Preparation and characterization of amoxicillin-loaded polyvinyl alcohol/sodium alginate nanofibrous mat: Drug release properties, antibacterial activity, and cytotoxicity. *Arab J Sci Eng*. 2025;50(1):77–91. doi:10.1007/s13369-024-09075-6

114. Kaur SP, Rao R, Nanda S. Amoxicillin: a broad spectrum antibiotic. *Int J Pharm Pharm Sci*. 2011;3(3):30-37. Available from: https://innovareacademics.in/journal/ijpps/Vol3Issue3/2249.pdf
115. Ayavoo T, Murugesan K, Gnanasekaran A. Roles and mechanisms of stem cell in wound healing. *Stem Cell Investig*. 2021;8:4. doi:10.21037/sci-2020-027
116. Ud-Din S, Bayat A. Non-invasive objective devices for monitoring the inflammatory, proliferative and remodelling phases of cutaneous wound healing and skin scarring. *Exp Dermatol*. 2016;25(8):579–585. doi:10.1111/exd.13027
117. Yang W, Xu H, Lan Y, et al. Preparation and characterisation of a novel silk fibroin/hyaluronic acid/sodium alginate scaffold for skin repair. *Int J Biol Macromol*. 2019;130:58–67. doi:10.1016/j.ijbiomac.2019.02.120
118. Aria M, Cuccurullo C. bibliometrix: An R-tool for comprehensive science mapping analysis. *J Informetrics*. 2017;11(4):959–975. doi:10.1016/j.joi.2017.08.007
119. Van Eck NJ, Waltman L. Software survey: VOSviewer, a computer program for bibliometric mapping. *Scientometrics*. 2010;84(2):523–538. doi:10.1007/s11192-009-0146-3

# Influence of drug incorporation strategy on structure and release behavior of alginate beads: A mechanistic study

# Wpływ strategii wprowadzania leku na strukturę i zachowanie uwalniania kulek alginianowych: badanie mechanistyczne

Jose Hernandez[1,A–F], Edith Cecilia Rivera-Meza[1,A,D], Adrian de Jesus Rivera-Ramirez[1,A,C], Mercedes Salazar-Hernandez[2,C,E,F], Rosa Hernandez-Soto[1,B,E,F], Alba N. Ardila A.[3,B,C,F]

[1] UPIIG, Instituto Politécnico Nacional, Av. Mineral de Valenciana 200-Interior, Col. Fraccionamiento Industrial Puerto Interior, 3, Silao, Gto., Mexico
[2] Departamento de Ingeniería en Minas, Metalurgia y Geología, División de Ingenierías, Universidad de Guanajuato, Guanajuato, Mexico
[3] Facultad de Ciencias Básicas, Sociales y Humanas, Politécnico Colombiano Jaime Isaza Cadavid, Medellín, Colombia

A – research concept and design; B – collection and/or assembly of data; C – data analysis and interpretation;
D – writing the article; E – critical revision of the article; F – final approval of the article

Polymers in Medicine, ISSN 0370-0747, eISSN 2451-2699 *Polim Med.* 2026;56(1):19–29

**Address for correspondence**
Jose Hernandez
E-mail: jahernandezma@ipn.mx

**Funding sources**
None declared

**Conflict of interest**
None declared

**Acknowledgements**
The authors wish to thank UPIIG for the infrastructure provided, as well as the Secretaría de Investigación y Posgrado (IPN) and the Laboratorio de Investigación y Caracterización de Minerales y Materiales (LICAMM-UG).

Received on April 7, 2026
Reviewed on May 19, 2026
Accepted on June 19, 2026

Published online on June 30, 2026

**Cite as**
Hernandez J, Rivera-Meza EC, Rivera-Ramirez AJ, Salazar-Hernandez M, Hernandez-Soto R, Ardila AN. Influence of drug incorporation strategy on structure and release behavior of alginate beads: a mechanistic study. *Polim Med*. 2026;56(1):19–29. doi:10.17219/pim/224828

**DOI**
10.17219/pim/224828



## Abstract

**Background.** Conventional excipients used in pharmaceutical formulations often exhibit limitations such as uncontrolled drug release and adverse patient responses, highlighting the need for improved drug delivery systems. Sodium alginate beads have been widely investigated as biocompatible carriers due to their ability to form ionically crosslinked hydrogels; however, the influence of drug incorporation strategies on their structural and functional performance remains insufficiently understood. In this study, alginate beads were used as delivery systems for acetylsalicylic acid (ASA) and acetaminophen (AP), comparing encapsulation during gelation with post-synthesis impregnation. The aim was to evaluate how these strategies affect morphology, drug loading, and release mechanisms. Encapsulation resulted in higher drug loading efficiencies (66.5% for AP and 81.8% for ASA) compared to impregnation (61.4% and 73.3%, respectively), as well as a more homogeneous drug distribution within the polymeric matrix. Morphological and structural analyses confirmed that encapsulated beads exhibited more uniform and compact structures, whereas impregnated systems showed heterogeneous drug localization and surface-associated deposits. In vitro release studies revealed that encapsulation promotes controlled and sustained release, while impregnation leads to faster release due to shorter diffusion pathways. Kinetic modeling indicated that AP release follows anomalous transport involving both diffusion and polymer relaxation, whereas ASA release is predominantly diffusion-controlled. These findings demonstrate that the drug incorporation strategy governs the internal structure of alginate beads and directly determines their release behavior, providing mechanistic insight into the rational design of polymeric drug delivery systems with tunable and predictable performance.

**Objectives.** The main objective of this study was to investigate sodium alginate beads as potential carriers for active pharmaceutical ingredients.

**Materials and methods.** Sodium alginate beads were prepared by ionotropic gelation and loaded with acetaminophen or acetylsalicylic acid either by encapsulation during gelation or by post-synthesis impregnation. The beads were characterized using FTIR, SEM, and XRD. Drug loading, swelling behavior, in vitro drug release, and release kinetics were also evaluated.

**Results.** Encapsulation produced beads with higher drug-loading efficiency and more homogeneous structures than impregnation. Consequently, encapsulated systems exhibited more controlled and sustained drug release, whereas impregnated beads showed faster release because of drug localization near the bead surface. Kinetic analysis indicated anomalous transport for acetaminophen and predominantly diffusion-controlled release for acetylsalicylic acid.

**Conclusions.** This study indicates that the drug incorporation strategy is a key factor governing the structural, functional, and release properties of alginate-based delivery systems.

## Streszczenie

Konwencjonalne substancje pomocnicze stosowane w preparatach farmaceutycznych często wykazują ograniczenia, takie jak niekontrolowane uwalnianie leku i niepożądane reakcje pacjentów, co wskazuje na potrzebę ulepszonych systemów dostarczania leków. Kulki alginianu sodu były szeroko badane jako biozgodne nośniki ze względu na ich zdolność do tworzenia jonowo usieciowanych hydrożeli; jednak wpływ strategii wprowadzania leków na ich właściwości strukturalne i funkcjonalne pozostaje nie do końca poznany. W niniejszym badaniu kulki alginianu zastosowano jako systemy dostarczania kwasu acetylosalicylowego (ASA) i acetaminofenu (AP), porównując enkapsulację podczas żelowania i impregnację po syntezie. Celem była ocena wpływu tych strategii na morfologię, nasycenie lekiem i mechanizmy uwalniania. Enkapsulacja skutkowała wyższą wydajnością nasycenia lekiem (66.5% dla AP i 81.8% dla ASA) w porównaniu z impregnacją (odpowiednio 61.4% i 73.3%), a także bardziej jednorodną dystrybucją leku w matrycy polimerowej. Analizy morfologiczne i strukturalne potwierdziły, że otoczone kapsułkami kulki wykazują bardziej jednorodną i zwartą strukturę, podczas gdy systemy impregnowane charakteryzują się heterogeniczną lokalizacją leku i osadami na powierzchni. Badania uwalniania in vitro wykazały, że otoczenie kapsułkami sprzyja kontrolowanemu i przedłużonemu uwalnianiu, podczas gdy impregnacja prowadzi do szybszego uwalniania dzięki krótszym szlakom dyfuzji. Modelowanie kinetyczne wskazało, że uwalnianie AP następuje w wyniku transportu anomalnego, obejmującego zarówno dyfuzję, jak i relaksację polimeru, podczas gdy uwalnianie ASA jest głównie kontrolowane przez dyfuzję. Odkrycia te dowodzą, że strategia wprowadzania leku determinuje strukturę wewnętrzną kulek alginianu i bezpośrednio wpływa na ich zachowanie podczas uwalniania; zapewnia to mechanistyczny wgląd w racjonalne projektowanie polimerycznych systemów dostarczania leków o regulowanej i przewidywalnej wydajności.

**Key words:** release, mechanism, kinetics, encapsulation, impregnation

**Słowa kluczowe:** uwalnianie, kinetyka, mechanizm, kapsułkowanie, impregnacja

# Introduction

Conventional pharmaceutical formulations frequently exhibit limitations such as uncontrolled drug release, gastrointestinal irritation, and variability in therapeutic response, which are often associated with both the active pharmaceutical ingredients (APIs) and the excipients employed.[1,2] These challenges have driven the development of advanced drug delivery systems capable of improving drug stability, bioavailability, and release control.[3] Among these systems, polymeric matrices based on natural biopolymers have gained significant attention due to their biocompatibility, low toxicity, and versatility.[4–6] In particular, sodium alginate has been extensively studied as a drug delivery material because of its ability to form hydrogels through ionic crosslinking with divalent cations, enabling the encapsulation and controlled release of active compounds.[5,7,8] The physicochemical properties of alginate-based systems, including porosity, swelling behavior,[9] and crosslinking density, are known to strongly influence drug release mechanisms, which may involve diffusion, polymer relaxation, or a combination of both.[8,10]

Despite the extensive literature, the distribution of the drug within the matrix significantly affects release behavior, yet systematic comparative studies on incorporation strategies remain limited, particularly in comparison with studies focused on crosslinking conditions and bead size.[7,8,11,12] However, comparatively less attention has been given to the role of drug incorporation strategies in determining the internal structure of the polymer matrix and its subsequent impact on drug release behavior.[10] The distribution of the drug within the matrix – whether homogeneously embedded or localized near the surface – can significantly affect both loading efficiency and release kinetics.[13] Drug incorporation into alginate matrices can be achieved through different approaches, including encapsulation during gel formation and post-synthesis impregnation.[10] These strategies are expected to produce distinct structural organizations within the beads, influencing drug–polymer interactions and mass transport phenomena.[14] Encapsulation typically promotes uniform drug entrapment within the polymeric network, whereas impregnation often results in heterogeneous distribution and surface localization of the drug.[13] Nevertheless, systematic comparative studies evaluating these approaches under similar experimental conditions remain limited. Despite the extensive use of alginate beads in drug delivery, limited attention has been given to how different drug incorporation strategies influence the internal structure of the matrix and, consequently, the release mechanism. Understanding this relationship is essential for the rational design of controlled release systems. Therefore, the aim of this study is to investigate how different drug incorporation strategies affect the internal structure of alginate beads and their release behavior. The study focuses on elucidating how the incorporation strategy affects bead morphology, drug loading, and release behavior, as well as the underlying transport mechanisms. By establishing structure–function relationships, this work contributes

to the rational design of alginate-based delivery systems with tunable release profiles and improved performance.

# Materials and methods

## Reagents

All reagents used were of analytical grade, and all aqueous solutions were prepared with deionized water. Calcium chloride ($CaCl_2$, ≥99.9%, Fermont, Monterrey, Nuevo León, México, Productos Químicos Monterrey, S.A. de C.V.), sodium alginate ($NaC_6H_7O_6$, ≥99.9%, Meyer, Ciudad de México, México, Química Suastes S.A. de C.V.), sodium chloride (NaCl, 99%, Meyer, Ciudad de México, México, Química Suastes S.A. de C.V.), hydrochloric acid (HCl, 36%, J.T. Baker, Madrid, Spain, Fisher Scientific S.L.), and sodium hydroxide (NaOH, ≥99.9%, Meyer, Ciudad de México, México, Química Suastes S.A. de C.V.) were employed. Pepsin (from porcine gastric mucosa, CAS 9001-75-6, St. Louis MO, USA, Sigma-Aldrich), acetylsalicylic acid ($C_9H_8O_4$, CAS 50-78-2, Wuppertal, Germany, Bayer), and acetaminophen ($C_8H_9NO_2$, CAS 103-90-2, New Brunswick, Nueva Jersey, USA, Johnson & Johnson) were purchased from Sigma-Aldrich.

## Preparation of SAP and API incorporation

Sodium alginate pearls (SAP) were prepared using the ionotropic gelation method. The selected conditions are consistent with widely reported protocols for alginate gelation and bead formation, which strongly influence structural integrity and encapsulation performance.[4,15] The selected alginate concentration, $CaCl_2$ concentration, and processing conditions were chosen based on previous studies reporting their influence on bead formation, encapsulation efficiency, and release behavior. A 4% (w/v) sodium alginate solution ($NaC_6H_7O_6$, 100% purity, Meyer) was maintained under constant stirring at 80°C until a homogeneous viscous solution was obtained. The resulting solution was then pumped dropwise into a 0.2 M calcium chloride solution ($CaCl_2$, Fermont, 100%) maintained at 4°C, as illustrated in Fig. 1.[16] The distance between the $CaCl_2$ solution and the hose (2.5 mm in diameter) was 8 cm while the pumping speed of the sodium alginate solution was 5 mL/min. The droplets immediately formed spherical gel beads due to ionic crosslinking between $Ca^{2+}$ and alginate chains.

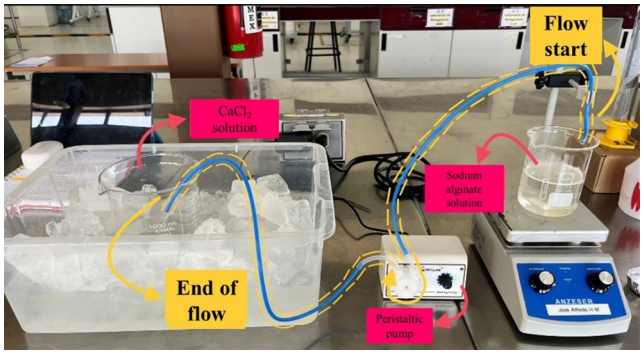


Fig. 1. Constant-flow system for the preparation of sodium alginate beads

The APIs were incorporated into the beads using two different methods: encapsulation and impregnation. These incorporation strategies were selected to evaluate how drug distribution within the polymeric matrix affects structural organization and release mechanisms, as drug localization has been reported to significantly influence mass transport behavior in polymeric systems.[9,10] For encapsulation, the API was mixed directly into the sodium alginate solution before gelation. The resulting mixture was then dropped into a $CaCl_2$ solution to form the beads. For impregnation, SAP were first prepared as blank beads. These preformed beads were then immersed in an API solution and stirred vigorously for 2 h at room temperature to allow diffusion of the active ingredient into the polymeric matrix.[17] The initial mass of API used was 0.5 g while the initial mass of ASA was 0.3 g. After incorporation, the API-loaded beads were stored at 4°C for 24 h to complete hardening, followed by filtration and drying in a convection oven (Memmert, model UNB 100) at 100°C for 1 h. The dried SAP-API were then stored in sealed amber containers under dark conditions to protect them from light exposure and extend their shelf life.

The in vitro release of the APIs was evaluated using a simulated gastric fluid (SGF) prepared according to the composition shown in Table 1. The release conditions were selected to simulate physiological gastric environments and to evaluate the performance of the delivery system under relevant conditions. The SGF was obtained by dissolving the components listed in Table 1 in 1 L of deionized water under vigorous stirring at room temperature. The solution was transferred to an amber glass container with a gas-tight cap and sterilized in an autoclave (Felisa, Zapopan, Jalisco, Mexico) at 121°C and 15 psi for 15 min.[18] Release studies were performed using SGF solutions with and without pancreatin to evaluate the behavior of both encapsulated and impregnated APIs.

A total of 0.3 g of alginate beads was accurately weighed and immersed in 100 mL of simulated gastric fluid within a dissolution apparatus (CROMTEK, Ethik, Santiago, Chile) maintained at 37°C. Aliquots were withdrawn every 10 min to determine the concentration of API. All experiments were performed in triplicate.[16,17] For ASA quantification,

Table 1. Composition of simulated gastric fluid (SGF)[18]

| Compound | Weight, g |
|---|---|
| HCl | 16.4* |
| NaCl | 4 |
| Pepsin | 10 |

*mL.

2 mL of each withdrawn sample was mixed in a 1 : 1 : 1 (v/v) ratio with water, sample, and NaOH (1 M), respectively, and the absorbance was measured at 297 nm using a UV–Vis spectrophotometer.[17] For API analysis, aliquots were diluted with 0.1 M HCl and the absorbance was recorded at 300 nm.[18] The release profile of the API was evaluated by calculating the fractional release ($M_t/M_\infty$) as a function of time in the table 2. Experimental data were fitted to various kinetic models commonly used to describe drug release from polymeric systems.[9,19] These models enable the identification of dominant mechanisms such as diffusion, swelling, and polymer relaxation.[8,20] The quality of the fit was assessed using the coefficient of determination ($R^2$) and the Akaike Information Criterion (AIC) for statistical comparison.[20]All experiments were performed in triplicate, and results are reported as mean ±standard deviation.

### Physicochemical and structural characterization of alginate beads loaded with active compounds

X-ray diffraction (XRD) patterns were obtained using a diffractometer (Rigaku Ultima IV) equipped with a Cu Kα radiation source (λ = 1.5418 Å). Data were collected over a 2θ range of 5–80° with a step size of 0.02°. Attenuated total reflectance–Fourier transform infrared spectroscopy (ATR-FTIR) analyses were performed using an infrared spectrometer (Nicolet iS10 Smart, Thermo Scientific) in the range of 4000–550 $cm^{-1}$, with 32 scans at a resolution of 4 $cm^{-1}$. Surface morphology and elemental composition were examined using scanning electron microscopy coupled with energy-dispersive X-ray spectroscopy (SEM–EDS) (JEOL JSM-6510 Plus). High-magnification micrographs were acquired to evaluate surface topology and particle size distribution. The size of SAP was determined using a stereomicroscope (Hinotek, model XTD-127) operated at magnifications ranging from ×10 to ×40 under reflected-light illumination. Bead diameters were measured by image analysis using ImageJ software, calculating the equivalent circular diameter of at least 30 beads per sample. Results are reported as mean diameter ± standard deviation. These characterization techniques were employed to correlate structural properties with the incorporation strategy and its impact on drug distribution and release behavior.

## Results and Discussion

### Effect of the incorporation strategy on bead formation and product yield

The formation of sodium alginate beads is strongly influenced by formulation and processing variables such as alginate concentration, solution viscosity, and gelation conditions. Among these factors, viscosity plays a key role in controlling droplet formation, bead integrity, and reproducibility during ionotropic gelation, since excessively high viscosity hinders solution flow, whereas low viscosity leads to unstable droplet formation and poor bead definition.[4,15,22] During preliminary trials, satisfactory bead formation for AP was achieved using 1% (w/v) sodium alginate, whereas ASA required a higher alginate concentration of 4% (w/v) to obtain stable and well-defined beads. This behavior suggests that the incorporation of each API modifies the physicochemical properties of the precursor solution differently, affecting its processability during gelation. Therefore, alginate concentration was adjusted to ensure adequate bead formation and structural stability for each system.[4,22] The total mass of SAP obtained for each API and incorporation strategy

**Table 2.** Mathematical models used to describe API release kinetics[9,21]

| | | |
|---|---|---|
| Power law | $\frac{M_t}{M_\infty} = kt^n$ | *k* is the incorporation constant of structural modifications and geometric characteristics of the system (release rate constant), and n is the release exponent (related to the drug release mechanism) |
| Peppas-Sahlin | $\frac{M_t}{M_\infty} = k_1 t^m + k_2 t^{2m}$ | |
| | $F = \frac{1}{1 + \frac{k_1}{k_2} t^m}$ | Amount of drug released due to the diffusion mechanism (Fickian, F) |
| | $R = \frac{k_1}{k_2} t^m$ | Contribution by swelling or relaxation (R) |

is summarized in Table 3. Differences in the recovered mass were observed between APIs and between incorporation methods, indicating that bead formation is affected not only by formulation composition but also by the incorporation strategy. In particular, encapsulation produced higher recovered mass than impregnation for both APIs, which may be associated with a more efficient retention of the drug within the polymeric network during bead formation. These results indicate that the incorporation strategy is not merely a loading step, but a key design parameter that influences bead formation and final product yield. This initial difference is relevant because it anticipates variations in subsequent properties such as morphology, drug distribution, and release performance.

**Table 3.** Total mass of alginate beads obtained for each API and incorporation strategy

| | | |
|---|---|---|
| | Impregnated | 13.61 ±0.54 |
| | Impregnated | 25.84 ±0.78 |

## Physical and functional properties of alginate beads

### Morphology

The morphology of alginate beads is a critical factor influencing drug distribution and release behavior. Optical microscopy images of SAP loaded with AP and ASA using encapsulation and impregnation methods are shown in Fig. 2 and 3, respectively. Encapsulated beads exhibited a predominantly spherical morphology with relatively uniform surfaces, indicating stable droplet formation during ionotropic gelation. In contrast, impregnated beads showed partially spherical or irregular geometries, characterized by flattened regions and increased surface roughness. These differences are associated with the absence of drug during bead formation in the impregnation method, which leads to less structural stabilization during gelation.

The more homogeneous morphology observed in encapsulated systems suggests a more uniform internal polymeric network, which may favor controlled diffusion of the drug. Conversely, the irregular structure of impregnated beads indicates heterogeneous drug distribution, likely localized near the surface, which can promote faster release behavior. These observations highlight that the incorporation strategy directly affects the structural organization of the beads and, consequently, their functional performance.[14,23] These morphological differences are consistent with previous reports indicating that drug incorporation methods influence bead structure and surface characteristics, which in turn affect drug release behavior.[24,25]

### Size determination

The average diameter of the alginate beads was determined for each API and incorporation method, and the results are presented in Table 4. Encapsulated beads exhibited slightly smaller and more uniform diameters compared to impregnated beads.

$$\mathrm{Dp} = \frac{\sum \text{diameter of each } SAP}{\text{Number of each } SAP} \qquad \text{Eq. (1)}$$

where Dp is the average diameter of the SAP. Table 4 shows the Dp for each pearl.

The differences in size distribution can be attributed to variations in solution viscosity and droplet formation

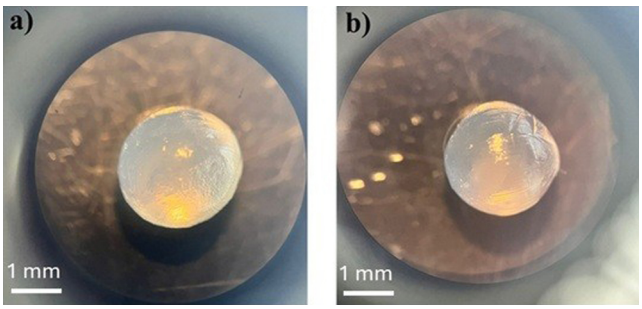


**Fig. 2.** Optical microscopy images of SAP-AP: (a) Enc and (b) Imp after exposure to SGF. The images illustrate the morphological integrity and surface characteristics of the beads under acidic conditions. Scale bar = 1 mm

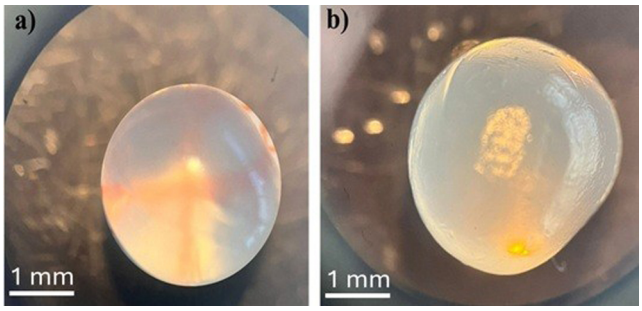


**Fig. 3.** Optical microscopy images of SAP-ASA: (a) Enc and (b) Imp after exposure to SGF. The images illustrate the morphological integrity and surface characteristics of the beads under acidic conditions. Scale bar = 1 mm.

**Table 4.** Average and standard deviation for each pearl type

| API Method | | Dp (mm) |
|---|---|---|
| AP | Encapsulated | 1.789 ± 0.203 |
| | Impregnated | 1.893 ± 0.202 |
| ASA | Encapsulated | 2.480 ± 0.224 |
| | Impregnated | 2.296 ± 0.226 |

during gelation. Encapsulation modifies the rheological properties of the alginate solution, leading to more stable droplet formation and reduced size variability. In contrast, impregnation does not influence bead formation directly, resulting in greater variability in bead size.

$$\phi = \frac{4\pi A}{p^2} \qquad \text{Eq. (2)}$$

and

$$R = \frac{4A}{\pi D_{max}^2} \qquad \text{Eq. (3)}$$

where A is the projected area, P is the perimeter and $D_{max}$ is the maximum Feret diameter. A narrower size distribution is generally associated with more predictable drug release profiles, whereas increased variability may lead to heterogeneous release behavior. Therefore, the observed differences in bead size further support the influence of the incorporation strategy on the structural characteristics of the system.

## Sphericity and roundness

The sphericity and roundness factors (Table 5) provide quantitative evidence of the morphological differences between encapsulated and impregnated beads. Encapsulated systems exhibited values closer to unity (ϕ ≈ 1), indicating near-spherical particles with uniform geometry. In contrast, impregnated beads showed lower sphericity and roundness values, confirming their irregular morphology. These geometric differences are relevant because particle shape influences surface area, diffusion pathways, and interactions with the dissolution medium. More spherical particles tend to exhibit more controlled and uniform release behavior, whereas irregular particles may facilitate faster release due to increased surface exposure.

## Drug content and loading efficiency

The drug content and loading efficiency (Table 6, 7) were significantly influenced by the incorporation strategy. Encapsulation resulted in higher drug loading and improved uniformity compared to impregnation for both APIs.

$$\%\text{API} = \left(\frac{\text{mass of API contained in SAP}}{\text{initial API mass}}\right) \times 100 \qquad \text{Eq. (4)}$$

This behavior can be attributed to the entrapment of the drug within the polymeric network during gelation, which minimizes drug loss and promotes homogeneous distribution. In contrast, impregnation relies on diffusion of the drug into preformed beads, leading to limited penetration and surface accumulation. These findings suggest that the incorporation strategy governs not only the amount of drug incorporated but also its spatial distribution within the matrix, which is expected to play a key role in determining release kinetics.[23,26,27] Taking these results into consideration, the mass balance of the API load in SAP was calculated and is presented in the following table, based on the equation shown below:

$$\%\text{API} = \text{API in SAP} + \text{API in supernatant} + \text{lost API} \qquad \text{Eq. (5)}$$

## Moisture content and swelling behavior

The swelling behavior of alginate beads is a key parameter affecting drug release, as it determines water uptake and matrix expansion. The results presented in Table 8 show similar swelling ratios for both incorporation methods, indicating that the polymeric network retains its hydrophilic nature regardless of the strategy used.

$$\%\text{Swelling ratio} = \left(\frac{w_{wet} - w_{dry}}{w_{wet}}\right) \times 100 \qquad \text{eq (7)}$$

where $W_{wet}$, $W_{dry}$ (g) are the masses of the wet and dry SAP, the values obtained being observed in Table 8. As can be seen, the humidity is similar regardless of the API trapping method used.

However, slight differences in swelling behavior may still influence release kinetics by modifying diffusion pathways

**Table 5.** SAP sphericity and roundness factor

| | | | |
|---|---|---|---|
| | Impregnated | 0.748 | 0.774 |
| | Impregnated | 0.660 | 0.843 |

**Table 6.** Yield of SAP obtained from different production methods

| | | |
|---|---|---|
| | Impregnated | 61.44 ±4.97 |
| | Impregnated | 73.74 ±5.97 |

**Table 7.** Mass balance in API load in SAP with different methods

| | | | | |
|---|---|---|---|---|
| | Impregnated | 0.307 | 0.138 | 0.055 |
| | Impregnated | 0.221 | 0.041 | 0.038 |

Table 8. Moisture content of SAP

| AI | Method | Swelling ratio, % |
|---|---|---|
| AP | Encapsulated | 151.55 ±13.8 |
| | Impregnated | 168.57 ±15.3 |
| ASA | Encapsulated | 166.15 ±15.1 |
| | Impregnated | 177.9 ±16.19 |

within the hydrogel matrix. These results suggest that, while swelling is primarily governed by polymer properties, the incorporation strategy may indirectly influence water uptake through changes in internal structure.[28–30]

## Evaluation of API release from SAP

The in vitro release profiles of AP and ASA from alginate beads prepared by encapsulation and impregnation are presented in Fig. 4. The release behavior differed significantly depending on the incorporation strategy, indicating that drug distribution within the polymeric matrix plays a key role in controlling mass transport. For ASA, encapsulated beads exhibited a more controlled release profile, characterized by a gradual increase in drug release over time. In contrast, impregnated beads showed a faster initial release, indicating that a significant fraction of the drug is located near the bead surface. This behavior is consistent with the expected differences in drug distribution between both incorporation strategies.

Similarly, for AP, impregnated beads exhibited a higher initial release compared to encapsulated systems. Encapsulation reduced the burst effect and promoted a more sustained release, suggesting that the drug is more effectively entrapped within the polymeric network. These results suggest that encapsulation improves control over drug release, whereas impregnation leads to faster release due to surface-localized drug. The differences observed in release behavior can be directly related to the structural characteristics described in the physical and functional properties of alginate beads section. Encapsulated beads exhibited more uniform morphology and internal structure, favoring diffusion-controlled release. In contrast, the heterogeneous structure of impregnated beads facilitates shorter diffusion pathways and faster release kinetics.

### Mechanistic analysis of drug release

To elucidate the dominant release mechanisms, experimental data were fitted to several kinetic models commonly used for polymeric systems (Table 9). These models allow differentiation between diffusion-controlled, swelling-controlled, and anomalous transport mechanisms.[8,31] For AP, the Korsmeyer–Peppas and Peppas–Sahlin models provided the best fit, indicating that release is governed by anomalous transport, involving both diffusion and polymer relaxation. This behavior is also consistent with

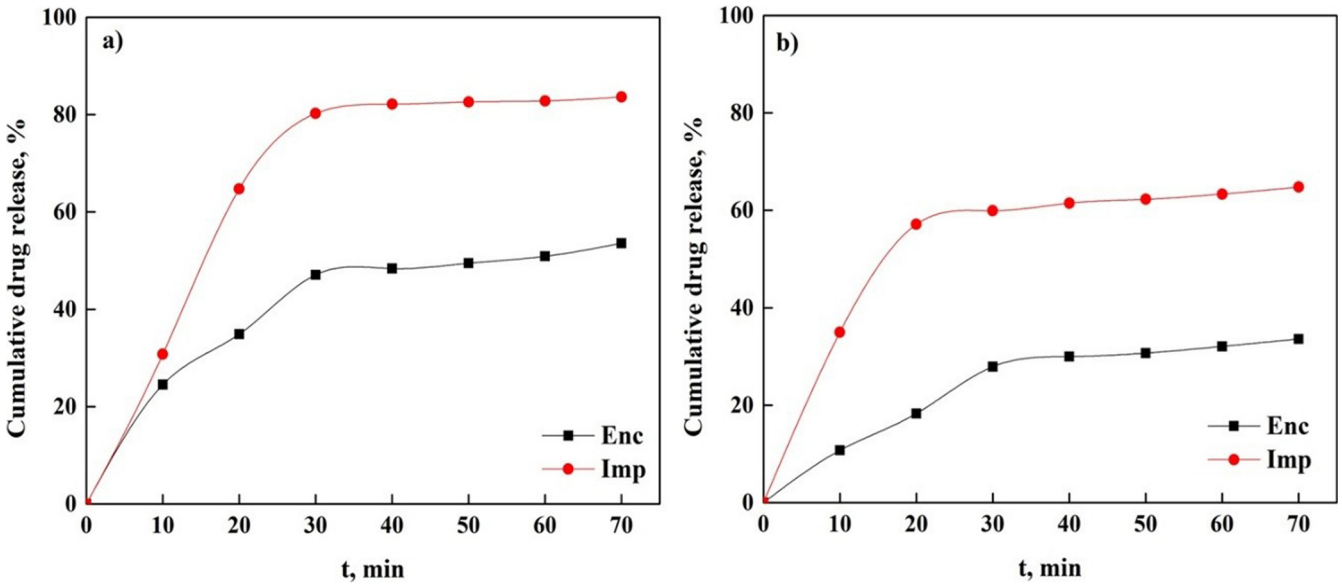


Fig. 4. In vitro release profiles of AP and ASA from alginate beads prepared by encapsulation and impregnation methods

Table 9. Parameters of API release models

| Sample | Higuchi | | | Korsmeyer–Peppas | | | | Peppas–Sahlin | | | | | Weibull | | | |
|---|---|---|---|---|---|---|---|---|---|---|---|---|---|---|---|---|
| | $K_H$ | $R^2$ | AIC | K | n | $R^2$ | AIC | $K_1$ | $K_2$ | m | $R^2$ | AIC | β | α | $R^2$ | AIC |
| AP-Enc | 4.30 | 0.96 | 44.6 | 0.03 | 0.66 | 0.96 | −14.8 | 0.03 | 0.01 | 0.43 | 0.95 | −14.6 | 0.83 | 0.02 | 0.95 | −12.6 |
| AP-Imp | 9.13 | 0.83 | 36.3 | 0.03 | 0.54 | 0.95 | −17.7 | 0.03 | 0.02 | 0.43 | 0.95 | −17.5 | 0.65 | 0.01 | 0.94 | −12.4 |
| ASA-Enc | 7.11 | 0.94 | 32.2 | 0.15 | 0.45 | 0.97 | −1.69 | 0.16 | 0.00 | 0.43 | 0.80 | −1.68 | 0.61 | 0.07 | 0.94 | −2.19 |
| ASA-Imp | 4.31 | 0.89 | 26.6 | 0.04 | 0.56 | 0.94 | −9.68 | 0.04 | 0.01 | 0.43 | 0.83 | −9.53 | 0.61 | 0.01 | 0.95 | −8.46 |

drug solubility differences between ASA and AP, which may influence diffusion through the hydrated matrix.

The values of the release exponent ($0.43 < n < 0.85$) suggest that AP release occurs through a combination of Fickian diffusion and matrix relaxation processes. In contrast, the release of ASA was better described by the Weibull model, suggesting a predominantly diffusion-controlled mechanism. The β parameter ($\beta < 1$) indicates an initial rapid release followed by a slower stage, consistent with drug diffusion from a polymeric matrix. The relative contributions of diffusion and polymer relaxation (Table 10) further support these findings. AP release is dominated by polymer relaxation, whereas ASA release is primarily governed by diffusion. These differences may be attributed to the physicochemical properties of each API and their interaction with the alginate matrix.

Importantly, the incorporation strategy significantly influences the dominant release mechanism. Encapsulation promotes a more homogeneous drug distribution within the matrix, leading to diffusion-controlled or mixed transport behavior. In contrast, impregnation results in heterogeneous drug localization and faster release dominated by surface desorption and diffusion. These findings indicate that the incorporation method is a key parameter governing both the kinetics and mechanism of drug release. The results are consistent with established models of drug transport in polymeric systems, where matrix structure and drug distribution determine the dominant release pathways.[9,10] Additionally, differences in drug solubility and molecular size may contribute to the observed variations in transport mechanisms between ASA and AP.

Table 10. Contribution of diffusion and polymer relaxation to API release

| | | | |
|---|---|---|---|
| | | | |
| | Impregnated | 0.7030 | 0.2970 |
| | | | |
| | Impregnated | 0.6920 | 0.3080 |

## Structural characterization of alginate beads

The structural and physicochemical properties of alginate beads prepared using different incorporation strategies were analyzed by FTIR, SEM, and XRD in order to establish correlations between matrix structure, drug distribution, and release behavior.

### FTIR analysis

FTIR spectra of alginate beads before and after drug incorporation are shown in Fig. 5. The spectra exhibit characteristic bands associated with alginate, including broad O–H stretching vibrations (~3200–3400 $cm^{-1}$), C–H stretching (~2900 $cm^{-1}$), and asymmetric and symmetric stretching of carboxylate groups (~1600 and ~1400 $cm^{-1}$), which are responsible for interactions with crosslinking ions. After drug incorporation, slight shifts and changes in band intensity were observed, particularly in the regions associated with hydroxyl and carboxyl groups.[4,32] These variations suggest potential interactions between the APIs and the polymeric matrix, such as hydrogen bonding or electrostatic interactions, which have been widely reported in alginate-based drug delivery systems.[7,13] Encapsulated systems showed more pronounced spectral changes compared to impregnated beads, indicating stronger interactions between the drug and the alginate matrix. In contrast, impregnated systems exhibited minimal spectral modifications, suggesting that the drug is mainly adsorbed on the surface rather than integrated

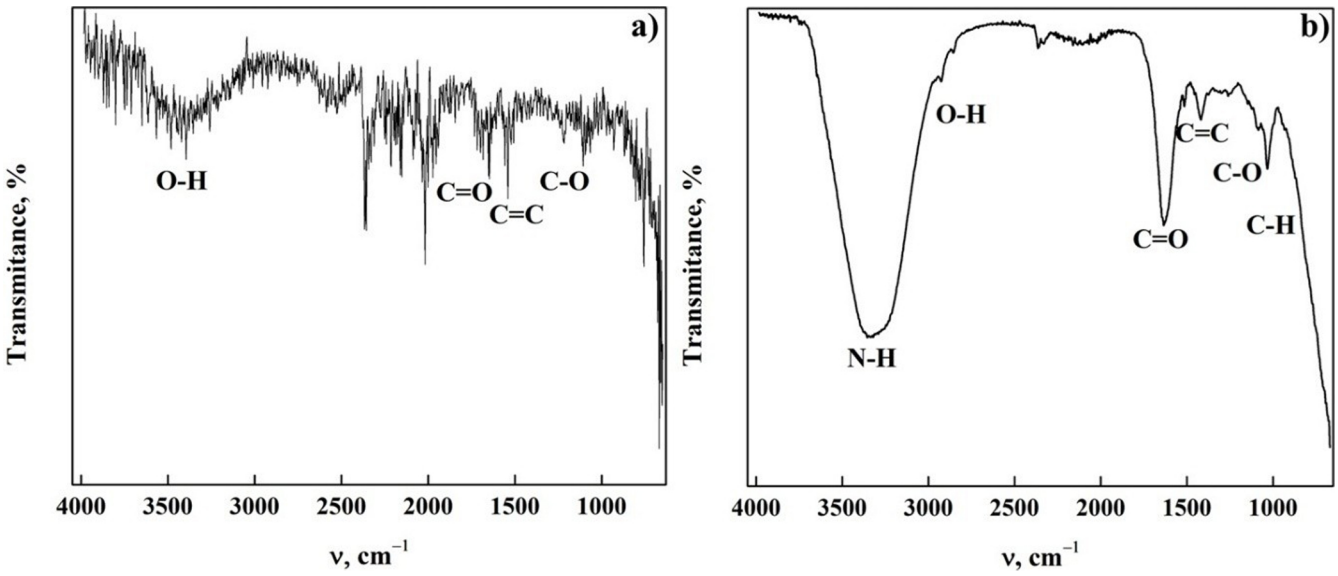


Fig. 5. FTIR spectra of alginate beads before and after drug incorporation using encapsulation and impregnation methods

into the polymer network. These findings support the hypothesis that encapsulation leads to a more homogeneous distribution of the drug within the matrix, whereas impregnation results in surface-localized drug, which is consistent with the release behavior observed in in the evaluation of API release from SAP section. These characteristic bands are consistent with those reported for alginate-based systems in previous studies.[4,31,32]

## SEM analysis

SEM images of alginate beads before and after drug incorporation are presented in Fig. 6. Encapsulated beads exhibited a relatively compact and homogeneous internal structure, whereas impregnated beads showed a more heterogeneous morphology with visible surface irregularities. After drug loading, encapsulated systems maintained their structural integrity, indicating that the drug is incorporated within the matrix without significantly altering the external morphology. In contrast, impregnated beads displayed surface deposits and irregularities, which can be attributed to drug accumulation on or near the surface. These morphological differences are directly related to the observed release behavior. Surface-localized drug in impregnated beads facilitates rapid dissolution and faster release, whereas the more uniform structure of encapsulated systems promotes controlled diffusion through the polymeric network.[15] Similar morphological changes associated with drug incorporation and surface deposition have been reported in alginate-based delivery systems, where surface-associated drug leads to faster release behavior compared to matrix-embedded systems.[14,33,34]

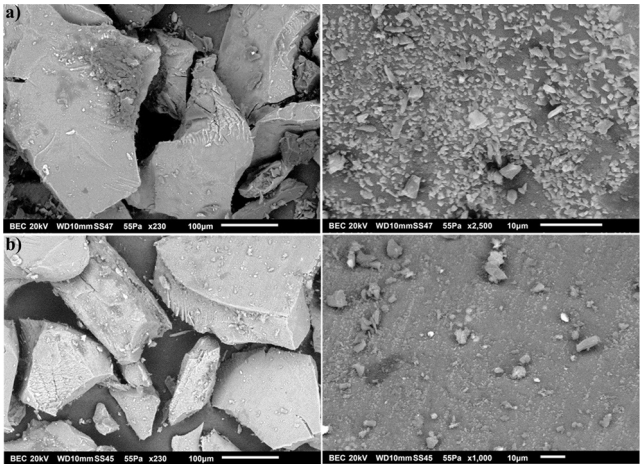


Fig. 6. SEM images of alginate beads prepared by encapsulation and impregnation before and after drug loading

## XRD analysis

XRD patterns of alginate beads are shown in Fig. 7. The diffractograms exhibit broad peaks characteristic of amorphous materials. This amorphous behavior is characteristic of alginate-based hydrogels, which typically lack long-range crystalline order due to their ionically crosslinked structure.[4,35] No major changes in crystallinity were observed after drug incorporation, although minor variations in peak intensity were detected in impregnated samples, which may be associated with partial surface crystallization. This behavior is consistent with molecular-level dispersion. The absence of distinct crystalline peaks indicates that the APIs are molecularly dispersed within the polymeric matrix rather than forming separate crystalline phases.[36–38] The absence of sharp crystalline peaks in encapsulated systems further supports the hypothesis of homogeneous drug distribution, whereas any minor changes observed in impregnated samples may be associated with partial surface crystallization of the drug. Overall, the XRD results suggest that

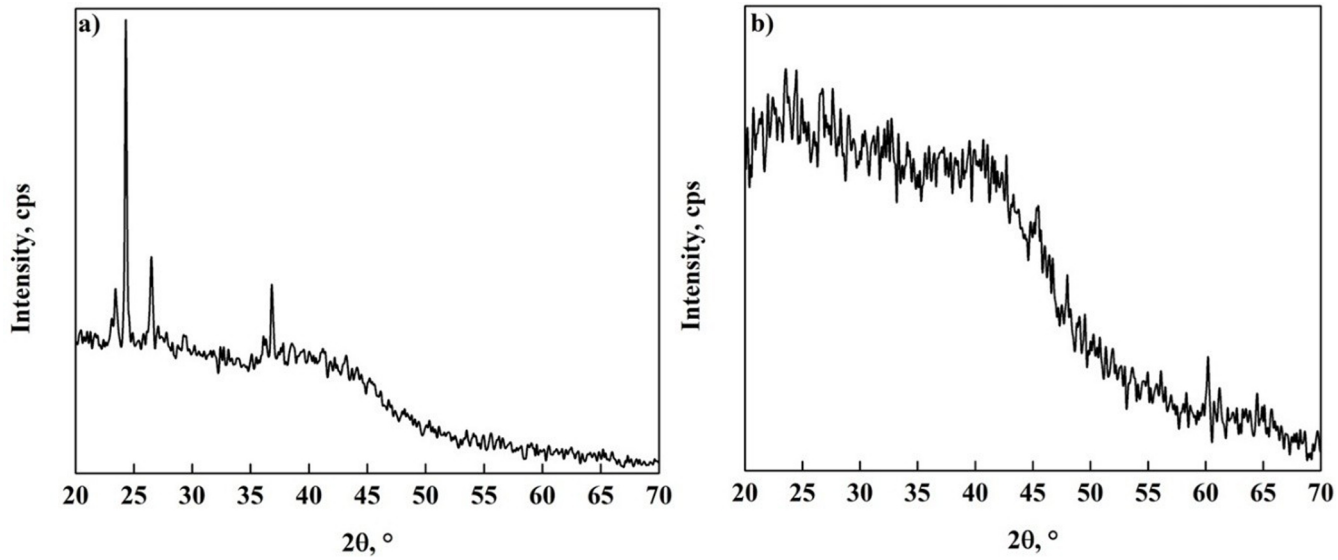


Fig. 7. XRD patterns of alginate beads prepared under different incorporation strategies

the structure of alginate beads is predominantly amorphous, which favors diffusion-controlled drug release.

The results obtained from FTIR, SEM, and XRD analyses consistently indicate that the drug incorporation method significantly alters the internal structure of the alginate matrix. This structural modification is directly related to the observed differences in drug release behavior, where encapsulation promotes a more homogeneous distribution and controlled release, while impregnation leads to surface localization and faster release profiles.

## Conclusions

This study indicates that the drug incorporation strategy is a key factor governing the structural, functional, and release properties of alginate-based delivery systems. The comparison between encapsulation and impregnation methods revealed significant differences in bead morphology, drug loading, and release behavior. Encapsulation resulted in more homogeneous structures, higher drug loading efficiency, and improved control over drug release, indicating effective integration of the APIs within the polymeric network. In contrast, impregnation led to heterogeneous drug distribution, with a significant fraction of the drug localized near the bead surface, resulting in faster release profiles. Kinetic modeling showed that AP release is governed by anomalous transport involving both diffusion and polymer relaxation, whereas ASA release is predominantly diffusion-controlled. These differences are directly related to the internal structure of the beads and the spatial distribution of the drug, which are determined by the incorporation strategy. Structural characterization by FTIR, SEM, and XRD supported these findings, confirming that encapsulation promotes a more uniform internal organization, while impregnation leads to surface-associated drug distribution. The consistency between structural analysis and release behavior highlights a clear structure–function relationship in alginate systems. Overall, this work provides mechanistic insight into how drug incorporation strategies influence polymeric delivery systems, demonstrating that the incorporation method is not merely a processing step but a critical design parameter. These findings contribute to the rational design of alginate-based carriers with tunable release profiles and potential applications in controlled drug delivery.

## Data Availability Statement

Not applicable.

### ORCID iDs

Jose Hernandez 0000-0002-0584-3715
Mercedes Salazar-Hernandez 0000-0001-8480-8725
Rosa Hernandez-Soto Rosa 0000-0001-7053-8808
Alba N. Ardila A. Alba 0000-0002-7675-0647

### References

1. Adepu S, Ramakrishna S. Controlled drug delivery systems: Current status and future directions. *Molecules*. 2021;26(19):5905. doi:10.3390/molecules26195905
2. Rouaz K, Chiclana-Rodríguez B, Nardi-Ricart A, et al. Excipients in the Paediatric Population: A Review. *Pharmaceutics*. 2021;13(3):387. doi:10.3390/pharmaceutics13030387
3. Taylor KMG, Aulton ME, eds. *Aulton's Pharmaceutics E-Book: The Design and Manufacture of Medicines*. 5th ed. Elsevier; 2017. ISBN: 978-0-7020-7005-1, 978-0-7020-7001-3.
4. Lee KY, Mooney DJ. Alginate: Properties and biomedical applications. *Prog Polym Sci*. 2012;37(1):106–126. doi:10.1016/j.progpolymsci.2011.06.003
5. Abourehab MAS, Rajendran RR, Singh A, et al. Alginate as a promising biopolymer in drug delivery and wound healing: A review of the state-of-the-art. *Int J Mol Sci*. 2022;23(16):9035. doi:10.3390/ijms23169035
6. Weng Y, Yang G, Li Y, et al. Alginate-based materials for enzyme encapsulation. *Adv Colloid Interface Sci*. 2023;318:102957. doi:10.1016/j.cis.2023.102957
7. Gunjal VB, Sonawane DS, Ahire SK, et al. A review on novel excipients. *Int J Pharm Sci*. 2023;1(9):304-320. doi:10.5281/zenodo.8344687
8. Peppas NA, Bures P, Leobandung W, Ichikawa H. Hydrogels in pharmaceutical formulations. *Eur J Pharm Biopharm*. 2000;50(1):27–46. doi:10.1016/s0939-6411(00)00090-4
9. Siepmann J, Peppas NA. Modeling of drug release from delivery systems based on hydroxypropyl methylcellulose (HPMC). *Adv Drug Deliv Rev*. 2001;48(2–3):139–157. doi:10.1016/s0169-409x(01)00112-0
10. Brazel CS, Peppas NA. Modeling of drug release from swellable polymers. *Eur J Pharm Biopharm*. 2000;49(1):47–58. doi:10.1016/s0939-6411(99)00058-2
11. Paul DR. Elaborations on the Higuchi model for drug delivery. *Int J Pharm*. 2011;418(1):13–17. doi:10.1016/j.ijpharm.2010.10.037
12. Kalkumbe MA, Waghmare S, Kamble H. Microencapsulation: A review. *Int Res J Modern Eng Technol Sci*. 2022;4(5):3844–3850. doi:10.56726/IRJMETS26546
13. Huang X, Brazel CS. On the importance and mechanisms of burst release in matrix-controlled drug delivery systems. *J Control Release*. 2001;73(2–3):121–136. doi:10.1016/s0168-3659(01)00248-6
14. Siepmann J, Siepmann F. Modeling of diffusion controlled drug delivery. *J Control Release*. 2012;161(2):351–362. doi:10.1016/j.jconrel.2011.10.006
15. Smrdel P, Bogataj M, Podlogar F, et al. Characterization of calcium alginate beads containing structurally similar drugs. *Drug Dev Ind Pharm*. 2006;32(5):623–633. doi:10.1080/03639040600599863
16. Jyothi NVN, Prasanna PM, Sakarkar SN, Prabha KS, Ramaiah PS, Srawan GY. Microencapsulation techniques, factors influencing encapsulation efficiency. *J Microencapsul*. 2010;27(3):187–197. doi:10.3109/02652040903131301
17. Kučuk N, Primožič M, Knez Ž, Leitgeb M. Alginate beads with encapsulated bioactive substances from *Mangifera indica* peels as promising peroral delivery systems. *Foods*. 2024;13(15):2404. doi:10.3390/foods13152404
18. Ong CKS, Lirk P, Tan CH, Seymour RA. An evidence-based update on nonsteroidal anti-inflammatory drugs. *Clin Med Res*. 2007;5(1):19-34. doi:10.3121/cmr.2007.698
19. Siepmann J, Peppas NA. Higuchi equation: Derivation, applications, use and misuse. *Int J Pharm*. 2011;418(1):6–12. doi:10.1016/j.ijpharm.2011.03.051
20. Bruschi ML. *Strategies to Modify the Drug Release from Pharmaceutical Systems*. Elsevier/Woodhead Publishing; 2015. ISBN:978-0-08-100092-2.
21. Kosmidis K, Argyrakis P, Macheras P. Fractal kinetics in drug release from finite fractal matrices. *J Chem Phys*. 2003;119(12):6373–6377. doi:10.1063/1.1603731
22. Kalogeropoulou F, Papailiou D, Protopapa C, et al. Design and development of low- and medium-viscosity alginate beads loaded with pluronic® F-127 nanomicelles. *Materials (Basel)*. 2023;16(13):4715. doi:10.3390/ma16134715
23. Sıçramaz H, Dönmez AB, Güven B, Ünal D, Aşbay E. Microstructure and release behavior of alginate–Natural hydrocolloid composites: A comparative study. *Polymers (Basel)*. 2025;17(4):531. doi:10.3390/polym17040531

24. Del Gaudio P, Colombo P, Colombo G, Russo P, Sonvico F. Mechanisms of formation and disintegration of alginate beads obtained by prilling. *Int J Pharm*. 2005;302(1–2):1–9. doi:10.1016/j.ijpharm.2005.05.041
25. Tavakol M, Vasheghani-Farahani E, Hashemi-Najafabadi S. The effect of polymer and $CaCl_2$ concentrations on the sulfasalazine release from alginate-N,O-carboxymethyl chitosan beads. *Prog Biomater*. 2013;2(1):10. doi:10.1186/2194-0517-2-10
26. Szekalska M, Wróblewska M, Czajkowska-Kośnik A, et al. The spray-dried alginate/gelatin microparticles with luliconazole as muco-adhesive drug delivery system. *Materials (Basel)*. 2023;16(1):403. doi:10.3390/ma16010403
27. Azad AK, Al-Mahmood SMA, Chatterjee B, Wan Sulaiman WMA, Elsayed TM, Doolaanea AA. Encapsulation of black seed oil in alginate beads as a pH-sensitive carrier for intestine-targeted drug delivery: In vitro, in vivo and ex vivo study. *Pharmaceutics*. 2020;12(3):219. doi:10.3390/pharmaceutics12030219
28. Kowalski G, Witczak M, Kuterasiński Ł. Structure effects on swelling properties of hydrogels based on sodium alginate and acrylic polymers. *Molecules*. 2024;29(9):1937. doi:10.3390/molecules29091937
29. Das MK, Senapati PC. Furosemide-loaded alginate microspheres prepared by ionic cross-linking technique: Morphology and release characteristics. *Indian J Pharm Sci*. 2008;70(1):77–84. doi:10.4103/0250-474X.40336
30. Bajpai SK, Kirar N. Swelling and drug release behavior of calcium alginate/poly (sodium acrylate) hydrogel beads. *Designed Monomers and Polymers*. 2016;19(1):89–98. doi:10.1080/15685551.2015.1092016
31. Dash S, Murthy PN, Nath L, Chowdhury P. Kinetic modeling on drug release from controlled drug delivery systems. *Acta Pol Pharm*. 2010;67(3):217–223. PMID:20524422.
32. Sriamornsak P, Thirawong N, Korkerd K. Swelling, erosion and release behavior of alginate-based matrix tablets. *Eur J Pharm Biopharm*. 2007;66(3):435–450. doi:10.1016/j.ejpb.2006.12.003
33. Van Haaren C, De Bock M, Kazarian SG. Advances in ATR-FTIR spectroscopic imaging for the analysis of tablet dissolution and drug release. *Molecules*. 2023;28(12):4705. doi:10.3390/molecules28124705
34. Witzler M, Vermeeren S, Kolevatov RO, et al. Evaluating release kinetics from alginate beads coated with polyelectrolyte layers for sustained drug delivery. *ACS Appl Biomater*. 2021;4(9):6719–6731. doi:10.1021/acsabm.1c00417
35. Khajuria DK, Vasireddi R, Priydarshi MK, Mahapatra DR. Ionic diffusion and drug release behavior of core–shell-functionalized alginate–chitosan-based hydrogel. *ACS Omega*. 2020;5(1):758–765. doi:10.1021/acsomega.9b03464
36. Ciarleglio G, Cinti F, Toto E, Santonicola MG. Synthesis and characterization of alginate gel beads with embedded zeolite structures as carriers of hydrophobic curcumin. *Gels*. 2023;9(9):714. doi:10.3390/gels9090714
37. Zhang F. Melt-Extruded Eudragit® FS-based granules for colonic drug delivery. *AAPS PharmSciTech*. 2016;17(1):56–67. doi:10.1208/s12249-015-0357-2
38. Unagolla JM, Jayasuriya AC. Drug transport mechanisms and in vitro release kinetics of vancomycin encapsulated chitosan-alginate polyelectrolyte microparticles as a controlled drug delivery system. *Eur J Pharm Sci*. 2018;114:199–209. doi:10.1016/j.ejps.2017.12.012

# Investigation of interactions between LDPE containers and ingredients of oil-based ophthalmic formulations

# Badanie interakcji pomiędzy opakowaniami LDPE a składnikami olejowych preparatów oftalmicznych

Marzena Jamrógiewicz[1,A–F], Katarzyna Czarnobaj[1,B,C], Katarzyna Krzemińska[2,B], Marcin Płaczek[2,B,C], Zofia Telefus[1,B], Julia Sołobodowska[1,B], Małgorzata Sznitowska[2,A,C,E,F]

[1] Department of Physical Chemistry, Faculty of Pharmacy, Medical University of Gdańsk, Poland
[2] Department of Pharmaceutical Technology, Faculty of Pharmacy, Medical University of Gdańsk, Poland

A – research concept and design; B – collection and/or assembly of data; C – data analysis and interpretation; D – writing the article; E – critical revision of the article; F – final approval of the article

Polymers in Medicine, ISSN 0370-0747, eISSN 2451-2699 *Polim Med*. 2026;56(1):31–40

**Address for correspondence**
Marzena Jamrógiewicz
E-mail: marzena.jamrogiewicz@gumed.edu.pl

**Funding sources**
This research was funded by the Medical Research Agency under grant No. 2024/ABM/03/KPO/KPOD.07.07-IW.07-0046/24-00.

**Conflict of interest**
None declared

**Acknowledgements**
The authors would like to express their sincere gratitude to the organizers of the *Physical Chemistry and Biophysics for Pharmacy 2025* conference for the opportunity to present and discuss the results included in this article.

Received on October 29, 2025
Reviewed on February 11, 2026
Accepted on February 18, 2026

Published online on June 30, 2026

**Cite as**
Jamrógiewicz M, Czarnobaj K, Krzemińska K, et al. Interactions between LDPE containers and oil-based ophthalmic formulations. *Polim Med*. 2026;56(1):31–40. doi:10.17219/pim/218264

**DOI**
10.17219/pim/218264



## Abstract

**Background.** This study presents the results of an investigation into the interactions between innovative ophthalmic formulations and commercially available low-density polyethylene (LDPE) containers. The newly developed formulations are self-emulsifying oils (SEOs) containing suspended drug particles, designed to form an emulsion immediately upon contact with tear fluid. Physicochemical and mechanical properties of the containers were evaluated. Interactions between 6 different LDPE containers and the SEO matrix (oil "O" and surfactant Tween 20 "T") were investigated, and the impact of the SEO formulations on the mechanical properties of the containers was assessed.

**Objectives.** The study aimed to identify potential interactions between SEO components and the packaging that may occur during storage under stress conditions, based on changes in morphology, structure, thermal behavior, and mechanical strength.

**Materials and methods.** The SEO carrier was prepared by mixing Miglyol® 812 with Tween® 20 at a concentration of 5% w/w, followed by sterile filtration. The suspensions were compounded aseptically using sterile, micronized sodium cefuroxime (CEF) and vancomycin hydrochloride (VAN) at a concentration of 5% w/w, along with sodium citrate (2% w/w). In accordance with stability testing guidelines, stress stability studies were conducted in a climatic chamber at 40°C/75% relative humidity and 60°C/75% relative humidity. To detect structural and physicochemical changes, advanced analytical techniques were employed, including Fourier-transform infrared (FTIR) and near-infrared (NIR) spectroscopy for the assessment of structural alterations and potential degradation, differential scanning calorimetry (DSC) for thermal analysis, and X-ray diffraction (XRD) for evaluation of material crystallinity. The mechanical strength of packaging material fragments after contact with the formulations was evaluated using a TA.XTplus texture analyzer.

**Results.** The experiments indicated potential migration (e.g., of plasticizers and residual monomers), as well as adsorption or absorption of excipient components. Subtle interactions were observed, accompanied by negligible changes in the mechanical strength of the packaging material.

**Conclusions.** The study confirmed the necessity of comprehensive compatibility testing between ophthalmic formulations and their packaging materials. A thorough understanding of these interactions is essential to ensure product stability, safety, and quality during storage and use.

## Streszczenie

**Wprowadzenie.** Artykuł przedstawia wyniki badań interakcji innowacyjnych preparatów okulistycznych z komercyjnymi opakowaniami z polietylenu o niskiej gęstości (LDPE). Opracowane formuły olejowe mają postać samoemulgujących zawiesin olejowych (SEO), przeznaczonych do natychmiastowego tworzenia emulsji z płynem łzowym po aplikacji. Zaplanowano badania fizykochemiczne i stresowe opakowań. Badano interakcje 6 różnych opakowań z matrycą SEO (olej „O" i surfaktant Tween 20 „T") oraz oceniono wpływ SEO na właściwości mechaniczne opakowań.

**Cel pracy.** Badania miały na celu identyfikację potencjalnych interakcji składników olejowego preparatu z opakowaniem, które mogą wystąpić podczas przechowywania preparatów, w oparciu o zmiany w materiale opakowania: morfologii, strukturze, własnościach termicznych i wytrzymałości mechanicznej.

**Materiał i metody.** Nośnik SEO przygotowano poprzez zmieszanie Miglyolu 812 z Tweenem 20 w stężeniu 5% w/w, a następnie poddano filtracji wyjaławiającej. Dodano mikronizowane proszki cefuroksymu sodowego (CEF) lub chlorowodorku wankomycyny (VAN) w stężeniu 5% w/w oraz cytrynian sodu (2% w/w), a następnie zhomogenizowano zawiesinę. Do badań przeznaczono próbki opakowań o wymiarach 5 × 5 mm, które umieszczano w probówkach Eppendorfa i zalewano 0,5 ml odpowiedniego płynu: oleju (O), oleju z Tween (O-T) lub zawiesiny (SEO-CEF, SEO-VAN).

**Wyniki.** Eksperymenty wskazały na możliwość migracji składników opakowania do preparatu (np. plastyfikatorów czy monomerów) oraz adsorpcji lub absorpcji do opakowania składników preparatu; w konsekwencji zanotowano również subtelne zmiany wytrzymałości opakowania.

**Wnioski.** Badanie dostarcza ważnych informacji, które muszą być uwzględnione przy wyborze opakowania dla kropli do oczu i wskazuje na przydatność użytych testów do oceny interakcji. Zrozumienie tych interakcji jest kluczowe dla zapewnienia stabilności, bezpieczeństwa i skuteczności terapeutycznej produktu podczas jego przechowywania i stosowania.


**Key words:** interactions, LDPE packaging, ophthalmic preparation, self-emulsifying oil

**Słowa kluczowe:** interakcje, opakowania LDPE, preparaty oftalmiczne, samoemulgujące krople olejowe

# Introduction

One of the crucial steps in introducing a new medicinal product to the market is the development of appropriate packaging. Pharmaceutical packaging plays a key role in ensuring the quality, safety, and efficacy of the drug product. Its primary function is to protect the formulation from adverse external factors (physical, chemical, and microbiological), such as light, moisture, oxygen, temperature fluctuations, and contamination, which may lead to degradation of the active substance or deterioration of product properties. The container should ensure product stability throughout its shelf life. Furthermore, the packaging material must not interact with the formulation components.[1]

One of the most commonly used materials in pharmaceutical packaging, including packaging for ophthalmic products, is low-density polyethylene (LDPE), followed by high-density polyethylene (HDPE) and polypropylene.[2,3] These polymers are widely used due to their favorable mechanical properties, chemical resistance, and relatively low production costs. In ophthalmic formulations, appropriate packaging plays a critical role in maintaining sterility, stability, and therapeutic efficacy throughout the product's shelf life. Ophthalmic solutions and suspensions are particularly sensitive to environmental factors such as light, oxygen, temperature fluctuations, and microbial contamination. Therefore, the selection of suitable packaging materials is essential to ensure patient safety and treatment efficacy.

Low-density polyethylene has a density ranging from 0.91 g/cm$^3$ to 0.93 g/cm$^3$. It is produced by radical polymerization of ethene under high temperature and pressure. The presence of side branches in the polymer chain prevents tight molecular packing, resulting in its relatively low density. This polymer is soft and resilient, resistant to puncture and tearing, and capable of withstanding repeated mechanical stress during use. These properties make it particularly suitable for squeeze bottles used in multidose ophthalmic products, where controlled dispensing and ease of handling are required. Although LDPE demonstrates good long-term stability, its resistance may significantly decrease under specific conditions, particularly following combined thermo- and photo-oxidative exposure.[3–5] Furthermore, LDPE is chemically inert, exhibits good heat-sealing properties, and is readily processable, which facilitates large-scale manufacturing and ensures tight container closure.[6] However, significant limitations of LDPE include low resistance to ultraviolet (UV) radiation and relatively high gas permeability.[7] These characteristics may adversely affect the stability of light- and oxygen-sensitive active pharmaceutical ingredients (APIs), potentially leading to gradual degradation during storage.

Low-density polyethylene used in pharmaceutical containers may interact with drug products through several mechanisms, including adsorption (adhesion of drug molecules to the polymer surface, potentially leading to dose loss), absorption (penetration of the active ingredient into the polymer matrix), migration of container components (e.g., plasticizers or other additives into the formulation), photodegradation (degradation induced by UV exposure), and gas permeability (increasing the risk of oxidative

degradation of formulation components).[7] Disruption of the polymer structure may result in significant loss of active ingredients, potentially leading to reduced therapeutic efficacy.[8] To mitigate these adverse effects, various material modification strategies have been developed. These strategies include the incorporation of colorants to improve UV protection, the addition of metal oxides or antioxidants to enhance barrier properties, and the application of surface coatings. Additionally, multilayer materials combining LDPE with other polymers or functional barrier layers are increasingly used to improve resistance to light, oxygen, and moisture. The appropriate selection and modification of packaging materials for ophthalmic products are essential to ensure drug stability, sterility, and therapeutic efficacy. Continuous advances in polymer engineering and multilayer technologies play a key role in meeting regulatory requirements and addressing the growing demand for high-quality, safe, and reliable ophthalmic drug delivery systems.

# Objectives

The aim of this study was to investigate the effects of self-emulsifying oils (SEOs) and antibiotic suspensions formulated in SEOs on the structural and physicochemical properties of commercially available packaging materials. In addition, the influence of SEO components on spectroscopic, thermal, and mechanical properties was evaluated following stress testing. The development of new medicinal products requires the submission of extensive documentation in the Common Technical Document (CTD) format to the relevant regulatory authority, such as the Polish Office for Registration of Medicinal Products (URPL). The Quality module (Module 3) of the CTD requires the submission of stability data, including information on formulation–packaging interactions. Therefore, comprehensive physicochemical and stress testing of the packaging materials was incorporated into the study design. To monitor potential interactions between drug components and the packaging, the applicability of attenuated total reflectance Fourier-transform infrared (ATR-FTIR) and near-infrared (ATR-NIR) spectroscopy, differential scanning calorimetry (DSC), and X-ray diffraction (XRD) was evaluated. The mechanical strength of the packaging material after exposure to the selected formulations was assessed using a TA.XTplus texture analyzer (Stable Micro Systems, Godalming, UK).

# Materials and methods

## Materials

The following substances were used to prepare SEOs containing suspended drug particles: sodium cefuroxime (CEF) and vancomycin hydrochloride (VAN) (each at 5% w/w; Zhejiang Changhai Pharmaceuticals, Shaoxing, China), Miglyol® 812 (fractionated coconut oil; Caesar & Loretz, Hilden, Germany), Tween® 20 (polysorbate 20, 5% w/w; Sigma-Aldrich, Steinheim, Germany), and sodium citrate (2% w/w; Sigma-Aldrich, Poznań, Poland).

## Methods

### Preparation of SEO formulations

The SEO carrier was prepared by mixing Miglyol® 812 with Tween® 20 at a concentration of 5% w/w. The mixture was subsequently sterile-filtered through hydrophobic polyethersulfone membrane filters (GPWP02500; Merck, Warsaw, Poland). Micronized, sterile powders of CEF and VAN (each at 5% w/w), along with sodium citrate (2% w/w), were added to the carrier, and the resulting suspension was homogenized. The following containers were included in the study: Amapack, Trzebnica, Poland (5 mL for aqueous solutions; Op1), Amapack (10 mL for oil-based solutions; Op2), Eprus, Bielsko-Biała, Poland (10 mL for aqueous solutions; Op3), Eprus (1 mL single-dose mini dropper with closure; Op4), Eprus (1 mL white bottle; Op5), and Gerresheimer, Bolesławiec, Poland (10 mL for oil-based solutions; Op6). Samples of the eye drop containers were cut into square or rectangular fragments measuring approx. from 5 × 5 mm to 10 × 10 mm. The fragments were placed in Eppendorf tubes and immersed in 0.5 mL of oil (O), oil–Tween mixture (O–T), and SEO-CEF and SEO-VAN suspensions, respectively. The prepared samples were incubated in a climatic chamber at 40°C and 60°C/75% relative humidity for 2 weeks. After incubation, the packaging material fragments were removed, gently wiped with tissue paper, and analyzed. Additionally, selected samples were washed with diethyl ether and reanalyzed after immersion in 1 mL of ether for 1 h. Structural changes and potential degradation were evaluated using FTIR and NIR spectroscopy, while DSC was employed to assess thermal properties.

### Infrared and near-infrared spectroscopy (FTIR/NIR)

Infrared and near-infrared spectra were recorded using a JASCO FT/IR-4700 spectrophotometer (JASCO Co., Tokyo, Japan) equipped with a diamond attenuated total reflectance (ATR) accessory. Measurements were performed at a resolution of 4 $cm^{-1}$ over the spectral ranges of 4000–400 $cm^{-1}$ (FTIR) and 8200–4000 $cm^{-1}$ (NIR).

### Differential scanning calorimetry

The thermal behavior of the samples was evaluated using a STAR®-1 System (Mettler Toledo, Greifensee, Switzerland) equipped with an intercooler. Approximately 3–5 mg of each sample was weighed into 40 µL aluminum

crucibles. Thermal analysis was performed over a temperature range from –30°C to 300°C at a heating rate of 10°C/min under a nitrogen purge at a flow rate of 60 mL/min. All measurements were normalized to sample mass.

### X-ray diffraction analysis

X-ray diffraction patterns of LDPE films were recorded using an X-ray powder diffractometer (SmartLab SE; Rigaku Corporation, Tokyo, Japan). Cu Kα radiation (λ = 1.5418 Å) was used as the X-ray source. The generator was operated at 40 kV and 50 mA. Diffraction data were collected over a 2θ range of 5° to 80°, with a scanning rate of 10.00°/min and a step size of 0.01°. All measurements were performed at room temperature under constant operating conditions.

### Texture analysis

The mechanical strength of container fragments was evaluated using a TA.XTplus texture analyzer (Stable Micro Systems) equipped with a 5 kg load cell. The force required to indent a spherical probe (P/5S, diameter 5 mm) into a plastic fragment (surface area approx. 1 $cm^2$) to a depth of 300 µm was measured. Prior to testing, the probe was positioned 1.5 mm above the sample surface and then lowered at a constant speed of 0.01 mm/s. Upon contact with the sample (trigger force = 1.0 g), the probe continued to move downward to a depth of 300 µm, after which it returned to the initial position at the same constant speed. During the test, the maximum force [N] and the work of compression [mJ], defined as the area under the force–distance curve, were recorded using Texture Exponent 32 software (Stable Micro Systems).

## Results

The prepared oil-based systems (SEOs) and their suspensions containing CEF and VAN were subjected to a series of analytical tests to evaluate their stability and compatibility with the selected packaging materials. Following incubation under stress conditions (40°C/75% relative humidity (RH) and 60°C/75% RH for 2 weeks), the samples were analyzed to detect changes in the active compounds and to assess potential interactions between the SEO components and the polymer matrix of the containers. A combination of complementary analytical techniques – FTIR and NIR spectroscopy, DSC, and XRD – was employed to identify structural and thermal alterations. In addition, texture analysis was performed to evaluate changes in the mechanical properties of the containers. The results provide insight into the physicochemical behavior of LDPE packaging materials following contact with oil, SEO formulations without active compounds, and SEO suspensions containing active ingredients.

## Spectroscopic and thermal data

Characteristic infrared (IR) absorption bands of polyethylene (PE) (Fig. 1) were observed in the mid-infrared

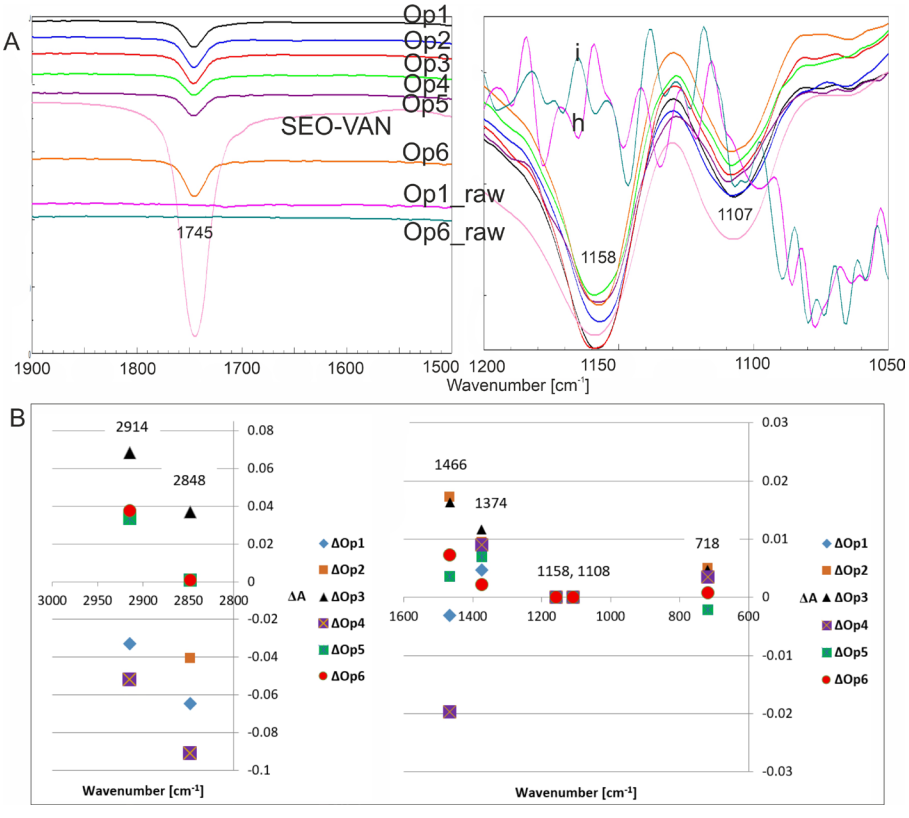


**Fig. 1.** FTIR spectra of packaging materials (Op1–Op6) recorded after incubation of polymer samples in SEO-VAN for 2 weeks at 60°C/75% relative humidity (RH). A. Two spectral ranges; B. Graph presenting ΔA values calculated as the difference between the absorbance (A) of the raw sample and the absorbance after stress testing for Op1–Op6

FTIR – Fourier-transform infrared spectroscopy; Op1–Op6 – tested containers for ophthalmic drop preparation; SEO-VAN – self-emulsifying oil (SEO) with suspended vancomycin hydrochloride particles; A – absorbance; ΔA – difference between the absorbance (A) of the raw sample and that after stress testing for Op1–Op6.

region at 2914 $cm^{-1}$ and 2848 $cm^{-1}$, corresponding to asymmetric and symmetric C–H stretching vibrations of $–CH_2–$ groups, respectively. Additional bands were detected at 1469 $cm^{-1}$ ($–CH_2$ bending), 1377 $cm^{-1}$ ($–CH_3$ bending), 1303 $cm^{-1}$ ($–CH_2$ twisting), and at 729 and 718 $cm^{-1}$ ($–CH_2$ rocking). In the near-infrared region, bands at 5818 $cm^{-1}$, 5789 $cm^{-1}$, 5781 $cm^{-1}$, 5771 $cm^{-1}$, 5695 $cm^{-1}$, 4323 $cm^{-1}$, and 4252 $cm^{-1}$ were attributed to overtones and combination bands of aliphatic C–H vibrations in methylene groups. The most pronounced differences between spectra of raw containers and those incubated with SEO formulations were observed at 2914 $cm^{-1}$ and 2848 $cm^{-1}$. Among the tested samples, only Op6 remained spectroscopically stable, showing no significant changes in these regions. The fingerprint region exhibited notable differences in absorption intensity at approx. 1745 $cm^{-1}$, corresponding to ester (R–COOR) groups, which may arise from PE oxidation or from the presence of Miglyol components.[7] This band was absent in the spectra of the untreated containers. After wiping and subsequent immersion in ether, 3 additional IR bands characteristic of the oil phase were identified at 1744 $cm^{-1}$, 1159 $cm^{-1}$, and 1109 $cm^{-1}$. The presence of these bands indicates sorption of oil components onto or into the packaging material following stress exposure at 60°C/75% RH for 2 weeks. According to the European Pharmacopoeia,[9] PE exhibits 2 characteristic bands at 1471 $cm^{-1}$ and 1465 $cm^{-1}$. However, all tested containers displayed a single band at 1466 $cm^{-1}$, consistent with LDPE.[10]

## Differential scanning calorimetry

The melting endotherms of LDPE containers (Op1–Op6) were observed in the temperature range of 108.69–116.51°C (Table 1). During the 2nd heating cycle, the small endothermic peaks detected in the 1st heating run within the 40–50°C range were no longer present (Fig. 2). Differences in the α-relaxation temperatures were observed among the individual container types and following incubation of the packaging materials in SEO at ambient temperature. Variations in these peaks between containers suggest differences in their thermal history and structural organization. No statistically significant differences in melting enthalpy ($\Delta H_m$) were observed between the tested samples (Table 1), indicating comparable degrees of crystallinity. Low-density polyethylene is a semi-crystalline polymer composed of crystalline domains dispersed within amorphous regions. In the 1st heating run, a small endothermic peak observed between 40°C and 60°C can be attributed to relaxation processes in the amorphous phase. These phenomena are consistent with the viscoelastic behavior of PE and correlate with internal friction peaks reported in the literature.[11–14] Plasticization of the amorphous regions may reduce stiffness, increase deformability, and alter mechanical strength, findings that are supported by the texture analysis results. After storage in SEO formulations at elevated temperatures, only negligible changes in the thermal characteristics of the containers were observed. During the 1st heating cycle, the peak temperatures were generally slightly lower than those of the untreated (raw) containers. However, in the case of Op4 incubated with SEO, an increase in peak temperature of approx. 10% was noted (Table 1). No significant differences were detected during the 2nd heating cycle. Overall, after storage under stress conditions (60°C/75%

**Table 1.** Results of differential scanning calorimetry (DSC) analysis of containers after incubation in SEO

| Sample/ parameter | Raw | SEO-CEF-Citr | SEO-VAN-Citr |
|---|---|---|---|
| Op1 | | | |
| Alpha relaxation | 46.49 | 70.7 | 71.41 |
| ΔH [J/g] | –59.13 | –56.95 | –58.73 |
| Peak [°C] | 111.98 | 107.96 | 111.06 |
| Op2 | | | |
| Alpha relaxation 1 | 43.54 | 32.71 | 29.96 |
| Alpha relaxation 2 | – | 70.46 | 70.78 |
| ΔH [J/g] | –65.78 | –65.85 | –58.56 |
| Peak [°C] | 108.69 | 109.98 | 109.44 |
| Op3 | | | |
| Alpha relaxation 1 | 45.55 | 30.78 | 31.05 |
| Alpha relaxation 2 | – | 70.69 | 69.89 |
| ΔH [J/g] | –59.4 | –62.19 | –56.4 |
| Peak [°C] | 112.62 | 111.65 | 110.9 |
| Op4 | | | |
| Alpha relaxation | 64.07 | 70.74 | 71.71 |
| ΔH [J/g] | –71.73 | –73.1 | –77.51 |
| Peak [°C] | 116.51 | 116.77 | 116.06 |
| Op5 | | | |
| Alpha relaxation 1 | 59.25 | 31.44 | 28.62 |
| Alpha relaxation 2 | – | 70.12 | 70.15 |
| ΔH [J/g] | –53.96 | –57.61 | –56.07 |
| Peak [°C] | 113.03 | 112.59 | 108.92 |
| Op6 | | | |
| Alpha relaxation 1 | 40.87 | 30.65 | 29.6 |
| Alpha relaxation 2 | – | 69.06 | 69.79 |
| ΔH [J/g] | –51.55 | –58.41 | –54.12 |
| Peak [°C] | 113.03 | 110.15 | 108.89 |

SEO-CEF – self-emulsifying oil (SEO) with suspended sodium cefuroxime; SEO-VAN – SEO with suspended vancomycin hydrochloride particles; A – absorbance; ΔA – difference between the absorbance (A) of the raw sample and that after stress testing for Op1–Op6.

A

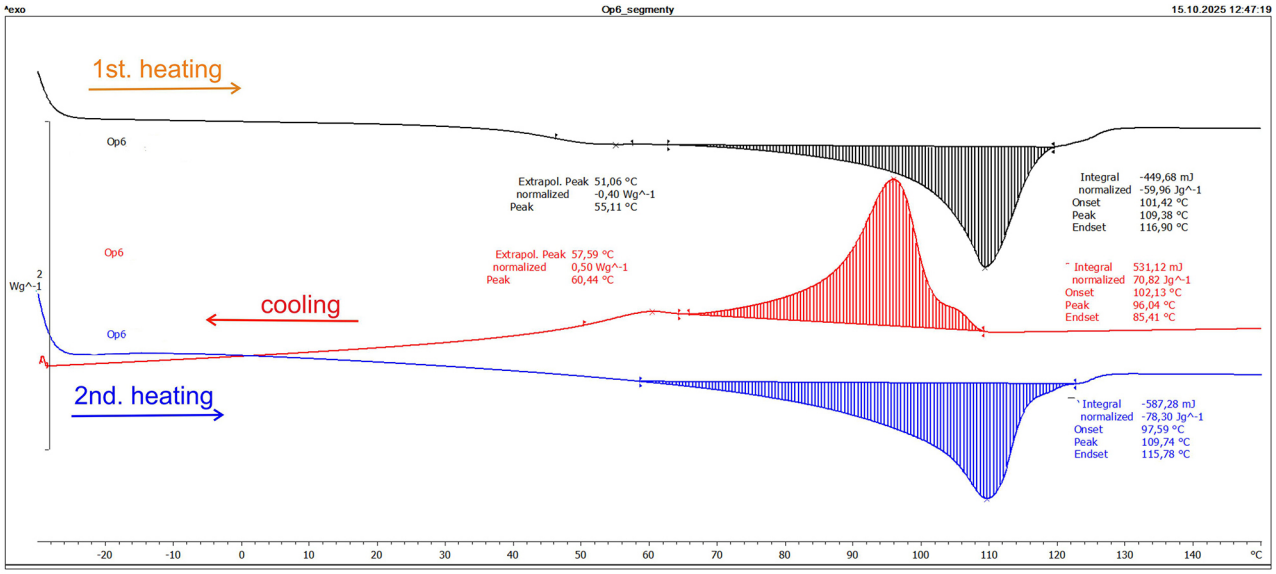


B

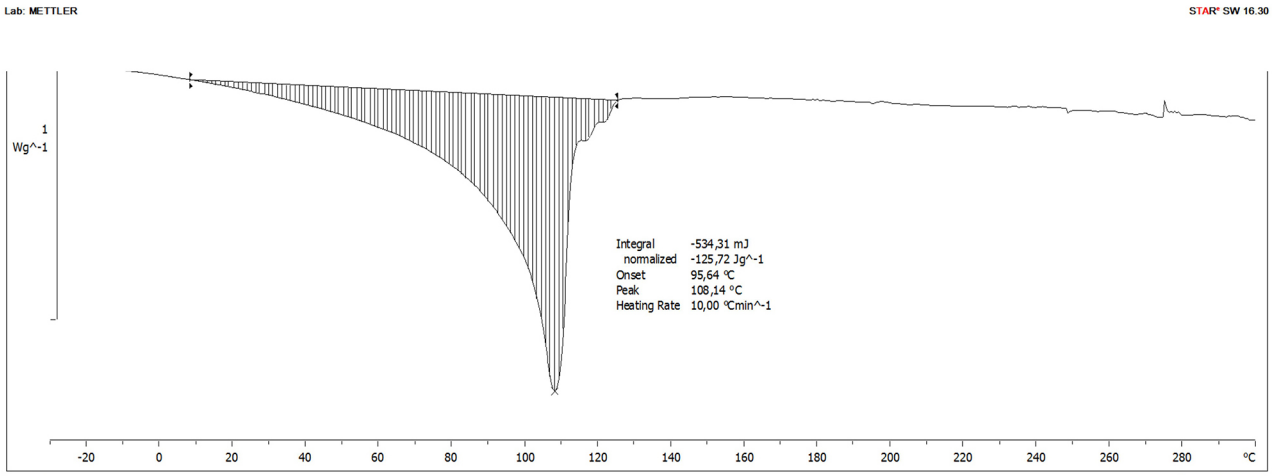


C

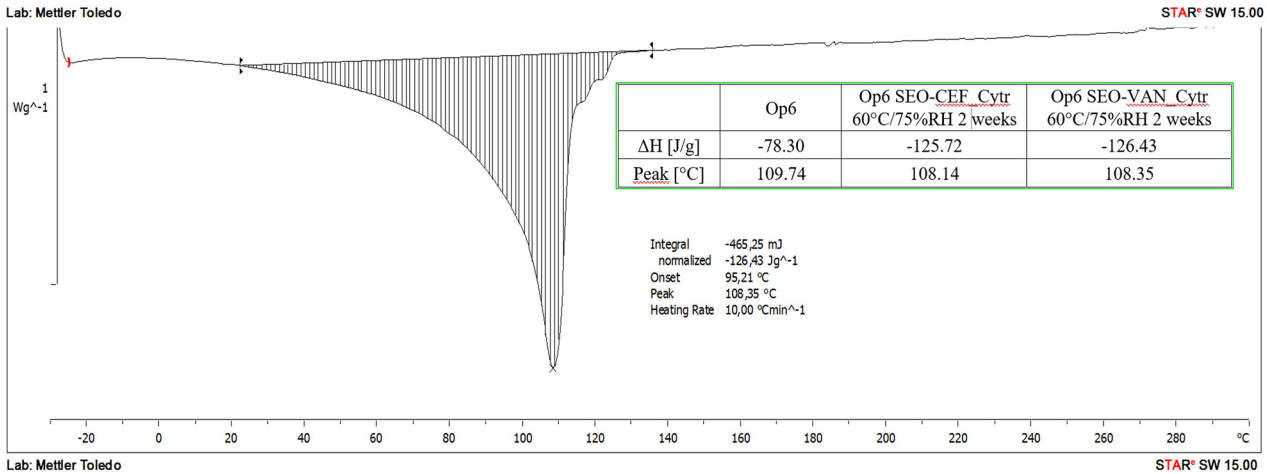


| | Op6 | Op6 SEO-CEF_Cytr 60°C/75%RH 2 weeks | Op6 SEO-VAN_Cytr 60°C/75%RH 2 weeks |
|---|---|---|---|
| ΔH [J/g] | -78.30 | -125.72 | -126.43 |
| Peak [°C] | 109.74 | 108.14 | 108.35 |

**Fig. 2.** DSC curves recorded for (A) raw Op6, (B) before contact with the preparation, and (C) after contact with the preparation during the 2nd heating cycle
DSC – differential scanning calorimetry; Op6 – tested commercial container designated as No. 6.

RH for 2 weeks) in SEO formulations containing APIs and sodium citrate, no evidence of substantial thermal interactions or structural alterations in the packaging materials was observed.

## Mechanical integrity and drug compatibility

The XRD patterns of LDPE are shown in Fig. 3. Peaks between 13° and 19° (2θ) are visible and correspond to reflections also recorded for the tape used to hold the container fragments in the instrument. The 2θ angles for LDPE were observed at 21.3°, 28.43°, and 36.04°. After incubation of the packaging with SEO, the XRD method indicated subtle θ/2θ shifts toward smaller angles, which may indicate an increase in the distance between crystalline planes (d-spacing). The plasticizer or oil can penetrate between the chains, pushing the structure apart, which was demonstrated during tests using the texturometer and FTIR. The differences in 2θ angles are mainly due to changes in the degree of crystallinity of LDPE after interaction with SEO (oil). The values of the shifts between the angles of the raw polymer and those of Op after incubation are presented in Fig. 4. For polymeric

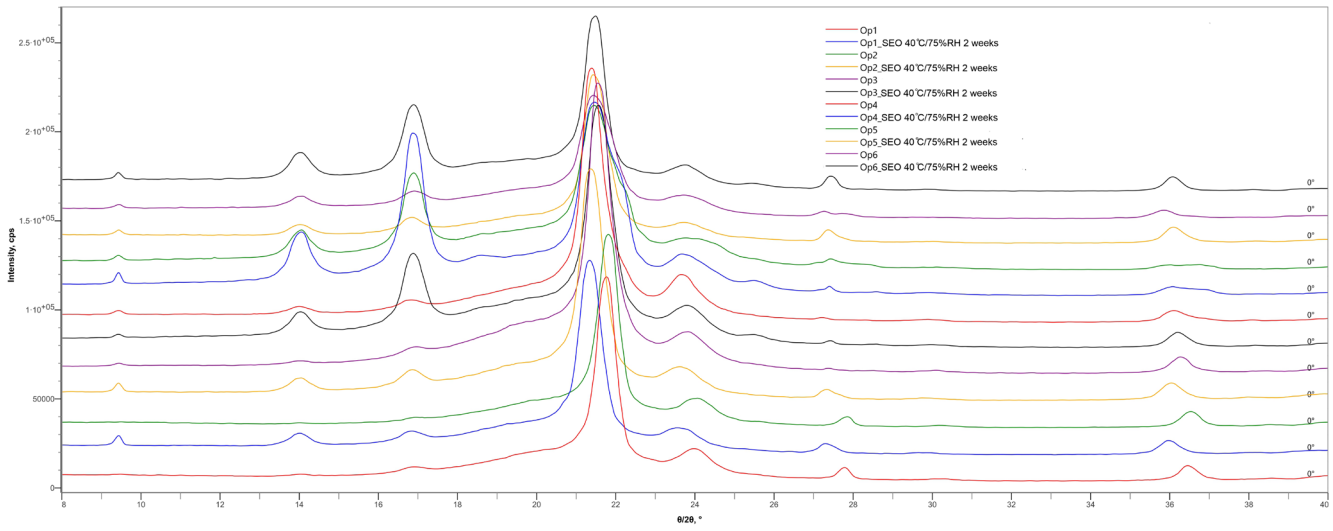


Fig. 3. X-ray diffractograms of raw containers (Op1–Op6) and after incubation in SEO (O–T) at 60°C/75% relative humidity (RH) for 2 weeks, according to the legend.

Op1–Op6 – tested commercial containers designated as No. 1–6; SEO (O–T) – self-emulsifying oil (oil–Tween 20) carrier.

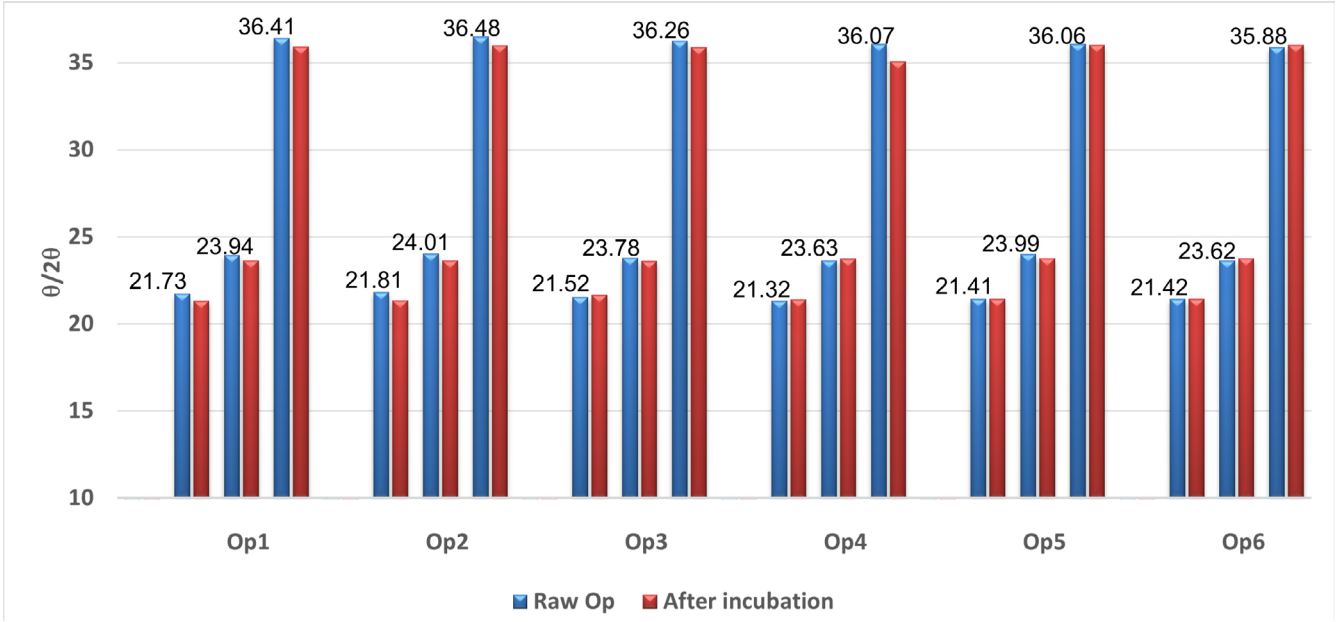


Fig. 4. Graph presenting differences in the XRD peaks of raw containers (Op1–Op6, blue) and after incubation (orange) in SEO (O–T) at 60°C/75% relative humidity (RH) for 2 weeks, according to the legend

XRD – X-ray diffraction; Op1–Op6 – tested commercial containers designated as No. 1–6; SEO (O–T) – self-emulsifying oil (oil–Tween 20) carrier.

packaging composites, diffraction peaks were observed at 2θ = 21.3° and 23.8°, corresponding to the (110) and (200) crystallographic planes, respectively, which has also been confirmed in the literature.[15] The graph below (Fig. 5) presents the results of the mechanical compression strength test of the tested packaging fragments, expressed as the maximum compression force [N]. Raw containers are not identical (Fig. 5A), but the data obtained during testing of the mechanical properties of selected package fragments (compression force at time T0) are similar (Fig. 5C). Regardless of the bottle type, their average values ranged from 17 N to 21 N (compression force) and from 3.7 mJ to 5.1 mJ

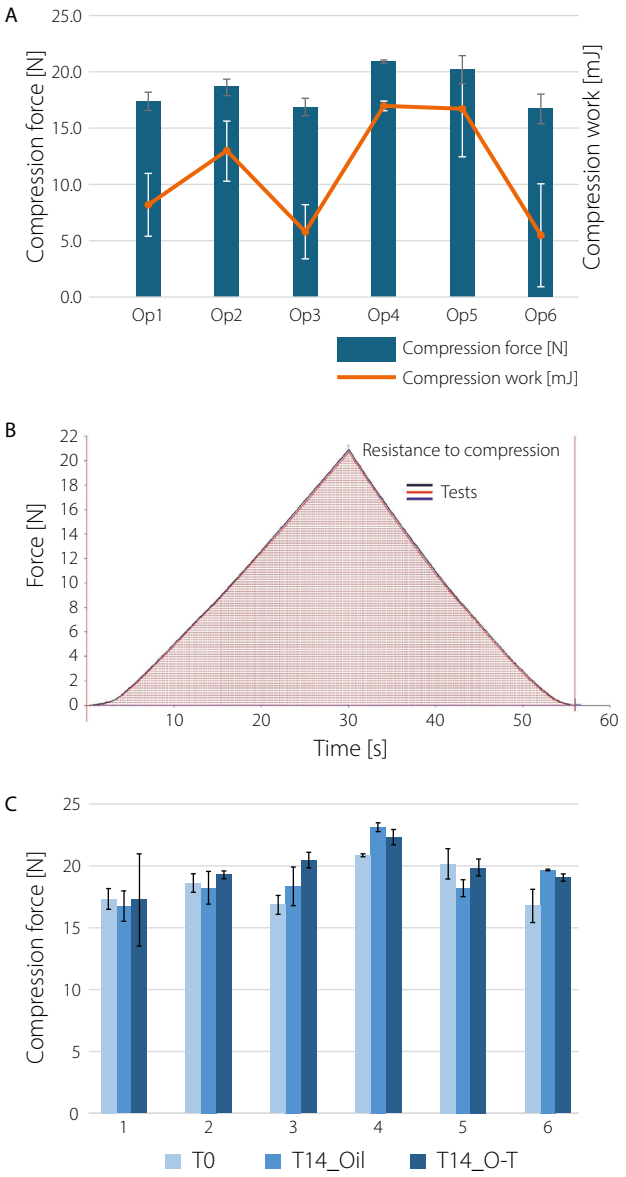


**Fig. 5.** Graph presenting the results of the mechanical compression strength test of the tested containers, expressed as (A) maximum compression force [N] and compression work [mJ]; B. Representative example of repeated testing of Op4, showing the maximum force [N] (peak of the curve) and the compression work (area under the force–time curve)

Op4 – tested commercial container designated as No. 4.

(compression work). We observed that the ease of penetration of the spherical probe into the package fragments depends on their thickness. The highest compression force and work were measured for bottles with the thinnest walls (500–600 µm) – Op4 (Fig. 5A,B). Although the tested package fragments were relatively small (approx. 1 $cm^2$), the wall thickness in different locations within a given fragment varied by up to approx. 100 µm (approx. 15%). For this reason, the results of mechanical measurements within a single fragment show considerable variability: the relative standard deviation (RSD) for compression work was 13–15% (Op1–Op3 stored in oil for 14 days, T14_Oil), and even 21.5–36.6% (force and compression work for Op1 stored for 14 days in the O–T mixture, T14_O–T).

# Discussion

The stability and compatibility of ophthalmic formulations with their primary packaging are critical factors in ensuring the safety and efficacy of drug delivery systems. This study evaluated the interactions between 3 distinct systems – pure oil, an oil-based self-emulsifying carrier (SEO), and SEO containing suspended CEF and VAN – and commercially used eye drop containers.

## Interpretation of spectroscopic and thermal data

These findings align with observations by Garrido-López et al.,[16] who described the migration of lipophilic components into PE. While such "scalping" can often lead to the loss of active ingredients or excipients, our data suggest a potential secondary benefit: the diffusion of oils into PE may act as a plasticizer, potentially enhancing chemical and oxidative stability or imparting radiopacity for specialized medical applications. Structural and thermal changes occurring in the samples after exposure to elevated temperature and humidity, simulating accelerated aging conditions, were analyzed using FTIR, NIR, DSC, XRD, and texture analysis to evaluate potential interactions between the formulation components and the packaging materials. The results obtained in this study enable the assessment of the influence of SEO composition and packaging type on the stability and safety of ophthalmic formulations. Fourier-transform infrared spectroscopy provided crucial evidence regarding the surface interactions between the lipophilic SEO and the polymer matrix. The identification of characteristic bands at 1744 $cm^{-1}$, 1159 $cm^{-1}$, and 1109 $cm^{-1}$ after stress testing confirms the formation of a persistent Miglyol-based film on the packaging surface. The fact that this residue remained after chemical cleaning (ether soaking) suggests a high affinity between the oil and the polyolefin chains. Differential scanning calorimetry analysis

further supported these observations. The consistency of melting profiles between raw and stressed containers indicates that the bulk thermal properties of the packaging remain intact. However, the subtle shifts of melting peaks observed in LDPE may suggest changes in the packing density of the amorphous phase, indicating that while the crystalline structure remains stable – as confirmed by the lack of significant changes in XRD diffraction peak intensities – the amorphous regions are susceptible to subtle structural rearrangements due to oil and polysorbate 20 penetration after 2 weeks at 60°C/75% RH.

The migration and adsorption of lipophilic cosmetic ingredients into polyolefins have already been confirmed using FTIR and DSC methods by Bolte et al.[17] for PE packaging. In this context, sorption ("scalping") phenomena, i.e., the adsorption or absorption of substances onto the surface or within the polymer matrix, may occur. In all samples tested, no noticeable changes in the diffraction peak intensities or in the widths of the crystalline peaks were observed. However, differences in peak positions during the first heating, even if not significant, may indicate variations in the crystallinity of the composite materials. Structural modifications in polymers – such as altered chain mobility – can occur after the introduction of oils, which is also manifested by subtle shifts in the α-relaxation temperatures in DSC curves.[18] Researchers attribute these processes to changes in the packing density of the amorphous phase.[18]

## Mechanical integrity and drug compatibility

Texture analysis confirmed that the structural integrity of the containers was not compromised. Storing the packaging in SEO at elevated temperature (40°C) for 14 days did not significantly alter the mechanical strength parameters. The variations observed in probe penetration were primarily a function of wall thickness rather than material degradation induced by the SEO carrier. This is a vital finding for the pharmaceutical industry, as it ensures that the physical protection provided by the bottle remains consistent throughout the product's shelf life.

## Clinical implications of active ingredient stability

The most significant finding of this study is the lack of interaction between the suspended APIs – CEF and VAN – and the packaging materials. More advanced methods, such as inductively coupled plasma–mass spectrometry (ICP–MS) or liquid chromatography–mass spectrometry (LC–MS), may be required to confirm the absence of APIs on the surface of the container.[9] The absence of drug detection within the polymer matrix suggests that the SEO system effectively sequestered these hydrophilic salts, preventing their migration or adsorption. This ensures that the concentration of the antibiotics remains stable within the formulation, which is paramount for the treatment of severe ocular infections where precise dosing is required.

# Limitations

This study has several limitations that should be acknowledged. One of the main constraints of the XRD analysis arises from the geometry of the packaging samples. The shape and curvature of the packaging materials may have affected the diffraction conditions, potentially influencing peak intensity and signal quality. As a result, the obtained data should be interpreted with caution.

Furthermore, to obtain a more comprehensive understanding of the interactions between the packaging materials and the oil-based suspension matrix, further investigations are warranted. In particular, Raman confocal microscopy mapping could provide spatially resolved information on chemical changes and diffusion phenomena, while ICP-MS analysis would allow for sensitive detection of potential elemental migration. These complementary techniques would contribute to a more complete characterization of packaging–matrix interactions.

# Conclusions

Physical and chemical characterization of LDPE containers was carried out to determine changes in their structural, thermal, functional group, and crystalline or amorphous properties after storage and incubation in O, O–T (SEO), SEO-CEF, and SEO-VAN under stress storage conditions. Basic characterization of PE containers enables the recording and understanding of their behavior in contact with the formulations. Fourier-transform infrared spectra allow observation of negligible interactions, visible as small (up to 8 $cm^{-1}$) band shifts. In general, independent of the active compound tested (CEF and VAN), only interactions related to the presence of O (oil) and contact with the containers under stress conditions were observed. Using the DSC method, small but detectable differences in the α-relaxation temperatures and melting enthalpy of LDPE containers were observed after stress testing. This research aimed to investigate the fundamental interactions between LDPE and SEO in the context of degradation studies. Oil–packaging and oil–surfactant interactions were minimal and consistent. No oil–surfactant incompatibilities were observed. The findings of this study may be incorporated into the registration documentation, specifically within the "Quality" section (Module 3)

of the CTD dossier. The polymeric materials that demonstrated stability under the tested conditions may be selected for the storage of commercial innovative SEO products.

## Data availability

The datasets generated and/or analyzed during the current study are available from the corresponding author on reasonable request.

## Consent for publication

Not applicable.

## Use of AI and AI-assisted technologies

Not applicable.

### ORCID iDs

Katarzyna Czarnobaj 0000-0001-7979-0102
Katarzyna Krzemińska 0000-0001-9711-7149
Marcin Płaczek 0000-0003-1679-5082
Małgorzata Sznitowska 0000-0003-0866-0452
Marzena Jamrógiewicz 0000-0002-2637-9886

### References

1. Pal R, Pandey P, Thakur S, et al. The significance of pharmaceutical packaging and materials in addressing challenges related to unpacking pharmaceutical products. *Int J Pharm Healthc Innov*. 2024;1:149-173. Accessed February 14, 2026. https://www.researchgate.net/profile/Rahul-Pal-25/publication/381126537_The_significance_of_pharmaceutical_packaging_and_materials_in_addressing_challenges_related_to_unpacking_pharmaceutical_products/links/665ebfd8bc86444c722dcdc3/The-significance-of-pharmaceutical-packaging-and-materials-in-addressing-challenges-related-to-unpacking-pharmaceutical-products.pdf.
2. Richard RME. Ophthalmic products. In: Watson J, Cogan L, eds. *Pharmacy Practice*. 6th ed. Edinburgh, UK–New York, USA: Elsevier; 2020. ISBN:978-0-7020-7430-1.
3. Vasile C, Pascu M. *Practical Guide to Polyethylene*. Shrewsbury, UK: RAPRA Technology; 2005. ISBN:978-1-85957-493-5.
4. Menzel T, Meides N, Mauel A, et al. Degradation of low-density polyethylene to nanoplastic particles by accelerated weathering. *Sci Total Environ*. 2022;826:154035. doi:10.1016/j.scitotenv.2022.154035
5. Rojas-Trejo MF, Valadez-Gonzalez A, Veleva L, Benavides R, Rodriguez-Hernandez MT, Moreno-Chulim MV. Impact of combined thermo- and photo-oxidation on the physicochemical properties of oxo-biodegradable low-density polyethylene films. *Polymers (Basel)*. 2025;17(2):193. doi:10.3390/polym17020193
6. Yuan CS, Hassan A, Ghazali MIH, Ismail AF. Heat sealability of laminated films with LLDPE and LDPE as the sealant materials in bar sealing application. *J Appl Polym Sci*. 2007;104(6):3736–3745. doi:10.1002/app.25863
7. Gugumus F. Physico-chemical aspects of polyethylene processing in an open mixer 2: Functional group formation on PE–LD processing. *Polym Degrad Stabil*. 2000;67(1):35–47. doi:10.1016/S0141-3910(99)00115-9
8. Ivanov I, Akhmedova D, Koroleva Y, Shatalov D. Sterility of ophthalmic solutions as a factor in the evolution of primary packaging for eye drops: A literature review. *Sci Pharm*. 2024;3(1):39–49. doi:10.58920/sciphar0301211
9. European Directorate for the Quality of Medicines & HealthCare. European Pharmacopoeia. General chapter 3.1.2: Polyolefins (301033). Strasbourg, France: European Directorate for the Quality of Medicines & HealthCare; 2025. https://pheur-online.edqm.eu/home/. Accessed February 14, 2026.
10. Jung MR, Horgen FD, Orski SV, et al. Validation of ATR FT-IR to identify polymers of plastic marine debris, including those ingested by marine organisms. *Mar Pollut Bull*. 2018;127:704–716. doi:10.1016/j.marpolbul.2017.12.061
11. Lee H, Cho K, Ahn TK, et al. Solid-state relaxations in linear low-density (1-octene comonomer), low-density, and high-density polyethylene blends. *J Polym Sci B Polym Phys*. 1997;35(10):1633–1642. doi:10.1002/(SICI)1099-0488(19970730)35:10%3C1633::AID-POLB15%3E3.0.CO;2-B
12. Lomovskoy VA, Shatokhina SA. Relaxation phenomena in low-density and high-density polyethylene. *Polymers (Basel)*. 2024;16(24):3510. doi:10.3390/polym16243510
13. Munaro M, Akcelrud L. Correlations between composition and crystallinity of LDPE/HDPE blends. *J Polym Res*. 2008;15(1):83–88. doi:10.1007/s10965-007-9146-2
14. Zaribaf FP, Gill HS, Pegg EC. Chemical stability of oil-infused polyethylene. *J Biomater Appl*. 2021;35(9):1168–1179. doi:10.1177/0885328220977353
15. Depan D, Chirdon W, Khattab A. Morphological and chemical analysis of low-density polyethylene crystallized on carbon and clay nanofillers. *Polymers (Basel)*. 2021;13(10):1558. doi:10.3390/polym13101558
16. Garrido-López Á, Santa-Cruz A, Moreno E, Cornago J, Cañas MC, Tena MT. Determination of cosmetic ingredients causing extrusion-coated and adhesive joint multilayer packaging delamination. *Packag Technol Sci*. 2009;22(7):415–429. doi:10.1002/pts.863
17. Bolte L, Gers-Barlag H, Heinsohn G, Daniels R. Migration of cosmetic components into polyolefins. *Adv Polym Technol*. 2024;2024(1):2680899. doi:10.1155/adv/2680899
18. Giannakas AE, Baikousi M, Karabagias VK, et al. Low-density polyethylene-based novel active packaging film for food shelf-life extension via thyme-oil control release from SBA-15 nanocarrier. *Nanomaterials*. 2024;14(5):423. doi:10.3390/nano14050423

# Biotechnological strategies to combat antibiotic resistance

# Strategie biotechnologiczne w walce z opornością na antybiotyki

Weronika Łakomy[1,A,B,D], Maria Myślińska[1,A,B,D], Ewa Tarnawska[1,A,B,D], Wojciech Rogóż[2,E,F], Karolina Kulig[2,C,E,F], Aleksandra Owczarzy[2,E,F], Małgorzata Maciążek-Jurczyk[2,E,F]

[1] Student Research Group at the Department of Physical Pharmacy, Faculty of Pharmaceutical Sciences in Sosnowiec, Medical University of Silesia, Katowice, Poland
[2] Department of Physical Pharmacy, Faculty of Pharmaceutical Sciences in Sosnowiec, Medical University of Silesia, Katowice, Poland

A – research concept and design; B – collection and/or assembly of data; C – data analysis and interpretation;
D – writing the article; E – critical revision of the article; F – final approval of the article

Polymers in Medicine, ISSN 0370-0747, eISSN 2451-2699 *Polim Med*. 2026;56(1):41–51

**Address for correspondence**
Małgorzata Maciążek-Jurczyk
E-mail: mmaciazek@sum.edu.pl

**Funding sources**
None declared

**Conflict of interest**
None declared

Received on December 18, 2025
Reviewed on January 14, 2026
Accepted on March 2, 2026

Published online as ahead of print on June 30, 2026

## Abstract

This article aims to present the current state of knowledge on four major biotechnological antimicrobial strategies and to evaluate their potential clinical applications in the context of increasing antibiotic resistance. Approaches such as phage therapy, CRISPR-Cas9 gene editing, nanoparticles, and antimicrobial peptides (AMPs) may significantly contribute to limiting the spread of resistance genes. Particular attention is given to advances in genetic engineering that enable precise targeting and elimination of resistance determinants, as well as to the therapeutic potential of the microbiome. A literature review of studies published between 2010 and 2025 was conducted using the following keywords: antimicrobial resistance, phage therapy, CRISPR-Cas9, AMPs, and nanotechnology. Both review articles and original studies, including preclinical and clinical data, were considered. Phage therapy demonstrates high efficacy against antibiotic-resistant pathogens, particularly in the form of phage cocktails and genetically engineered phages. Antimicrobial peptides exhibit broad-spectrum activity and can be structurally optimized to improve stability and selectivity. CRISPR-Cas9 systems enable targeted elimination of resistance genes or direct disruption of pathogen genomes, while nanotechnology facilitates drug delivery, biofilm penetration, and bactericidal activity, particularly through metal-based nanoparticles. Notably, all approaches show potential for synergistic use with conventional antibiotics. Biotechnological treatment strategies may become a key component in combating antibiotic resistance. However, their clinical implementation requires further research, comprehensive safety evaluation, regulatory development, and integration into medical practice. Advances in these areas could significantly reduce the global burden of infectious diseases.

## Streszczenie

Celem niniejszego artykułu jest przedstawienie aktualnego stanu wiedzy na temat czterech głównych biotechnologicznych strategii przeciwdrobnoustrojowych oraz ocena ich potencjalnych zastosowań klinicznych w kontekście narastającej oporności na antybiotyki. Metody takie jak terapia fagowa, edycja genów CRISPR-Cas9 czy zastosowanie nanocząsteczek i peptydów przeciwdrobnoustrojowych mogą znacząco przyczynić się do ograniczenia rozprzestrzeniania się genów oporności. Szczególną uwagę zwrócono na innowacje w inżynierii genetycznej, które pozwalają na precyzyjne niszczenie genów oporności, a także na wykorzystanie mikrobiomu jako potencjalnego narzędzia terapeutycznego. Przeprowadzono przegląd literatury naukowej opublikowanej w latach 2010–2025, przeszukując bazy danych za pomocą słów kluczowych: oporność na antybiotyki, terapia fagowa, CRISPR-Cas9, peptydy przeciwdrobnoustrojowe, nanotechnologia. Uwzględniono zarówno artykuły przeglądowe, jak i oryginalne badania obejmujące dane przedkliniczne i kliniczne. Terapia fagowa wykazuje wysoką skuteczność w zwalczaniu szczepów opornych na antybiotyki, zwłaszcza w postaci koktajli fagowych i fagów modyfikowanych genetycznie. Peptydy przeciwdrobnoustrojowe charakteryzują się

**Cite as**
Łakomy W, Myślińska M, Tarnawska E, et al. Biotechnological strategies to combat antibiotic resistance. *Polim Med*. 2026;56(1):41–51. doi:10.17219/pim/218777

**DOI**
10.17219/pim/218777

szerokim spektrum działania i mogą być modyfikowane strukturalnie w celu zwiększenia stabilności i selektywności. Systemy CRISPR-Cas9 umożliwiają precyzyjną eliminację genów oporności lub zniszczenie genomu patogenu, a nanotechnologia umożliwia skuteczne dostarczanie leków, penetrację biofilmu i działanie bakteriobójcze poprzez nanocząstki metali. Wszystkie te metody wykazują potencjał synergii z antybiotykami. Biotechnologiczne strategie leczenia mogą w przyszłości stać się kluczowym elementem w walce z opornością na antybiotyki. Ich wdrożenie wymaga dalszych badań klinicznych, oceny bezpieczeństwa, opracowania ram prawnych i integracji z praktyką medyczną. Postęp w tych obszarach mógłby znacząco zmniejszyć globalne obciążenie chorobami zakaźnymi.

**Key words:** nanotechnology, antimicrobial peptides, antimicrobial resistance, CRISPR-Cas9, phage therapy

**Słowa kluczowe:** nanotechnologia, peptydy przeciwdrobnoustrojowe, terapia fagowa, oporność na środki przeciwdrobnoustrojowe, CRISPR-Cas9

## Highlights

- Biotechnological antimicrobial strategies address antimicrobial resistance using phage therapy, CRISPR-Cas9, peptides, and nanotechnology.
- Phage therapy shows high efficacy against multidrug-resistant pathogens and enables precision antimicrobial treatment.
- CRISPR-Cas9 targets resistance genes, while peptides and nanoparticles enhance antimicrobial activity and biofilm penetration.
- Biotechnological strategies combined with antibiotics may improve infection control and reduce antimicrobial resistance.

## Highlights

- Biotechnological antimicrobial strategies address antimicrobial resistance using phage therapy, CRISPR-Cas9, peptides, and nanotechnology.
- Phage therapy shows high efficacy against multidrug-resistant pathogens and enables precision antimicrobial treatment.
- CRISPR-Cas9 targets resistance genes, while peptides and nanoparticles enhance antimicrobial activity and biofilm penetration.
- Biotechnological strategies combined with antibiotics may improve infection control and reduce antimicrobial resistance.

## Introduction

### The problem of antibiotic resistance and the limitations of conventional therapy

Pathogenic microorganisms have accompanied human populations throughout history, contributing substantially to morbidity and mortality. The 20$^{th}$ century marked a major breakthrough in the treatment of bacterial infections with the discovery of penicillin and other antimicrobial agents. However, the widespread and often inappropriate use of antibiotics, combined with the natural evolutionary adaptability of pathogens, has led to the emergence of multiple resistance mechanisms and a progressive decline in treatment efficacy.[1]

Antimicrobial agents include antibiotics, antivirals, antifungals, and antiparasitic drugs. They are used to inhibit the growth and replication of microorganisms or to eliminate them, thereby preventing and treating infectious diseases in humans, animals, and plants. These agents may be natural, semi-synthetic, or synthetic and act through a variety of mechanisms. Antimicrobial resistance (AMR) is defined as the ability of microorganisms to survive and remain viable despite exposure to antimicrobial agents. This reduces the effectiveness of therapy and can render infections difficult or even impossible to treat. As a consequence, AMR contributes to increased disease transmission, greater infection severity, long-term health complications, and mortality. Although AMR is a natural phenomenon driven by genetic variation, its accelerated emergence and spread are largely attributable to human activity, particularly the inappropriate and excessive use of antimicrobials in human medicine, veterinary practice, and agriculture.[2]

Bacterial resistance represents a major challenge for healthcare systems worldwide, as the increasing use of antibiotics promotes the emergence of resistant strains. This results in reduced treatment effectiveness, prolonged hospital stays, increased healthcare costs, and higher mortality rates. Individuals with compromised immune systems, including patients with cancer, HIV infection, or diabetes, are particularly vulnerable to its consequences.

In addition, limited public awareness and the inappropriate prescribing and use of antimicrobial agents by both healthcare professionals and patients further exacerbate the problem. If current trends persist, even minor injuries or common infections may become life-threatening, marking a transition toward a so-called "post-antibiotic era." International organizations such as the World Health Organization (WHO), the European Centre for Disease Prevention and Control (ECDC), and the Centers for Disease Control

and Prevention (CDC) have implemented coordinated strategies to address AMR, including risk assessment, identification of contributing factors, and the development of control measures. According to a 2019 CDC report, AMR threats are classified into several categories. Urgent threats include infections caused by carbapenem-resistant *Acinetobacter* spp., *Candida auris*, *Clostridioides difficile*, drug-resistant *Neisseria gonorrhoeae*, and carbapenem-resistant Enterobacterales. Serious threats include multidrug-resistant *Pseudomonas aeruginosa*, antibiotic-resistant *Campylobacter* spp., and vancomycin-resistant *Enterococcus* (VRE). Based on resistance profiles, microorganisms are further classified as multidrug-resistant (MDR), extensively drug-resistant (XDR), or pan-drug-resistant (PDR).[1,3]

In low- and middle-income countries, AMR is further exacerbated by limited healthcare infrastructure, insufficient funding, and inadequate regulation of antibiotic use. Multidrug-resistant Gram-negative bacteria pose a particularly serious threat, especially among neonates. These include members of the family Enterobacteriaceae, notably strains producing extended-spectrum β-lactamases (ESBLs) as well as carbapenem-resistant organisms. Key examples include *Klebsiella pneumoniae* producing carbapenemases such as KPC (*K. pneumoniae* carbapenemase) and strains harboring New Delhi metallo-β-lactamase (NDM), as well as NDM-producing *Escherichia coli*. In response to this growing threat, global initiatives such as NeoAMR have been launched to develop strategies for antibiotic management in neonatal sepsis, particularly in low- and middle-income settings. The NeoAMR initiative involves more than 40 partners across 25 countries and focuses on four main areas: identification of key pathogens responsible for neonatal sepsis, surveillance of resistance patterns, standardization of diagnostic protocols, and optimization of empirical antibiotic therapy. The project has collected over 36,000 clinical samples and conducted microbiological analyses and genotyping of isolates to identify dominant MDR strains. The findings revealed substantial geographical variation in pathogen distribution, along with an alarmingly high prevalence of resistance to first-line antibiotics, including aminopenicillins and third-generation cephalosporins. Based on these data, region-specific recommendations for the empirical treatment of neonatal sepsis were developed, taking into account local resistance patterns.[3] NeoAMR also serves as a platform for scientific and educational collaboration, supporting the development of local diagnostic capacity and the establishment of AMR surveillance networks in high-burden regions. This initiative represents a modern, integrated approach to addressing AMR in one of the most vulnerable patient populations – newborns – and may serve as a model for future AMR control programs.[4]

# Objectives

Developing and implementing strategies to limit the emergence and spread of antibiotic resistance is essential, as bacteria employ a range of sophisticated molecular defense mechanisms. These include genetic mutations, acquisition of resistance genes, and the use of mobile genetic elements, all of which contribute to the persistence and dissemination of resistance. A comprehensive understanding of the molecular and genetic basis of MDR, the mechanisms underlying its mobilization, and the dynamics of its spread in both environmental and human populations is critical for designing effective strategies to combat AMR.[1–3]

## Bacterial resistance mechanisms

Bacterial resistance to antimicrobial agents is a major factor limiting the effectiveness of infection treatment. Bacteria employ a variety of resistance strategies, both intrinsic and acquired, that enable them to survive and proliferate in the presence of antibiotics. Understanding these mechanisms is essential for the development of effective alternative therapies and for limiting the further spread of AMR. This section outlines the key mechanisms of bacterial resistance, with particular emphasis on the role of horizontal gene transfer in their dissemination.[5]

### Main types of bacterial resistance mechanisms

Resistance mechanisms can be broadly classified into several categories based on their mode of action and spectrum of activity against different classes of antibiotics.

1. Enzymatic inactivation of antibiotics: This is one of the most common resistance mechanisms and involves the production of bacterial enzymes that degrade or structurally modify antibiotic molecules. Examples include β-lactamases (e.g., ESBL, KPC, NDM), which hydrolyze the β-lactam ring of penicillins and cephalosporins,[1,6,7] as well as enzymes such as acetyltransferases, phosphotransferases, and nucleotidyl transferases, which modify aminoglycosides.[8,9]
2. Modification of antibiotic target sites: This mechanism involves genetic mutations or structural alterations in bacterial molecules that serve as targets for antimicrobial agents. Examples include methylation of ribosomal RNA mediated by erm genes in Streptococcus spp., which reduces susceptibility to macrolides,[10] as well as alterations in penicillin-binding proteins (PBPs) that underlie β-lactam resistance in methicillin-resistant Staphylococcus aureus (MRSA).[11]
3. Reduced membrane permeability: This mechanism is particularly important in Gram-negative bacteria, where decreased permeability of the outer membrane limits antibiotic entry through porin channels. Mutations in genes encoding porins (e.g., OmpF and OmpC

in *E. coli*) can reduce susceptibility to β-lactams, including carbapenems.[12]

4. Active efflux of antibiotics (efflux pumps): Bacteria can actively expel antibiotics from the cell via membrane-associated transport proteins. Examples include the MexAB–OprM efflux system in *P. aeruginosa* and the NorA pump in *S. aureus*.[13] This mechanism is a major contributor to MDR.
5. Bypass of metabolic pathways: Bacteria may evade the effects of antibiotics by utilizing alternative enzymes or metabolic pathways that are not targeted by the drug. A classic example is resistance to trimethoprim–sulfamethoxazole in *E. coli*, which is mediated by the production of a modified dihydrofolate reductase (DHFR) enzyme encoded by altered *dhfr* genes.[14]

Table 1 summarizes the mechanisms of bacterial resistance and provides representative examples of their occurrence. Many multidrug-resistant strains, including MDR, XDR, and PDR phenotypes, exhibit multiple resistance mechanisms simultaneously, which significantly complicates the treatment of infections.[15]

**Table 1.** Mechanisms of bacterial resistance and their occurrence

| Resistance mechanism | Description of action | Examples of bacteria/genes |
|---|---|---|
| Enzymatic inactivation | Enzymatic degradation or modification of the antibiotic | *E. coli* (ESBL, NDM), *K. pneumoniae* (KPC)[8,9] |
| Target modification | Mutations or structural modifications of target proteins | MRSA (PBP2a), *S. pneumoniae* (23S rRNA)[11] |
| Reduced permeability | Loss/change of porins reducing penetration of the biological membrane by the drug | *P. aeruginosa*, *E. coli* (OmpF, OmpC)[12] |
| Efflux pumps | Actively pumping the antibiotic out of the cell | *S. aureus* (NorA), *P. aeruginosa* (MexAB-OprM)[13] |
| Bypassing the metabolic pathway | Production of an alternative enzyme or pathway that is drug insensitive | *S. aureus* (mutation in the DHFR gene)[14] |

### The importance of gene transfer

Horizontal gene transfer (HGT) plays a key role in the spread of bacterial resistance. It allows for the rapid transfer of resistance genes between different species and strains of bacteria, regardless of phylogenetic relatedness. Horizontal gene transfer can occur according to one of the following patterns:

- Conjugation: Involves the direct transfer of genetic material, typically plasmids, between bacterial cells via cell-to-cell contact. This is the most common mechanism for the dissemination of genes encoding enzymes such as ESBLs, KPC, and NDM β-lactamases.[16]
- Transformation: The uptake of free extracellular DNA by competent bacteria. For example, *Streptococcus pneumoniae* can incorporate DNA fragments containing penicillin resistance genes into its genome.[17]
- Transduction: The transfer of genetic material mediated by bacteriophages. Although less common than conjugation, this mechanism can also contribute to the spread of resistance genes.[18]

Genetic determinants of antibiotic resistance may be located on plasmids, transposons, integrons, and complex mosaic genetic elements composed of multiple mobile DNA sequences. Plasmids are extrachromosomal, autonomously replicating DNA molecules, typically circular, while transposons are mobile elements capable of relocating within the genome. Integrons are genetic platforms that capture and express gene cassettes through site-specific recombination. For example, class 1 integrons, commonly found in Enterobacterales, contain gene cassettes encoding multiple resistance determinants, along with integrase genes that facilitate their integration and expression within the host genome.[19] The dissemination of resistance genes is strongly influenced by environmental factors, including selective pressure exerted by antibiotic use, co-selection mechanisms (e.g., the co-occurrence of antibiotic resistance and heavy metal tolerance genes on the same plasmid), and the formation of biofilms, which promote horizontal gene transfer.[20] Importantly, metagenomic studies have demonstrated that antibiotic resistance genes are also present in microorganisms inhabiting environments with minimal human impact. These findings suggest that such genes are part of the natural resistome; however, anthropogenic activity significantly enhances their mobilization and spread.[20]

## The aim of this work

The increasing resistance of microorganisms to antimicrobial agents represents one of the most serious public health challenges of the 21st century. It is estimated that antibiotic-resistant bacterial infections directly caused approx. 1.27 million deaths worldwide in 2019, exceeding those attributed to HIV/AIDS or malaria, while deaths associated with AMR reached 4.95 million globally.[20] Projections suggest that by 2050, infections caused by antibiotic-resistant bacteria could result in up to 10 million deaths annually, potentially surpassing cancer as a leading cause of mortality.[20] The primary drivers of this crisis include the overuse and misuse of antibiotics in human medicine, veterinary practice, and agriculture, as well as the limited development of new antimicrobial classes.[21] In response to these challenges, there is an urgent need to explore innovative therapeutic strategies. Modern biotechnology offers several promising approaches to combating infections caused by drug-resistant microorganisms. This review focuses on 4 such strategies: phage therapy, antimicrobial

peptides (AMPs), CRISPR-Cas9-based genome editing, and nanotechnology.[22] Each approach is characterized by a distinct mechanism of action and is currently at a different stage of clinical development. This paper aims to present and discuss biotechnological strategies for combating antibiotic resistance and to evaluate their potential clinical applications.

## Methodology of literature search and selection

The literature review was conducted using the MEDLINE (via PubMed), Scopus, and Web of Science databases, with a particular focus on publications from 2010 to 2025. The search strategy was based on the following keywords: AMR, phage therapy, CRISPR-Cas9, AMPs, and nanotechnology. Both review articles and original studies reporting preclinical and clinical data were included in the analysis.

## Results

### Phage therapy

Phage therapy involves the use of bacteriophages – viruses that specifically infect bacteria – to treat infections. A key characteristic of phages is their high host specificity, as a given phage typically targets only particular bacterial species or strains. This specificity enables the elimination of antibiotic-resistant bacteria without harming human cells or disrupting the normal microbiota.[23]

The clinical potential of phage therapy has been demonstrated in numerous case reports and preliminary studies. For example, successful treatment has been reported in infections caused by *Acinetobacter baumannii*, *P. aeruginosa*, MRSA, and *Klebsiella pneumoniae*. Importantly, phages are capable of infecting and disrupting biofilm-forming bacteria.[23,24] In addition, both in vitro and in vivo studies have demonstrated potential synergistic effects between bacteriophages and conventional antibiotics.[25]

At present, novel strategies are being developed to enhance the efficacy of phage therapy. One such approach is the use of phage cocktails, which consist of combinations of multiple bacteriophages capable of targeting different strains of a given bacterial species or even multiple species. This strategy is particularly advantageous in the treatment of polymicrobial infections. The use of phage cocktails may improve therapeutic efficacy while reducing the risk of resistance to individual phages.[25]

A growing body of evidence supports the effectiveness of phage therapy using phage cocktails. One of the first randomized clinical trials in this field was conducted by Jault et al. as part of the PhagoBurn project. The study evaluated a cocktail of twelve natural lytic bacteriophages targeting *P. aeruginosa* (PP1131) in patients with burn wound infections. Although the clinical efficacy was limited – primarily due to insufficient concentrations of active phages – the study demonstrated the safety of phage therapy and laid the groundwork for the development of standardized clinical protocols.[26] More recent studies have focused on optimizing the design of phage cocktails. For example, Vaitekenas et al. emphasized the importance of phage diversity within therapeutic mixtures. The inclusion of phages targeting different bacterial receptors – such as lipopolysaccharides (LPS), type IV pili (T4P), outer membrane proteins, or efflux pump structures – can reduce the likelihood of resistance development while enhancing therapeutic efficacy. This approach is particularly relevant in infections caused by *P. aeruginosa* in patients with cystic fibrosis, where complex biofilm structures are commonly observed.[27] In addition, Rastegar et al. investigated combination therapy using bacteriophages and antibiotics against biofilms formed by XDR *A. baumannii*. Their study evaluated a four-phage cocktail (SA1, Eva, Ftm, Gln) in combination with antibiotics (ampicillin/sulbactam, meropenem, and colistin). Phages were selected based on activity against clinical biofilm-forming isolates. The results demonstrated that phage–antibiotic combination therapy significantly enhanced biofilm eradication, indicating a synergistic effect. These findings highlight the potential of phage therapy as an adjunctive strategy in the treatment of infections caused by XDR *A. baumannii*, particularly in the context of increasing resistance to conventional therapies.[28]

Another promising direction in the development of phage therapy is the use of genetically engineered bacteriophages. These phages can be modified to enhance lytic activity, broaden host range, or introduce additional therapeutic functions. For example, some engineered phages can be equipped with CRISPR-Cas9 systems, enabling the targeted disruption of resistance genes within the bacterial genome. Other modifications include the ability to degrade biofilms or to evade bacterial defense mechanisms, such as restriction–modification systems.[21]

In a study by Selle et al., recombinant bacteriophages were engineered to selectively target *C. difficile* using a CRISPR-Cas3 system. These engineered phages, referred to as crPhage, contained customized CRISPR sequences designed to target the bacterial genome. Both in vitro and in vivo (murine) models demonstrated that crPhage more effectively reduced *C. difficile* burden compared to wild-type phages, while also limiting intestinal tissue damage. Importantly, these modifications decreased the risk of lysogeny and associated adverse effects, such as increased expression of bacterial toxins.[29,30]

Recombinant bacteriophages are also being developed as engineered constructs that combine features of multiple natural phages or are synthetically designed based on genomic sequences of known bacteriophages. Such phages may exhibit enhanced stability, increased activity, and reduced susceptibility to neutralization by the host immune system.[31] Phages can be modified in vitro using approaches such as CRISPR-Cas9-mediated editing (discussed later

in this paper) or homologous recombination (HDR), allowing them to be tailored to specific therapeutic needs. These modifications enable not only efficient bacterial killing but also the selective modulation of the host microbiota. This strategy offers new opportunities for personalized phage therapy and the treatment of diseases associated with microbiota dysbiosis.[32] A compelling example of this approach is provided by Peters et al., who investigated short-term co-evolution of two bacteriophages (LP-048 and LP-125) and their interactions with phage-resistant *Listeria monocytogenes*. The study demonstrated that phage exposure exerted selective pressure on bacterial populations, leading to the emergence of phage-resistant strains. Importantly, co-infection with both phages resulted in spontaneous genetic recombination, giving rise to novel phage variants capable of infecting bacterial strains resistant to the original phages. These recombination events involved genes encoding proteins likely associated with host recognition and DNA interaction. These findings suggest that phage co-evolution and recombination may serve as natural mechanisms to expand host range and enhance the effectiveness of phage therapy against resistant bacterial populations.[33]

The advantages of phage therapy include the ability of bacteriophages to self-replicate at the site of infection, high tolerability in humans, and effectiveness against antibiotic-resistant strains.[23,24] However, several challenges remain. These include the narrow host range of individual phages, the need for personalized therapy, and the associated high costs, as well as the potential for bacteria to develop resistance to phages. Additional limitations include possible host immune responses to phages and the lack of standardized regulatory frameworks governing their clinical use.[25,34]

An example of a clinical facility offering phage therapy is the Phage Therapy Center at the Ludwik Hirszfeld Institute of Immunology and Experimental Therapy, Polish Academy of Sciences, in Wrocław. Operating since 2005, the center provides treatment within the framework of a therapeutic experiment, primarily for patients with chronic infections unresponsive to conventional antibiotic therapy. The treatment process begins with patient qualification, including the evaluation of medical history, prior treatments, and microbiological documentation. A key step is phage typing, which involves the laboratory selection of bacteriophages active against the bacterial strain isolated from the patient. The center offers treatment for infections caused by pathogens such as *S. aureus* (including MRSA), *P. aeruginosa*, *E. coli*, *K. pneumoniae*, *Enterococcus faecalis*, and *Proteus mirabilis*. Therapy is initiated after obtaining informed consent and may be administered via oral, rectal, or topical routes. Treatment typically lasts 6–8 weeks and is closely supervised by a multidisciplinary team. Reported effectiveness reaches approx. 40% in patients with chronic infections.[34]

## Antimicrobial peptides

Antimicrobial peptides are small bioactive molecules that constitute a key component of the innate immune system in many organisms. Their antimicrobial activity primarily involves disruption of microbial cell membranes, leading to rapid pathogen elimination. In addition, many AMPs interfere with intracellular processes, including protein, RNA, and DNA synthesis. Antimicrobial peptides exhibit a broad spectrum of activity against Gram-positive and Gram-negative bacteria, fungi, viruses, and certain parasites. Due to their distinct mechanism of action, resistance to AMPs develops less frequently compared to conventional antibiotics.[21,22] Antimicrobial peptides can be classified into several categories based on their origin, biosynthesis, structural characteristics, and biological functions (Table 2).

Certain clinically used antimicrobial agents, such as polymyxins (e.g., colistin), daptomycin, and glycopeptides (e.g., vancomycin), share functional similarities with AMPs, although they are not always classified as classical AMPs. Current research focuses on modifying naturally occurring peptides (e.g., melittin) and designing synthetic peptides with enhanced stability, selectivity, and reduced toxicity. An example of such an approach is murepavadin, a synthetic antimicrobial peptide with high specificity against *P. aeruginosa*. Murepavadin exerts its activity by binding to the outer membrane protein LptD, which is involved in LPS transport, leading to membrane destabilization and bacterial cell death. In addition, it demonstrates the ability to penetrate and disrupt bacterial biofilms, representing a significant advantage over many conventional antibiotics. Preclinical and clinical studies have demonstrated rapid bactericidal activity, high efficacy, and favorable safety profiles. As a result, murepavadin is considered a promising therapeutic candidate for the treatment of infections caused by MDR Gram-negative bacteria, particularly in the context of increasing resistance to existing antibiotics.[35]

Antimicrobial peptides may originate from natural sources (e.g., colistin, gramicidin) or be synthetically designed (e.g., pexiganan, omiganan). Natural AMPs are produced by a wide range of organisms, including bacteria (which produce bacteriocins such as colicins), fungi (e.g., copsin, plectasin), plants (e.g., plant defensins), insects (e.g., cecropins and insect defensins), and mammals, including humans (e.g., cathelicidins and defensins).[35–37] Increasing research efforts are focused on the development of peptide hybrids and AMP-based conjugates with nanoparticles or antibodies. These approaches aim to improve peptide stability, bioavailability, and target specificity. An example of such a strategy is the use of targeted nanocarriers, such as melittin-loaded nanoparticles, which have been investigated in early-stage studies, particularly in oncology. This approach enables controlled peptide release while reducing toxicity, including hemolytic effects.[35]

**Table 2.** Classification of antimicrobial peptides

| Criterion | Categories | Characteristics/Examples |
|---|---|---|
| 1. Origin | Eukaryotic | Mammals (human – LL-37, HBD-3), amphibians, fish, plants (γ-thionine), invertebrates (drosomycin) |
| | Prokaryotic | Polymyxins, gramicidins, bacitracin (products of bacterial metabolism) |
| 2. Method of biosynthesis | Ribosomal | Coded in DNA, synthesized in a cell, e.g., cathelicidins, defensins |
| | Non-ribosomal | Synthesis by enzymes, e.g., polymyxins, bacitracin |
| 3. Structure | Linear α-helical | LL-37, cecropine B |
| | β-sheet | Defensins α, β, θ |
| | Cyclic | Defensins θ, bactenecin |
| | Rich in specific amino acids | Indolicidin (tryptophan), OaBac (proline and arginine) |
| 4. Molecular family | Defensins<br>– α-defensins<br>– β-defensins<br>– θ-defensins<br>– of plants/invertebrates | 3 disulfide bridges, molecular weight 3–5 kDa<br>– HNP-1 to -4 (neutrophils), HD-5 and HD-6 (Paneth cells)<br>– HBD-1 to -4, secreted by epithelium<br>– RTD (macaques), BTD (baboons) – cyclic, absent in humans<br>– γ-thionins (plants), drosomycin (insects) |
| | Cathelicidins<br>– LL-37<br>– other | Precursor: pre-propeptide with cathelin domain<br>– The only human cathelicidin identified, active throughout the body<br>– CAP-18 (rabbit), SMAP29 (sheep), Saha-CATH (Tasmanian devil) |
| 5. Biological function | Direct action | Destruction of the cell membrane, disruption of DNA, RNA, and wall synthesis |
| | Immunomodulation | Cytokine induction, chemotaxis, activation of immune cells |
| | Neutralization of toxins | Anti-endotoxin activity (e.g., LPS) |
| | Anti-cancer activity | Magainin 2, chrysofsin 1, cecropin B |
| 6. Unusual examples (species) | Komodo dragon | cAMPs homologous to histones (VK6–VK25) |
| | Giant panda | Cathelicidin-AM – fast antibacterial effect |
| | Tasmanian devil | Saha-CATH cathelicidins 1 to 6, broad spectrum of action |

LPS – lipopolysaccharide; cAMP – cationic antimicrobial peptides.

Similarly, Xuan et al. described a synthetic antimicrobial peptide, SAAP-148, which exhibited potent antibacterial activity against pathogens such as *S. aureus* and *Acinetobacter baumannii*. The peptide demonstrated the ability to penetrate biofilms and eliminate bacteria in regions that are difficult to access with conventional antibiotics. Importantly, SAAP-148 showed enhanced synergistic effects when combined with tetracyclines, highlighting the potential of AMPs as components of combination therapies for drug-resistant infections.[38] Research has also focused on the topical application of AMPs, including their incorporation into antimicrobial dressings and bioactive implant coatings.[35,36] For example, Liu et al. developed a hydrogel coating containing WR and Bac2A peptides, which demonstrated durability, bioactivity in vivo, and strong antibacterial and anticoagulant properties in animal models. Such coatings may be applied to medical devices, including catheters, stents, and vascular grafts, to prevent infection and thrombosis.[39]

Another distinguishing feature of AMPs is their immunomodulatory activity. In addition to direct antimicrobial effects, AMPs can modulate the host immune response by promoting immune cell migration, regulating cytokine production, and enhancing wound healing. For example, LL-37 and defensins have been shown to play key roles in these processes.[35] As a result, AMPs are increasingly recognized as multifunctional molecules with both antimicrobial and therapeutic properties. Preclinical studies indicate that AMPs can enhance the efficacy of conventional antibiotics, for instance by facilitating their penetration into bacterial biofilms. Some peptides, such as IDR-1018, not only inhibit bacterial growth but also reduce biofilm formation and inflammation, making them promising candidates for the treatment of chronic wounds and skin infections.[40] Antimicrobial peptides can also be incorporated into combination therapies with other non-conventional approaches, such as bacteriophages or nanomaterials, enabling the development of multimodal treatment strategies with enhanced efficacy. Another promising direction involves antibody–peptide conjugates, which allow targeted delivery of AMPs to specific pathogens.[36] Despite their therapeutic potential, the clinical application of AMPs remains limited by challenges such as susceptibility to enzymatic degradation, short half-life, and potential cytotoxicity. Consequently, significant research efforts are focused on improving their stability and safety through strategies such as peptide cyclization, incorporation of D-amino acids, and encapsulation in nanocarriers (e.g., liposomes or hydrogels). These approaches enhance delivery efficiency and may facilitate broader clinical implementation of AMP-based therapies.[35,36]

## CRISPR-Cas9 and genome editing

The CRISPR-Cas9 system is an adaptive defense mechanism in bacteria that has been transformed into a precise tool for genome editing. Its action is based on a complex of the Cas9 protein and a synthetic single-stranded guide RNA, known as single guide RNA (sgRNA). This RNA contains two functional parts: a crRNA sequence, responsible for recognizing a specific DNA fragment, and trans-activating CRISPR RNA (tracrRNA), which stabilizes the complex with the Cas9 protein.

After the Cas9–sgRNA complex is formed, the genome is searched for a sequence complementary to the guide RNA (gRNA), i.e., the editing target. An important condition for its recognition is the presence of a short DNA motif called the protospacer adjacent motif (PAM), which most often takes the form of the trinucleotide sequence "NGG." When the Cas9 protein locates the correct target site with an adjacent PAM motif in the DNA, a local fragment of the double helix unfolds. The gRNA hybridizes with one of the DNA strands, allowing the enzyme to precisely align itself. Once the match is confirmed, Cas9 activates its two cutting domains – HNH, which cleaves the strand complementary to the RNA, and RuvC, which cleaves the opposite strand. The result of the enzyme's action is a double-strand break (DSB). Damaged DNA must be repaired by endogenous cellular mechanisms. Most often, non-homologous end joining (NHEJ) occurs, which involves rapid joining of the cut ends without the use of a template. This process is efficient, but often introduces minor errors, such as insertions or deletions, which can lead to gene inactivation. The second possible scenario is repair by HDR, which requires the presence of an externally supplied DNA template. This allows for precise modification, e.g., repair of a mutation or introduction of a new sequence.[41] In therapeutic applications, this strategy can be used to eliminate resistance genes or selectively destroy pathogenic bacteria.[21,42]

In clinical practice and preclinical studies, CRISPR-Cas9 systems are primarily used in two therapeutic strategies. The first involves the precise excision of genes encoding antibiotic resistance factors, such as *mcr-1* or *blaNDM*, which in turn restores bacterial sensitivity to conventional antibiotics. The second strategy involves the complete destruction of the pathogen's genome, leading to bacterial cell death. Both methods use modified bacteriophages – phagemids – as vectors for the selective delivery of CRISPR-Cas9 elements to target cells. This approach allows for the effective elimination of resistant strains without affecting the rest of the microbiome.[21,42]

In 2024, the first-ever clinical trial using CRISPR-Cas3 therapy, delivered via a phage vector, was conducted, targeting *E. coli* strains in uncomplicated urinary tract infections (UTIs) in women. The trial, called ELIMINATE, was conducted by Locus Biosciences and aimed to evaluate the safety, tolerability, and efficacy of a preparation containing a cocktail of engineered phages integrated with the CRISPR-Cas3 system. The study group consisted of 39 adult women aged 18–70. All participants had confirmed active UTI of bacterial etiology (*E. coli*) and a history of at least 1 previous episode of UTI within the past year. The goal of the treatment was to reduce bacterial colonization and clinical symptoms. The therapeutic design was based on a cocktail of three modified lytic bacteriophages that naturally infect *E. coli*. Each phage was additionally equipped with a construct containing the CRISPR-Cas3 system, targeting highly conserved regions of the bacterial genome. After entering the bacterial cell, the phages induced a lytic cycle of infection, and Cas3 initiated extensive DNA degradation, which ultimately led to the complete destruction of the bacterial cell. The observed mechanism was significantly more effective than the precise DNA cleavage characteristic of the Cas9 protein. Importantly, no serious adverse effects were reported. No bacterial resistance to phages or CRISPR-Cas3 was observed either. The described study provides the first clinical evidence of the effectiveness of CRISPR-Cas3 as a therapeutic tool in the treatment of bacterial infections in humans. This technology combines the selectivity of bacteriophages with precise destruction of the microbial genome, making it a potentially groundbreaking solution in the fight against antibiotic resistance.[43] Further clinical trials are currently underway using CRISPR-Cas9 systems as an alternative approach for the treatment of infections caused by resistant strains, including *P. aeruginosa* and *K. pneumoniae*.[21,42]

The advantages of this approach include high precision, the ability to adapt the therapy to new strains, and minimal impact on the microbiome.[23] The challenges, however, include difficulties in delivering CRISPR-Cas9 systems to sites of infection, the possibility of immune reactions, and the risk of so-called off-target effects, i.e., unintended DNA cleavage outside the target sequence. This phenomenon results from the fact that gRNA can bind not only to a perfectly matched site in the genome but also to other highly similar sequences, leading to unintended genetic modifications. Such mutations can disrupt the function of important genes, increasing the risk of, among other things, cellular toxicity and carcinogenesis. A study conducted by Feng Zhang's team using the GUIDE-seq method demonstrated that Cas9 can cleave DNA at numerous unintended locations, raising concerns about the safety of this technology.[44] Similar conclusions were reported by Schaefer et al., who observed unexpected mutations in mice treated with CRISPR-based therapy.[45] In response to these challenges, more precise variants of Cas9 are being developed, along with improved gRNA design strategies aimed at minimizing off-target effects.[46] Nevertheless, CRISPR-Cas9 remains one of the most promising strategies in addressing the growing problem of AMR.[23]

## Nanotechnology

Nanotechnology in antimicrobial medicine is developing dynamically as an innovative approach to combating antibiotic resistance. The use of nanomaterials such as metal nanoparticles (silver, gold, copper), metal oxides (e.g., ZnO, $TiO_2$), and polymer and lipid carriers enables the delivery of drugs to hard-to-reach sites of infection, penetration of bacterial biofilms, and direct bactericidal action. These nanoparticles are characterized by sizes ranging from 1 to 100 nm, which allows them to readily penetrate cell membranes and interact with microbial macromolecules at the molecular level.[47,48] Silver nanoparticles (AgNPs) exhibit strong antimicrobial activity against Gram-positive and Gram-negative bacteria, acting by damaging cell membranes, generating reactive oxygen species (ROS), and disrupting metabolic processes.[47,49] Their effectiveness against antibiotic-resistant strains makes them a promising tool for combating MDR pathogens. Furthermore, nanosilver can be combined with conventional antibiotics, leading to a synergistic effect – reducing the required doses and potentially delaying the development of resistance.

An example of this is the study by Panáček et al., which evaluated the effectiveness of combining AgNPs with various antibiotics (including ampicillin, gentamicin, and streptomycin) against selected strains of *E. coli* and *S. aureus*. It was shown that the combinations of antibacterial agents significantly increased antimicrobial activity, especially when compared to antibiotics used in monotherapy. The observed synergistic effect allowed the minimum inhibitory concentration (MIC) to be reduced severalfold. On this basis, the authors indicated that nanosilver may enhance the activity of conventional drugs and constitute an effective antimicrobial strategy against drug-resistant strains.[50] Gold nanoparticles (AuNPs) also exhibit high antibacterial activity, as demonstrated by the study of Muhammad Ilyas et al.[51] Their aim was to investigate the antimicrobial properties of AuNPs against selected bacterial pathogens. The authors used AuNPs synthesized biologically using *Delphinium denudatum* leaf extract and then assessed their effects on *E. coli*, *S. aureus*, *P. aeruginosa*, and *Salmonella typhi*. The results showed that AuNPs exhibited clear bactericidal activity, with effectiveness dependent on particle concentration and size. The authors also noted that nanoparticles likely interact with the bacterial cell membrane, causing damage and disruption of metabolic processes. This study confirms the potential of AuNPs as an alternative or complement to conventional antimicrobial therapy.[51]

Nanocarriers such as liposomes, dendrimers, or polymer nanoparticles (e.g., made of poly(lactic-co-glycolic acid) (PLGA)) can function as drug delivery systems while protecting active substances against degradation, increasing their bioavailability, and directing them to sites of infection. Examples include nanocarriers of colistin or vancomycin, which improve antibiotic penetration into bacterial biofilms and reduce drug toxicity. A study conducted by Zhang et al. assessed the effectiveness of colistin-loaded PLGA nanoparticles in the treatment of infections caused by MDR strains of *P. aeruginosa*. To conduct this study, nanoparticles were prepared by emulsification and solvent evaporation and then evaluated in vitro and in vivo (in a mouse model). It was found that colistin encapsulated in nanocarriers exhibited increased biofilm penetration and antibacterial effectiveness while reducing renal toxicity compared to the free form of the drug. These results confirm the potential of nanotechnology to treat antibiotic-resistant bacterial infections more safely and effectively.[44]

An innovative approach is the so-called "intelligent nanomaterials", which respond to environmental conditions such as pH, the presence of bacterial enzymes, or light. These allow controlled drug release in response to stimuli.[47] Nanotechnology is also widely used in diagnostics, offering fast, sensitive, and specific methods for detecting pathogens and resistance markers. Knowledge of their occurrence is extremely valuable because it enables rapid adaptation of pharmacotherapy to the properties of pathogens. An example of the effective use of nanotechnology in diagnostics is a study conducted by Hong-zhi Pan et al.[52] It describes an electrochemical nanosensor based on AuNPs and graphene-modified electrodes, used to detect the presence of a resistance gene encoding *Klebsiella pneumoniae* carbapenemase. To conduct this study, the authors used hybridization of specific DNA probes with the target gene fragment and detection of the electrochemical signal, which enabled detection of the gene with high sensitivity and a short analysis time. The results showed that this platform enables rapid detection of resistance genes without the need for DNA amplification, making it a promising tool in microbiological diagnostics, especially in hospital settings.[52]

The advantages of nanotechnology include increased therapeutic effectiveness, the ability to deliver drugs to hard-to-reach sites, the ability to overcome biological barriers, and the potential reduction of antibiotic doses. Challenges include the toxicity of some nanomaterials, tissue accumulation, the lack of long-term safety studies, and the need for legal regulations regarding their use.[47,48]

## Discussion

Summarizing the main findings, all discussed strategies – phage therapy, AMPs, CRISPR-Cas9 gene editing, and nanotechnology – are characterized by high therapeutic potential. Their strength lies in the possibility of selective action against MDR pathogens and their effectiveness against biofilms. The weakness lies in the limited number of clinical trials, difficulties in standardizing methods, and issues related to safety and legal regulations. Compared to previous studies, there is an increasing emphasis

on personalized therapy and the combination of different strategies in a multimodal approach. Differences in research results arise mainly from variations in experimental models and the limited scale of clinical trials. It is important for clinicians that these innovative methods may complement or replace conventional antibiotics in the future, especially in the treatment of infections caused by MDR and XDR strains. Further clinical trials are necessary to determine the long-term effectiveness and safety of these new therapies. Challenges also include unanswered questions regarding interactions with the microbiome, the risk of immunogenicity, and the potential for secondary resistance.

## Conclusions

Microbial resistance to conventional antibiotics necessitates the introduction of innovative treatment methods. Biotechnological strategies such as phage therapy, AMPs, CRISPR-Cas9 systems, and nanotechnology open up new therapeutic possibilities. Their development may significantly affect clinical practice in the future but requires further research, funding, and the establishment of an appropriate legislative framework. The implementation of these methods should go hand in hand with public education, the rational use of antibiotics, and interdisciplinary collaboration. Shortening the path from basic research to clinical practice is crucial for effectively combating the growing problem of AMR.

## Use of AI and AI-assisted technologies

Not applicable.

### References


1. Abushaheen MA, Muzaheed, Fatani AJ, et al. Antimicrobial resistance, mechanisms and its clinical significance. *Disease-a-Month*. 2020;66(6):100971. doi:10.1016/j.disamonth.2020.100971
2. World Health Organization (WHO). Antimicrobial resistance. Geneva, Switzerland: World Health Organization (WHO); 2023. Accessed April 1, 2026. https://www.who.int/news-room/fact-sheets/detail/antimicrobial-resistance
3. Saha M, Sarkar A. Review on multiple facets of drug resistance: A rising challenge in the 21st century. *J Xenobiot*. 2021;11(4):197–214. doi:10.3390/jox11040013
4. Sands K, Carvalho MJ, Portal E, et al. Characterization of antimicrobial-resistant Gram-negative bacteria that cause neonatal sepsis in seven low- and middle-income countries. *Nat Microbiol*. 2021;6(4):512–523. doi:10.1038/s41564-021-00870-7
5. Laxminarayan R, Matsoso P, Pant S, et al. Access to effective antimicrobials: A worldwide challenge. *Lancet*. 2016;387(10014):168–175. doi:10.1016/S0140-6736(15)00474-2
6. Bush K, Bradford PA. Interplay between β-lactamases and new β-lactamase inhibitors. *Nat Rev Microbiol*. 2019;17(5):295–306. doi:10.1038/s41579-019-0159-8
7. Wu W, Feng Y, Tang G, Qiao F, McNally A, Zong Z. NDM metallo-β-lactamases and their bacterial producers in healthcare settings. *Clin Microbiol Rev*. 2019;32(2):e00115-18. doi:10.1128/CMR.00115-18
8. Ramirez MS, Tolmasky ME. Aminoglycoside modifying enzymes. *Drug Resist Updat*. 2010;13(6):151–171. doi:10.1016/j.drup.2010.08.003
9. Rogóż W, Kulig K, Knopik-Kocłęga M, Szkudlarek A, Maciążek-Jurczyk M. Analysis of antibiotic resistance genetic conditioning of Enterobacteriaceae NDM-1 family members and the related epidemiological threat in Poland. *Med Res J*. 2019;4(4):216–224. doi:10.5603/MRJ.a2019.0039
10. Miklasińska-Majdanik M. Mechanisms of resistance to macrolide antibiotics among *Staphylococcus aureus*. *Antibiotics (Basel)*. 2021;10(11):1406. doi:10.3390/antibiotics10111406
11. Chambers HF, DeLeo FR. Waves of resistance: *Staphylococcus aureus* in the antibiotic era. *Nat Rev Microbiol*. 2009;7(9):629–641. doi:10.1038/nrmicro2200
12. Doumith M, Ellington MJ, Livermore DM, Woodford N. Molecular mechanisms disrupting porin expression in ertapenem-resistant *Klebsiella* and *Enterobacter* spp. clinical isolates from the UK. *J Antimicrob Chemother*. 2009;63(4):659–667. doi:10.1093/jac/dkp029
13. Poole K. Efflux-mediated antimicrobial resistance. *J Antimicrob Chemother*. 2005;56(1):20–51. doi:10.1093/jac/dki171
14. Eliopoulos GM, Huovinen P. Resistance to trimethoprim-sulfamethoxazole. *Clin Infect Dis*. 2001;32(11):1608–1614. doi:10.1086/320532
15. Tacconelli E, Carrara E, Savoldi A, et al. Discovery, research, and development of new antibiotics: The WHO priority list of antibiotic-resistant bacteria and tuberculosis. *Lancet Infect Dis*. 2018;18(3):318–327. doi:10.1016/S1473-3099(17)30753-3
16. Partridge SR, Kwong SM, Firth N, Jensen SO. Mobile genetic elements associated with antimicrobial resistance. *Clin Microbiol Rev*. 2018;31(4):e00088-17. doi:10.1128/CMR.00088-17
17. Domenech A, Slager J, Veening JW. Antibiotic-induced cell chaining triggers pneumococcal competence by reshaping quorum sensing to autocrine-like signaling. *Cell Rep*. 2018;25(9):2390–2400.e3. doi:10.1016/j.celrep.2018.11.007
18. Davies EV, Winstanley C, Fothergill JL, James CE. The role of temperate bacteriophages in bacterial infection. *FEMS Microbiol Lett*. 2016;363(5):fnw015. doi:10.1093/femsle/fnw015
19. Gillings MR, Gaze WH, Pruden A, Smalla K, Tiedje JM, Zhu YG. Using the class 1 integron-integrase gene as a proxy for anthropogenic pollution. *ISME J*. 2015;9(6):1269–1279. doi:10.1038/ismej.2014.226
20. Berendonk TU, Manaia CM, Merlin C, et al. Tackling antibiotic resistance: The environmental framework. *Nat Rev Microbiol*. 2015;13(5):310–317. doi:10.1038/nrmicro3439
21. Pacia DM, Brown BL, Minssen T, Darrow JJ. CRISPR-phage antibacterials to address the antibiotic resistance crisis: Scientific, economic, and regulatory considerations. *J Law Biosci*. 2024;11(1):lsad030. doi:10.1093/jlb/lsad030
22. Lazar V, Oprea E, Ditu LM. Resistance, tolerance, virulence and bacterial pathogen fitness: Current state and envisioned solutions for the near future. *Pathogens*. 2023;12(5):746. doi:10.3390/pathogens12050746
23. Ahmed M, Kayode H, Okesanya O, et al. CRISPR-cas systems in the fight against antimicrobial resistance: Current status, potentials, and future directions. *Infect Drug Resist*. 2024;17:5229–5245. doi:10.2147/IDR.S494327
24. Sawa T, Moriyama K, Kinoshita M. Current status of bacteriophage therapy for severe bacterial infections. *J Intensive Care*. 2024;12(1):44. doi:10.1186/s40560-024-00759-7
25. Kapoor A, Mudaliar SB, Bhat VG, Chakraborty I, Prasad ASB, Mazumder N. Phage therapy: A novel approach against multidrug-resistant pathogens. *3 Biotech*. 2024;14(10):256. doi:10.1007/s13205-024-04101-8
26. Jault P, Leclerc T, Jennes S, et al. Efficacy and tolerability of a cocktail of bacteriophages to treat burn wounds infected by *Pseudomonas aeruginosa* (PhagoBurn): A randomised, controlled, double-blind phase 1/2 trial. *Lancet Infect Dis*. 2019;19(1):35–45. doi:10.1016/S1473-3099(18)30482-1
27. Vaitekenas A, Tai AS, Ramsay JP, Stick SM, Kicic A. *Pseudomonas aeruginosa* resistance to bacteriophages and its prevention by strategic therapeutic cocktail formulation. *Antibiotics (Basel)*. 2021;10(2):145. doi:10.3390/antibiotics10020145
28. Rastegar S, Skurnik M, Tadjrobehkar O, et al. Synergistic effects of bacteriophage cocktail and antibiotics combinations against extensively drug-resistant *Acinetobacter baumannii*. *BMC Infect Dis*. 2024;24(1):1208. doi:10.1186/s12879-024-10081-0
29. Selle K, Fletcher JR, Tuson H, et al. In vivo targeting of *Clostridioides difficile* using phage-delivered CRISPR-Cas3 antimicrobials. *mBio*. 2020;11(2):e00019-20. doi:10.1128/mBio.00019-20

30. Balcha FB, Neja SA. CRISPR-Cas9 mediated phage therapy as an alternative to antibiotics. *Animal Dis*. 2023;3(1):4. doi:10.1186/s44149-023--00065-z
31. Zalewska-Piątek B, Piątek R. Bacteriophages as potential tools for use in antimicrobial therapy and vaccine development. *Pharmaceuticals (Basel)*. 2021;14(4):331. doi:10.3390/ph14040331
32. Łobocka M, Dąbrowska K, Górski A. Engineered bacteriophage therapeutics: Rationale, challenges and future. *BioDrugs*. 2021;35(3):255–280. doi:10.1007/s40259-021-00480-z
33. Peters TL, Song Y, Bryan DW, Hudson LK, Denes TG. Mutant and recombinant phages selected from in vitro coevolution conditions overcome phage-resistant *Listeria monocytogenes*. *Appl Environ Microbiol*. 2020;86(22):e02138-20. doi:10.1128/AEM.02138-20
34. Instytut Immunologii i Terapii Doświadczalnej im. Ludwika Hirszfelda Polskiej Akademii Nauk. Ośrodek Terapii Fagowej. Wrocław, Poland: Instytut Immunologii i Terapii Doświadczalnej im. Ludwika Hirszfelda Polskiej Akademii Nauk; 2025. Accessed April 1, 2026. https://hirszfeld.pl/struktura/centrum-medyczne/osrodek-terapii-fagowej/
35. Zheng S, Tu Y, Li B, et al. Antimicrobial peptide biological activity, delivery systems and clinical translation status and challenges. *J Transl Med*. 2025;23(1):292. doi:10.1186/s12967-025-06321-9
36. Sharma D, Dhiman I, Das S, et al. Recent advances in therapeutic peptides: Innovations and applications in treating infections and diseases. *ACS Omega*. 2025;10(17):17087–17107. doi:10.1021/acsomega.5c02077
37. Fry DE. Antimicrobial peptides. *Surg Infect*. 2018;19(8):804–811. doi:10.1089/sur.2018.194
38. Xuan J, Feng W, Wang J, et al. Antimicrobial peptides for combating drug-resistant bacterial infections. *Drug Resist Updat*. 2023;68:100954. doi:10.1016/j.drup.2023.100954
39. Liu K, Zhang F, Wei Y, et al. Dressing blood-contacting materials by a stable hydrogel coating with embedded antimicrobial peptides for robust antibacterial and antithrombus properties. *ACS Appl Mater Interfaces*. 2021;13(33):38947–38958. doi:10.1021/acsami.1c05167
40. Mookherjee N, Anderson MA, Haagsman HP, Davidson DJ. Antimicrobial host defence peptides: Functions and clinical potential. *Nat Rev Drug Discov*. 2020;19(5):311–332. doi:10.1038/s41573-019-0058-8
41. Janik E, Niemcewicz M, Ceremuga M, Krzowski L, Saluk-Bijak J, Bijak M. Various aspects of a gene editing system: CRISPR-Cas9. *Int J Mol Sci*. 2020;21(24):9604. doi:10.3390/ijms21249604
42. Bikard D, Barrangou R. Using CRISPR-Cas systems as antimicrobials. *Curr Opin Microbiol*. 2017;37:155–160. doi:10.1016/j.mib.2017.08.005
43. Kim P, Sanchez AM, Penke TJR, et al. Safety, pharmacokinetics, and pharmacodynamics of LBP-EC01, a CRISPR-Cas3-enhanced bacteriophage cocktail, in uncomplicated urinary tract infections due to *Escherichia coli* (ELIMINATE): The randomised, open-label, first part of a two-part phase 2 trial. *Lancet Infect Dis*. 2024;24(12):1319–1332. doi:10.1016/S1473-3099(24)00424-9
44. Zhang L, Pornpattananangkul D, Hu CMJ, Huang CM. Development of nanoparticles for antimicrobial drug delivery. *Curr Med Chem*. 2010; 17(6): 585–594. doi: 10.2174/092986710790416290
45. Schaefer KA, Wu WH, Colgan DF, et al. Unexpected mutations after CRISPR–Cas9 editing in vivo. Nat Methods. 2017; 14(6): 547–548. doi:10.1038/nmeth.4293
46. Tsai SQ, Zheng Z, Nguyen NT, et al. GUIDE-seq enables genome-wide profiling of off-target cleavage by CRISPR-Cas nucleases. *Nat Biotechnol*. 2015;33(2):187–197. doi:10.1038/nbt.3117
47. Hetta HF, Ramadan YN, Al-Harbi AI, et al. Nanotechnology as a promising approach to combat multidrug resistant bacteria: A comprehensive review and future perspectives. *Biomedicines*. 2023;11(2):413. doi:10.3390/biomedicines11020413
48. Pelgrift RY, Friedman AJ. Nanotechnology as a therapeutic tool to combat microbial resistance. *Adv Drug Deliv Rev*. 2013;65(13–14):1803–1815. doi:10.1016/j.addr.2013.07.011
49. Shaikh S, Nazam N, Rizvi SMD, et al. Mechanistic insights into the antimicrobial actions of metallic nanoparticles and their implications for multidrug resistance. *Int J Mol Sci*. 2019;20(10):2468. doi:10.3390/ijms20102468
50. Panáček A, Kvítek L, Smékalová M, et al. Bacterial resistance to silver nanoparticles and how to overcome it. *Nat Nanotechnol*. 2018;13(1):65–71. doi:10.1038/s41565-017-0013-y
51. Muhammad Ilyas M, Arif M, Ahmad A, et al. Biogenic synthesis of gold nanoparticles, characterization and their biomedical applications. *Int J Biomed Mater Res*. 2022;10(2):39–52. doi:10.11648/j.ijbmr.20221002.12.
52. Pan HZ, Yu HW, Wang N, et al. Electrochemical DNA biosensor based on a glassy carbon electrode modified with gold nanoparticles and graphene for sensitive determination of *Klebsiella pneumoniae* carbapenemase. *J Biotechnol*. 2015;214:133–138. doi:10.1016/j.jbiotec.2015.09.015

# Zinc oxide nanoparticles potentiate the antibacterial and antibiofilm efficacy of imipenem against *Klebsiella pneumoniae*

Deyar Jassim Shawi[A,B], Ayaid Khadem Zgair[A,C–F]

Department of Biology, College of Science, University of Baghdad, Iraq

A – research concept and design; B – collection and/or assembly of data; C – data analysis and interpretation;
D – writing the article; E – critical revision of the article; F – final approval of the article

Polymers in Medicine, ISSN 0370-0747, eISSN 2451-2699 *Polim Med*. 2026;56(1):53–63

**Address for correspondence**
Ayaid Khadem Zgair
E-mail: ayaid.zgair@sc.uobaghdad.edu.iq

**Funding sources**
None declared

**Conflict of interest**
None declared

**Acknowledgements**
The authors thank all staff members of the Department of Biology, College of Science, University of Baghdad, for their support during the experimental work. Furthermore, the authors thank the hospitals and clinical laboratories that helped the researchers isolate and identify the bacterial isolates.

Received: February 7, 2026
Revised: March 4, 2026
Accepted: March 30, 2026
Final review: March 6, 2026

Published online on June 30, 2026

## Abstract

**Background.** Biofilm extracellular polymeric matrix (EPS) biomass plays a central role in bacterial resistance to carbapenems, especially imipenem (IPM), which poses a serious threat to public health.

**Objectives.** The present study aims to use ZnO NPs to improve the susceptibility of imipenem-resistant *Klebsiella pneumoniae* (IRKP) to imipenem (IPM) and to reduce biofilm extracellular polymeric matrix (EPS) biomass.

**Materials and methods.** Susceptibility to IPM and biofilm formation were evaluated in 20 uropathogenic *K. pneumoniae* isolates. ZnO NPs were prepared using an extract of *Thymus vulgaris* leaves. The effects of sub-minimum inhibitory concentrations (MICs) of IPM and ZnO NPs on biofilm formation were evaluated. The additive effect of sub-MICs of ZnO NPs on IRKP susceptibility to IPM and biofilm formation was assessed.

**Results.** The diameter of the prepared ZnO NPs was less than 50 nm. Biofilm formation negatively correlated with inhibition zone diameter ($r = -0.819$, $p = 0.001$) and positively with IPM MICs ($r = 0.79$, $p = 0.001$). Sub-MICs of IPM and ZnO NPs reduced biofilm formation on polystyrene in a concentration-dependent manner. The synergistic role of sub-MICs of ZnO NPs in decreasing the MICs of IPM against *K. pneumoniae* was observed, from $250 \pm 50$ µg/mL to $116.6 \pm 14.4$ µg/mL (at ½, ¼, and ⅛ MICs of ZnO NPs), while 1⁄16 MIC of ZnO NPs decreased the MICs of IPM to $125 \pm 25$ µg/mL. The 1⁄32 and 1⁄64 MICs of ZnO NPs reduced the MICs of IPM to $141.6 \pm 14.4$ µg/mL and $158.3 \pm 80.36$ µg/mL, respectively. The greatest reduction in biofilm extracellular polymeric matrix (EPS) formation was observed at the highest concentrations of the IPM/ZnO NP combination, while the lowest reduction was observed at the lowest concentrations of both materials ($p < 0.05$).

**Conclusions.** The present study demonstrated a synergistic effect of sub-MIC ZnO NPs on the antibacterial and antibiofilm activities of imipenem against *K. pneumoniae* (IRKP).

**Key words:** *Klebsiella pneumoniae*, ZnO NPs, imipenem, biofilm formation

**Cite as**
Shawi DJ, Zgair AK. Zinc oxide nanoparticles potentiate the antibacterial and antibiofilm efficacy of imipenem against *Klebsiella pneumoniae*. *Polim Med*. 2026;56(1):53–63. doi:10.17219/pim/220166

**DOI**
10.17219/pim/220166

# Background

Biofilm-associated infections with this bacterial species are difficult to treat because the extracellular polymeric matrix (EPS) of the biofilm acts as a barrier, reducing antibiotic penetration and promoting bacterial resistance.[1] Therefore, new strategies to reduce biofilm formation may help limit and enhance the activity of antibiotics against resistant bacteria. New approaches in materials science have focused on polymers and nanoparticles (NPs) as multifunctional platforms for antibacterial applications.[2] Natural and synthetic polymers play a significant role in the design of functional nanoparticles, which serve as stabilizers, carriers, or surface modifiers. Polymeric materials can modify nanoparticle size, surface charge, dispersibility, and interactions with biological cellular processes; they can improve biocompatibility and antimicrobial activity.[3] Furthermore, polymer–nanoparticle composites offer tunable physicochemical properties that can be used to disrupt bacterial membrane systems, alter biofilm structure, and improve drug activity in terms of delivery efficiency against bacterial cellular processes.[4]

The rise in antimicrobial resistance among Gram-negative pathogens has become a critical global health concern, especially during periods of limited availability of effective antibiotics. Imipenem (IPM) is a beta-lactam antibiotic commonly used to treat infections caused by multidrug-resistant (MDR) organisms, including *Klebsiella pneumoniae*.[5] This bacterial species is an opportunistic pathogen responsible for several infectious diseases, including wound and soft tissue infections, pneumonia, bloodstream infections (septicemia), liver abscess (invasive *Klebsiella* syndrome), eye infections, and urinary tract infections (UTIs).[6] The resistance of this bacterial species to a wide spectrum of antibiotics and its ability to adhere to biotic and abiotic surfaces (forming biofilms) are associated with increased virulence.[7]

Metal oxide nanoparticles are of great importance due to their antimicrobial properties and multiple effects on cellular processes. One of the most important is zinc oxide (ZnO) nanoparticles, valued for their chemical stability, low cost, and recognized biocompatibility in biological systems. ZnO NPs exhibit broad-spectrum antibacterial activity via multiple mechanisms, including the production of reactive oxygen species, disruption of bacterial cell membranes, and the release of $Zn^{2+}$ ions, which interfere with bacterial metabolic processes.[8] On the other hand, the nanoscale size of ZnO NPs and their high surface-to-volume ratio facilitate interactions with bacterial metabolism and the polymers of biofilm matrices.[9]

The combination of nanoparticles with polymer-based systems disrupts bacterial cell function by controlling nanoparticle aggregation and enhancing interactions with microbial populations, including the biofilm matrix. This process has shown that nanoparticles can more effectively penetrate biofilm matrices and improve antibiotic activity.[10] Thus, combining nanoparticles with antibiotics can act synergistically by increasing bacterial cell membrane permeability, reducing efflux pump activity, and facilitating antibiotic penetration into the biofilm matrix.[11]

# Objectives

The additive antibacterial and antibiofilm effects of ZnO NPs on imipenem activity are highlighted, underscoring the roles of material properties and nanoscale interactions in improving antibacterial outcomes. This approach demonstrates a new strategy to enhance imipenem activity against imipenem-resistant *K. pneumoniae*, a serious public health threat.

# Materials and methods

## Ethical approval

The study was approved by the Human Ethics Committee of the Department of Biology, College of Science, University of Baghdad, Iraq, with reference No. CSEC/1025/0112, on October 9, 2025.

## Bacterial isolates

Aseptic midstream urine samples were collected from 183 patients diagnosed with urinary tract infections (UTIs) who attended Al-Yarmouk Teaching Hospital, Baghdad, Iraq, for routine clinical evaluation. Patients who had received antibiotic therapy within 72 h prior to sample collection were excluded, and informed consent was obtained from all participants. The urine samples were cultured on MacConkey agar (HiMedia, Mumbai, India) and incubated at 37°C for 18 h. Large, mucoid, pink colonies (lactose-fermenting colonies) were selected for further identification. Gram staining was performed, followed by biochemical tests, including oxidase, indole, urease, and citrate utilization tests. A VITEK DensiCheck instrument and fluorescence system (bioMérieux, Marcy-l'Étoile, France) (ID-GNB card) were used to identify the isolates as *K. pneumoniae*. All confirmed *K. pneumoniae* isolates were stored at –80°C in tryptic soy broth (TSB) supplemented with 20% (v/v) glycerol for long-term preservation until further use.

### Kirby–Bauer method

This method was used to determine the response of *K. pneumoniae* isolates to imipenem (IPM). Bacterial suspensions were prepared and adjusted to a turbidity equivalent to a 0.5 McFarland standard and then uniformly inoculated onto Mueller–Hinton agar (MHA; HiMedia, India). Imipenem disks were placed on the MHA surface, and

the plates were incubated for 18 h at 37°C. Inhibition zones were measured in millimeters. Inhibition zone diameters were measured as the total diameter, including the 6 mm disk diameter, in accordance with Clinical and Laboratory Standards Institute (CLSI) guidelines. The isolates were categorized as susceptible (S), intermediate (I), or resistant (R) to IPM based on CLSI breakpoints.[12,13]

## ZnO NPs preparation

The previously described standard method was followed for biosynthesis using Thymus vulgaris leaves purchased from local markets in Baghdad, Iraq. The leaves were washed several times to remove dust, then dried and ground into a powder. Fifty grams of the powder were added to 500 mL of distilled water and heated to 80°C for 45 min. The mixture was cooled to room temperature and filtered through Whatman filter paper (No. 1) to remove solids. The clear suspension was stored at 4°C until use.[14]

Fifty milliliters of the leaf extract were added dropwise to a 0.1 M $Zn(NO_3)_2{\cdot}6H_2O$ (Sigma-Aldrich, St. Louis, USA) solution prepared in deionized double-distilled water (1:1, v/v). The reaction was carried out at ambient room temperature (21°C), maintained in the laboratory without the use of an incubator, under continuous magnetic stirring (Heidolph Instruments, Germany). The pH was adjusted to 8 with 0.1 M NaOH until the mixture turned milky white and was then heated at 80°C for 3 h to obtain a brownish paste. The sedimented growth fluid was separated from the ZnO NPs by centrifugation at 7,000 × g for 10 min (Benchtop High Speed Centrifuge CFG-17H, Scitek, China). The solid powder was removed using methanol. Following the ethanol wash, distilled water was used several times to further wash the ZnO NPs. The ZnO NPs were dried in an oven (Memmert GmbH, Schwabach, Germany) at 70°C until completely dry.[14]

The prepared ZnO NPs were characterized using atomic force microscopy (AFM; Innova® AFM; Bruker, Santa Barbara, USA). For AFM analysis, a thin film of the nanoparticles was deposited on a glass substrate. Scanning electron microscopy (SEM) was also performed (Zeiss EVO® LS 15; Carl Zeiss AG, Jena, Germany); a smear of ZnO NPs was prepared on a glass surface and coated with a thin layer of platinum to enhance conductivity for imaging.[14,15]

## MTT assay

In this method, the cytotoxicity of ZnO NPs on MCF-7 human breast cancer cells was evaluated using the MTT assay, a colorimetric indicator of cell viability. MCF-7 cells (ATCC) were cultured in RPMI-1640 medium (Sigma-Aldrich, USA) supplemented with 10% fetal bovine serum (FBS, Sigma-Aldrich, USA) and 1% penicillin/streptomycin (MSE SAS, France) and maintained at 37°C in a humidified atmosphere containing 5% $CO_2$. Cells were seeded into 96-well tissue culture plates at a density of $10^4$ cells/well, incubated overnight, and then treated under the above conditions for 24 h and 72 h.[16]

A stock solution of ZnO NPs was prepared, and serial two-fold dilutions were made in complete culture medium (100, 50, 25, 10, 5, and 1 µg/mL). The negative control consisted of untreated cells cultured in medium alone. The growth medium was removed, and 100 µL of medium containing ZnO NPs was added, followed by incubation for 24 h under standard culture conditions. Following treatment, the medium was discarded, and 20 µL of MTT solution (1 mg/mL) was added to each well and incubated for 4 h at 37°C to allow viable cells to reduce MTT into insoluble purple formazan crystals. (Note: the 4 h incubation refers specifically to the formazan development step, not the treatment duration). The MTT solution was then removed, and 100 µL of dimethyl sulfoxide (DMSO) was added to dissolve the formazan crystals. Absorbance was measured at 570 nm using a microplate reader (Bio-Rad, USA).[17,18] Cell viability was expressed as a percentage relative to untreated control cells using the following formula:

$$\text{Cell viability}\left(\%\right) = \left(\frac{\text{Abs}_{\text{treated}}}{\text{Abs}_{\text{control}}}\right) \times 100$$

## Minimum inhibitory concentrations

The broth microdilution method was used to determine the minimum inhibitory concentrations (MICs) of IPM and ZnO NPs against *K. pneumoniae* isolates. Two-fold serial dilutions of IPM (Medscape, New York City, USA) were prepared in Mueller–Hinton broth (MHB; HiMedia, India) in a U-shaped microtiter plate. The standardized bacterial inoculum was adjusted to an optical density of 0.1 at 600 nm, equivalent to approximately 1–2 × $10^8$ CFU/mL (0.5 McFarland standard), and then diluted 1 : 100 in MHB to achieve a final inoculum of approximately 5 × $10^5$ CFU/mL per well, consistent with CLSI M07 broth microdilution guidelines. Five microliters of *K. pneumoniae* suspension were added to each well. The bacterial suspension was prepared by washing the overnight growth of *K. pneumoniae* with sterile phosphate-buffered saline (PBS; 0.1 M, pH 7.2) using centrifugation at 6,500 × g for 10 min (Benchtop High Speed Centrifuge CFG-17H, Scitek, China). The bacterial suspension was adjusted to an optical density of 0.1 at 600 nm (Thermo Fisher Scientific, USA). Plates were incubated at 37°C for 18 h, and MICs were defined as the lowest concentrations that completely inhibited visible bacterial growth. Three controls were prepared: MHB with bacterial isolate (first control), wells containing MHB only (second control), and two-fold serial dilutions of antibiotic only (third control). A similar method was followed to measure the MICs of ZnO NPs against *K. pneumoniae* isolates.[15,19]

## Biofilm formation

In this method, 100 µL of sterile Tryptic Soy Broth (TSB; HiMedia, India) supplemented with 0.25% (w/v) glucose was added to the wells of flat-bottom polystyrene tissue culture plates. TSB was supplemented with 0.25% (w/v) glucose to enhance biofilm formation on polystyrene surfaces, as glucose promotes the production of extracellular polymeric substances. Five microliters of a standard inoculum of *K. pneumoniae* were added to each well (as described in the method for MIC evaluation), and the plates were incubated at 37°C for 24 h. The TSB was discarded, and the plates were washed three times with distilled water. The plates were then dried and stained with 100 µL of 0.4% Hucker crystal violet for 15 min, followed by washing five times with distilled water. After the wells were dried, 100 µL of anhydrous ethanol (Sigma-Aldrich, USA) was added to each well. Absorbance was measured at 590 nm using a microplate reader (BioTek 800 TS; BioTek, Winooski, USA). The experiment was performed in triplicate.[19,20]

## Effect of sub-MICs on biofilm formation

In this experiment, the effects of sub-MIC concentrations of IPM and ZnO NPs on biofilm formation by *K. pneumoniae* isolates were investigated. A biofilm formation assay similar to that previously described,[19] with minor modifications, was used. Serial dilutions of sub-MICs of either ZnO NPs or IPM were prepared in TSB (HiMedia, India) and dispensed into the flat-bottom wells of a 96-well polystyrene microtiter plate. Five microliters of a standard *K. pneumoniae* inoculum (as described in the MIC evaluation method) were added to the wells, and the plates were incubated at 37°C for 24 h. Following incubation, the wells were washed three times with distilled water, dried, and stained with 0.4% Hucker crystal violet for 15 min. After drying, anhydrous ethanol was added to each well. Absorbance was measured at 590 nm using a microplate reader (BioTek 800 TS; BioTek, Winooski, USA). The experiment was repeated three times.[19]

## Synergistic effect of ZnO NPs and IPM on MICs

The checkerboard microdilution method, performed in a 96-well U-bottom polystyrene microtiter plate, was used to evaluate the synergistic effect of ZnO NPs on the susceptibility (as measured by MICs) of *K. pneumoniae* (resistant to IPM) to IPM. Briefly, 100 µL of sterile MHB (HiMedia, India) was added to each well. Two-fold serial dilutions of IPM were prepared horizontally across the plate (columns 1–12), yielding final concentrations ranging from 1000 to 0.48 µg/mL. Two-fold serial dilutions of ZnO NPs corresponding to sub-MICs (½ MIC to $\frac{1}{128}$ MIC) were prepared vertically from row A to row G. Five microliters of a standard inoculum of *K. pneumoniae* (as described in the MIC preparation method) were added to the wells. The plates were gently shaken and incubated at 37°C for 24 h. The MIC was defined as the lowest concentration of IPM that inhibited visible bacterial growth. Row H was considered the first control, showing the MIC of IPM (without ZnO NPs). Control groups were as follows: first control – IPM serial dilutions without ZnO NPs; second control – bacterial growth control (MHB + bacteria only); third control – sterility control (MHB only); fourth control – ZnO NPs at sub-MIC concentrations with bacterial inoculum without IPM; fifth control – IPM serial dilutions without nanoparticles. The experiment was repeated three times.

## Synergistic effect of ZnO NPs and IPM on biofilm formation

A similar procedure was followed to assess the synergistic effect of ZnO NPs on the MICs of IPM against an IPM-resistant *K. pneumoniae* isolate that produced the highest level of biofilm biomass, with minor modifications. TSB was used instead of MHB, and a 96-well flat-bottom polystyrene microtiter plate was used instead of a 96-well U-bottom plate. After incubation, the plates were washed three times with distilled water, dried, and stained with 100 µL of 0.4% Hucker crystal violet for 15 min. After washing and drying, 100 µL of anhydrous ethanol (Sigma-Aldrich, USA) was added to each well. Absorbance was measured at 590 nm using a microplate reader (BioTek 800 TS; BioTek, Winooski, USA). The experiment was repeated three times.[19–21]

## Statistical analyses

The statistical analyses and graphs were generated using Origin v. 8.4 (OriginLab, Northampton, USA). The chi-square test was performed using SPSS v. 26 (IBM, USA) for comparisons of categorical resistance data. Data were presented as means ± standard error (M ± SE). Student's t-test and one-way analysis of variance (ANOVA) were used to assess statistical significance. Correlations were evaluated using Pearson's correlation coefficient. A p-value of less than 0.05 was considered statistically significant.

# Results

## Bacterial isolates and IPM susceptibility

In the present study, twenty *K. pneumoniae* isolates were obtained from 183 urine samples collected from patients with UTIs. The isolates were initially identified using biochemical tests, and species-level identification was subsequently confirmed using the VITEK® 2 system. In the current study, the incidence of UTIs caused by *K. pneumoniae* was 10.92%.

The Kirby–Bauer disk diffusion method showed that the inhibition zone diameters of the twenty *K. pneumoniae* isolates ranged from 7.5 ± 0.8 mm (Kp14) to 31.7 ± 3.2 mm (Kp8). All inhibition zone diameters reported represent the total diameter, including the 6 mm disk diameter, consistent with CLSI measurement guidelines. MIC values were also used to assess the susceptibility of these isolates to IPM. The MICs of IPM against the 20 isolates ranged from 0.24 µg/mL (Kp1, Kp6, Kp8) to 250 µg/mL (Kp4, Kp9, Kp14, Kp20), confirming the inverse relationship between MIC and inhibition zone diameter. The current study indicates variable susceptibility to IPM. Of the 20 isolates, 7 (35%) were susceptible to IPM, 1 (5%) was intermediate (I), and 12 (60%) were resistant to IPM. This finding indicates a high prevalence of IPM resistance. Overall, an inverse relationship between inhibition zone diameter and MIC was observed, supporting the validity of the susceptibility testing (Table 1).

**Table 1.** Imipenem susceptibility of twenty *K. pneumoniae* isolates, as determined according to CLSI guidelines, and their ability to form biofilms. This table presents inhibition zone diameters (mm), minimum inhibitory concentrations (MIC, µg/mL), and biofilm formation measured as absorbance at 590 nm for the isolates. The isolates were categorized as susceptible (S), intermediate (I), or resistant (R) to IPM based on CLSI breakpoints

| No. of isolates | Inhibition zone (mm) of IPM | MIC (µg/mL) of IPM | Category | Biofilm (OD 590 nm) |
|---|---|---|---|---|
| Kp1 | 25 ± 3.2 | 0.24 | S | 0.28 ± 0.19 |
| Kp2 | 14 ± 1.9 | 62.5 | R | 0.60 ± 0.18 |
| Kp3 | 21.1 ± 2.9 | 1.95 | I | 0.46 ± 0.14 |
| Kp4 | 9.4 ± 1.5 | 250 | R | 0.77 ± 0.17 |
| Kp5 | 24.5 ± 3.4 | 0.48 | S | 0.55 ± 0.13 |
| Kp6 | 28.3 ± 4.8 | 0.24 | S | 0.47 ± 0.11 |
| Kp7 | 16.8 ± 2.2 | 62.5 | R | 0.59 ± 0.26 |
| Kp8 | 31.7 ± 3.2 | 0.24 | S | 0.23 ± 0.19 |
| Kp9 | 9.3 ± 0.8 | 250 | R | 0.79 ± 0.28 |
| Kp10 | 12 ± 1.6 | 125 | R | 0.68 ± 0.22 |
| Kp11 | 24 ± 3.6 | 0.97 | S | 0.27 ± 0.21 |
| Kp12 | 17 ± 3.2 | 31.25 | R | 0.43 ± 0.16 |
| Kp13 | 12 ± 1.2 | 62.5 | R | 0.59 ± 0.26 |
| Kp14 | 7.5 ± 0.8 | 250 | R | 0.82 ± 0.30 |
| Kp15 | 15 ± 1.7 | 15.6 | R | 0.53 ± 0.15 |
| Kp16 | 27 ± 3.6 | 0.48 | S | 0.40 ± 0.13 |
| Kp17 | 25 ± 3.8 | 0.97 | S | 0.64 ± 0.15 |
| Kp18 | 18 ± 2.6 | 15.6 | R | 0.60 ± 0.11 |
| Kp19 | 11 ± 1.3 | 125 | R | 0.62 ± 0.24 |
| Kp20 | 8.1 ± 1.4 | 250 | R | 0.73 ± 0.21 |

## Biofilm formation and IPM response

Table 1 shows that all studied isolates produced biofilm to varying extents, with optical density values ranging from 0.23 ± 0.19 to 0.82 ± 0.30. Based on biofilm production, 14 (70%) of the *K. pneumoniae* isolates were classified as strong biofilm producers, 5 (25%) as moderate producers, and 1 (5%) as a weak biofilm producer. The study showed that susceptible isolates had low to moderate biofilm production ($OD_{590} \approx 0.27–0.47$), the intermediate isolate (Kp3) had moderate biofilm formation ($OD_{590} = 0.46 \pm 0.13$), while resistant isolates had moderate to strong biofilm formation ($OD_{590} \approx 0.53–0.82$). The relatively high SD observed for Kp1 (0.28 ± 0.19) reflects biological variability in biofilm production between experimental replicates, which is characteristic of weak biofilm producers exhibiting inconsistent surface attachment behavior.

Figure 1 shows a strong correlation between biofilm formation and IPM inhibition zone diameters (r = –0.819, p = 0.00096; Fig. 1A), highlighting increased resistance in high-biofilm-producing isolates. However, a significant positive correlation was observed between biofilm formation and IPM MICs in 20 isolates of *K. pneumoniae* (r = 0.79, p = 0.00024; Fig. 1B). The current findings show a significant association between increased biofilm formation and increased IPM resistance in *K. pneumoniae*.

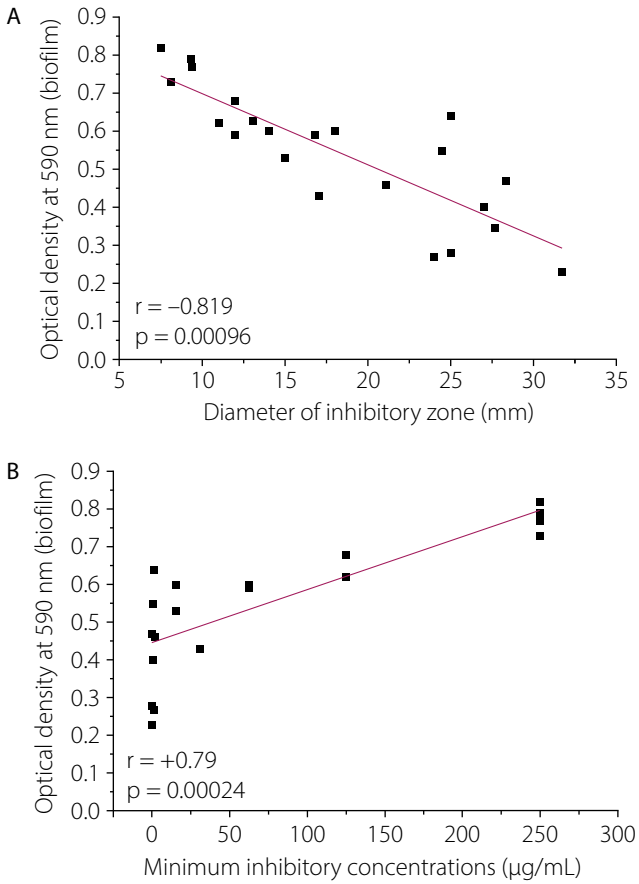


**Fig. 1.** Correlation between biofilm formation, expressed as crystal violet absorbance at 590 nm, and inhibition zone diameters of IPM against 20 *K. pneumoniae* isolates (A), as well as MIC values (B).

r – Pearson correlation coefficient; $p < 0.05$.

## ZnO NPs preparation and characterization

Figure 2A shows an atomic force microscopy (AFM) image of the surface topography of the synthesized ZnO NPs. The nanoparticles are uniformly distributed and have diameters of less than 50 nm, indicating successful preparation. The three-dimensional distribution shows that most particles are spherical to slightly irregular aggregated structures. Figure 2B shows a scanning electron microscopy (SEM) image of ZnO nanoparticles at × 100,000 magnification (scale bar = 500 nm). The nanoparticles exhibited an almost spherical morphology with slight agglomeration. The particle size observed in SEM is consistent with AFM measurements, confirming nanoscale dimensions below 50 nm. Overall, both AFM and SEM analyses confirm the successful synthesis of ZnO nanoparticles with nanoscale size, uniform dispersion, and typical spherical morphology, suitable for further physicochemical and biological applications.

## MTT assay

The cytotoxic effect of ZnO nanoparticles on MCF-7 breast cancer cells, assessed by the MTT assay, was demonstrated in this study. Figure 3A shows that MCF-7 cells were exposed to increasing concentrations of ZnO NPs (0–100 µg/mL) for 24 h, and cell viability was measured by determining the optical density (OD) at 570 nm. A concentration-dependent reduction in metabolic activity was observed. The greatest decrease in cancer cell viability was observed at higher ZnO NP concentrations (25, 50, and 100 µg/mL) compared with the untreated control (0 µg/mL). Data are presented as mean ± SD, and statistically significant differences relative to the control are indicated by asterisks (*, $p < 0.05$). Figure 3B shows the concentration–response curve, presenting percentage cell viability as a function of the $\log_{10}$ concentration of ZnO NPs. The half-maximal inhibitory concentration ($IC_{50}$) was determined to be 47.9 µg/mL, confirming the moderate cytotoxic effect of ZnO NPs against MCF-7 cells.

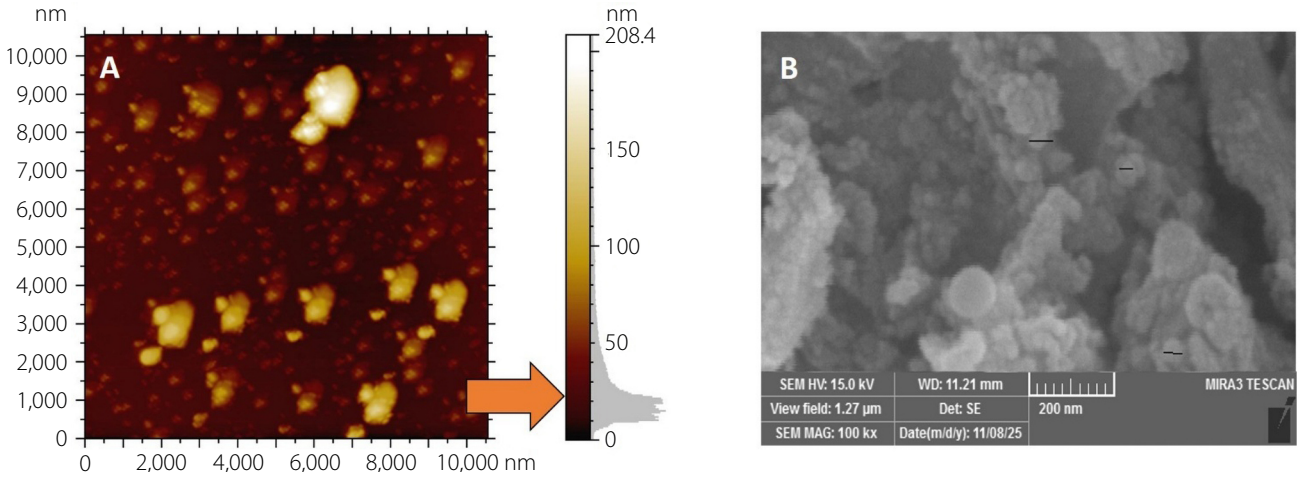


Fig. 2. A. Atomic force microscopy (AFM) 2D topography image of the ZnO nanoparticle (ZnO NP) surface. The orange arrow indicates the particle diameter, which is below 50 nm; B. Scanning electron microscopy (SEM) image of ZnO NPs at ×100,000 magnification (scale bar = 500 nm). The black bars confirm particle sizes below 50 nm

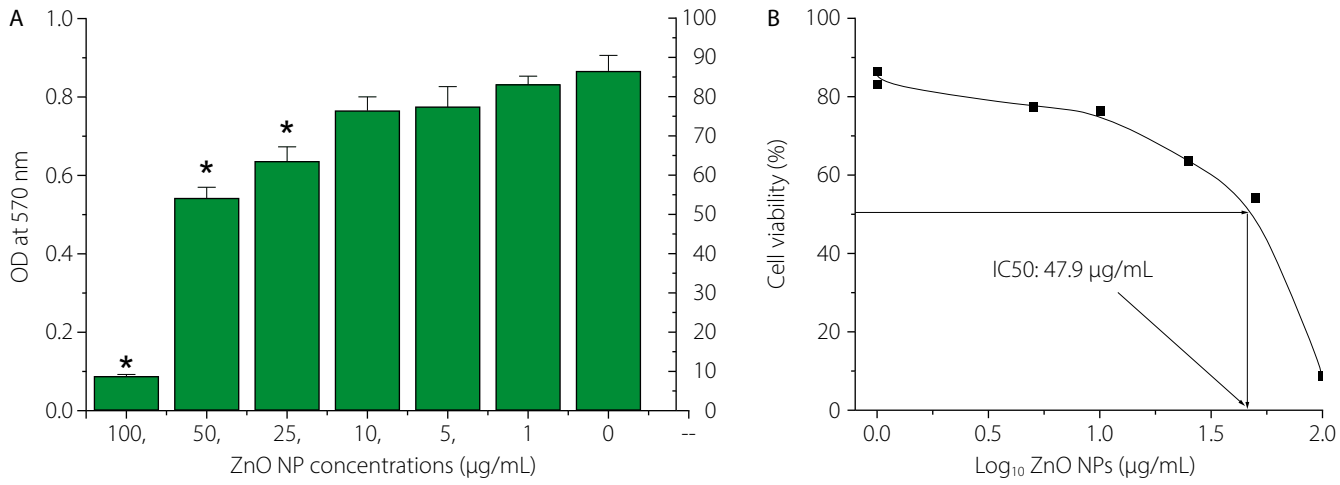


Fig. 3. Cytotoxic effect of ZnO NPs on MCF-7 cells assessed by the MTT assay. A. MCF-7 breast cancer cells were treated with increasing concentrations of ZnO NPs (0–100 µg/mL) for 24 h, and cell viability was evaluated by measuring optical density (OD) at 570 nm. Data are presented as mean ± SD. Asterisks indicate significant differences compared with the untreated control ($p < 0.05$); B. Concentration–response curve showing percentage cell viability plotted against the $\log_{10}$ concentration of ZnO nanoparticles. The half-maximal inhibitory concentration ($IC_{50}$) was 47.9 µg/mL

## Effect of sub-MICs of IPM on biofilm formation

Figure 4 shows the impact of sub-MICs of IPM on biofilm formation in imipenem-resistant *K. pneumoniae* (IRKP) isolates (12 isolates), which strongly produced biofilm biomass. Across the isolates, biofilm biomass increased as the imipenem concentration decreased from ½ MIC to ⅟₃₂ MIC. The strongest biofilm production was observed when the isolates were exposed to the lowest antibiotic concentrations (⅟₁₆ and ⅟₃₂ MIC), with several isolates approaching control levels. However, higher antibiotic concentrations (½ and ¼ MIC) resulted in lower biofilm biomass formation. The highest concentrations of IPM (½, ¼, and ⅛ MICs) significantly reduced biofilm formation compared with the control in *K. pneumoniae* isolates not exposed to IPM ($p < 0.05$).

## Effect of sub-MICs of ZnO NPs on biofilm formation

Figure 5 shows the concentration-dependent inhibitory effect of ZnO NPs on biofilm biomass formation by 12 isolates of *K. pneumoniae* on polystyrene microtiter plates. Exposure to ZnO NPs decreased biofilm biomass. The highest concentration (½ MIC) produced the most significant inhibition compared with the control ($p < 0.05$). The antibiofilm effect of ZnO NPs decreased with decreasing concentrations of ZnO NPs (¼ MIC to ⅟₃₂ MIC). Strong biofilm producers showed a decrease in biofilm production even at lower ZnO NP concentrations up to ⅟₁₆ MIC ($p < 0.05$). These data demonstrate that ZnO NPs exhibit significant concentration-dependent antibiofilm activity against *K. pneumoniae*.

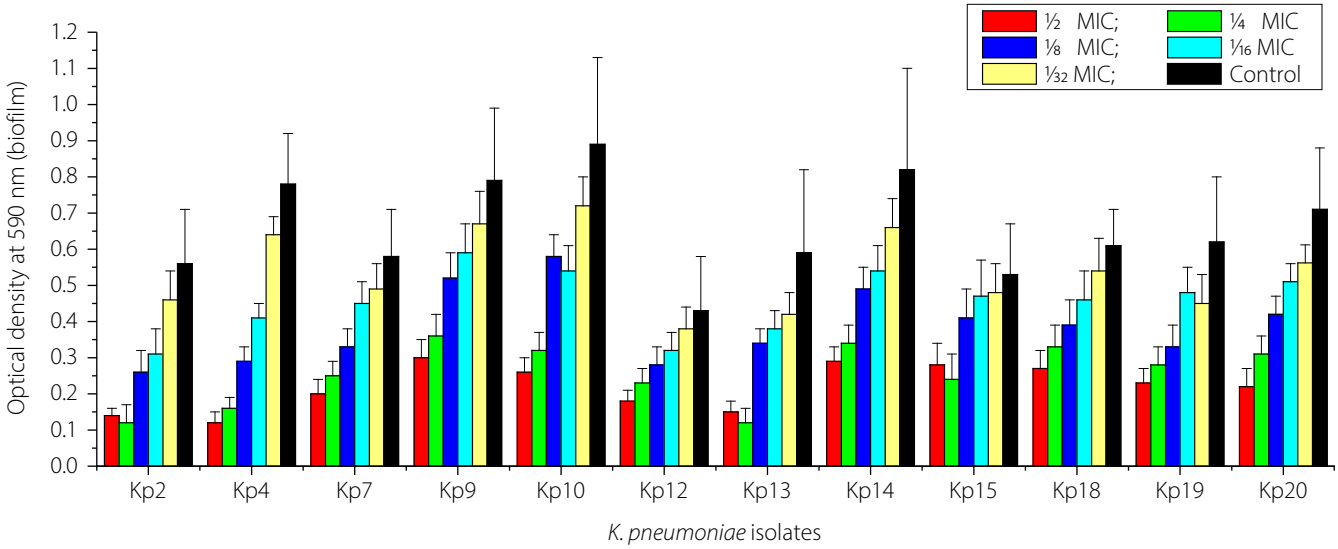


**Fig. 4.** Effect of sub-minimum inhibitory concentrations (sub-MICs) of imipenem (IPM) on biofilm formation by 12 *K. pneumoniae* isolates on polystyrene microtiter plates. The antibiofilm effect of sub-MICs of IPM was concentration dependent. Y-axis, biofilm biomass ($OD_{590}$); X-axis, *K. pneumoniae* isolates. Data are presented as mean ± SD

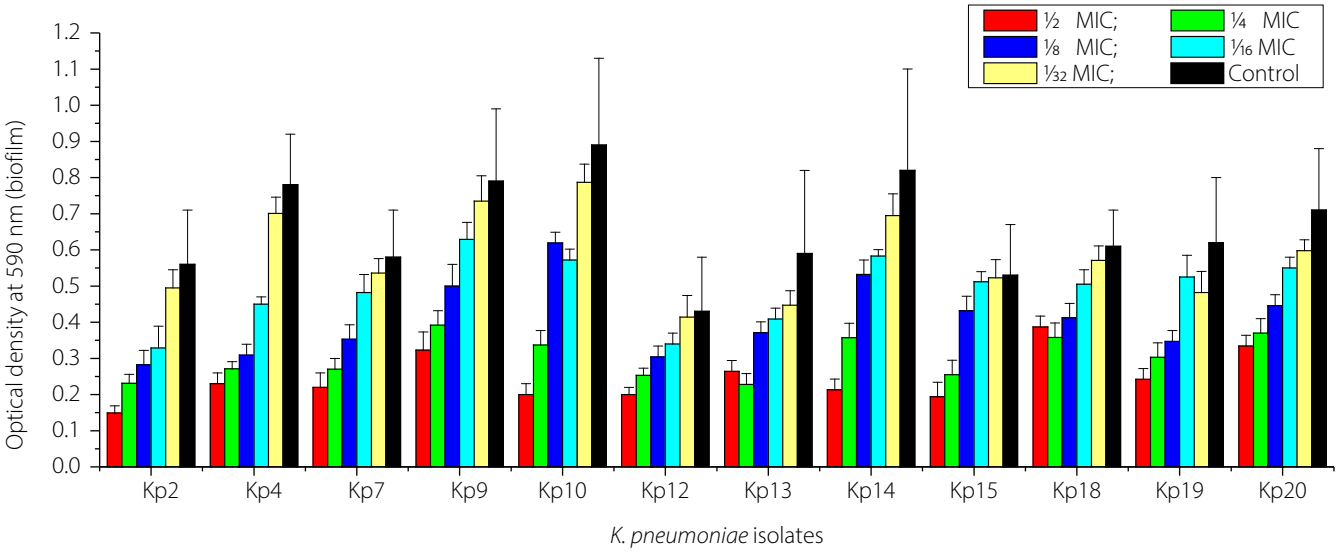


**Fig. 5.** Concentration-dependent inhibition of *K. pneumoniae* biofilm formation by zinc oxide nanoparticles (ZnO NPs). Biofilm formation by 12 *K. pneumoniae* isolates on polystyrene was quantified as optical density at 590 nm. Isolates were treated with sub-MICs of ZnO NPs (½, ¼, ⅛, ⅟₁₆, and ⅟₃₂ MIC). Y-axis, biofilm biomass ($OD_{590}$); X-axis, *K. pneumoniae* isolates. Data are presented as mean ± SD

## Additive effect of ZnO NPs and IPM on MICs

The effect of different concentrations of ZnO NPs (sub-MICs) on the susceptibility of Kp14 (*K. pneumoniae* isolate exhibiting the highest level of biofilm formation and resistance to IPM) to IPM is shown in Fig. 6. The results showed that all tested sub-MICs of ZnO NPs significantly reduced ($p < 0.05$) the minimum inhibitory concentration (MIC) of IPM required to completely inhibit the growth of Kp14, compared with the control treatment (MICs of IPM without ZnO NPs). The greatest decreases in the MIC of IPM were observed in the presence of ½ MIC, ¼ MIC, and ⅛ MIC of ZnO NPs. These concentrations of ZnO NPs reduced the MIC of IPM against Kp14 from 250 ± 50 µg/mL to 116.6 ± 14.4 µg/mL, while 1/16 MIC of ZnO NPs decreased the MIC of IPM from 250 ± 50 µg/mL to 125 ± 25 µg/mL. Furthermore, 1/32 and 1/64 MICs of ZnO NPs reduced the MIC of IPM against Kp14 from 250 ± 50 µg/mL to 141.6 ± 14.4 µg/mL and 158.3 ± 80.36 µg/mL, respectively. Despite the reduction in MIC values, Kp14 remained classified as clinically resistant to IPM, as the post-treatment MICs substantially exceeded the CLSI susceptibility breakpoint of ≤1 µg/mL. These findings are therefore described as ZnO NPs potentiating imipenem activity, rather than fully restoring susceptibility.

The fractional inhibitory concentration index (FICI) was calculated for each ZnO NP sub-MIC concentration tested (Table 2). FICI values ranged from approximately 0.97 (at ½ MIC ZnO NPs) to 1.13 (at 1/64 MIC ZnO NPs), indicating additive interactions across all tested concentrations. A FICI ≤ 0.5 is defined as synergistic, 0.5–1.0 as additive, 1.0–2.0 as indifferent, and > 2.0 as antagonistic. The results therefore confirm an additive potentiation effect rather than classical synergy.

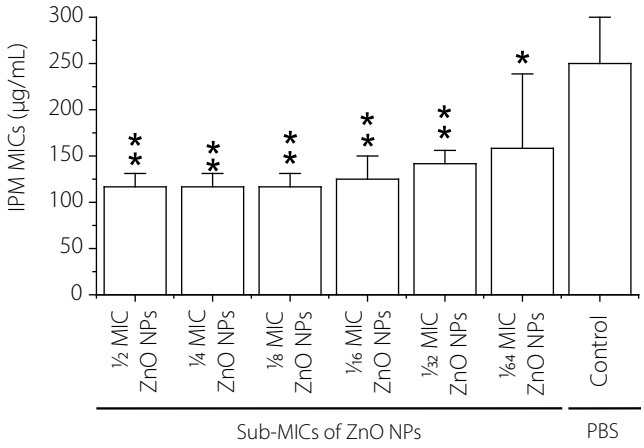


Fig. 6. Additive effect of sub-inhibitory concentrations (½ MIC, ¼ MIC, ⅛ MIC, 1/16 MIC, 1/32 MIC, and 1/64 MIC) of ZnO NPs on reducing the MIC of IPM against Kp14. Asterisks indicate significant differences compared with the control (MIC of IPM against Kp14 with Sub-MICs of ZnO NPs): *$p < 0.05$; **$p < 0.005$.

## Additive effect of ZnO NPs and imipenem on biofilm formation

Table 3 shows the effect of sub-inhibitory concentrations of ZnO NPs and IPM on biofilm formation by Kp14. The results showed the highest inhibition of biofilm formation when Kp14 was exposed to ½ MIC of ZnO NPs and ½ MIC of IPM compared with three controls (first, second, and third controls). The lowest inhibition of biofilm formation was observed when the bacterial isolate (Kp14) was

Table 2. Fractional inhibitory concentration index (FICI) values for the combination of ZnO NPs and IPM against Kp14, calculated using the checkerboard microdilution assay. FICI = (MIC of IPM in combination/MIC of IPM alone) + (concentration of ZnO NPs used/MIC of ZnO NPs alone). Interpretation: ≤0.5, synergistic; 0.5–1.0, additive; 1.0–2.0, indifferent; >2.0, antagonistic

| | | | |
|---|---|---|---|
| ¼ MIC ZnO NPs | 116.6 ± 14.4 | 0.72 | Additive |
| 1/16 MIC ZnO NPs | 125 ± 25 | 0.81 | Additive |
| 1/64 MIC ZnO NPs | 158.3 ± 80.4 | 1.13 | Indifferent |

Table 3. Biofilm formation, expressed as optical density at 590 nm, of *K. pneumoniae* (Kp14) after incubation for 24 h at 37°C under exposure to sub-MICs of ZnO NPs, sub-MICs of imipenem (IPM), and their combination. First control, biofilm formation of Kp14 under exposure to sub-MICs of IPM; second control, biofilm formation of Kp14 under exposure to sub-MICs of ZnO NPs; third control, biofilm formation of Kp14 without exposure to sub-MICs of IPM or ZnO NPs. #$p < 0.05$ vs first control; ^$p < 0.05$ vs second control; *$p < 0.05$ vs third control

| Sub-MICs of ZnO NPs | ½ MIC of IPM | ¼ MIC of IPM | ⅛ MIC of IPM | 1/16 MIC of IPM | 1/32 MIC of IPM | 1/64 MIC of IPM | 2nd control |
|---|---|---|---|---|---|---|---|
| ½ MIC of ZnO NPs | 0.14 ± 0.05*#^ | 0.18 ± 0.04*#^ | 0.19 ± 0.03*#^ | 0.20 ± 0.04*#^ | 0.22 ± 0.05*#^ | 0.23 ± 0.06*#^ | 0.33 ± 0.03 |
| ¼ MIC of ZnO NPs | 0.16 ± 0.04*#^ | 0.19 ± 0.05*#^ | 0.20 ± 0.04*#^ | 0.23 ± 0.05*#^ | 0.26 ± 0.06*#^ | 0.31 ± 0.07*# | 0.357 ± 0.04 |
| ⅛ MIC of ZnO NPs | 0.19 ± 0.05*#^ | 0.17 ± 0.04*#^ | 0.21 ± 0.05*#^ | 0.24 ± 0.05*#^ | 0.31 ± 0.06*#^ | 0.39 ± 0.08*#^ | 0.532 ± 0.04 |
| 1/16 MIC of ZnO NPs | 0.17 ± 0.05*#^ | 0.21 ± 0.05*#^ | 0.20 ± 0.06*#^ | 0.25 ± 0.06*#^ | 0.35 ± 0.07*#^ | 0.48 ± 0.09*#^ | 0.583 ± 0.0177 |
| 1/32 MIC of ZnO NPs | 0.19 ± 0.05*#^ | 0.20 ± 0.05*#^ | 0.21 ± 0.04*#^ | 0.26 ± 0.06*#^ | 0.32 ± 0.08*#^ | 0.51 ± 0.10*#^ | 0.695 ± 0.06 |
| 1/64 MIC of ZnO NPs | 0.15 ± 0.04*#^ | 0.20 ± 0.06*#^ | 0.23 ± 0.05*#^ | 0.29 ± 0.06*#^ | 0.39 ± 0.09*# | 0.59 ± 0.11*#^ | 0.701 ± 0.04 |
| 1st control | 0.29 ± 0.04 | 0.34 ± 0.05 | 0.49 ± 0.06 | 0.54 ± 0.07 | 0.66 ± 0.08 | 0.70 ± 0.102 | 0.83 ± 0.23 (3rd control) |

exposed to ¼ sub-MICs of both agents (ZnO NPs and IPM), although these concentrations still reduced biofilm formation significantly compared with the three controls. The present study, for the first time, shows that sub-MICs of IPM and ZnO NPs in combination reduce biofilm formation by Kp14 (IRKP) more than exposure to either sub-MIC alone. The present study confirms the synergistic effect of sub-inhibitory concentrations of ZnO NPs in reducing biofilm formation by Kp14 under sub-MIC IPM stress. This finding explains one mechanism by which ZnO NPs reduce Kp14 resistance to IPM.

## Discussion

The growing resistance of pathogenic bacteria to a wide range of antibiotics has become a significant global challenge and represents a serious public health threat. Moreover, no new effective antibiotics have been discovered in recent years to counteract the increasing proportion of antibiotic-resistant bacteria. The recent World Health Organization report has classified carbapenem (imipenem)-resistant bacteria as a high priority for the development of new antimicrobials. Carbapenem-resistant *K. pneumoniae* (CRKP) infections are associated with mortality rates exceeding 28.7% in hospitalized patients, particularly among immunocompromised individuals with pneumonia and sepsis.[22] The emergence and spread of infections caused by multidrug-resistant (MDR) or extensively drug-resistant (XDR) bacteria increase the risk of morbidity and mortality among infected patients.[23,24]

The present study elucidates the moderate incidence of *K. pneumoniae* in urinary tract infections (UTIs). The incidence of UTIs caused by *K. pneumoniae* is 16.2% in Iraq, and it is the second most common uropathogen, accounting for 15% to 23% of culture-positive UTIs.[25] Sub-inhibitory concentrations of imipenem and ZnO NPs, applied separately, reduced biofilm formation by imipenem-resistant *K. pneumoniae* (IRKP) on polystyrene microtiter plates. The novelty of the current study lies in demonstrating the enhancing effect of ZnO NPs on the antibacterial activity of imipenem (IPM) against IRKP, as well as their combined antibiofilm effect. However, despite this enhancement, the increased bacterial susceptibility did not reach the threshold for clinical susceptibility to imipenem, as MIC values decreased from 250 ± 50 μg/mL to 116.6 ± 14.4 μg/mL, still exceeding the CLSI susceptibility breakpoint of ≤1 μg/mL.[13] These findings offer a promising strategy to combat the growing challenge of antimicrobial resistance in this opportunistic pathogen.

The strong negative correlation between biofilm formation and inhibition zone diameter (r = −0.819) directly supports the established barrier function of the extracellular polymeric substance (EPS) matrix. The EPS matrix physically restricts antibiotic diffusion, reduces the local antibiotic concentration at the bacterial cell surface, and creates a microenvironment characterized by reduced pH and oxygen tension, which further diminishes antibiotic efficacy. Collectively, these factors explain the observed inverse relationship between biofilm production and IPM susceptibility.

It is important to note that although ZnO NPs significantly reduced the MIC of IPM against Kp14, the post-treatment MIC still substantially exceeds the CLSI susceptibility breakpoint of ≤1 μg/mL for IPM. Therefore, these findings are more accurately described as ZnO NPs potentiating imipenem activity rather than fully restoring susceptibility. This potentiation effect, while not sufficient to reclassify the isolate as clinically susceptible, may contribute to improved clinical outcomes when higher antibiotic concentrations are achieved at the site of infection. Clinically, this implies that the concentrations required to achieve meaningful IPM potentiation would substantially exceed standard therapeutic doses, and thus the current findings cannot be directly translated into revised dosing recommendations without extensive pharmacokinetic/pharmacodynamic (PK/PD) modeling and in vivo validation. Nevertheless, the demonstrated potentiation provides proof of concept that ZnO NPs can modulate carbapenem activity through membrane permeabilization and biofilm disruption.

The cytotoxicity of ZnO NPs against MCF-7 cells yielded an $IC_{50}$ of 47.9 μg/mL. Importantly, the sub-MIC concentrations of ZnO NPs used in the synergy experiments were substantially below this $IC_{50}$ value, suggesting a potential therapeutic safety margin. This differential selectivity – antibacterial activity at concentrations below the eukaryotic cytotoxic threshold – is an essential consideration in evaluating ZnO NPs as candidate adjunct antimicrobial agents. However, in vivo validation of this safety margin remains necessary prior to clinical translation.

*Thymus vulgaris* was selected as the green synthesis agent for ZnO NPs based on its well-documented phytochemical profile, particularly its high content of thymol, carvacrol, and flavonoids, which function as reducing and capping agents during nanoparticle biosynthesis. These phenolic compounds stabilize the nanoparticle surface, control particle size, and may also contribute residual antimicrobial activity. Furthermore, *Thymus vulgaris* extracts are widely available, low-cost, non-toxic, and environmentally sustainable compared with chemical reducing agents, aligning with the green chemistry principles that guided this study.

The synergistic antibacterial activity can be explained by multiple mechanisms of action of ZnO NPs. Previous studies have reported that ZnO NPs can induce oxidative stress by generating reactive oxygen species (ROS), such as superoxide and hydroxyl radicals.[26,27] These reactive species lead to lipid peroxidation, protein denaturation, and DNA damage, ultimately disrupting cellular structure and bacterial function.[28] Furthermore, the dissolution of ZnO NPs releases $Zn^{2+}$ ions that interfere with key cellular enzymatic processes, disrupt membrane potential, and suppress

essential bacterial cell functions.[29] The interaction of ZnO NPs with protein components of the bacterial cell membrane enhances membrane damage, increases membrane permeability, and facilitates the uptake of antibiotics.[30] This increased permeability likely plays a significant role in the observed potentiation, enabling IPM to reach its intracellular targets more effectively.

In addition to planktonic growth, the combined effect of ZnO NPs and IPM inhibits *K. pneumoniae* biofilm formation in vitro. The primary role of biofilms is to promote bacterial resistance to antibiotics and host immune responses by reducing antibiotic penetration and decreasing the effectiveness of phagocytic cells in clearing bacterial cells in vivo.[31] Several previous studies have shown that ZnO NPs exhibit antibiofilm activity by disrupting the extracellular polymeric substance (EPS) matrix, reducing bacterial adhesion to surfaces, and interfering with quorum-sensing mechanisms.[32,33] The combination of ZnO NPs and imipenem enhances these effects, as compromised bacterial cells within the biofilm matrix become more susceptible to both agents, leading to disruption of the biofilm structure. This is consistent with previous findings showing that other carbapenems (e.g., meropenem) exhibit antibiofilm activity when combined with ZnO NPs against carbapenem-resistant *K. pneumoniae*.[34]

These outcomes have important implications. *K. pneumoniae* is one of the pathogens responsible for hospital-acquired infections, and carbapenem-resistant isolates, particularly IRKP, represent a serious threat to public health.[23,24,35,36] The combined effect of ZnO NPs and IPM reduces the effective imipenem dose required for treatment, potentially decreasing antibiotic-associated toxicities and slowing the progression of further resistance. This line of research is therefore highly relevant for addressing multidrug resistance. The current study highlights the need for further research to clarify the mechanisms underlying the enhancing effect of ZnO NPs on imipenem activity. Molecular studies should investigate the roles of genes associated with *K. pneumoniae* resistance to imipenem, as well as those involved in biofilm formation and polymerization. Such studies may help elucidate how the combined action of these agents improves antibiotic efficacy. Another important aspect is the need for in vivo validation of the enhancing effect of ZnO NPs on imipenem activity in infections caused by carbapenem-resistant bacteria, which remain a major public health concern. Future in vivo studies will employ a murine UTI model (transurethral instillation of *K. pneumoniae* in C57BL/6 mice) to evaluate the efficacy and safety of combined ZnO NP and imipenem treatment, consistent with established models for carbapenem-resistant *K. pneumoniae* infections. These limitations are being addressed in ongoing research projects in our laboratory.

# Conclusions

The present study determined the incidence of UTIs caused by *K. pneumoniae* resistant to IPM. A significant relationship was observed between the ability of *K. pneumoniae* to form biofilms and its resistance to IPM. Sub-MICs of IPM and ZnO NPs significantly reduced biofilm formation. The current study demonstrates, for the first time, the additive effect of sub-MIC ZnO NPs in reducing biofilm formation and potentiating imipenem activity against *K. pneumoniae*. These findings suggest the potential use of ZnO NPs to enhance the effectiveness of IPM against IPM-resistant *K. pneumoniae*.

## ORCID iDs

Deyar Jassim Shawi 0009-0005-2234-6592
Ayaid Khadem Zgair 0000-0002-2356-3338

## References

1. Nagham SM, Obaid MM, Jasem MJ, Noaman TM. Impact of biofilm formation on antibiotic resistance in *Escherichia coli*. *World J Exp Biosci*. 2024;12(2):44–48. doi:10.65329/wjeb.v12.02.004
2. Campos JV, Pontes JTC, Canales CSC, Roque-Borda CA, Pavan FR. Advancing nanotechnology: Targeting biofilm-forming bacteria with antimicrobial peptides. *BME Front*. 2025;6:0104. doi:10.34133/bmef.0104
3. Hajareh Haghighi F, Mercurio M, Cerra S, et al. Surface modification of $TiO_2$ nanoparticles with organic molecules and their biological applications. *J Mater Chem B*. 2023;11(11):2334–2366. doi:10.1039/D2TB02576K
4. Hosnedlova B, Kabanov D, Kepinska M, et al. Effect of biosynthesized silver nanoparticles on bacterial biofilm changes in *S. aureus* and *E. coli*. *Nanomaterials*. 2022;12(13):2183. doi:10.3390/nano12132183
5. Fu Y, Zhang Y, Zhao J, et al. Emergence of co-resistance to imipenem/relebactam and ceftazidime/avibactam in clinical *Klebsiella pneumoniae* ST11 clone due to KPC-2 N132S and CTX-M-65 S130G/P167S substitutions. *Antimicrob Agents Chemother*. 2025;69(12):e00891-25. doi:10.1128/aac.00891-25
6. Chen HQ, Mo ZH, Wei WX. Case report: Trauma-induced *Klebsiella pneumoniae* invasive syndrome presenting with liver abscess, lung abscess, endophthalmitis, and purulent meningitis. *Front Med (Lausanne)*. 2025;11:1513831. doi:10.3389/fmed.2024.1513831
7. Mendes G, Santos ML, Ramalho JF, Duarte A, Caneiras C. Virulence factors in carbapenem-resistant hypervirulent *Klebsiella pneumoniae*. *Front Microbiol*. 2023;14:1325077. doi:10.3389/fmicb.2023.1325077
8. Ashaduzzaman M, Al Muhit MA, Dey SC, et al. Microwave assisted starch stabilized green synthesis of zinc oxide nanoparticles for antibacterial and photocatalytic applications. *Sci Rep*. 2025;15(1):28288. doi:10.1038/s41598-025-14193-8
9. Masadeh MM, Bany-Ali NM, Khanfar MS, Alzoubi KH, Masadeh MM, Al Momany EM. Synergistic antibacterial effect of ZnO nanoparticles and antibiotics against multidrug-resistant biofilm bacteria. *Curr Drug Deliv*. 2025;22(1):92–106. doi:10.2174/0115672018279213240110045557
10. Rodríguez-Suárez JM, Gershenson A, Onuh TU, Butler CS. The heterogeneous diffusion of polystyrene nanoparticles and the effect on the expression of quorum-sensing genes and EPS production as a function of particle charge and biofilm age. *Environ Sci Nano*. 2023;10(9):2551–2565. doi:10.1039/D3EN00219E
11. Norouzalinia F, Asadpour L, Mokhtary M. Anti-microbial, anti-biofilm, and efflux pump inhibitory effects of ellagic acid–bonded magnetic nanoparticles against *Escherichia coli* isolates. *Int Microbiol*. 2024;28(3):563–573. doi:10.1007/s10123-024-00560-4
12. Talib MM, Ghafil JA. Comparative adhesion of *Pseudomonas aeruginosa* to human oral mucosal epithelial cells and polystyrene surfaces. *J Fac Med Baghdad*. 2024;66(3):344–349. doi:10.32007/jfacmedbaghdad.6632328
13. Clinical and Laboratory Standards Institute (CLSI). *CLSI M100. Performance Standards for Antimicrobial Susceptibility Testing*. 34th ed. Malvern, USA: Clinical and Laboratory Standards Institute (CLSI); 2024. ISBN: 978-1-68440-305-9, 978-1-68440-306-6.

14. Karam ST, Abdulrahman AF. Green synthesis and characterization of ZnO nanoparticles by using thyme plant leaf extract. *Photonics*. 2022;9(8):594. doi:10.3390/photonics9080594
15. Sadiq SI, Ghafil JA. Polyhydroxybutyrate nanoparticle improving the sensitivity of *Pseudomonas aeruginosa* to ceftriaxone and reducing the biofilm formation in vitro. *Polim Med*. 2025;55(1):31–39. doi:10.17219/pim/203765
16. Mosmann T. Rapid colorimetric assay for cellular growth and survival: Application to proliferation and cytotoxicity assays. *J Immunol Methods*. 1983;65(1–2):55–63. doi:10.1016/0022-1759(83)90303-4
17. Plumb JA. Cell sensitivity assays: The MTT assay. *Methods Mol Med*. 1999;28:25–30. doi:10.1385/1-59259-687-8:25
18. Berridge MV, Herst PM, Tan AS. Tetrazolium dyes as tools in cell biology: New insights into their cellular reduction. *Biotechnol Annu Rev*. 2005;11:127–152. doi:10.1016/S1387-2656(05)11004-7
19. Abd Al-Mutalib L, Zgair A. Effect of subinhibitory doses of rifaximin on in vitro *Pseudomonas aeruginosa* adherence and biofilm formation to biotic and abiotic surface models. *Polim Med*. 2023;53(2):97–103. doi:10.17219/pim/166584
20. Talib MM, Ghafil JA. Effect of sub-minimum inhibitory concentrations of ceftriaxone on the *Pseudomonas aeruginosa* adhesion to human oral mucosal epithelial cells and biofilm formation to polystyrene in vitro. *Pharm Sci Asia*. 2024;51(2):180–189. doi:10.29090/psa.2024.02.24.1752
21. Mohammed HA, Zgair AK. Detection of quorum sensing genes of *Pseudomonas aeruginosa* isolated from different areas in Iraq. *Iraqi J Sci*. 2022;63(11):4665–4673. doi:10.24996/ijs.2022.63.11.5
22. Zhou C, Sun L, Li H, Huang L, Liu X. Risk factors and mortality of elderly patients with hospital-acquired pneumonia of carbapenem-resistant *Klebsiella pneumoniae* infection. *Infect Drug Resist*. 2023;16:6767–6779. doi:10.2147/IDR.S431085
23. World Health Organization (WHO). *WHO Bacterial Priority Pathogens List 2024: Bacterial Pathogens of Public Health Importance, to Guide Research, Development, and Strategies to Prevent and Control Antimicrobial Resistance*. Geneva, Switzerland: World Health Organization (WHO); 2024. ISBN:978-92-4-009346-1.
24. Mondol SM, Islam MdR, Mia MdE, et al. Molecular and genomic insights into multidrug-resistant (MDR) and extensively drug-resistant (XDR) *Pseudomonas aeruginosa* causing burn wound infections in Bangladesh. *Sci Rep*. 2025;15(1):32629. doi:10.1038/s41598-025-19576-5
25. Polse RF, Qarani SM, Assafi MS, Sabaly N, Ali F. Incidence and Antibiotic Sensitivity of *Klebsiella pneumoniae* isolated from urinary tract infection patients in Zakho emergency hospital/Iraq. *J Educ Sci*. 2020;29(3):257–268. doi:10.33899/edusj.2020.126827.1056
26. Mendes CR, Dilarri G, Forsan CF, et al. Antibacterial action and target mechanisms of zinc oxide nanoparticles against bacterial pathogens. *Sci Rep*. 2022;12(1):2658. doi:10.1038/s41598-022-06657-y
27. Sirelkhatim A, Mahmud S, Seeni A, et al. Review on zinc oxide nanoparticles: Antibacterial activity and toxicity mechanism. *Nanomicro Lett*. 2015;7(3):219–242. doi:10.1007/s40820-015-0040-x
28. Jiang S, Lin K, Cai M. ZnO nanomaterials: Current advancements in antibacterial mechanisms and applications. *Front Chem*. 2020;8:580. doi:10.3389/fchem.2020.00580
29. Emram R, Sionov RV, Gutkin V, Wilensky A, Steinberg D, Assad R. Mechanism of action of zinc oxide nanoparticles as an antibacterial agent against *Streptococcus mutans*. *Biomolecules*. 2025;15(12):1660. doi:10.3390/biom15121660
30. Mahgoub SM, Mohamed EA, Aziz SAAA, et al. Synergistic potential of clindamycin hydrochloride loaded on zinc oxide nanoparticles: A novel approach to combat multidrug-resistant infections. *Sci Rep*. 2025;15(1):44665. doi:10.1038/s41598-025-30573-6
31. Mohamed AA, Saed S, El-Sayed SR, et al. A combined therapy of meropenem–ZnO nanoparticles efficiently eliminates carbapenem-resistant *Klebsiella pneumoniae* biofilms, with reduced nephrotoxicity (in vitro). *Lett Appl Microbiol*. 2024;77(12):ovae136. doi:10.1093/lambio/ovae136
32. Banerjee S, Vishakha K, Das S, et al. Antibacterial, anti-biofilm activity and mechanism of action of pancreatin doped zinc oxide nanoparticles against methicillin resistant *Staphylococcus aureus*. *Colloids Surf B Biointerfaces*. 2020;190:110921. doi:10.1016/j.colsurfb.2020.110921
33. Kumarage PM, Gul T, Green NJ, et al. Recent advances in gold and zinc oxide nanoparticles: Antibiofilm action, mechanisms beyond ROS generation, and in vivo efficacy. *Microbiol Res*. 2026;306:128441. doi:10.1016/j.micres.2026.128441
34. Mohsenzadeh A, Mohsenzadeh H, Mohammadi A, et al. Synergistic effects of zinc oxide nanoparticles and Meropenem on biofilm formation in *Pseudomonas aeruginosa*. *Cell Mol Biomed Rep*. 2025;5(2):121–134. doi:10.55705/cmbr.2025.481668.1280
35. Khan BK, Ud Din MA, Mohammed MT, Batool M, Ullah H. Antagonism and antibiofilm activity of sterile microbiota growth medium against *Klebsiella pneumoniae* in vitro. *World J Exp Biosci*. 2025;13(2):33–36. doi:10.65329/wjeb.v13.02.003
36. Ebrahimi FA, Siasi E, Yazdian F, Ashrafi F. Nanotechnology meets superbugs: Biocompatible polymeric nanoparticles combat MDR *Klebsiella pneumoniae* via gene suppression and biofilm inhibition. *Sci Rep*. 2025;15(1):37708. doi:10.1038/s41598-025-21606-1

# Molecular insights into sub-inhibitory ceftriaxone-mediated modulation of *Pseudomonas aeruginosa* biofilm architecture, quorum sensing networks, and antibiotic–target docking interactions

Nabaa Amer Jaber[B,E,F], Jenan Atiyah Ghafil[A–F]

Department of Biology, College of Science, University of Baghdad, Iraq

A – research concept and design; B – collection and/or assembly of data; C – data analysis and interpretation;
D – writing the article; E – critical revision of the article; F – final approval of the article

Polymers in Medicine, ISSN 0370-0747, eISSN 2451-2699 *Polim Med*. 2026;56(1):65–74

**Address for correspondence**
Jenan A. Ghafil
E-mail: genan.atiyah@sc.uobaghdad.edu.iq

**Funding sources**
None declared

**Conflict of interest**
None declared

**Acknowledgements**
None declared

Received on April 18, 2026
Reviewed on May 26, 2026
Accepted on June 15, 2026

Published online on June 30, 2026

## Abstract

**Background.** *Pseudomonas aeruginosa* biofilm polymer matrix formation contributes to antibiotic tolerance. The antibiofilm effects of sub-minimum inhibitory concentrations (MICs) of ceftriaxone (CTX), the molecular mechanisms by which these sub-MICs modulate biofilm polymer production and quorum sensing (QS), and the binding interactions of CTX with key biofilm regulatory proteins (LasR and RhlR QS receptors) have not been previously investigated.

**Objectives.** To determine the role of sub-MIC CTX in regulating biofilm polymer matrix formation, bacterial adhesion, QS gene expression (*rhlR* and *lasR*), and to perform molecular docking analysis of CTX interactions with LasR and RhlR QS receptor proteins and biofilm EPS polymer-associated targets.

**Materials and methods.** MICs and biofilm formation were determined. The effects of CTX sub-MICs on biofilm formation, adhesion to mouse bladder epithelial cells (BECs), and QS gene expression (*rhlR* and *lasR*, by qRT-PCR) were assessed. In silico molecular docking of CTX against the ligand-binding domains of LasR (PDB: 2UV0) and RhlR (PDB: 3T5K) was performed using AutoDock Vina. Interaction fingerprinting with biofilm EPS polymer-associated enzymes (AlgD and PelB) was also performed.

**Results.** CTX sub-MICs regulated biofilm formation in an isolate-dependent manner, reduced *P. aeruginosa* adhesion to mouse BECs, and downregulated the *rhlR* and *lasR* genes in a concentration-dependent manner. Molecular docking revealed that CTX binds favorably within the ligand-binding pockets of LasR (−8.3 kcal/mol) and RhlR (−7.1 kcal/mol) via hydrogen bonding and hydrophobic interactions, suggesting competitive interference with QS autoinducer binding. CTX also exhibited affinity for AlgD (−7.6 kcal/mol), a key enzyme in alginate polymer biosynthesis.

**Conclusions.** CTX sub-MICs modulate biofilm EPS polymer matrix formation and epithelial adhesion by downregulating QS regulatory genes. *lasR* was more responsive to CTX sub-MIC stress than *rhlR*. Molecular docking supports a direct molecular interaction mechanism through which CTX may interfere with QS receptor signaling and alginate polymer biosynthesis, providing a structural basis for its antibiofilm activity at sub-inhibitory concentrations.

**Key words:** *Pseudomonas aeruginosa*, alginate, molecular docking, ceftriaxone, quorum sensing

**Cite as**
Jaber NA, Ghafil JA. Molecular insights into sub-inhibitory ceftriaxone-mediated modulation of *Pseudomonas aeruginosa* biofilm architecture, quorum sensing networks, and antibiotic–target docking interactions. *Polim Med*. 2026;56(1):65–74. doi: 10.17219/pim/224596

**DOI**
10.17219/pim/224596

## Background

The formidable opportunistic pathogen *Pseudomonas aeruginosa* causes persistent infections in immunosuppressed patients and in individuals with cystic fibrosis, burns, urinary tract infections (UTIs), and infections associated with indwelling medical devices.[1,2] Its primary virulence factor is its ability to form biofilms. A biofilm is a structured, multicellular community of bacteria enclosed within a self-produced extracellular matrix. This mode of growth creates a microenvironment that promotes bacterial proliferation and shields the bacteria from antibiotics and the host immune system.[3] Consequently, it often leads to chronic and difficult-to-treat infections.[4] This inherent resistance to antibiotics contributes to high morbidity and mortality rates, presenting a significant challenge for managing *P. aeruginosa* infections in clinical settings.[5]

The extracellular matrix of *P. aeruginosa* biofilms is a complex mixture of biopolymers that confer structural stability, antibiotic recalcitrance, and protection from host immunity. Chief among these are three distinct exopolysaccharide (EPS) polymers: alginate, Pel, and Psl. [6] Alginate is a linear polymer of β-1,4-linked mannuronate and guluronate residues, which forms a viscous, hydrogel-like capsule that impedes antibiotic penetration and protects bacteria from desiccation and immune surveillance.[7] Pel is a cationic, partially deacetylated polymer of β-1,4-linked galactosamine and *N*-acetylgalactosamine, critical for maintaining biofilm cohesion and pellicle formation. Psl is a neutral pentasaccharide repeat-unit polymer rich in mannose and glucose, predominantly associated with surface attachment and the initial stages of biofilm development.[8] Together, these EPS polymers represent the structural 'scaffold' of the biofilm and are prime targets for anti-biofilm therapeutic strategies. Understanding how antibiotics at sub-inhibitory concentrations alter EPS polymer production is therefore critical for comprehending biofilm modulation.

The cell-to-cell communication system known as quorum sensing (QS) is involved in the pathogenicity of *P. aeruginosa*. The Las and Rhl systems are the primary circuits in *P. aeruginosa* that function hierarchically yet interactively. Both systems have a transcriptional regulator (LasR and RhlR, respectively) and its cognate autoinducer synthase.[9] The LasR system is the primary regulator that drives activation of the RhlR system. Both systems regulate the expression of various virulence factors, including elastase, rhamnolipids, and pyocyanin, and are essential for the formation and maintenance of strong biofilms.[10] Crucially, QS governs EPS polymer gene clusters: LasR and RhlR directly regulate alginate biosynthesis genes, including *algD*, and modulate Pel and Psl biosynthesis operons, thereby linking intercellular signaling to biofilm polymer matrix composition.[11]

Ceftriaxone (CTX) is a third-generation cephalosporin antibiotic active against both Gram-positive and Gram-negative bacteria and is a drug of choice for treating pneumonia, meningitis, sepsis, and complicated urinary tract infections.[12] The bactericidal and antibiofilm effects of CTX on *P. aeruginosa* have been reported in previous studies.[13,14] A previous study showed that sub-MICs of CTX inhibit biofilm formation through mechanisms involving QS.[14] However, the structural basis for how CTX may directly interact with QS receptor proteins (LasR and RhlR) and biofilm EPS polymer biosynthetic enzymes at the molecular level has not been examined. Molecular docking is a validated computational approach that predicts the binding mode and affinity of a ligand within a target protein's active site, enabling the rationalization of observed biological effects.[15] Given the polymer-centric nature of *P. aeruginosa* biofilm resistance, elucidating the molecular interactions between CTX and biofilm-associated target proteins has direct relevance to the development of novel antibiofilm strategies and polymer-targeted therapies.

## Objectives

The present study aims to evaluate the effect of sub-MICs of CTX on *P. aeruginosa* biofilm formation on abiotic surfaces and adhesion to mouse bladder epithelial cells; to elucidate the molecular mechanism of biofilm inhibition by assessing the effect of sub-MIC concentrations of CTX on QS regulatory genes (*lasR* and *rhlR*); and to perform docking analysis to investigate the binding interactions of CTX with the LasR and RhlR QS receptor proteins and biofilm EPS polymer biosynthetic enzymes (AlgD and PelB), thereby providing a structural basis for the observed antibiofilm activities.

## Materials and methods

### Bacterial isolation and identification

Midstream urine specimens were collected from 260 inpatients at Baghdad Teaching Hospital, Baghdad, Iraq, who had UTIs. The samples were collected in sterile containers. Patients were not allowed to receive antibiotic treatment within 3 days prior to sample collection. All patients signed the consent form before sample collection. The samples were inoculated onto MacConkey agar (HiMedia, Mumbai, India) and Cetrimide agar (HiMedia, Mumbai, India) plates and incubated at 37°C for 18 h. Biochemical tests (oxidase and catalase) and Gram staining were performed. The VITEK 2 system (bioMérieux, Marcy-l'Étoile, France) with the ID-GNB card was used for identification.[16] Purified isolates were stored at –20°C in nutrient broth supplemented with 20% glycerol. The authors followed good laboratory practices when handling the biohazardous materials used in the current study.[17]

## Antimicrobial susceptibility testing and minimum inhibitory concentration

Kirby–Bauer disk diffusion on Mueller–Hinton agar (MHA; HiMedia) using CTX disks (30 µg) was performed. Inhibition zone diameters were interpreted according to CLSI breakpoint guidelines.[18] Minimum inhibitory concentrations (MICs) were determined using the broth microdilution method in Mueller–Hinton broth (MHB; HiMedia), with serial twofold dilutions of CTX (Panpharma, France) prepared from a 2 mg/mL stock solution.[19]

## Biofilm formation assay

Biofilm formation was evaluated using the microtiter plate crystal violet assay on polystyrene 96-well plates. Briefly, 100 µL Tryptic Soy Broth (TSB, 0.25 g/L glucose, HiMedia, India) with 5 µL bacterial suspension (0.5 McFarland) was incubated at 37°C for 24 h. Wells were washed, fixed at 65°C for 60 min, stained with 0.4% crystal violet (15 min), washed, and destained with anhydrous ethanol. Absorbance at 590 nm ($OD_{590}$) was measured with a microplate reader (BioTek 800 TS, Winooski, USA). Experiments were performed in triplicate, and biofilm classification was based on cut-off optical density values.[14]

## Effect of CTX sub-MICs on biofilm polymer formation

The effect of CTX sub-MICs (½ MIC, ¼ MIC, ⅛ MIC, 1/16 MIC, 1/32 MIC, and 1/64 MIC) on biofilm formation was assessed on polystyrene surfaces using the method described above. Three controls were included: TSB alone (negative), TSB with bacterial inoculum without antibiotic (positive biofilm control), and CTX serial dilutions in TSB without bacteria (background control). All experiments were performed in triplicate.

## Effect of CTX sub-MICs on adhesion to mouse bladder epithelial cells

The effect of CTX sub-MICs (½ MIC, ¼ MIC, ⅛ MIC, 1/16 MIC, and 1/32 MIC) on the adhesion of *P. aeruginosa* to mouse bladder epithelial cells (BECs) was evaluated. Mouse BECs were prepared in vitro by gently scraping the inner epithelial layer of the bladder obtained from healthy mice.[20] Cells were maintained in Minimum Essential Medium (MEM; Sigma-Aldrich, St. Louis, USA) supplemented with 10% fetal bovine serum (Biowest, USA), 2 mM L-glutamine, and 1 mM sodium pyruvate. After incubation, non-adherent bacteria were removed by washing, and viable adherent bacteria were counted by serial tenfold dilution and plate counting on nutrient agar. Smears stained with Leishman stain were examined microscopically. Bacteria treated with phosphate-buffered saline (PBS; 0.1 M, pH 7.2) instead of CTX served as untreated controls.

## Gene expression: qRT-PCR

The effects of sub-MICs of CTX (½ MIC, ¼ MIC, ⅛ MIC, 1/16 MIC, and 1/32 MIC) on the expression of QS regulatory genes (*rhlR* and *lasR*) were evaluated using the isolate producing the highest level of biofilm formation. Total RNA was extracted with TRIzol reagent (Thermo Fisher Scientific, Waltham, USA). cDNA was synthesized with the RevertAid First Strand cDNA Synthesis Kit (Thermo Fisher Scientific). qRT-PCR was performed on a Rotor-Gene Q thermocycler (Qiagen, Hilden, Germany) using TOPreal qPCR ×2PreMIX SYBR Green (Enzynomics, Daejeon, South Korea). Gene expression was normalized to the housekeeping gene *rpoD* using the 2^−ΔΔCT method.[15,21] Data are expressed as fold change relative to the PBS-treated control.

## Molecular docking of ceftriaxone with biofilm-associated target proteins

In silico molecular docking was performed to investigate the binding interactions of CTX with QS receptor proteins (LasR and RhlR) and key biofilm EPS polymer biosynthetic enzymes (AlgD and PelB).

Ligand preparation: The three-dimensional structure of ceftriaxone (PubChem CID: 5479530; molecular formula: $C_{18}H_{18}N_8O_7S_3$; molecular weight: 554.58 g/mol) was retrieved from the PubChem database. The structure was converted to PDBQT format using Open Babel v. 3.1. Energy minimization was performed using the MMFF94 force field within Avogadro v. 1.2 prior to docking.

Target protein preparation: Crystal structures were downloaded from the Protein Data Bank (PDB): LasR ligand-binding domain in complex with *N*-(3-oxododecanoyl)-L-homoserine lactone (PDB: 2UV0, resolution: 1.9 Å), RhlR ligand-binding domain (PDB: 3T5K, resolution: 1.6 Å), AlgD GDP-mannose dehydrogenase (PDB: 1MV8), and PelB from the Pel biosynthetic operon (PDB: 5TCB). Water molecules and co-crystallized ligands were removed using PyMOL v. 2.5 (Schrödinger, New York, USA). Polar hydrogen atoms were added, and Gasteiger partial charges were assigned using AutoDockTools v. 1.5.7 (Scripps Research Institute, La Jolla, USA).

Docking simulations: Molecular docking was performed using AutoDock Vina v. 1.2 (Scripps Research Institute).[22] The docking grid box was centered on the co-crystallized ligand binding site for each target (LasR: center x = 15.5, y = 18.3, z = 22.7; RhlR: center x = −4.2, y = 12.8, z = 5.4; AlgD: center x = 8.1, y = 22.5, z = −3.9; PelB: center x = 5.2, y = −8.7, z = 14.2), with box dimensions of 25 × 25 × 25 Å and an exhaustiveness parameter of 8. The top-ranked binding pose (lowest binding energy) was selected for analysis. Protein–ligand interactions were visualized using BIOVIA Discovery Studio Visualizer v. 21.1 (Dassault Systèmes, Vélizy-Villacoublay, France) and LigPlot+ v. 2.2 (EMBL-EBI, Hinxton, UK). Binding interactions (hydrogen

bonds and hydrophobic contacts) were identified, and the interacting residues were recorded.[22]

Validation: The docking protocol was validated by re-docking the co-crystallized native ligand of each target protein into its respective binding site. Acceptable re-docking was confirmed by a root-mean-square deviation (RMSD) of ≤2.0 Å between the re-docked and crystallographic poses, consistent with standard validation criteria.

## Statistical analyses

Origin v. 8.4 (OriginLab, Northampton, USA) was used to prepare graphs and perform data analysis. Data are presented as means ± standard error. Student's t-test and one-way ANOVA were used to evaluate group differences. Correlation was assessed by Pearson's correlation coefficient (r). A $p < 0.05$ was considered statistically significant.

# Results

## Bacterial isolates and CTX susceptibility

Twenty *P. aeruginosa* isolates were obtained from 260 midstream urine samples (incidence: 7.66%). The Kirby–Bauer disk diffusion method showed inhibitory zone diameters ranging from 7 ± 0.78 mm (Pa15) to 28 ± 4.8 mm (Pa7). MIC values ranged from 1.95 µg/mL (Pa2, Pa7, Pa17) to 250 µg/mL (Pa1, Pa5, Pa10, Pa15), confirming an inverse relationship between inhibition zone diameter and MIC (Table 1).

## Biofilm formation

All 20 isolates produced biofilm to varying extents, with $OD_{590}$ values ranging from 0.21 ± 0.17 to 0.66 ± 0.10. Five isolates (Pa1, Pa4, Pa5, Pa10, Pa15) were strong biofilm formers ($OD_{590} > 0.50$). Eight isolates were moderate biofilm formers, and four were weak biofilm formers. A significant negative correlation was observed between CTX inhibition zone diameter and biofilm formation ($r = -0.68$, $p < 0.001$), and a significant positive correlation was found between MIC values and biofilm biomass ($r = +0.70$, $p < 0.001$) (Fig. 1). These findings indicate that strong biofilm formation is associated with reduced susceptibility to CTX, consistent with the protective role of EPS polymer matrices (alginate, Pel, Psl) in shielding bacterial cells from antibiotic penetration.

## Effect of CTX sub-MICs on biofilm formation

CTX sub-MICs (½, ¼, ⅛, 1/16, 1/32 MIC) produced heterogeneous effects on biofilm formation across the 20 isolates.

**Table 1.** Antimicrobial susceptibility and biofilm formation of 20 clinical *P. aeruginosa* isolates. Isolates were cultured in Mueller–Hinton broth at 37°C under aerobic conditions for MIC determination and Tryptic Soy Broth supplemented with 0.25% glucose at 37°C for biofilm assays

| Isolate | Inhibitory zone (mm) | MIC (µg/mL) | Biofilm OD590 (mean ± SD) |
|---|---|---|---|
| Pa1 | 7 ± 1.1 | 250 | 0.56 ± 0.15 |
| Pa2 | 26 ± 2.7 | 1.95 | 0.26 ± 0.14 |
| Pa3 | 12 ± 1.4 | 62.5 | 0.46 ± 0.13 |
| Pa4 | 17 ± 2.7 | 31.25 | 0.66 ± 0.10 |
| Pa5 | 8 ± 1.3 | 250 | 0.59 ± 0.14 |
| Pa6 | 22 ± 3.4 | 3.9 | 0.42 ± 0.09 |
| Pa7 | 28 ± 4.8 | 1.95 | 0.36 ± 0.09 |
| Pa8 | 14 ± 2.1 | 62.5 | 0.45 ± 0.21 |
| Pa9 | 19 ± 2.8 | 15.6 | 0.33 ± 0.14 |
| Pa10 | 9 ± 0.9 | 250 | 0.61 ± 0.21 |
| Pa11 | 11 ± 1.4 | 125 | 0.52 ± 0.18 |
| Pa12 | 22 ± 3.6 | 3.9 | 0.21 ± 0.17 |
| Pa13 | 17 ± 3.2 | 31.25 | 0.33 ± 0.13 |
| Pa14 | 12 ± 1.2 | 62.5 | 0.45 ± 0.21 |
| Pa15 | 7 ± 0.78 | 250 | 0.58 ± 0.22 |
| Pa16 | 15 ± 1.7 | 15.6 | 0.41 ± 0.12 |
| Pa17 | 27 ± 3.6 | 1.95 | 0.31 ± 0.11 |
| Pa18 | 25 ± 3.8 | 3.9 | 0.49 ± 0.11 |
| Pa19 | 18 ± 2.8 | 15.6 | 0.46 ± 0.09 |
| Pa20 | 10 ± 1.03 | 125 | 0.48 ± 0.19 |

MIC – minimum inhibitory concentration; OD – optical density.

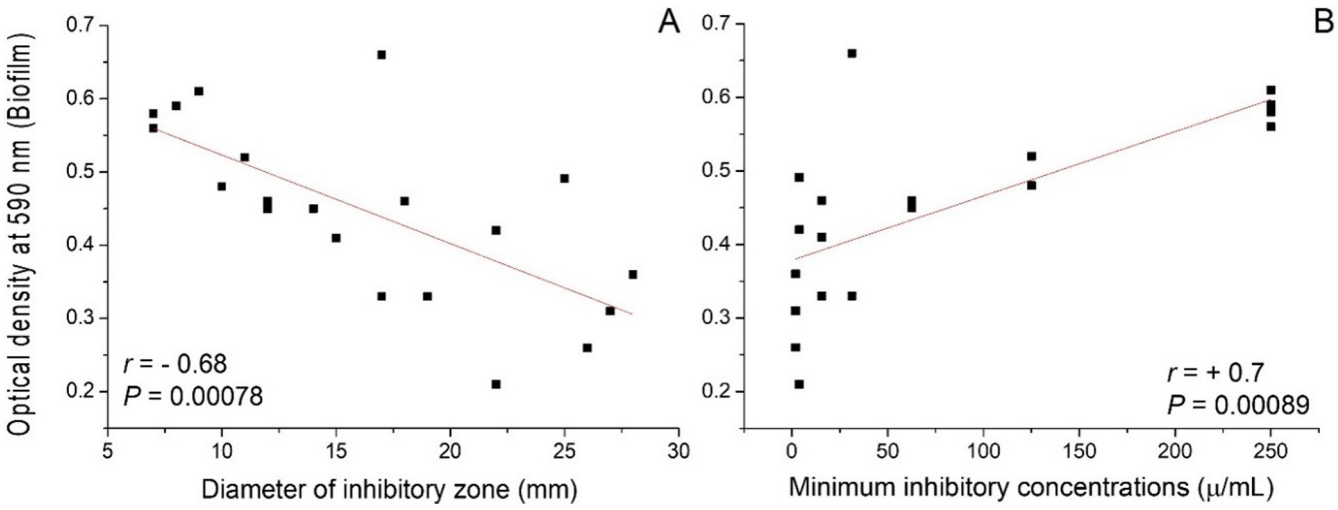


Fig. 1. Correlation analysis between ceftriaxone (CTX) susceptibility and biofilm formation in 20 *P. aeruginosa* isolates. Biofilm formation ($OD_{590}$) showed a significant negative correlation with inhibition zone diameter (mm) (A) and a significant positive correlation with MICs (µg/mL) (B). r, Pearson's correlation coefficient. Statistical significance was assessed using the p-value

The majority of isolates (Pa1–Pa8, Pa10–Pa11, Pa14–Pa20) exhibited a concentration-dependent reduction in biofilm biomass. Two isolates (Pa9 and Pa13) showed a paradoxical, transient increase in biofilm formation at intermediate sub-MIC concentrations (⅛–1⁄16 MIC), suggesting a stress-induced adaptive biofilm response. One isolate (Pa12) showed no significant change across all CTX sub-MICs (Fig. 2).

This paradoxical effect in a subset of strains likely reflects the upregulation of EPS polymer biosynthesis, particularly alginate overproduction, as a stress-response mechanism to a sublethal antibiotic challenge, a phenomenon associated with *mucA* mutation and sigma factor AlgT/U activation.[23]

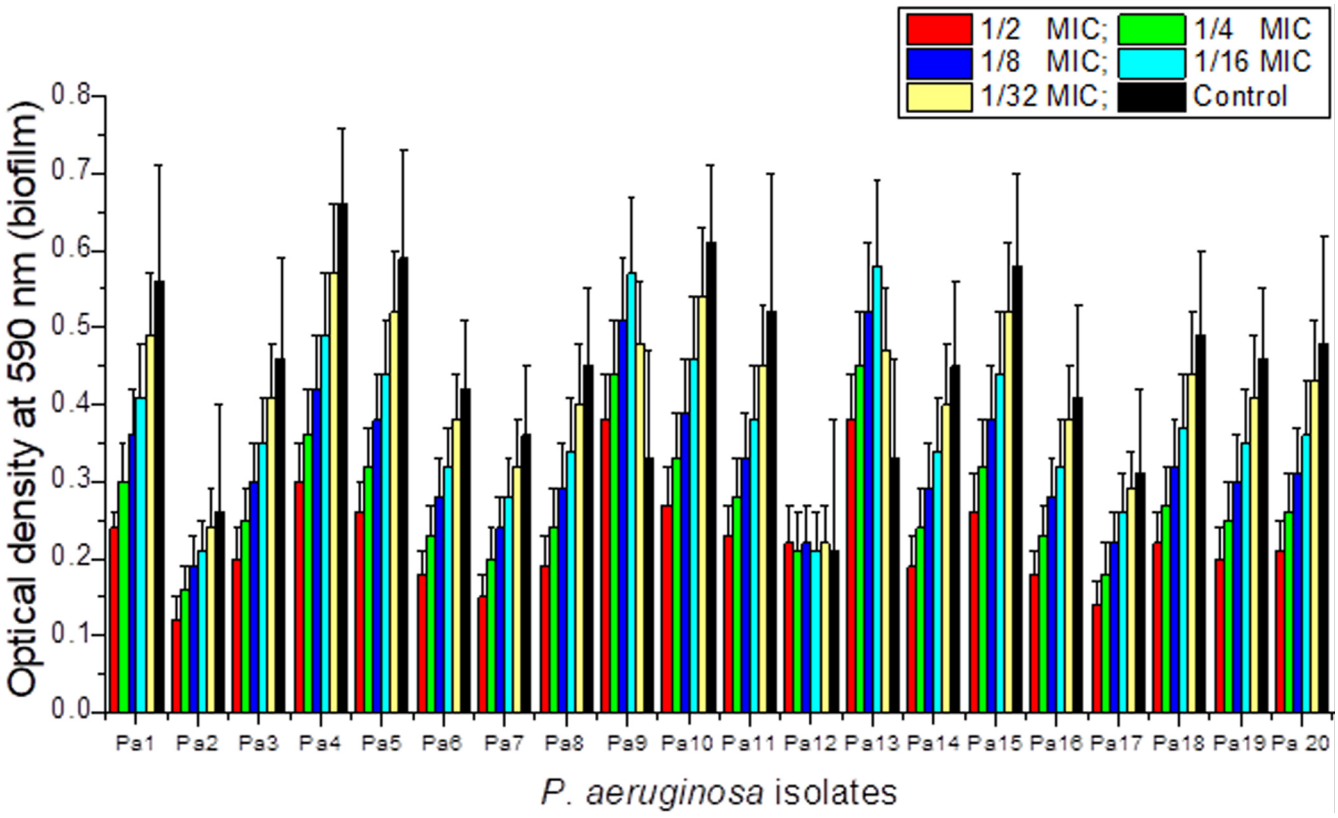


Fig. 2. Effect of CTX sub-MICs (½, ¼, ⅛, 1⁄16, and 1⁄32 MIC) on biofilm formation ($OD_{590}$) across 20 clinical *P. aeruginosa* UTI isolates, showing concentration-dependent suppression in 17 of 20 isolates, a paradoxical increase in Pa9 and Pa13, and no change in Pa12

## Effect of CTX sub-MICs on adhesion to mouse BECs

CTX sub-MICs reduced the number of viable Pa4 cells adherent to mouse BECs in a concentration-dependent manner. The greatest reduction was observed at ½ MIC. Significant decreases were observed at ½, ¼, ⅛, and 1⁄16 MIC concentrations. No significant effect was observed at 1⁄32MIC ($p > 0.05$; fig. 3). Microscopic examination (Fig. 4) confirmed a concentration-dependent reduction in bacterial adhesion to BECs. The reduction in surface adhesion at sub-inhibitory CTX concentrations may reflect diminished Psl polymer-mediated surface attachment, as Psl is a key mediator of initial surface colonization and its regulation falls under the QS network modulated by LasR and RhlR.

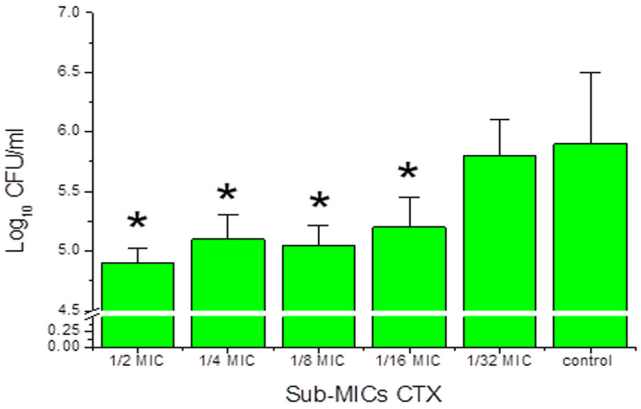


Fig. 3. Effect of different CTX sub-MIC concentrations on the ability of *P. aeruginosa* Pa4 to adhere to mouse BECs in vitro. Adhesion ability was determined by the number of viable bacterial cells, expressed as CFU/mL. Asterisks indicate a significant difference compared with the control (adhesion of Pa4 not exposed to CTX). A p-value <0.05 was considered statistically significant

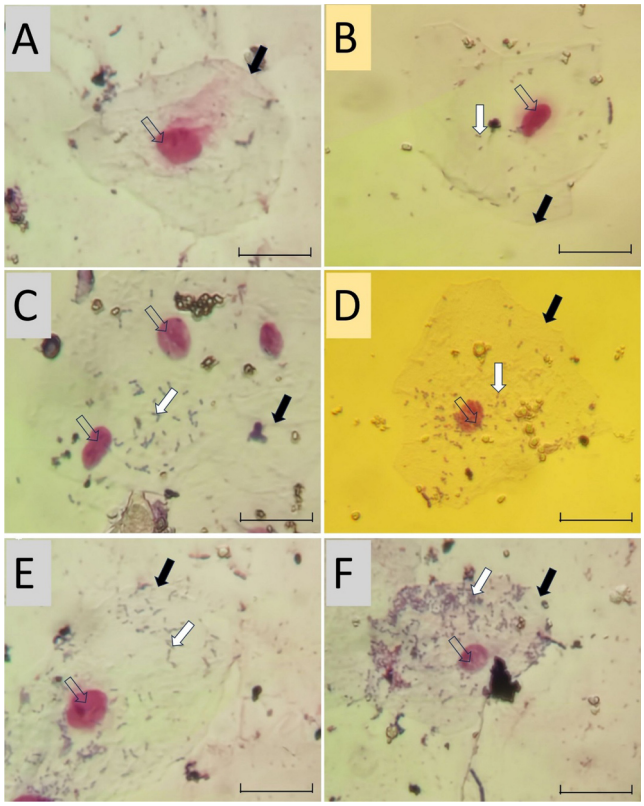


Fig. 4. Light micrographs showing the adhesion of *P. aeruginosa* (Pa4) treated with different CTX sub-MIC concentrations to mouse bladder epithelial cells (BECs). Bacterial treatments included ½ MIC (B), ¼ MIC (C), ⅛ MIC (D), and 1⁄32 MIC (E). Image A shows mouse BECs not exposed to Pa4 (negative control), whereas image F shows mouse BECs exposed to Pa4 without CTX treatment (positive control). Cells were stained with Leishman stain, and images were captured using a smartphone camera (Honor 400) mounted on a compound light microscope. White arrows indicate adherent bacteria, open arrows indicate epithelial cell nuclei, and black arrows indicate the epithelial cell membrane. Scale bar = 75 µm

## Effect of CTX sub-MICs on rhlR and LasR gene expression

Sub-MICs of CTX significantly downregulated QS gene expression (*rhlR* and *lasR*) in Pa4 in a concentration-dependent manner (Fig. 5). At ½ MIC, *lasR* and *rhlR* expression decreased to 0.28- and 0.42-fold, respectively. *lasR* exhibited greater sensitivity to CTX than *rhlR* at all sub-MIC concentrations. Since LasR directly governs the *algD* gene cluster and Pel/Psl biosynthesis operons, the observed downregulation of *lasR* by CTX sub-MICs provides a transcriptional mechanism for the concurrent reduction in biofilm EPS polymer matrix formation.

## Molecular docking of ceftriaxone with biofilm-associated target proteins

Re-docking validation: The re-docking RMSD values for all four target proteins were ≤1.8 Å (LasR: 1.3 Å; RhlR: 1.6 Å; AlgD: 1.7 Å; PelB: 1.5 Å), confirming the reliability of the docking protocol.

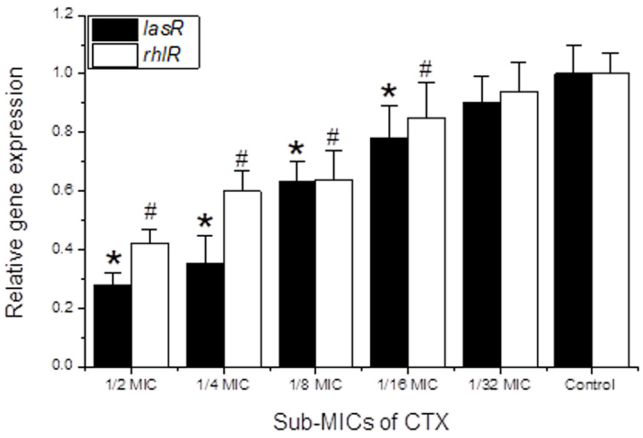


Fig. 5. Impact of sub-MICs of ceftriaxone (CTX) on *lasR* and *rhlR* quorum-sensing (QS) gene expression in *P. aeruginosa* Pa4. Relative expression levels of *lasR* and *rhlR* were quantified by qRT-PCR and normalized to a housekeeping gene using the 2^ΔΔCt method. Exposure to sub-MIC concentrations of CTX resulted in concentration-dependent downregulation of both genes, with *lasR* showing greater sensitivity than *rhlR*. Data are presented as mean ± SD; *indicates a significant difference ($p < 0.05$) compared with the control (*lasR* gene expression in Pa4 not exposed to CTX); # indicates a significant difference ($p < 0.05$) compared with the control (*rhlR* gene expression in Pa4 not exposed to CTX)

CTX–LasR interaction: Molecular docking of CTX into the LasR ligand-binding domain (PDB: 2UV0) yielded a binding energy of –8.3 kcal/mol, which is comparable to that of the native autoinducer *N*-(3-oxododecanoyl)-L-homoserine lactone (3-oxo-C12-HSL; –8.7 kcal/mol). CTX occupied the hydrophobic pocket of LasR, with hydrogen bond formation involving residues Trp60, Asp73, Tyr93, and Ser129 through its aminothiazole ring and oxime functional group. Hydrophobic contacts were established with Ala127, Tyr134, Leu125, and Phe163. The favorable docking energy and overlap with the autoinducer-binding site suggest that CTX may competitively displace the native QS signal from LasR, thereby inhibiting LasR-dependent transcriptional activation of virulence and EPS polymer biosynthesis genes (Table 2, Fig. 6A).

CTX–RhlR interaction: Docking of CTX into the RhlR ligand-binding domain (PDB: 3T5K) yielded a binding energy of –7.1 kcal/mol. Key hydrogen bonds were formed with Asp38, Tyr64, and Arg61, while hydrophobic contacts involved Ile40, Leu62, Phe82, and Val111. The lower binding energy compared with LasR is consistent with the experimentally observed greater sensitivity of *lasR* gene expression to CTX sub-MIC stress (Table 2, Fig. 6B).

CTX–AlgD interaction: AlgD (GDP-mannose dehydrogenase; PDB: 1MV8) is the rate-limiting enzyme in alginate polymer biosynthesis. Docking of CTX against AlgD yielded a binding energy of –7.6 kcal/mol, with key interactions involving the NAD+-binding residues Lys59, Thr145, and Arg264 via hydrogen bonding. These interactions were concentrated at the coenzyme-binding cleft, suggesting that CTX may interfere with the enzymatic activity of AlgD and thereby reduce alginate EPS polymer production (Table 2, Fig. 6C).

CTX–PelB interaction: Docking against PelB (PDB: 5TCB), a key outer-membrane auxiliary protein involved in Pel polysaccharide secretion, yielded a binding energy of –6.4 kcal/mol, with hydrogen bonding to Arg135, Tyr175, and Asn201. This interaction may interfere with Pel polymer export (Table 2, Fig. 6D). The binding energies are summarized in Table 2.

**Table 2.** Summary of molecular docking results for ceftriaxone (CTX) against biofilm-associated target proteins of *Pseudomonas aeruginosa*

| Target protein | PDB ID | Binding energy, kcal/mol (kJ/mol) | Key interacting residues | Biological role |
|---|---|---|---|---|
| LasR (LBD) | 2UV0 | –8.3 (–34.7 kJ/mol) | Trp60, Asp73, Tyr93, Ser129, Phe163 | QS master regulator; algD/pel/psl activator |
| RhlR (LBD) | 3T5K | –7.1 (–29.7 kJ/mol) | Asp38, Tyr64, Arg61, Phe82 | QS secondary regulator; rhamnolipid activator |
| AlgD | 1MV8 | –7.6 (–31.8 kJ/mol) | Lys59, Thr145, Arg264 | Alginate polymer biosynthesis |
| PelB | 5TCB | –6.4 (–26.8 kJ/mol) | Arg135, Tyr175, Asn201 | Pel polymer secretion |

LBD – ligand-binding domain; QS – quorum sensing; kcal/mol – kilocalories per mole; kJ/mol – kilojoules per mole.

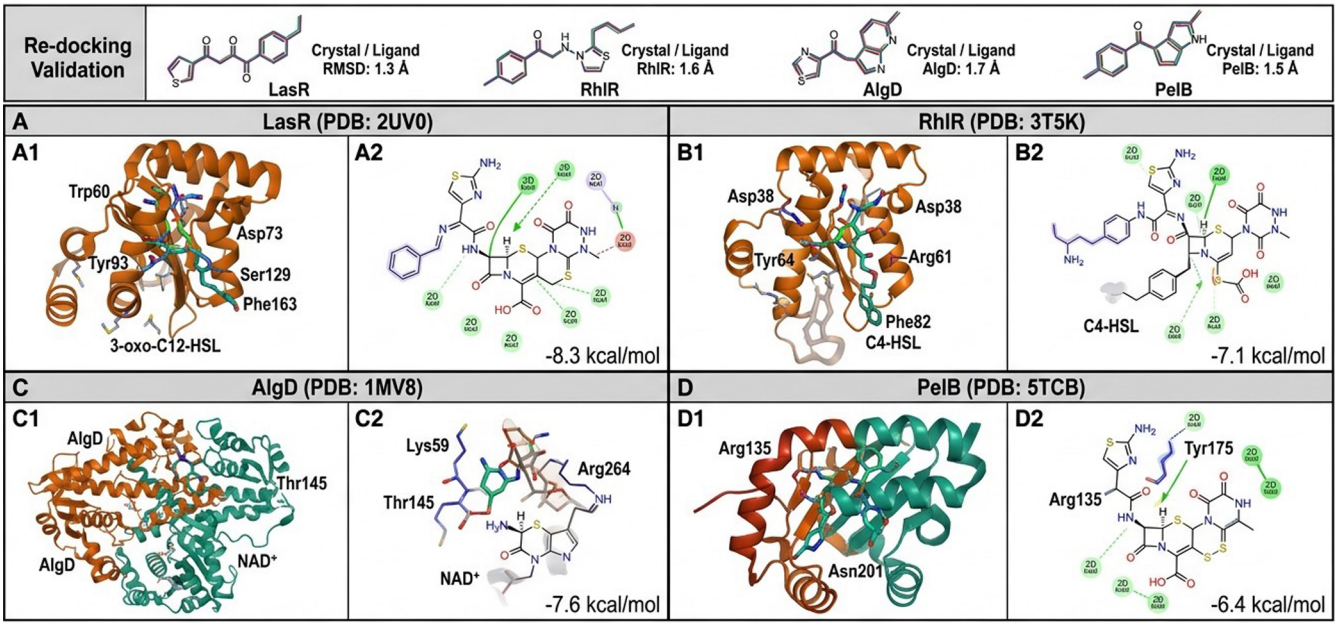


**Fig. 6.** Molecular docking analysis of ceftriaxone (CTX) with biofilm-associated target proteins. (A) Interaction of CTX with the LasR ligand-binding domain (PDB: 2UV0), demonstrating occupation of the hydrophobic pocket and overlap with the autoinducer-binding site. (B) Docking of CTX into the RhlR ligand-binding domain (PDB: 3T5K). (C) Interaction of CTX with the rate-limiting enzyme AlgD (PDB: 1MV8), highlighting binding at the $NAD^+$ coenzyme-binding cleft. (D) Docking of CTX against the outer-membrane auxiliary protein PelB (PDB: 5TCB). Panels A1, B1, C1, and D1 show the 3D binding poses. Panels A2, B2, C2, and D2 show the 2D interaction diagrams

## Discussion

UTIs caused by *P. aeruginosa* are among the most challenging conditions for physicians to manage owing to its extensive antibiotic resistance.[24,25] Biofilm formation is a central virulence mechanism, and the EPS polymer matrix comprising alginate, Pel, and Psl plays a decisive role in antibiotic tolerance and persistent infection.[23,26]

The present study demonstrates that sub-MIC concentrations of CTX modulate *P. aeruginosa* biofilm formation and epithelial cell adhesion through QS gene downregulation and provides novel molecular docking evidence for direct CTX interactions with QS receptor proteins and biofilm EPS polymer biosynthetic enzymes.

In the present study, mouse BECs were used as a biotic model to study bacterial adhesion rather than human BECs because both cell types may yield comparable data on the adhesion of *P. aeruginosa* to biotic surfaces. The mouse BEC model was used because these cells are available in our laboratory, are easy to handle, and offer ethical advantages for preliminary adhesion studies.

All *P. aeruginosa* isolates from UTI urine samples formed biofilms at varying levels. The significant positive correlation between MIC and biofilm biomass ($r = +0.70$, $p < 0.001$) confirms that biofilm formation contributes to antibiotic tolerance. This correlation is mechanistically explained by the biofilm EPS polymer matrix: alginate and Pel polysaccharides create a physical diffusion barrier that reduces effective intra-biofilm CTX concentrations, while Psl reinforces surface adhesion. Isolates forming stronger biofilms thus require higher antibiotic concentrations for inhibition.[27]

Crystal violet staining is the preferred method for measuring biofilm biomass; it has been extensively validated in *P. aeruginosa* biofilm research and is used in several studies.[13,14,18] This method measures the total biofilm biomass (including both bacterial cells and the biofilm extracellular matrix) and provides a statistically validated measure of treatment-induced suppression of biofilm formation.

Although direct quantification of EPS polymers would further support these data, we believe that combining biofilm biomass measurements with qRT-PCR gene expression analysis to determine how CTX affects biofilm formation yields valuable mechanistic insights into CTX-mediated biofilm modulation.

Sub-MICs of CTX reduced biofilm formation in the majority (17/20) of isolates in a concentration-dependent manner. Not only did CTX reduce biofilm formation, but previous studies have also shown that CTX possesses antibiofilm activity and that different β-lactam antibiotics can reduce biofilm formation by *P. aeruginosa*.

In the present study, the *rhlR* and *lasR* genes were chosen because they represent the 2 main quorum-sensing systems of *P. aeruginosa*. The 2 systems work together hierarchically to regulate biofilm formation and exopolysaccharide (EPS) production. The *lasR* gene is the master regulator of QS and activates the *rhlR* system, which in turn regulates the *algD*, *pel*, and *psl* operons. Therefore, these 2 genes are critical for understanding QS inhibition by CTX.[28]

At the molecular level, the concurrent downregulation of *lasR* and *rhlR* by CTX sub-MICs provides a transcriptional explanation for reduced EPS polymer production: LasR directly activates the *algD* biosynthetic gene cluster (required for alginate polymer synthesis) and the *pel*/*psl* operons responsible for Pel and Psl polysaccharide production.[29] Downregulation of LasR therefore simultaneously reduces alginate viscosity, Pel-mediated cohesion, and Psl-mediated surface attachment, collectively dismantling the biofilm polymer scaffold.[10,11]

Paradoxically, two isolates (Pa9 and Pa13) showed a transient increase in biofilm formation at intermediate sub-MIC concentrations. This stress-induced response is consistent with the well-characterized "alarm" mechanism in *P. aeruginosa*, whereby sublethal antibiotic stress triggers the AlgT/U sigma factor, leading to mucoid conversion and alginate overproduction as a protective response.

Importantly, the *mucA* gene encodes a negative regulator (anti-sigma factor) of AlgT/U, thereby suppressing alginate overproduction in *P. aeruginosa*. Under antibiotic stress, *mucA* is frequently mutated, resulting in constitutive overproduction of alginate and enhanced biofilm tolerance.[23,30]

These findings underscore the risk of using subtherapeutic antibiotic concentrations, as they may drive selection for mucoid, hyper-biofilm-forming phenotypes and promote the emergence of new antibiotic-resistant *P. aeruginosa* isolates, making the treatment of bacterial infections a major challenge for physicians.

The present study demonstrated that sub-MICs of CTX downregulated the expression of *lasR* and *rhlR* in a concentration-dependent manner, with *lasR* exhibiting greater sensitivity. This hierarchy aligns with the upstream regulatory position of the Las system: LasR activates *rhlR* expression, meaning that CTX-mediated interference with LasR signaling has compounding downstream effects across the entire QS network.

Our molecular docking data provide a structural mechanism for this preferential sensitivity: CTX binds within the LasR ligand-binding domain with a binding energy (–8.3 kcal/mol) close to that of the native autoinducer (–8.7 kcal/mol), suggesting competitive displacement of 3-oxo-C12-HSL from the LasR binding pocket. This would prevent LasR dimerization and DNA binding, thereby repressing LasR-dependent transcription of virulence and EPS polymer biosynthesis genes.[31]

The molecular docking interaction of CTX with AlgD (binding energy: –7.6 kcal/mol) at the NAD+-binding site is particularly significant. AlgD catalyzes the irreversible oxidation of GDP-mannose to GDP-mannuronic acid, the committed step in alginate polymer biosynthesis. Inhibition of AlgD would reduce the pool of alginate monomers, directly impairing alginate EPS polymer production. Similarly, CTX interaction with PelB (–6.4 kcal/mol),

an auxiliary protein involved in Pel polysaccharide secretion, suggests an additional mechanism by which CTX may disrupt Pel polymer assembly at the bacterial outer membrane.[32,33]

These computational findings collectively suggest that CTX exerts antibiofilm effects through a multi-target mechanism: (i) QS receptor antagonism (LasR and RhlR), (ii) transcriptional downregulation of EPS polymer gene clusters, and (iii) potential direct enzymatic interference with alginate and Pel biosynthetic enzymes.

A previous study by Talib and Ghafil demonstrated the effects of CTX sub-MICs on *P. aeruginosa* biofilm formation and adhesion to human oral mucosal epithelial cells,[14] while Naga et al. reported QS gene modulation by a ceftriaxone–nickel complex.[15] The present study extends these findings by focusing on UTI-derived isolates, mouse BEC adhesion, and, critically, by providing the first molecular docking analysis of CTX binding to *P. aeruginosa* QS receptors and EPS polymer biosynthetic enzymes, offering a mechanistic structural framework for the observed biological activities. These docking insights align with emerging polymer-focused antibiofilm strategies that target EPS biosynthesis as a therapeutic vulnerability.[34]

The molecular docking analysis in the present study showed favorable binding energies and suitable binding-site localization for CTX interactions with LasR, RhlR, AlgD, and PelB. However, the current predictions remain computational and cannot be confirmed without direct biophysical evidence. In contrast to QS gene downregulation (validated by qRT-PCR), the proposed CTX–protein interactions remain mechanistic hypotheses that require validation using surface plasmon resonance (SPR), isothermal titration calorimetry (ITC), or enzyme inhibition assays. Therefore, QS inhibition via *lasR*/*rhlR* transcriptional suppression represents the primary validated mechanism of antibiofilm activity identified in this study, whereas targeting of EPS biosynthetic enzymes (AlgD and PelB) should be considered a plausible secondary mechanism pending experimental validation.

## Limitations

This study has several limitations. First, only a single high-biofilm-forming isolate (Pa4) was used for QS gene expression and adhesion experiments, as the study aimed to characterize the effects of multiple sub-MIC concentrations rather than a single concentration. However, several previous studies used a single isolate to examine the effects of antibiotics on biofilm formation, and other studies investigated QS gene expression in a single bacterial isolate (*P. aeruginosa* and *Vibrio harveyi*).[13,18,35,36]

Second, the molecular docking analysis is computational in nature and requires experimental validation by surface plasmon resonance, isothermal titration calorimetry, or co-crystallography to confirm direct CTX binding to LasR, RhlR, AlgD, and PelB proteins. Third, all experiments were conducted in vitro, and the relevance of sub-MIC CTX effects on biofilm EPS polymer dynamics in vivo requires further investigation in animal infection models. In our laboratory, we plan to extend the findings of the current study using a murine animal model. The project has been prepared and will commence upon receipt of final approval.

Finally, this study did not directly quantify EPS polymer components (alginate, Pel, and Psl) by chemical analysis, which would strengthen the correlation between QS gene downregulation and EPS polymer reduction. In future studies, we suggest evaluating existing QS inhibitors (e.g., furanones and salicylate analogs) and biofilm disruptors (e.g., DNase and chelating agents); the potential of CTX–QS inhibitor combinations remains unexplored. This approach would have high clinical relevance for the treatment of recalcitrant UTIs.

## Conclusions

The present study shows that *P. aeruginosa* isolates from urine samples form variable levels of biofilm. Sub-inhibitory concentrations of CTX exerted heterogeneous effects on biofilm formation but reduced biofilm formation in most (17/20) isolates and decreased *P. aeruginosa* (Pa4) adhesion to mouse BECs.

The sub-inhibitory concentrations of CTX downregulated the QS regulatory genes *lasR* and *rhlR*, with *lasR* being more sensitive. Molecular docking analysis demonstrates that CTX binds favorably to the ligand-binding pockets of the LasR and RhlR QS receptor proteins, competitively displacing native autoinducers and providing a structural basis for QS inhibition.

Additional docking interactions with AlgD and PelB suggest that CTX may directly interfere with alginate and Pel EPS polymer biosynthesis. These findings position CTX as a multitarget antibiofilm and anti-QS agent, with potential implications for polymer-focused therapeutic strategies targeting *P. aeruginosa* biofilm EPS matrix formation.

## Data availability

The datasets generated and/or analyzed during the current study are available from the corresponding author on reasonable request. Molecular docking files (input/output) are available upon request.

## Consent for publication

Not applicable. No personal data, images, or information that could identify individuals are included in this manuscript.

## Ethical approval

This study was approved by the Ethics Committee of the University of Baghdad, Iraq (CSEC/1025/0122; October 12, 2025), since it was a retrospective analysis of routinely collected clinical data; individual patient consent was waived in accordance with national ethical guidelines and the Declaration of Helsinki.

### ORCID iDs

Nabaa Amer Jaber 0009-0003-9166-248X
Jenan Atiyah Ghafil 0000-0003-1461-302X

### References

1. Moursi SA, Saleem M, Alharbi MS, et al. Resistance patterns and virulence factors of *Pseudomonas aeruginosa* in hospitalized patients: A Saudi Arabian study. *Sci Rep*. 2025;15(1):38118. doi:10.1038/s41598-025-18388-x
2. Miller E, Jamal H, Patel P. Recurrent bacteremia in the setting of *Pseudomonas* endocarditis of the tricuspid valve and indwelling medical devices. *Cureus*. 2024;16(12):e76368. doi:10.7759/cureus.76368
3. Tegegne DT, Abbott IJ, Poźniak B. Catheter-associated urinary tract infections: Understanding the interplay between bacterial biofilm and antimicrobial resistance. *Int J Mol Sci*. 2025;26(18):9193. doi:10.3390/ijms26189193
4. Horcajada JP, Gales A, Isler B, et al. How do I manage difficult-to-treat *Pseudomonas aeruginosa* infections? Key questions for today's clinicians. *Clin Microbiol Infect*. 2025;31(11):1797–1806. doi:10.1016/j.cmi.2025.08.018
5. Horcajada JP, Montero M, Oliver A, et al. Epidemiology and treatment of multidrug-resistant and extensively drug-resistant *Pseudomonas aeruginosa* infections. *Clin Microbiol Rev*. 2019;32(4):e00031-19. doi:10.1128/CMR.00031-19
6. Colvin KM, Gordon VD, Murakami K, et al. The Pel polysaccharide can serve a structural and protective role in the biofilm matrix of *Pseudomonas aeruginosa*. *PLoS Pathog*. 2011;7(1):e1001264. doi:10.1371/journal.ppat.1001264
7. Billings N, Ramirez Millan M, Caldara M, et al. The Extracellular Matrix Component Psl Provides Fast-Acting Antibiotic Defense in Pseudomonas aeruginosa Biofilms. *PLoS Pathog*. 2013;9(8):e1003526. doi:10.1371/journal.ppat.1003526
8. Hay ID, Rehman ZU, Moradali MF, Wang Y, Rehm BHA. Microbial alginate production, modification and its applications. *Microb Biotechnol*. 2013;6(6):637–650. doi:10.1111/1751-7915.12076
9. Wu L, Liu Y, Deng J, Gui S, Nie H. Integrated analysis of electrical stimulation effects on Pseudomonas aeruginosa PAO1 inoculated denitrifying community: targeted and untargeted metabolomic analysis of phenazine biosynthesis and quorum sensing. *Front Microbiol*. 2025;16:1621417. doi:10.3389/fmicb.2025.1621417
10. Ramesh R, Rekha ND, Gopal S. Pseudomonas aeruginosa biofilm: treatment strategies to combat infection. *Arch Microbiol*. 2025;207(6):141. doi:10.1007/s00203-025-04346-8
11. Irie Y, Starkey M, Edwards AN, Wozniak DJ, Romeo T, Parsek MR. *Pseudomonas aeruginosa* biofilm matrix polysaccharide Psl is regulated transcriptionally by RpoS and post-transcriptionally by RsmA. *Mol Microbiol*. 2010;78(1):158–172. doi:10.1111/j.1365-2958.2010.07320.x
12. Brust-Sisti L, Hu GY, Bridgeman M, Brunetti L, Gonzalez J. Comparative efficacy of high- and low-dose ceftriaxone regimens: A systematic review and meta-analysis. *Ann Pharmacother*. 2026;60(4):357–365. doi:10.1177/10600280251346777
13. Sadiq SI, Ghafil JA. Polyhydroxybutyrate nanoparticle improving the sensitivity of *Pseudomonas aeruginosa* to ceftriaxone and reducing the biofilm formation in vitro. *Polim Med*. 2025;55(1):31–39. doi:10.17219/pim/203765
14. Talib MM, Ghafil JA. Effect of sub-minimum inhibitory concentrations of ceftriaxone on the *Pseudomonas aeruginosa* adhesion to human oral mucosal epithelial cells and biofilm formation to polystyrene in vitro. *Pharm Sci Asia*. 2024;51(2):180–189. doi:10.29090/psa.2024.02.24.1752
15. Naga NG, El-Badan DE, Mabrouk MEM, Rateb HS, Ghanem KM, Shaaban MI. Innovative application of ceftriaxone as a quorum sensing inhibitor in *Pseudomonas aeruginosa*. *Sci Rep*. 2025;15(1):5022. doi:10.1038/s41598-025-87609-0
16. Talib MM, Ghafil JA. Comparative adhesion of *Pseudomonas aeruginosa* to human oral mucosal epithelial cells and polystyrene surfaces. *J Fac Med Baghdad*. 2024;66(3):344–349. doi:10.32007/jfacmedbaghdad.6632328
17. Ficociello B, Giordano D, Incoronato F, Farinella A, Pietrangeli B. WHO Laboratory Biosafety Manual: A new approach to security. *Ann Work Expo Health*. 2023;67(4):425–429. doi:10.1093/annweh/wxac086
18. Al-mutalib LAA, Zgair AK. Sub-inhibitory doses of Ofloxacin reduce adhesion and biofilm formation of *Pseudomonas aeruginosa* to biotic and abiotic surfaces. *Pharm Sci Asia*. 2023;50(3):196–203. doi:10.29090/psa.2023.03.23.377
19. Abbasi Z, Sadiq SI, Obaid M. Antibacterial effect of *Thymus vulgaris* essential oil against ceftazidime-resistant *Enterococcus faecalis*. *World J Exp Biosci*. 2025;13(1):15–18. doi:10.65329/wjeb.v13.01.004
20. Zgair AK, Al-Adressi AMH. *Stenotrophomonas maltophilia* fimbrin stimulates mouse bladder innate immune response. *Eur J Clin Microbiol Infect Dis*. 2013;32(1):139–146. doi:10.1007/s10096-012-1729-0
21. Livak KJ, Schmittgen TD. Analysis of relative gene expression data using real-time quantitative PCR and the 2−ΔΔCT method. *Methods*. 2001;25(4):402–408. doi:10.1006/meth.2001.1262
22. Trott O, Olson AJ. AutoDock Vina: Improving the speed and accuracy of docking with a new scoring function, efficient optimization, and multithreading. *J Comput Chem*. 2010;31(2):455–461. doi:10.1002/jcc.21334
23. Wiens JR, Vasil AI, Schurr MJ, Vasil ML. Iron-regulated expression of alginate production, mucoid phenotype, and biofilm formation by *Pseudomonas aeruginosa*. *mBio*. 2014;5(1):e01010-13. doi:10.1128/mBio.01010-13
24. Bontemps-Gallo S. The cost of chronicity: *Pseudomonas aeruginosa's* silent evolution in the urinary tract. *Microbiol Spectr*. 2026;14(1):e03381-25. doi:10.1128/spectrum.03381-25
25. Saleh FM, Mohammed HA. Variations in *Pseudomonas aeruginosa* biofilm formation influence virulence and amoxicillin resistance. *World J Exp Biosci*. 2025;13(1):19–23. doi:10.65329/wjeb.v13.01.005
26. Taha AB. Bacteriological profile, antibiotic susceptibility, and biofilm formation in children with chronic suppurative otitis media. *Int J Pediatr Otorhinolaryngol*. 2025;188:112208. doi:10.1016/j.ijporl.2024.112208
27. Arami N, Tajani AS, Hashemi M, et al. Targeted inhibition of PqsR in *Pseudomonas aeruginosa* PAO1 quorum-sensing network by chalcones as promising antibacterial compounds. *Mol Biol Rep*. 2025;52(1):175. doi:10.1007/s11033-025-10270-3
28. Elnegery AA, Mowafy WK, Zahra TA, Abou El-Khier NT. Study of quorum-sensing LasR and RhlR genes and their dependent virulence factors in *Pseudomonas aeruginosa* isolates from infected burn wounds. *Access Microbiol*. 2021;3(3):000211. doi:10.1099/acmi.0.000211
29. Amer AN, Attia N, Baecker D, Mansour RE, El-Soudany I. Growth-phase-dependent modulation of quorum sensing and virulence factors in *Pseudomonas aeruginosa* ATCC 27853 by sub-MICs of antibiotics. *Antibiotics (Basel)*. 2025;14(7):731. doi:10.3390/antibiotics14070731
30. Chen P, Qin J, Su HK, Du L, Zeng Q. Harmine acts as a quorum sensing inhibitor decreasing the virulence and antibiotic resistance of *Pseudomonas aeruginosa*. *BMC Infect Dis*. 2024;24(1):760. doi:10.1186/s12879-024-09639-9
31. Yakobi SH, Nwodo UU. Structure-based screening and molecular dynamics of phytophytochemicals against *Pseudomonas aeruginosa* quorum sensing systems. *J Genet Eng Biotechnol*. 2025;23(4):100603. doi:10.1016/j.jgeb.2025.100603
32. Moradali MF, Ghods S, Rehm BHA. *Pseudomonas aeruginosa* lifestyle: A paradigm for adaptation, survival, and persistence. *Front Cell Infect Microbiol*. 2017;7:39. doi:10.3389/fcimb.2017.00039
33. Franklin MJ, Nivens DE, Weadge JT, Howell PL. Biosynthesis of the *Pseudomonas aeruginosa* extracellular polysaccharides, alginate, Pel, and Psl. *Front Microbiol*. 2011;2:167. doi:10.3389/fmicb.2011.00167
34. Al-Maddboly LA, El-Salam MA, Bastos JK, Hasby EA, Kushkevych I, El-Morsi RM. Anti-biofilm and anti-quorum sensing activities of galloylquinic acid against clinical isolates of multidrug-resistant *Pseudomonas aeruginosa* in open wound infection: In vitro and in vivo efficacy studies. *BMC Microbiol*. 2025;25(1):206. doi:10.1186/s12866-024-03712-8
35. Anetzberger C, Schell U, Jung K. Single cell analysis of *Vibrio harveyi* uncovers functional heterogeneity in response to quorum sensing signals. *BMC Microbiol*. 2012;12(1):209. doi:10.1186/1471-2180-12-209
36. Kok LC, Tsai CC, Liao YH, et al. Roles of transcriptional factor PsrA in the regulation of quorum sensing in *Pseudomonas aeruginosa* PAO1. *Front Microbiol*. 2024;15:1424330. doi:10.3389/fmicb.2024.1424330

# Microwave plasma-induced effects on human immune lymphocytes

Atheer Q. Muryoush[1,B–D], Jenan Hussein Taha[2,B–E], Sura Allawi Obaid[3,B,E], Bahaa Al-Rubaii[3,D,E]

[1] Department of Physics, College of Science for Women, Baghdad University, Iraq
[2] Physiology and Medical Physics Department, College of Medicine, University of Al-Nahrain, Baghdad, Iraq
[3] Biology Department, College of Science, University of Baghdad, Baghdad, Iraq

A – research concept and design; B – collection and/or assembly of data; C – data analysis and interpretation; D – writing the article; E – critical revision of the article; F – final approval of the article

Polymers in Medicine, ISSN 0370-0747, eISSN 2451-2699 *Polim Med*. 2026;56(1):75–81

**Address for correspondence**
Bahaa Al-Rubaii
E-mail: bahaa.abdullah@sc.uobaghdad.edu.iq

**Funding sources**
None declared

**Conflict of interest**
None declared

**Acknowledgements**
None declared

Received on December 3, 2025
Reviewed on January 30, 2026
Accepted on February 26, 2026

Published online on June 30, 2026

## Abstract

**Background.** Microwave plasma generates reactive oxygen and nitrogen species, making it popular in biomedical research. These species affect human cell shape, viability, and function. Plasma-induced biochemical changes affect lymphocytes, which regulate immunological responses.

**Objectives.** This study aims to investigate the effects of microwave plasma on lymphocyte cells to estimate how different exposure times affect their biological responses. Lymphocytes were exposed to microwave plasma for different time intervals.

**Materials and methods.** Healthy men aged 25–30 years provided 5 mL venous blood samples in sterile heparinized tubes. After stimulation with phytohemagglutinin (PHA), lymphocytes were grown in RPMI-1640 medium at 37°C for 72 h. After incubation, cells were centrifuged, red blood cells were lysed with a hypotonic solution, and fixed with methanol:acetic acid (3:1). The fixed cell suspension was air-dried and Giemsa-stained on glass slides.

**Results.** Studies have indicated that exposure to plasma alters the morphology and behavior of lymphocytes. Reactive species that interact with cell membranes and intracellular components may cause these alterations. Plasma has potential in biomedical applications, but exposure parameters must be carefully controlled. Short-term plasma exposure appears to boost cell proliferation in healthy lymphocytes, bolstering the immune response. In contrast, extended plasma exposure (≥25 min) may reduce pathological cell proliferation in diseased cells.

**Conclusions.** Short-duration plasma treatment promotes normal cell function, while extended exposure times target diseased cells. Microwave plasma has 2 effects depending on exposure time. Plasma exerts different biological effects depending on exposure time. Short exposure boosts normal lymphocyte activity and proliferation, but long exposure suppresses aberrant cells. Thus, microwave plasma is attractive for biomedical applications when exposure parameters are well controlled.

**Key words:** plasma, lymphocytes, immune system, tissue culture

**Cite as**
Muryoush AQ, Taha JH, Obaid SA, Al-Rubaii B. Microwave plasma-induced effects on human immune lymphocytes. *Polim Med*. 2026;56(1):75–81. doi: 10.17219/pim/218614

**DOI**
10.17219/pim/218614

## Highlights

- Microwave plasma modulates lymphocyte morphology and function: Exposure to plasma-generated reactive oxygen and nitrogen species significantly alters lymphocyte shape, viability, and biological behavior.
- Exposure time determines biological response: Short-term microwave plasma exposure enhances normal lymphocyte proliferation and immune activation, while prolonged exposure (≥25 minutes) suppresses pathological cell growth.
- Reactive species drive cellular biochemical changes: Plasma-induced oxidative and nitrosative stress interacts with cell membranes and intracellular components, influencing immune cell regulation.
- Therapeutic potential with controlled parameters: Microwave plasma shows promise in biomedical and immunological applications, provided exposure duration is carefully optimized to balance immune stimulation and anti-proliferative effects.

## Background

Cold plasma has emerged as a novel and versatile technology, gaining significant attention in recent years due to its broad spectrum of applications in medicine, therapeutics, biology, and even industry. As a partially ionized gas, cold plasma constitutes a reactive environment enriched with free electrons, ions, ultraviolet radiation, and reactive oxygen and nitrogen species (RONS).[1,2] These components collectively enable cold plasma to interact directly with cellular structures and biological processes.[3,4] These processes occur without inducing considerable thermal damage, which distinguishes it from conventional thermal approaches.[5,6] Cell division is a fundamental biological process that governs tissue growth, repair, and regeneration, and its deregulation plays a critical role in the onset and progression of cancer.[6,7] Recent investigations have demonstrated that the biological effects of cold plasma on lymphocytes are highly dependent on both the type of cells exposed and the parameters of plasma treatment, such as intensity and duration.[8,9] In normal cells, low-dose exposure to cold plasma has been reported to enhance proliferative activity and promote regenerative responses, whereas high-dose exposure can inhibit or completely suppress cell division by inducing oxidative stress pathways.[10,11] Conversely, in malignant cells, cold plasma has shown pronounced efficacy in slowing down or arresting cellular proliferation, in addition to triggering programmed cell death (apoptosis).[12,13] These unique dual effects of cold plasma, promoting regeneration in normal cells while suppressing proliferation in cancerous cells, underscore its potential as a promising adjunctive tool in oncology and regenerative medicine. The tissue culture technique is a widely used method for observing dividing lymphocytes (blast cells) and determining the mitotic index (MI), which examines the abnormal behavior of living cells as a result of exposure to external agents, whether therapeutic or harmful.[14] Such agents may include cold exposure, mutagens, carcinogens, and various types of radiation such as plasma.[15] The tissue culture method has been widely applied in cytogenetic studies due to the relative ease of obtaining blood samples by venipuncture compared with collecting epithelial cells from the oral cavity, which requires a longer duration.[16] There are many reports addressing the application of this method in studying cases of leukemia, chromosomal abnormalities, and various types of genetic mutations.[17,18] Current research increasingly utilizes the MI assay in lymphocytes because of their high mitotic activity. This process indicates the ability of living organisms to resist external influences. An increase in dividing lymphocytes indicates enhanced mitotic activity, whereas a decrease reflects suppression of cell division.[19,20] This phenomenon has been used as a marker to study the effects of mutagens and other factors on chromosomes. The MI, defined as the percentage of dividing cells among 1,000 observed cells, is considered an important cytogenetic parameter in assessing mitotic activity and the potential of cells to continue dividing or to display signs of apoptosis.[21,22] Therefore, the MI is used to diagnose the causes of reduced mitotic activity and to propose solutions for enhancing the overall ability of cells to divide.[23,24]

## Materials and methods

### Blood culture

A venous blood sample (5 mL) was collected from healthy male volunteers aged between 25–30 years and transferred into sterile heparinized tubes containing 0.2 mL of heparin as an anticoagulant. The samples were cultured at 37°C. For each sample, 0.5 mL of whole blood was added to 5 mL of RPMI-1640 culture medium (Sigma-Aldrich, St. Louis, USA). To stimulate lymphocyte proliferation, 0.2 mL of phytohemagglutinin (PHA; Sigma-Aldrich) was added, and the cultures were incubated for 72 h at 37°C. Following incubation, the tubes were centrifuged at 1,500 rpm for 10 min, and the supernatant was discarded. Then, 2 mL of hypotonic solution (KCl) was added to lyse the red blood cells. After 10 min, the tubes were centrifuged again under the same conditions, and the cells were fixed by adding 3 mL of freshly prepared fixative (methanol:acetic acid 3:1). The fixation process was repeated 3 times until the cell suspension became clear and free of debris. Drops of the final

suspension were placed onto clean, cold glass slides, air-dried, and stained with Giemsa stain. The stained preparations were examined microscopically to identify mitotic cells, and the MI and blastogenic index (BI) were calculated as follows[24,25]:

- mitotic index assay (MI) = (Number of mitotic cells)/(1000 cells) (×100%)
- blastogenic index assay (BI) = (Number of blast cells)/(1000 cells) (×100%)

## Results

The tissue culture technique, specifically the blood culture method, was employed in this study due to its high reliability and effectiveness in observing lymphocyte cells during their active stages of division, particularly the blast transformation phase. This method allows for the stimulation and monitoring of lymphocytes as they progress through the cell cycle, making it especially useful for cytogenetic and cellular analyses. Furthermore, it provides optimal conditions for calculating the mitotic index, an important parameter used to assess the rate of cell division.

Through this assay, it becomes possible to evaluate any abnormal cellular behavior or disruptions in normal mitotic activity and the blastogenesis index of lymphocyte cells that may occur as a result of different exposure times to various external agents, such as chemical substances, environmental factors, or radiation. This makes the technique a valuable tool for understanding the biological effects of such agents on living cells.

## Discussion

The results demonstrated that short-term exposure of lymphocytes to cold plasma, ranging from 5 min to 20 min, significantly promoted lymphocyte proliferation. This enhancement was evidenced by an increased number of cells primed for division, leading to a higher proportion of actively dividing cells. These observations are supported by the quantitative data presented in the corresponding tables and figures. In contrast, prolonged plasma exposure of 25 min resulted in an inhibitory effect on lymphocyte proliferation. This suppression was characterized by a marked decrease in the number of cells prepared for mitosis, with values significantly lower than those observed in the control group. These findings provide scientific and medical insights, highlighting that plasma can exert beneficial effects in both scenarios, depending on the type of cells being treated. In the case of healthy lymphocytes, short-term plasma exposure appears to enhance cell proliferation, thereby strengthening and supporting the immune response. Conversely, in diseased or abnormal cells, prolonged plasma exposure (≥25 min) may exert inhibitory effects, slowing down or preventing pathological cell proliferation. As illustrated in the figures, the enhanced effect of cold plasma observed in female lymphocytes may be attributed to the interaction between female hormones, cell membrane composition, and a relatively stronger immune response, resulting in increased sensitivity to plasma-generated reactive species. Molecular techniques can be utilized to investigate the effects of cold plasma on target cell genes and related molecular pathways. Such molecular biological approaches have been widely applied across numerous experimental studies in the life sciences in general and in medical research in particular.[26–29]

## Limitations

The current investigation was constrained by the limited sample size and the exclusive use of in vitro experiments. The molecular mechanisms related to plasma-induced cellular responses were not examined. Additional research with more extensive experimental models is necessary to validate the results.

## Conclusions

Accordingly, it can be concluded that brief plasma exposure is beneficial for supporting normal cellular activity, whereas longer exposure durations may be more suitable for the therapeutic targeting of diseased cells. The biological effects of cold plasma are primarily mediated through the generation of reactive oxygen and nitrogen species (ROS and RNS), which interact with cellular membranes and proteins, leading to alterations in cell viability and immune activity.

### Data availability

The datasets generated and/or analyzed during the current study are available from the corresponding author on reasonable request.

### Consent for publication

Not applicable.

### Use of AI and AI-assisted technologies

Not applicable

### ORCID iDs

Atheer Q. Muryoush 0000-0003-4777-6546
Jenan Hussein Taha 0000-0003-1966-7166
Sura Allawi Obaid 0000-0002-8625-5498
Bahaa Al-Rubaii 0000-0003-4546-1815

**Table 1.** Mitotic and blastogenesis index of lymphocyte cells at 25 min exposure time

| Number of samples | Control | | Treated | |
|---|---|---|---|---|
| Male group | mitotic index ±SD | blastogenesis index ±SD | mitotic index ±SD | blastogenesis index ±SD |
| 1 | 0.4 ±0.12 | 4.2 ±0.22 | 0.3 ±0.20 | 3.3±0.11 |
| 2 | 0.5 ±0.03 | 2.2 ±0.13 | 0.4 ±0.10 | 1.5±0.12 |
| 3 | 0.3 ±0.12 | 3.5 ±0.12 | 0.2 ±0.12 | 2.1±0.11 |
| 4 | 0.2 ±0.08 | 3.5 ±0.09 | 0.2 ±0.08 | 2.2 ±0.22 |
| 5 | 0.4 ±0.09 | 3.5 ±0.19 | 0.3 ±0.19 | 2.1±0.21 |
| 6 | 0.4 ±0.46 | 3.8 ±0.46 | 0.3 ±0.46 | 2.9 ±0.11 |
| 7 | 0.4 ±0.45 | 3.2 ±0.16 | 0.2 ±0.25 | 2.1 ±0.13 |
| 8 | 0.2 ±0.03 | 2.5 ±0.03 | 0.1 ±0.13 | 1.1 ±0.10 |
| 9 | 0.3 ±0.46 | 2.5 ±0.46 | 0.2 ±0.21 | 1.3 ±0.16 |
| 10 | 0.2 ±0.09 | 4 ±0.99 | 0.1 ±0.19 | 3.1 ±0.20 |
| Average | 0.33±0.05 | 3.29 | 0.23±0.06 | 2.17 ±0.05 |

SD – standard deviation.

**Table 2.** Mitotic and blastogenesis index of lymphocyte cells at 20 min exposure time

| Number of samples | Control | | Treated | |
|---|---|---|---|---|
| Male group | mitotic index ±SD | blastogenesis index ±SD | mitotic index ±SD | blastogenesis index ±SD |
| 1 | 0.4 ± 0.12 | 4.2 ±0.22 | 1.0 ±0.12 | 5.2 ±0.12 |
| 2 | 0.5 ± 0.03 | 2.2 ±0.13 | 0.8 ±0.03 | 3.2 ±0.03 |
| 3 | 0.3 ± 0.12 | 3.5 ±0.12 | 0.7 ±0.12 | 4.5 ±0.12 |
| 4 | 0.2 ± 0.08 | 3.5 ±0.09 | 1.0 ±0.09 | 3.5 ±0.09 |
| 5 | 0.4 ± 0.09 | 3.5 ±0.19 | 0.9 ±0.09 | 4.5 ±0.09 |
| 6 | 0.4 ± 0.46 | 3.8 ±0.46 | 0.4 ±0.46 | 4.8 ±0.46 |
| 7 | 0.4 ± 0.45 | 3.2 ±0.16 | 0.85 ±0.46 | 4.2 ±0.46 |
| 8 | 0.2 ± 0.03 | 2.5 ±0.03 | 0.9 ±0.03 | 3.5 ±0.03 |
| 9 | 0.3 ± 0.46 | 2.5 ±0.46 | 0.9 ±0.46 | 3.5 ±0.46 |
| 10 | 0.2 ± 0.09 | 4 ±0.99 | 1.1 ±0.09 | 5 ±0.09 |
| Average | 0.33 ±0.05 | 3.29 ±0.03 | 1.76 ±0.12 | 4.19 ±0.12 |

SD – standard deviation.

**Table 3.** Mitotic and blastogenesis index of lymphocyte cells at 15 min exposure time

| Number of samples | Control | | Treated | |
|---|---|---|---|---|
| Male group | mitotic index ±SD | blastogenesis index ±SD | mitotic index ±SD | blastogenesis index ±SD |
| 1 | 0.4 ±0.12 | 4.2 ±0.22 | 0.8 ±0.12 | 4.5 ±0.22 |
| 2 | 0.5 ±0.03 | 2.2 ±0.13 | 0.8 ±0.03 | 2.5 ±0.13 |
| 3 | 0.3 ±0.12 | 3.5 ±0.12 | 0.7 ±0.12 | 3.8 ±0.12 |
| 4 | 0.2 ±0.08 | 3.5 ±0.09 | 0.6 ±0.09 | 3.9 ±0.09 |
| 5 | 0.4 ±0.09 | 3.5 ±0.19 | 0.4 ±0.09 | 3.6 ±0.19 |
| 6 | 0.4 ±0.46 | 3.8 ±0.46 | 0.4 ±0.46 | 3.9 ±0.46 |
| 7 | 0.4 ±0.45 | 3.2 ±0.16 | 0.8 ±0.46 | 3.7 ±0.16 |
| 8 | 0.2 ±0.03 | 2.5 ±0.03 | 0.6 ±0.03 | 2.9 ±0.03 |
| 9 | 0.3 ±0.46 | 2.5 ±0.46 | 0.5 ±0.46 | 2.9 ±0.46 |
| 10 | 0.2 ±0.09 | 4 ±0.99 | 0.6 ±0.09 | 4.7 ±0.99 |
| Average | 0.33±0.05 | 3.29 ±0.06 | 0.62 ±0.04 | 3.6 ±0.03 |

SD – standard deviation.

**Table 4.** Mitotic and blastogenesis index of lymphocyte cells at 10 min exposure time

| Number of samples | Control | | Treated | |
|---|---|---|---|---|
| Male group | mitotic index ±SD | blastogenesis index ±SD | mitotic index ±SD | blastogenesis index ±SD |
| 1 | 0.4 ±0.12 | 4.2 ±0.22 | 0.6 ±0.12 | 4.3 ±0.32 |
| 2 | 0.5 ±0.03 | 2.2 ±0.13 | 0.5 ±0.03 | 2.3 ±0.23 |
| 3 | 0.3 ±0.12 | 3.5 ±0.12 | 0.3 ±0.12 | 3.6 ±0.22 |
| 4 | 0.2 ±0.08 | 3.5 ±0.09 | 0.2 ±0.09 | 3.6 ± 0.1 |
| 5 | 0.4 ± 0.09 | 3.5 ±0.19 | 0.4 ±0.09 | 3.6 ±0.19 |
| 6 | 0.4 ±0.46 | 3.8 ±0.46 | 0.4 ±0.46 | 3.9 ±0.16 |
| 7 | 0.4 ±0.45 | 3.2 ±0.16 | 0.4 ±0.46 | 3.4 ±0.26 |
| 8 | 0.2 ±0.03 | 2.5 ±0.03 | 0.2 ±0.03 | 2.6 ±0.13 |
| 9 | 0.3 ±0.46 | 2.5 ±0.46 | 0.4 ±0.46 | 2.6 ±0.12 |
| 10 | 0.2 ±0.09 | 4 ±0.99 | 0.2 ±0.09 | 4.5 ±0.99 |
| Average | 0.33 ±0.05 | 3.29 | 0.4 ±0.06 | 3.4 ±0.99 |

SD – standard deviation.

**Table 5.** Mitotic and blastogenesis index of lymphocyte cells at 5 min exposure time

| Number of samples | Control | | Treated | |
|---|---|---|---|---|
| Male group | mitotic index ±SD | blastogenesis index ±SD | mitotic index ±SD | blastogenesis index ±SD |
| 1 | 0.4 ±0.12 | 4.2 ±0.22 | 0.5 ±0.11 | 4.5 ±0.22 |
| 2 | 0.5 ±0.03 | 2.2 ±0.13 | 0.5 ±0.01 | 2.2 ±0.13 |
| 3 | 0.3 ±0.12 | 3.5 ±0.12 | 0.5 ±0.11 | 3.5 ±0.12 |
| 4 | 0.2 ±0.08 | 3.5 ±0.09 | 0.4 ±0.19 | 3.5 ±0.09 |
| 5 | 0.4 ±0.09 | 3.5 ±0.19 | 0.6 ±0.09 | 3.5 ±0.19 |
| 6 | 0.4 ±0.46 | 3.8 ±0.46 | 0.4 ±0.26 | 3.8 ±0.46 |
| 7 | 0.4 ±0.45 | 3.2 ±0.16 | 0.4 ±0.16 | 3.2 ±0.16 |
| 8 | 0.2 ±0.03 | 2.5 ±0.03 | 0.3 ±0.13 | 2.5 ±0.03 |
| 9 | 0.3 ±0.46 | 2.5 ±0.46 | 0.5 ±0.11 | 2.5 ±0.23 |
| 10 | 0.2 ±0.09 | 4 ±0.99 | 0.3 ±0.11 | 4.5 ±0.11 |
| Average | 0.33 ±0.05 | 3.29 | 0.42 ±0.44 | 3.37 ±0.23 |

SD – standard deviation.

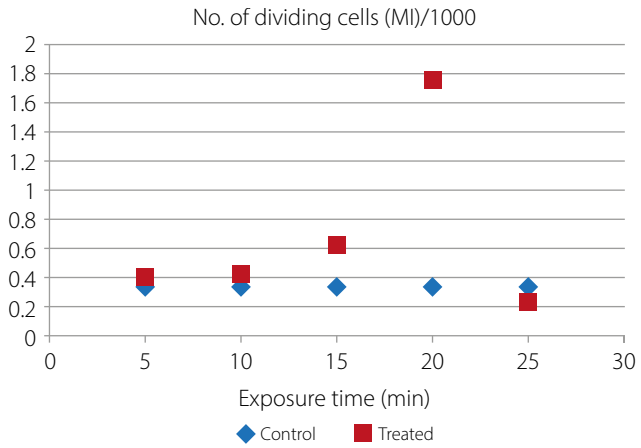


**Fig. 1.** Number of dividing lymphocyte cells for the male group

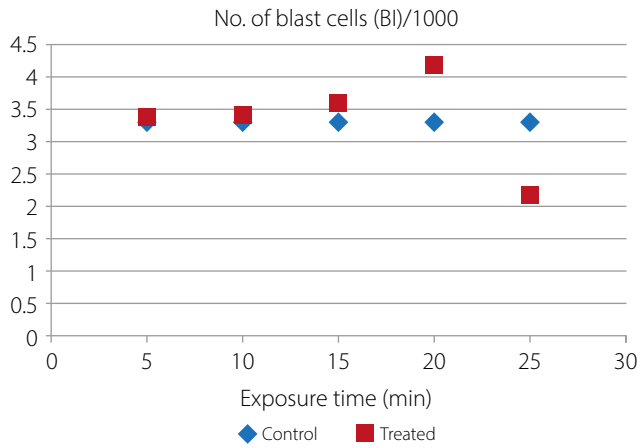


**Fig. 2.** Number of blast lymphocyte cells for the male group

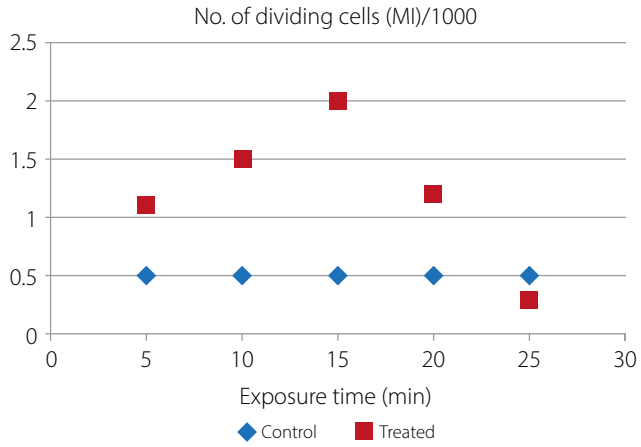


Fig. 3. Number of dividing lymphocyte cells for the female group

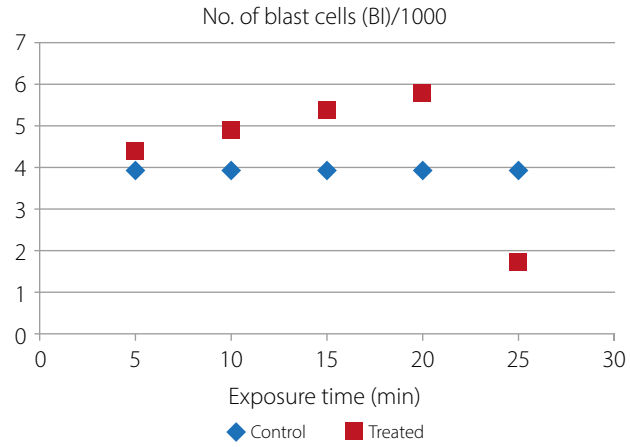


Fig. 4. Number of blast lymphocyte cells for the female group

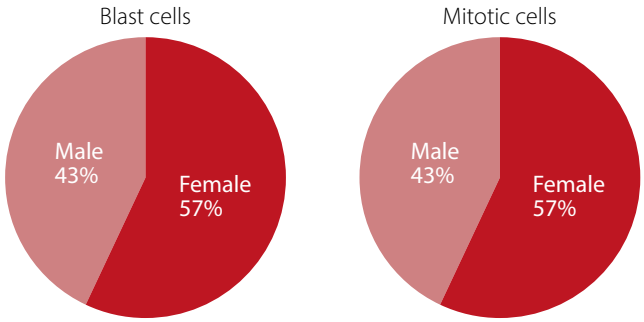


Fig. 5. Comparison of the percentage of plasma effects between men and women

## References


1. Muryoush AQ. The effect of cold plasma on pH, creatine, and the concentration of the most trace elements in human's nails by using X-ray fluorescent method. *Iraqi J Sci*. 2022;63(5):2057–2062. doi:10.24996/ijs.2022.63.5.21
2. Guo Y, Zhang X, Xing Y, et al. Atmospheric pressure plasma treatment increases the antioxidant capacity of the serum in vitro. *Sci Rep*. 2025;15(1):19127. doi:10.1038/s41598-025-03914-8
3. Deltadahl S, Gilbey J, Van Laer C, et al. Deep generative classification of blood cell morphology. *Nat Mach Intell*. 2025;7(11):1791–1803. doi:10.1038/s42256-025-01122-7
4. Merino A, Puigví L, Boldú L, Alférez S, Rodellar J. Optimizing morphology through blood cell image analysis. *Int J Lab Hematol*. 2018;40(Suppl 1):54–61. doi:10.1111/ijlh.12832
5. Wu J, Dong L, Xiang J, Di G. Static electric field exposure decreases white blood cell count in peripheral blood through activating hypothalamic–pituitary–adrenal axis. *Int J Environ Health Res*. 2024;34(1):305–315. doi:10.1080/09603123.2022.2148636
6. Brech A, Kubinyi G, Németh Z, Bakos J, Fiocchi S, Thuróczy G. Genotoxic effects of intermediate frequency magnetic fields on blood leukocytes in vitro. *Mutat Res Genet Toxicol Environ Mutagen*. 2019;845:403060. doi:10.1016/j.mrgentox.2019.05.016
7. Heshusius S, Heideveld E, Burger P, et al. Large-scale in vitro production of red blood cells from human peripheral blood mononuclear cells. *Blood Adv*. 2019;3(21):3337–3350. doi:10.1182/bloodadvances.2019000689
8. Leon-Ferre RA, Jonas SF, Salgado R, et al. Tumor-infiltrating lymphocytes in triple-negative breast cancer. *JAMA*. 2024;331(13):1135. doi:10.1001/jama.2024.3056
9. Nahrendorf M, Ginhoux F, Swirski FK. Immune system influence on physiology. *Science*. 2025;389(6760):594–599. doi:10.1126/science.adx4380
10. Zhao H, He Y, Ling X, et al. Profiles of lymphocyte subtypes in HIV-infected people with different immunologic responses to antiretroviral therapy. *J Med Virol*. 2024;96(11):e70081. doi:10.1002/jmv.70081
11. Loureiro A, Pais C, Sampaio P. Relevance of macrophage extracellular traps in C. albicans killing. *Front Immunol*. 2019;10:2767. doi:10.3389/fimmu.2019.02767
12. *Modern Genetic Analysis*. 3rd ed. New York, USA: W.H. Freeman; 2002. ISBN:978-0-7167-4714-7.
13. Belli M, Tabocchini MA. Ionizing radiation-induced epigenetic modifications and their relevance to radiation protection. *Int J Mol Sci*. 2020;21(17):5993. doi:10.3390/ijms21175993
14. Seghatchian J, Amiral J. Spotlight on the current perspectives on applications of human blood cell culture and organoids: Introductory remarks. Transfus Apher Sci. 2020;59(4):102861. doi:10.1016/j.transci.2020.102861
15. Navakatikian M, Tomashevskaya L. Behavioral and endocrinal effects of microwaves of non-thermal intensity. In: Carpenter DO, Ayrapetian SN, eds. *Biological Effects of Electric and Magnetic Fields*. Vol 1. San Diego, USA: Academic Press; 1994:236–239. ISBN:978-0-12-160261-1, 978-0-12-160262-8.
16. Gao S, Yang SH, Wang HY, Wang GS, Yin PG. Excellent electromagnetic wave absorbing properties of two-dimensional carbon-based nanocomposite supported by transition metal carbides $Fe_3C$. *Carbon*. 2020;162:438–444. doi:10.1016/j.carbon.2020.02.031
17. Santini R, Santini P, Danze JM, Le Ruz P, Seigne M. Investigation on the health of people living near mobile telephone relay stations: I/Incidence according to distance and sex [in French]. Pathol Biol (Paris). 2002;50(6):369–373. doi:10.1016/s0369-8114(02)00311-5
18. Tamarin RH. *Principles of Genetics*. 7th ed. Boston, USA: McGraw-Hill; 2004. ISBN:978-0-07-124320-9.

19. Moraes AP, Vale AAD, Santos RR, et al. Chromosome number overview in Habenaria (Habenariinae, Orchideae, Orchidaceae): a new smallest diploid number and insight on chromosome number evolution in a karyotypically variable genus [published online as ahead of print on November 18, 2025]. *Botanical Journal of the Linnean Society*. 2025. doi:10.1093/botlinnean/boaf088
20. Matsuda Y, Uchimura A, Satoh Y, et al. Spectra and characteristics of somatic mutations induced by ionizing radiation in hematopoietic stem cells. *Proc Natl Acad Sci U S A*. 2023;120(15):e2216550120. doi:10.1073/pnas.2216550120
21. Claessen MJAG, Yagci N, Fu K, et al. Production and stability of cultured red blood cells depends on the concentration of cholesterol in culture medium. *Sci Rep*. 2024;14(1):15592. doi:10.1038/s41598-024-66440-z
22. Chen Z, Liu P, Xia X, Cao C, Ding Z, Li X. Low ambient temperature exposure increases the risk of ischemic stroke by promoting platelet activation. *Sci Total Environ*. 2024;912:169235. doi:10.1016/j.scitotenv.2023.169235
23. Mahon CR, Lehman DC, eds. *Textbook of Diagnostic Microbiology*. 6th ed. St. Louis, USA: Elsevier Saunders; 2019. ISBN:978-0-323-48218-9.
24. Rosenberg SA. Lymphocytes as a living drug for cancer. Science. 2024;385(6704):25–26. doi:10.1126/science.adp1130
25. Abdullah MM, AL-Rubaii BAL. Effect of Lactobacillus supernatant on swarming-related gene expression in Proteus mirabilis isolated from urinary tract infections. *Ukr J Nephrol Dial*. 2024;4(84):39–48. doi:10.31450/ukrjnd.4(84).2024.05
26. Ibrahim GJ, Laftaah BA. The efficiency of certain amino acids in regulating *chABCI* gene expression in *Proteus mirabilis*. *Iraqi J Sci*. 2024;65(9):4983–4992. doi:10.24996/ijs.2024.65.9.15
27. Jassim TS, Talib SS, Jaber NR, Sahib DH, Ali RW, Al-Rubaii BA. Impact of hepatitis C virus on *IFITM3* gene expression: A comprehensive analysis incorporating serological detection and viral load quantification via qPCR. Polim Med. 2025;55(1):21–30. doi:10.17219/pim/199333
28. Khudair S, Al-Rasheed IA, Ibrahim TK, Saleh TH, Al-Rubaii BA. Molecular study of *CACNA1A*, *ATP1A2*, and *SCN1A* genes and its association with the migraine disease in Iraq. *Ibom Med J*. 2026;19(1):132–143. doi:10.61386/imj.v19i1.922
29. Baqey DAASA, Sultan RS, Hamoode RH, Al-Rubaii BAL. Metabolic markers of insulin resistance in Iraqi type 2 diabetes mellitus patients infected with H. pylori. *East Ukr Med J*. 2025;13(2):417–423. doi:10.21272/eumj.2025;13(2):417-423

# Sustainable polymers: A report from the Interdisciplinary Symposium in Tübingen, October 9, 2025

Charlotte Elisabeth Scheherazade Schmidt[A–F]

Faculty of Medicine, Eberhard Karls University, Tübingen, Germany

A – research concept and design; B – collection and/or assembly of data; C – data analysis and interpretation;
D – writing the article; E – critical revision of the article; F – final approval of the article

Polymers in Medicine, ISSN 0370-0747, eISSN 2451-2699 *Polim Med*. 2026;56(1):83–91

**Address for correspondence**
Charlotte Elisabeth Scheherazade Schmidt
E-mail: e_c_s_schmidt@yahoo.com

**Funding sources**
None declared

**Conflict of interest**
None declared

**Acknowledgements**
I sincerely thank Professor Monika Rieger for her trust and supervision of this project, which provided valuable insights and experience. I am also deeply grateful to Professor Florian Lotz for his continuous inspiration and steadfast support throughout my interdisciplinary journey. His generous commitment to in-depth discussions and encouragement has enriched my work across ecology, chemistry, medicine, clinical and laboratory research, and academia. Without his mentorship and collaborative spirit, this work would not have been possible. I also thank Christine Shojaei Kawan for her invaluable editorial guidance in refining this manuscript. I gratefully acknowledge the German Academic Exchange Service (DAAD) for its support (Funding Program ID: 57595573), which enabled my initial engagement in both laboratory and clinical research as a physician.

Received on December 27, 2025
Reviewed on February 8, 2026
Accepted on February 26, 2026

Published online on June 30, 2026

**Cite as**
Schmidt ECS. Sustainable polymers: A report from the Interdisciplinary Symposium in Tübingen, October 9, 2025. *Polim Med*. 2026;56(1):83–91. doi:10.17219/pim/218618

**DOI**
10.17219/pim/218618



## Abstract

Plastics play a major role in daily life, with unprecedented levels of usage. As anthropogenically produced polymers should be optimized with regard to biodegradability and biocompatibility, green chemistry strategies offer promising pathways. In this context, the symposium on sustainable polymers in Tübingen presented a comprehensive overview of recent advances in polymer research, addressing synthesis and degradation pathways along with environmentally benign catalysts. These developments benefit not only industrial efficiency but also resource conservation and environmental protection. Beyond these sustainability-driven concepts, innovative approaches to biocompatible biomaterials for medical applications and advanced polymer systems for therapeutic drug delivery were highlighted. This conference report presents current polymer research, including contributions from the medical, pharmacological, and ecological fields. To foster interdisciplinary exchange on sustainable polymers, the Tübingen Symposium was initiated by the interdisciplinary faculty College of Fellows: Center for Interdisciplinary and Intercultural Studies at Eberhard Karls University Tübingen, Baden-Württemberg, on October 9, 2025, from 8:30 a.m. to 5:30 p.m., at the Ernst von Sieglin Lecture Hall.

**Key words:** polymers, nanomedicine, environmental health, microbiology, chemistry

## Highlights

- Advances in sustainable polymers and green chemistry: The Tübingen Symposium highlighted cutting-edge research in biodegradable polymers, environmentally benign catalysts, and sustainable polymer synthesis to enhance resource conservation and environmental protection.
- Innovative biomaterials and drug delivery systems: Emerging biocompatible polymer-based biomaterials and advanced therapeutic drug delivery platforms demonstrated the expanding medical and pharmacological applications of sustainable polymers.
- Interdisciplinary collaboration in polymer science: The 2025 Tübingen Symposium fostered cross-disciplinary exchange among experts in medicine, pharmacology, ecology, and materials science, promoting integrated solutions for sustainable polymer development.

## Introduction

The Anthropocene is defined as a geological epoch shaped by human activity. One of its defining characteristics is the large-scale production and consumption of polymers. With 445 million metric tons of thermoplastics feeding international markets in 2025,[1] there appears to be a substantial demand for anthropogenically produced polymers in everyday applications as well as in scientific and medical contexts. Consequently, it is necessary to optimize eco-friendly and cost-efficient polymer synthesis pathways and to identify biodegradable and biocompatible biopolymers.[2] A scientific approach addressing sustainable polymers would help address numerous challenges in environmental and human health sciences. Ever since 2011, sustainability lectures have been held annually in Tübingen. The 2025 meeting was dedicated to sustainability projects in chemistry, advancing them through research, teaching, and science communication. The event was held in the Ernst von Sieglin Lecture Hall, located within Hohentübingen Castle. The lecture on polymer sustainability took place in the very building where Friedrich Miescher isolated, in 1869, a fundamental biopolymer of our cells: DNA. With the advancement of plastic synthesis and production methods, a new generation of polymers has emerged. Thorough investigations into the sustainability of polymers reveal a high degree of complexity, which clearly merits deeper understanding. In parallel, analytical investigations have enabled scientists to address fundamental questions associated with these materials and their sustainability. Thus, the symposium provided a forum for addressing ecological questions such as biocompatibility and biodegradability.

The "Sustainable Polymers" symposium aimed to: 1) present concepts for polymer production incorporating $CO_2$ capture; 2) promote the use of less toxic catalysts in polymer synthesis; 3) address polymer degradation strategies to reduce annual plastic waste; 4) outline the role of bacteria as biological tools for polymer synthesis; 5) advance the understanding of bacterial degradation processes of naturally occurring polymers such as caoutchouc, while further elucidating their limitations with respect to anthropogenically produced polymers; and 6) highlight the application of nanosized polymers as drug-coating materials in medical therapies as a novel approach. The program covered polymer synthesis and degradation strategies alongside the use of polymers in drug delivery and medical applications and was presented to an interdisciplinary audience, largely consisting of students and scientists in chemistry. Given that the symposium was open to academics from all disciplines, the aim was to present current problems and solution-oriented content and to promote participation in future events, thereby making it possible to benefit from expertise from across the globe (Fig. 1).

The College of Fellows at the University of Tübingen, which supported the organization of this event, is a young initiative first launched in 2022, aiming to provide international research fellows with the opportunity to collaborate across disciplines and explore disciplinary boundaries in an open, pressure-free environment. Open to the entire academic community, the symposium fostered dialogue, knowledge sharing, and networking.

The idea of polymer sustainability was strongly supported by chemists, and the Tübingen Symposium was initially established to foster knowledge exchange among them. Beyond chemical strategies – such as developing bio-based polymers from plant-derived epoxide resins combined with $CO_2$ capture – the symposium integrated other disciplines, providing valuable impetus for future research at the interface of sustainability, biotechnology, and medical applications. Notably, advances in pharmacology and microbiology have also contributed to polymer science, further expanding knowledge relevant to human health.

On October 9, 2025, the Department of Inorganic Chemistry in Tübingen hosted the symposium on sustainable polymers, which was attended by approx. 50 participants – primarily members of the Faculty of Chemistry. Nine invited speakers from 4 countries and institutions shared their expertise in polymer science, providing a holistic overview of current environmental challenges and medical limitations in nanopolymer-based drug delivery systems.

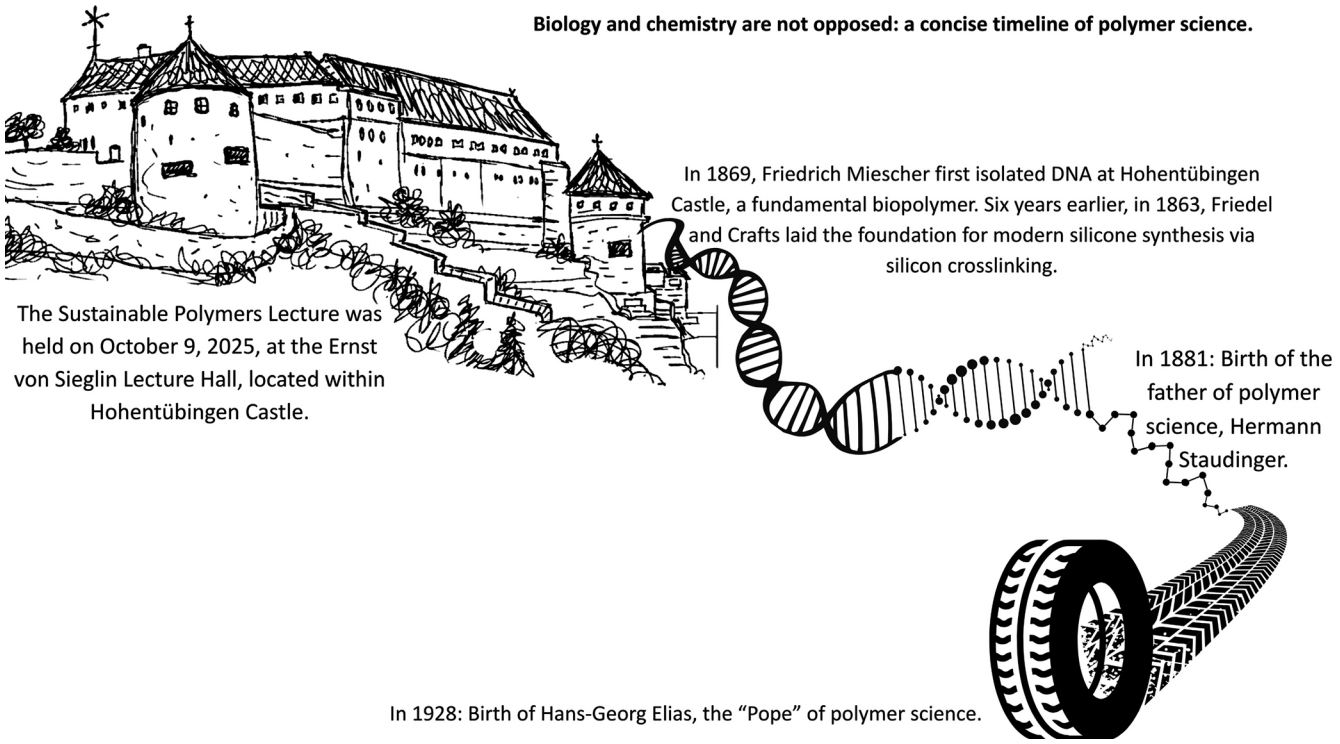


Fig. 1. Biology and chemistry are not opposed: a concise timeline of polymer science

Overall, the speakers highlighted emerging ecological crises and potential future economic impacts, emphasizing the urgency of addressing these challenges to prevent further escalation. A distinctive feature of the symposium was the opportunity to examine polymer science from the perspectives of chemistry, medicine, and microbiology. The one-day symposium included short discussion sessions following each lecture. Issues addressed included rising $CO_2$ emissions, plastic waste, reliance on petroleum and rare earth elements, and the prolonged degradation of plastics. Proposed solutions included integrating $CO_2$ into catalytic synthesis, recovering rare earth elements, developing biodegradable thermoplastics with $CO_2$-binding capacity, and employing cultivated bacterial strains as an ecological alternative to conventional polymer production. In addition, applications of nanopolymers for targeted drug delivery were discussed. Participants suggested that future events should maintain a similar balance between polymer research and its advancements, and environmental and health-related topics (Table 1).

Table 1. Invited speakers and topics from the Interdisciplinary Symposium about Sustainable Polymers

| Discipline | Speaker | Institution | Title | Topics |
|---|---|---|---|---|
| Inorganic Chemistry | Prof. Dr. Reiner Anwander | Eberhard Karls University Tübingen | Opening Remarks | • Sustainability topics since 2011 • Summer Course 2025: Emerging Concepts & Issues in Polymer Synthesis & Degradation |
| | Prof. Dr. Megan E. Fieser | University of Southern California, Los Angeles Wrigley Institute for Environment and Sustainability, University of Southern California | Simple Rare Earth Metal Catalyst Systems for the (De) polymerization of Emerging Polyesters and Polycarbonates | • Chemistry under mission: teams POL & DEPOL • Epoxide/anhydride copolymerization: opportunities and challenges • Tunable Lewis acidity • Impact of catalyst structure • Anhydride mixtures • Lanthanide scope • Impact of $H_2O$ • Metal ionic liquids • Catalyst impact on molecular weight • Ring-closing depolymerization • Impact of substituted urea |
| | Prof. Dr. Arjan W. Kleij | Institut Català d'Investigació Química | Catalysis as a Key Driver for the Transformation of Biomass into Engineering Polymers | • ROCOP of polylimonene carbonate (PLC) • PLC recycling • Bio-based epoxy adhesives and polycaprolactone (PLCO) • ROP/ROMP of aliphatic polycarbonates • ROCOP of cyclic anhydrides • Fatty acid-based polyesters • Bio-based carbon feedstock • Catalysis & polymer engineering • De- and repolymerization of PLC via terpene-based polymers (TBD) • Bio-based bifunctional monomers |

Table 1. Invited speakers and topics from the Interdisciplinary Symposium about Sustainable Polymers

| Discipline | Speaker | Institution | Title | Topics |
|---|---|---|---|---|
| | Paul Preisenberger | Eberhard Karls University Tübingen | Isoselective Ring-Opening Polymerization of Racemic β-Butyrolactone Using Calcium Catalysts | • ROP study of PHA biopolyesters • Poly-3-hydroxybutyrate (PHB) with potentially high biodegradability • Elongation at break: 5% • Challenges in industrial scalability • Depolymerization of *A. faecalis* & *P. pickettii* • Calcium-binding complex for ring-opening polymerization of β-butyrolactone with regard to medical compatibility and cost-effective scaling |
| | Prof. Dr. Erwan Le Roux | University of Bergen | Mechanistic and Selectivity Studies of N-Heterocyclic Carbene Pincer Metal Catalysts in $CO_2$-Derived Polymer Synthesis | • $CO_2$-based polymer synthesis • ROCOP of epoxides with $CO_2$: $CO_2$–polyurethane synthesis • Catalytic ROCOP: key to selectivity & activity • Bimetallic and monometallic systems for ROCOP • Titanium as a less toxic, non-endangered element • NHC-based group complexes • Nature of the NHC backbone • V-complexes • "Ate" complex formation |
| | Philipp Wetzel | Eberhard Karls University Tübingen | Recycled Rare-Earth Metals for Isoprene Polymerization | • Natural caoutchouc (degradability: *S. coelicolor*, *P. citronellolis*) • Nd-catalyzed rubber polymerization of polyisoprene • Annual Nd material demand for renewables in 2030 & 2050 • Alkali baking |
| Microbiology | Philipp Fink | Eberhard Karls University Tübingen | A Novel Strategy for Sustainable PHB Production in Filamentous Cyanobacteria | • Plastic waste • Cyanobacteria & oxygenic photosynthesis • PHB in *Synechocystis* sp. PCC 6803 • *Nostoc* sp. PCC 7120 • PHB production • New production strategy using an inducer • Inducible PHB production: NosPHB4.0 (1); NosPHB4.0 (2) • Tetracycline at different concentrations |
| | Prof. Dr. Dieter Jendrossek | University of Stuttgart | Enzymatic Biodegradation of Rubber and Fossil Hydrocarbon Polymers | • *Steroidobacter gummioxidans* • Rubber oxygenase A (RoxA) • RoxA & RoxB comparison • Degradation of polyethylene, polystyrene, PVC • Myths of the superworm and its degrading enzymes • Polyethylene is not biodegradable |
| Pharmaceutical Technology | Yasaman Pourdakheli-Hamedani | Eberhard Karls University Tübingen | Poly(solketal acrylate) as a Versatile Tool for Ocular Delivery Applications | • Ocular barriers • Polymer synthesis & characterization • Nanoparticle formulation and encapsulation • Evaluation in vitro & ex vivo |

## $CO_2$ integration and plastic pollution challenges

From the outset of the symposium, the urgency of addressing global plastic pollution was underscored – most notably through the observation that every individual on the planet has a plastic counterpart,[3] as stated by chemist Professor Dr. Arjan Kleij (Tarragona, Spain) (Fig. 2). Kleij introduced $CO_2$ as a potential feedstock to circumvent conventional petroleum-based polymer synthesis: "Bio-based carbon constitutes a versatile feedstock,"[4] enabling the transition toward more sustainable material platforms.

Kleij's group has developed catalytic methods to incorporate $CO_2$ into substances such as fatty acids, sugars, and terpenes (secondary plant metabolites)[5] to create novel bio-based polymeric materials. Key synthetic strategies include ring-opening polymerization techniques (ROP), ring-opening copolymerization (ROCOP) of polylimonene carbonate (PLC) and fatty acids,[6] and ring-opening metathesis polymerization (ROMP) of cyclic anhydrides for the synthesis of "renewable and biodegradable polymers such as aliphatic polyesters."[7] These synthetic pathways are grounded in catalytic processes and are designed with sustainability in mind, strategically utilizing atmospheric $CO_2$ as a carbon source. Kleij also addressed the topic of aliphatic polycarbonates synthesized through ROP and ROMP, which are expected to gain considerable relevance in the biomedical field due to their favorable biodegradability and modular structural properties.[8]

Finally, Kleij highlighted depolymerization and subsequent repolymerization approaches, exemplified by terpene-based polymers (TBD)-mediated degradation and reformation of polycaprolactone (PCL), presenting it as a model system for circular polymer chemistry.[9]

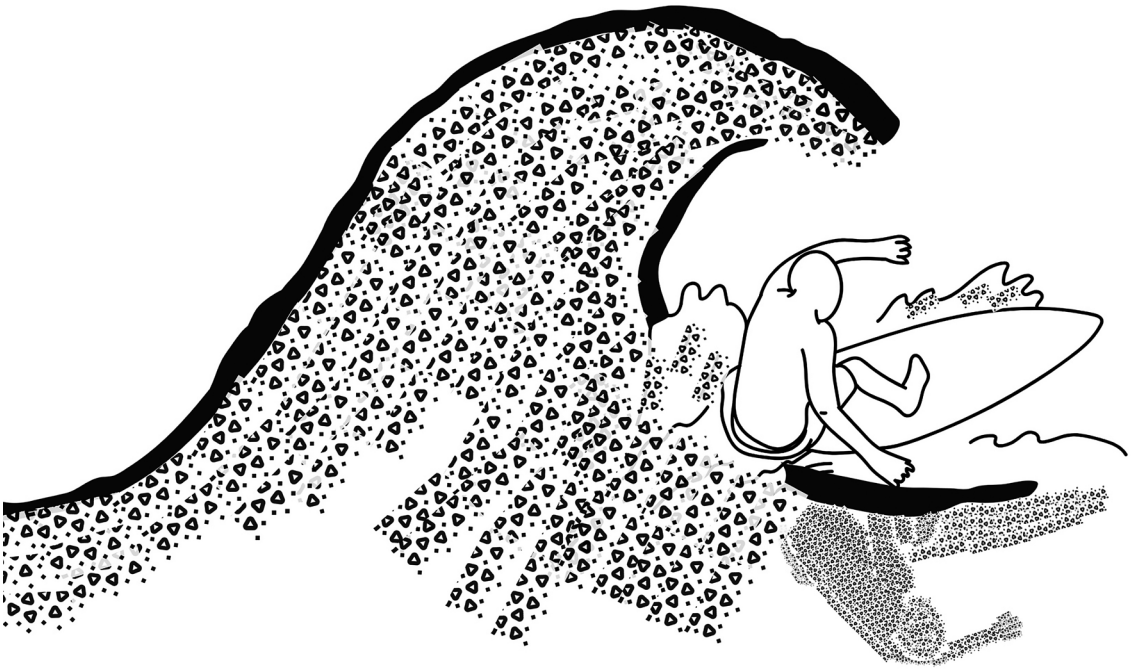

**Breaking the plastic wave because "every individual on the planet has a plastic counterpart."**

Fig. 2. "Every individual on the planet has a plastic counterpart"

## N-heterocyclic carbenes: A pivotal role for lower energy and toxicity in polymer synthesis

Professor Dr. Erwan Le Roux (Bergen, Norway) also presented novel strategies for $CO_2$-derived polymer synthesis, highlighting the significance of these less energy-intensive processes as a sustainable alternative. In particular, he emphasized their potential to generate new polycarbonate materials while circumventing the use of toxic chemical intermediates such as bisphenol A and phosgene.[5]

He and his research team have identified N-heterocyclic carbenes (NHCs) as remarkably adaptable molecular scaffolds, particularly in the context of $CO_2$-binding ROCOP. N-heterocyclic carbenes, coordinated with Group 4 transition metals such as titanium (Ti), zirconium (Zr), and hafnium (Hf), function as stable, electron-rich ligands with strong σ-donor capacity. Their incorporation permits precise control over the electronic and steric environment of the catalyst, thereby enhancing reactivity and selectivity and enabling the design of tailored polymer architectures. Ring-opening copolymerization catalyzed by NHC-based Group 4 complexes permits up to 99% alternating $CO_2$ insertion into polycarbonates.[6]

Furthermore, Le Roux emphasized that the nature of the NHC backbone – specifically whether it is saturated or unsaturated – plays a pivotal role in the formation of catalytically active species. Demonstrating remarkable efficiency in terpolymerization, Hf- and Ti-NHC catalysts facilitate the selective synthesis of diblock terpolymers from a diverse array of cyclic anhydrides (Fig. 3).

## New horizons in synthesis, upcycling and depolymerization with Team POL (Polymerization) and Team DEPOL (Depolymerization)

Professor Dr. Megan Fieser (Los Angeles, USA) has held the title of New Horizons Fellow at Eberhard Karls University Tübingen since 2024, in recognition of her pioneering research at the interface of polymer synthesis, recycling, and upcycling. Her research program is structured into two teams: Team POL (polymerization) and Team DEPOL (depolymerization processes). Accordingly, Team POL represents polymer synthesis activities, whereas Team DEPOL focuses on the development of tailored depolymerization procedures. The POL group investigates copolymerizations involving diverse epoxides and cyclic anhydrides, providing the opportunity to construct over 400 distinct polyester structures. Notably, these structures can be modified after polymerization and are likely to be both degradable and biocompatible. Although biocompatibility is achieved, the resulting polymers often fall short of reaching sufficiently high molecular weights and exhibit undesirable side reactions. Moreover, a universal "one-size-fits-all"

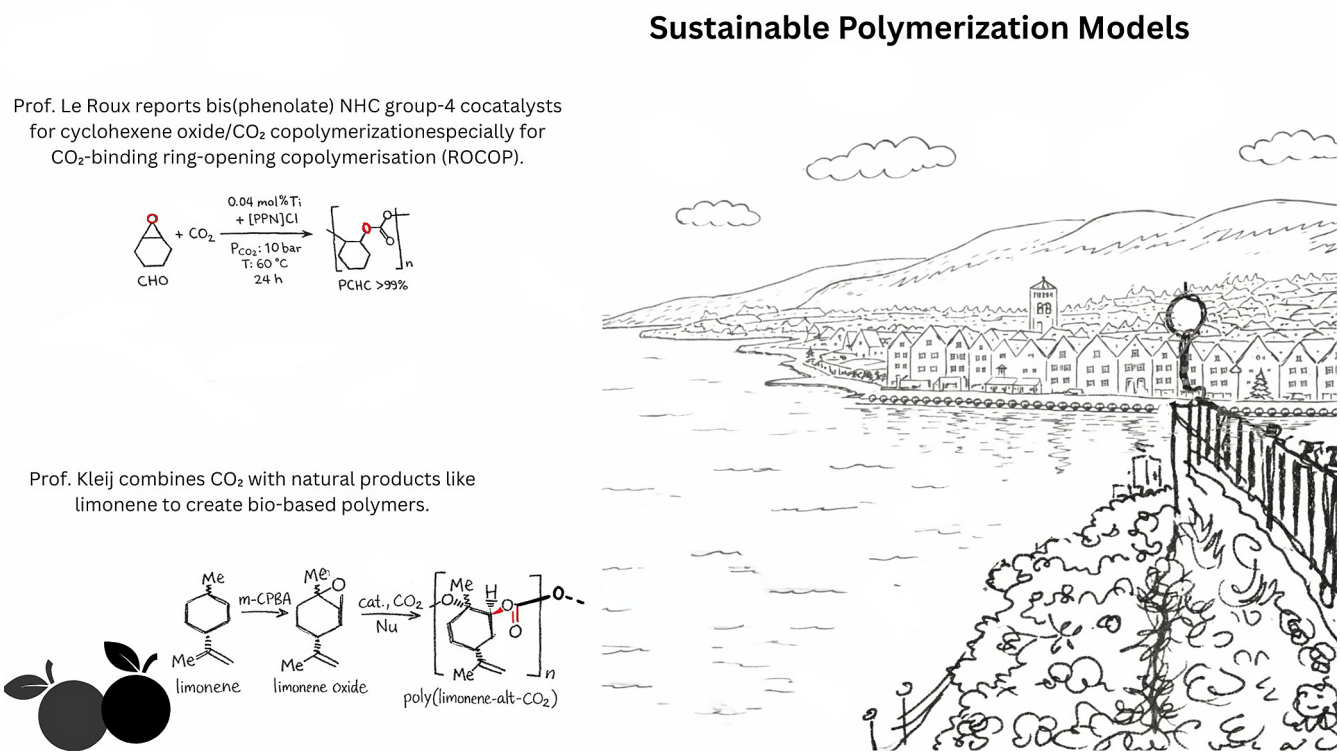


Fig. 3. Sustainable polymerization models

catalyst remains elusive, and the catalysts that are effective tend to be both atom- and time-intensive to produce.[7] By leveraging the effects of Lewis acidity and the size of lanthanide salts, the ring-opening copolymerization of diverse epoxides and cyclic anhydrides is significantly enhanced.[8] Fieser's other research team has developed divergent strategies for the depolymerization of polyesters, opening selective degradation pathways tailored to the polymers' structure and intended recovery applications.[9]

## Lanthanide baking for neodymium recovery

Philipp Wetzel, a researcher in the group of Professor Dr. Reiner Anwander (Tübingen, Germany), addressed problems related to the limited availability of rare-earth materials. Polyisoprene, a key material for rubber wheels, is the product of vulcanized caoutchouc (chemically crosslinked using sulfur). Globally, approx. 14.2 million tons of polyisoprene enter the market each year. Rare-earth metals are required for the polymerization process. On average, around 30 g of neodymium (Nd) are required per ton of polyisoprene produced. Given the scarcity of neodymium and the growing uncertainties in its supply amid increasing market demand, Philipp Wetzel presented a chemical extraction technique via alkali baking as an effective method for recovery.

## Calcium-catalyzed synthesis of biodegradable β-butyrolactone

Paul Preisenberger and Nicolas Czimber, researchers in the group of Professor Dr. Reiner Anwander (Tübingen), presented a calcium-based catalyst complex for the synthesis of β-butyrolactone (BBL), a biodegradable compound. Beta-butyrolactone can be polymerized using this catalyst, analogous to those employed in lactide ROP. This method offers improved initiation control by leveraging calcium as an inexpensive and non-toxic metal to effectively conduct the ROP of BBL. It thus presents a promising route for scalable and environmentally compatible biopolymer synthesis.

## Bacteria-produced polymer: PHB – a biodegradable, biocompatible $CO_2$ storage polymer

Philipp Fink, who works under the supervision of Professor Dr. Karl Forchhammer (Tübingen), presented his concept of harnessing cyanobacteria as functional natural production platforms for the biosynthesis of biodegradable and biocompatible polyhydroxybutyrate (PHB). It serves as a carbon storage polymer and can accumulate to as much as 90% of the cell dry weight (CDW) under nutrient-limiting conditions.[10] In this context, he aimed to overcome the limitations of low PHB yield during autotrophic

growth in cyanobacteria[10] by integrating continuous PHB biosynthetic machinery[11] from *Cupriavidus necator* into genetically amenable filamentous cyanobacteria of the genus Nostoc sp. PCC7120. Preliminary findings demonstrated that the resulting transformants successfully initiated PHB production.[10] Fink underscored the potential industrial applicability of cyanobacteria for PHB production, achieving up to 30% (w/w) PHB relative to CDW, while noting that further optimization and development remain possible (Fig. 4).

## Bacteria-produced oligomers: plastic degradation

Professor Dr. Dieter Jendrossek (Stuttgart, Germany) provided insights into bacterial polymer degradation. Caoutchouc, poly-(1,4-cis-isoprene), is harvested from *Hevea brasiliensis*, the rubber tree, and *Taraxacum kok-saghyz*, the Russian dandelion. During the industrial processing of polyisoprene rubber, effluents are released into both aquatic and terrestrial ecosystems. As a result, polyisoprene-degrading bacteria originally assigned to the genus *Xanthomonas* and later reclassified as *Steroidobacter gummioxidans* were identified. Their capacity to degrade polyisoprene is attributed to depolymerizing enzymes, namely rubber oxygenase A (RoxA)[12], rubber oxygenase B (RoxB), and latex clearing protein (Lcp).[13] The oligo-isoprenoid degradation products vary depending on the enzyme involved.

Rubber oxygenase A generates $C_{15}$ oligo-isoprenoids and is structurally characterized by a dead-end binding pocket that determines a precise cleavage pattern. This enzyme operates via an exo-type cleavage mechanism and undergoes open–closed conformational transitions. In contrast, RoxB utilizes a substrate-penetrating tunnel, enabling endo-type cleavage of the polyisoprene backbone.[14] Consequently, RoxB produces a heterogeneous mixture of oligo-isoprenoids, typically including $C_{20}$, $C_{25}$, $C_{30}$, and higher chain lengths.[15]

Latex clearing proteins (Lcps), which are structurally distinct from both RoxA and RoxB, also catalyze endo-type cleavage through a mechanism similar to that of RoxB.[14] The resulting degradation products resemble those generated by RoxB, comprising oligo-isoprenoids ranging from $C_{20}$ to $C_{30}$ and beyond. Collectively, these findings underscore the metabolic capacity of bacteria to degrade natural rubber.

## Microbiological capacities and limitations in polymer degradation

In a second presentation, Prof. Jendrossek reported on his long-term, biannual literature searches, consistently using the search terms "PE" and "degradation" to assess the publication landscape. He identified an exponential increase in publications addressing the bacterial degradation of industrial polymers.[14] The publishing momentum shows no indication of decline and has expanded to include studies on mealworms and larvae, which, according to some authors, are reported to digest polyvinyl chloride (PVC), polyethylene (PE), and polystyrene (PS) through the

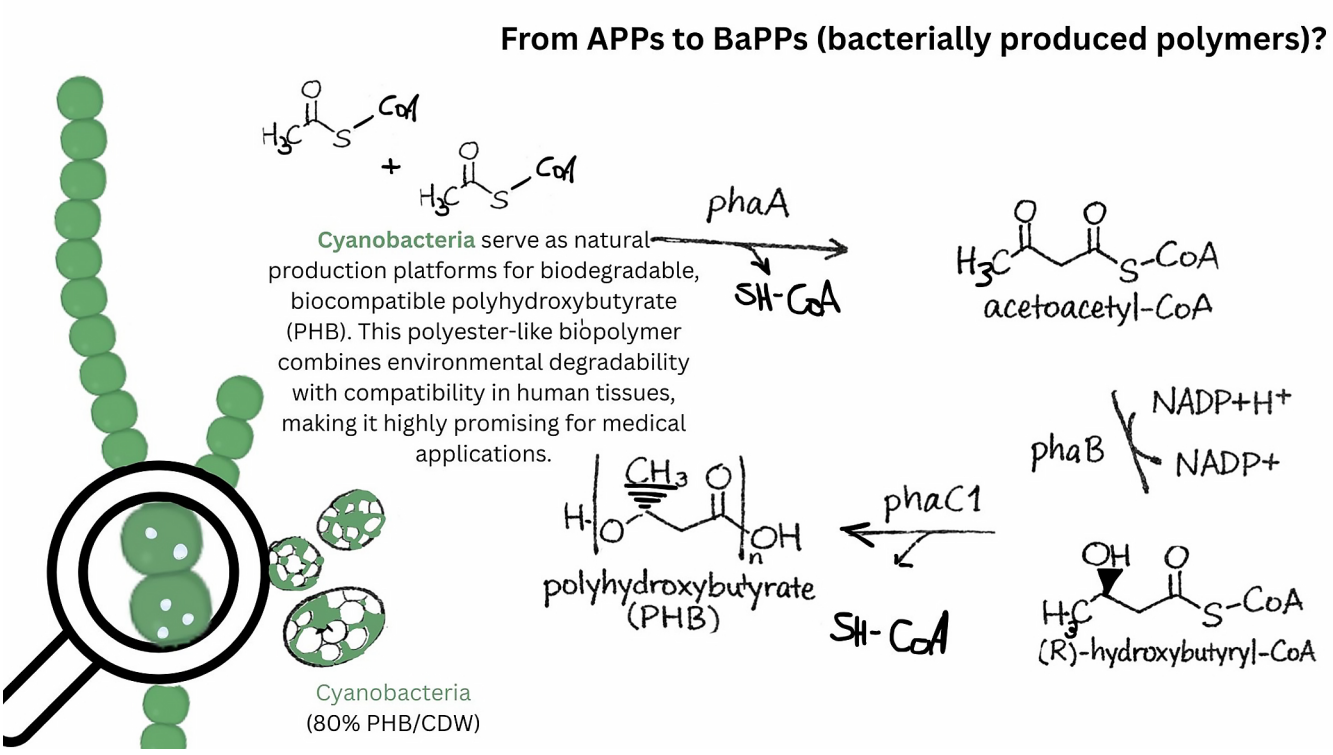


Fig. 4. From APPs to BaPPs (bacterially produced polymers)?

action of specialized enzymes.[14,16,17] Professor Jendrossek subsequently evaluated these claims using isotopic analysis following the Pee Dee standard from South Carolina. His findings indicated that the calculations reported in the publication by Yang et al.[17] were not consistent with the isotopic data.[18]

## Precise polymers: nanoparticles for drug delivery

In her presentation entitled "Poly(solketal acrylate) as a versatile tool for ocular delivery applications", Yasaman Pourdakheli-Hamedani, under the supervision of Prof. Dr. Friederike Adams (Stuttgart) and Dr. Sven Schnichels (Tübingen), introduced a novel perspective on sustainable polymers, focusing on the application of non-toxic, spherical nanopolymer structures for localized gene therapy. Her studies involve polymer synthesis and characterization, nanoparticle formulation and encapsulation, and evaluation of their application both in vitro and ex vivo. Her ambition is to develop these nanoparticles (NPs) as drug delivery agents administered via local ocular injection. Local ocular injection is employed to circumvent the first-pass effect, minimize systemic toxicity, and facilitate gene therapy for age-related macular degeneration, diabetic retinopathy, retinitis pigmentosa, and Leber congenital amaurosis.[19] Furthermore, Pourdakheli-Hamedani outlined several challenges faced by nanoparticle-based ocular drug delivery, including diffusion limitations, nanoparticle aggregation, epithelial barriers, tear clearance, and limited permeability.[20] Additionally, nanoparticle-based drug delivery systems must overcome ocular barriers such as tight junctions, efflux pumps, enzymatic degradation, limited permeability of large particles, and immune responses.[20] In Pourdakheli-Hamedani's study, poly(solketal acrylate) ($PSA_{100}$), a homopolymer, was selected as the amphiphilic carrier polymer that self-assembles into micellar nanostructures. She explained that the well-dispersed spherical NPs, "exhibiting minimal aggregation and a negative surface charge, facilitate efficient diffusion in the vitreous humor."[20] She demonstrated that $PSA_{100}$ nanoparticles ($PSA_{100}$-NPs) maintained ideal cell viability across all particle concentrations. In vitro tests with retinal pigment epithelium ARPE-19 cells and primary-derived Müller cells showed time- and concentration-dependent uptake of Nile red-loaded $PSA_{100}$-NPs. The final ex vivo test on porcine retina was successfully conducted, demonstrating uptake of Nile red–loaded $PSA_{100}$-NPs in the outer nuclear layer, inner nuclear layer, and ganglion cell layer.

## Conclusions

The Tübingen symposium on sustainable polymers was a unique opportunity for researchers to network and engage in broad interdisciplinary exchange on topics that provide valuable impetus and are exploratory in nature. In particular, the combination of environmental degradability and human biocompatibility offers promising opportunities for applications, especially in the field of medicine.[2] One salient observation from the symposium is the need to open the field to researchers from other disciplines. Polymer research is a broad domain in which green chemistry is far from the only discipline playing a major role. Bacteria-based polymer production, as envisioned by microbiologists, holds significant potential for the development of future biodegradable and biocompatible materials. Another point of interest was the limited effectiveness of current biological degradation processes, as claims regarding some worms' ability to degrade plastics were shown to be unfounded. Moving forward, events in polymer science, such as the Sustainable Polymer Symposium, should be leveraged to promote the exchange of current research while more extensively incorporating contributions from medical, pharmacological, and ecological disciplines in future gatherings.

## Use of AI and AI-assisted technologies

Not applicable.

### ORCID iDs

Charlotte Elisabeth Scheherazade Schmidt 0009-0005-6551-3696

### References

1. Sasu DD. Production forecast of thermoplastics worldwide from 2025 to 2050. New York, USA: *Statista Inc*. 2023. https://www.statista.com/statistics/664906/plastics-production-volume-forecast-worldwide/ Accessed October 10, 2025.
2. Sam G, Chen S, Rehm BHA. Functionalisation of polyhydroxybutyrate for diagnostic uses. *New Biotechnol*. 2025;85:9–15. doi:10.1016/j.nbt.2024.11.002
3. Taft M. For every person on Earth, there are 21,000 pieces of plastic in the ocean. New York, USA: *Gizmodo*; 2023. https://gizmodo.com/170-trillion-plastic-pieces-ocean-pollution-1850212628. Accessed October 10, 2025.
4. Kleij AW. Catalysis as a key driver for the transformation of biomass into engineering polymers [PowerPoint presentation]. Presented at: Sustainable Polymers Symposium; October 9, 2025; Tübingen, Germany.
5. Hanssens J, Meneses D, Saya JM, Orru RVA. Terpenes and terpenoids: how can we use them? *Eur J Org Chem*. 2025;28:e202401151. doi:10.1002/ejoc.202401151
6. Brandolese A, Battistel E, Hauenstein O, Kleij AW. Catalytic ring-opening copolymerization of fatty acid epoxides: access to functional biopolyesters. *Macromolecules*. 2022;55(7):2566–2573. doi:10.1021/acs.macromol.2c00321
7. Sanford MJ, Peña Carrodeguas L, Van Zee NJ, Kleij AW, Coates GW. Alternating copolymerization of propylene oxide and cyclohexene oxide with tricyclic anhydrides: access to partially renewable aliphatic polyesters with high glass transition temperatures. *Macromolecules*. 2016;49(17):6394–6400. doi:10.1021/acs.macromol.6b01425
8. Shi W, Senthamarai T, Lanzi M, Orlando P, Nogués Martín R, Kleij AW. Access to highly functional and polymerizable carbonate-drug conjugates. *ChemSusChem*. 2025;18:e202500031. doi:10.1002/cssc.202500031

9. Lamparelli DH, Villar-Yanez A, Dittrich L, et al. Bicyclic guanidine promoted mechanistically divergent depolymerization and recycling of a bio-based polycarbonate. *Angew Chem Int Ed*. 2023;135(51):e202314659. doi:10.1002/anie.202314659
10. Fink P, Menzel C, Kwon J-H, Forchhammer K. A novel recombinant PHB production platform in filamentous cyanobacteria avoiding nitrogen starvation while preserving cell viability. *Microb Cell Fact*. 2025;24(1):43. doi:10.1186/s12934-025-02650-y
11. Fink P. Genome integration of PHB operon in Nostoc sp. PCC7120: Stable, constitutive PHB production of NosPHB3.0. [PowerPoint presentation]. Presented at: Sustainable Polymers Symposium; October 9, 2025; Tübingen, Germany.
12. Birke J, Jendrossek D. Rubber oxygenase and latex clearing protein cleave rubber to different products and use different cleavage mechanisms. *Appl Environ Microbiol*. 2014;80(16):4772–4781. doi:10.1128/AEM.01271-14
13. Prakash T, Yadav SR, Brüger M, Jendrossek D. Cleavage of natural rubber by rubber oxygenases in Gram-negative bacteria. *Appl Microbiol Biotechnol*. 2024;108:191. doi:10.1007/s00253-023-12940-3
14. Jendrossek D. Enzymatic biodegradation of rubber and fossil hydrocarbon polymers. [PowerPoint presentation]. Presented at: Sustainable Polymers Symposium; October 9, 2025; Tübingen, Germany.
15. Birke J, Röther W, Jendrossek D. RoxB is a novel type of rubber oxygenase that combines properties of rubber oxygenase RoxA and latex clearing protein (Lcp). *Appl Environ Microbiol*. 2017;83(14):e00721-17. doi:10.1128/AEM.00721-17
16. Sanluis-Verdes A, Colomer-Vidal P, Rodriguez-Ventura F, et al. Wax worm saliva and the enzymes therein are the key to polyethylene degradation by *Galleria mellonella*. *Nat Commun*. 2022;13:5568. doi:10.1038/s41467-022-33127-w
17. Yang Y, Yang J, Wu WM, et al. Biodegradation and mineralization of polystyrene by plastic-eating mealworms: Part 1. Chemical and physical characterization and isotopic tests. *Environ Sci Technol*. 2015;49(20):12080–12086. doi:10.1021/acs.est.5b02661
18. Jendrossek D. Polyethylene and related hydrocarbon polymers („plastics") are not biodegradable. *New Biotechnol*. 2024;83:231–238. doi:10.1016/j.nbt.2024.08.503
19. Hurst J, Adams F, Schnichels S. The future of nanomaterials tackling the challenge of delivering nucleic acids to the retina. *Adv Funct Mater*. 2024;34:407173. doi:10.1002/adfm.202407173
20. Pourdakheli-Hamedani Y. *Poly(solketal acrylate) as a versatile tool for ocular delivery applications*. [PowerPoint presentation]. Presented at: Sustainable Polymers Symposium; October 9, 2025; Tübingen, Germany.